Technical Report

TR-01-21

Äspö Hard Rock Laboratory

Analysis of fracture networks based on the integration of structural and hydrogeological observations on different scales

Paul Bossart
Geotechnical Institute Ltd., Bern

Jan Hermanson
Golder Associates, Stockholm

Martin Mazurek
University of Bern

May 2001

Svensk Kärnbränslehantering AB
Swedish Nuclear Fuel
and Waste Management Co
Box 5864
SE-102 40 Stockholm Sweden
Tel 08-459 84 00
+46 8 459 84 00
Fax 08-661 57 19
+46 8 661 57 19

Äspö Hard Rock Laboratory

Analysis of fracture networks based on the integration of structural and hydrogeological observations on different scales

Paul Bossart
Geotechnical Institute Ltd., Bern

Jan Hermanson
Golder Associates, Stockholm

Martin Mazurek
University of Bern

May 2001

The full report including all Appendices is available as a pdf-file on the enclosed CD-ROM disc. The printed version contains only the main text and a list of the Appendices.

Abstract

Fracture networks at Äspö have been studied for several rock types exhibiting different degrees of ductile and brittle deformation, as well as on different scales. Mesoscopic fault systems have been characterised and classified in MAZUREK et al. (1996); this report focuses mainly on fracture networks derived on smaller scales, but also includes mesoscopic and larger scales.

The TRUE-1 block has been selected for detailed structural analysis on a small scale due to the high density of relevant information. In addition to the data obtained from core materials, structural maps, BIP data and the results of hydrotests were synthesised to derive a conceptual structural model. The approach used to derive this conceptual model is based on the integration of deterministic structural evidence, probabilistic information and both upscaling and downscaling of observations and concepts derived on different scales.

Twelve fracture networks mapped at different sites and scales and exhibiting various styles of tectonic deformation were analysed for fractal properties and structural and hydraulic interconnectedness. It was shown that these analysed fracture networks are not self-similar. An important result is the structural and hydraulic interconnectedness of fracture networks on all scales in the Äspö rocks, which is further corroborated by geochemical evidence.

Due to the structural and hydraulic interconnectedness of fracture systems on all scales at Äspö, contaminants from waste canisters placed in tectonically low deformation environments would be transported - after having passed through the engineered barriers - from low-permeability fractures towards higher permeability fractures and may thus eventually reach high-permeability features.

Contents

1 Introduction 1

1.1 Overview 1

1.2 Goals of the phase III work 1

1.3 Specific notation 2

2 Derivation of a structural / hydraulic conceptual model on the metre - decametre scale (TRUE-1 block) 3

2.1 Introduction 3

2.2 Database 3

2.2.1 Tunnel and borehole geometry 4

2.2.2 Geological and structural drillcore logging 5

2.2.3 Borehole Image Processing System (BIP) 9

2.2.4 Tunnel mapping 10

2.2.5 Line counting in the tunnel 10

2.3 Results 11

2.3.1 Lithologies and structures in the TRUE-1 block 11

2.3.2 Database analysis of the TRUE-1 core logs and Borehole Image Processing System (BIP) 13

2.3.3 Comparison of tunnel maps and line countings at the TRUE-1 site with SKB standard tunnel mapping data 18

2.4 Deterministic Conceptual Structural Model of the TRUE-1 site 22

2.4.1 Methodology 22

2.4.2 The fracture network 25

2.4.3 Visualisation of core logging and BIP data 27

2.4.4 Prerequisites for the deterministic structural model 29

2.4.5 The deterministic model 33

2.5 A stochastic geometric model of the fracture network in the TRUE-1 volume 37
2.5.1 Principle 37
2.5.2 Previous work 38
2.5.3 Fracture size estimation 39
2.5.4 Fracture intensity 43
2.5.5 Summary of the stochastic geometric DFN model 44
2.6 Derivation of the integrated structural model 51
2.6.1 Integration of deterministic and stochastic models 52
2.6.2 Visualisation of the results 55
2.7 Constraints on the structural model based on hydrogeological observations 55
2.7.1 Available hydraulic data 55
2.7.2 Evaluation of hydraulic tests 57
2.7.3 Connectivity of the fracture network 62
2.7.4 Relationships between structures and hydraulics in the TRUE-1 boreholes 67
2.7.5 Specific constraints on hydrogeological testing and conceptual structural models 69
2.8 Conceptual model for tracer transport in “Feature A” and a generic block model of the TRUE-1 site 71
2.8.1 Conceptualisation of “Feature A” 71
2.8.2 Generic block model of the TRUE-1 block 78

3 Large-scale structures and flowpaths, scaling relationships 81

3.1 Introduction 81
3.2 Database 81
3.3 Methodology 83
3.4 Results 95
3.5 Structural and hydrogeological constraints 97
3.6 Integration of hydrochemical evidence 99
3.7 Conclusions 100

4 Summary of concepts: water flowpaths between waste canisters and the biosphere 101

4.1 Fracture geometries of different scales 101

4.2 Implications for contaminant transport between the repository and the biosphere 103

Acknowledgements 105

References 107

List of Appendices

Appendix 1 The drillcore database

Appendix 2 The BIP database

Appendix 3 The line counting database

Appendix 4 The tunnel wall fracture trace map of the TRUE-1 block

Appendix 5 The deterministic structural model: visualisation of fractures in the TRUE-1 block

Appendix 6 Constraints on the structural model based on hydrogeological observations

Appendix 7 Scaling relationships: cumulative fracture frequencies of structural maps

Executive Summary

The present report is the last report in the framework of the Fracture Classification and Characterisation project (FCC). The previous investigations were documented in a series of technical reports and in an international co-operation report (MAZUREK et al. 1996). The following executive summary is related mainly to this previous reporting in order to find the link to the whole FCC project.

The objectives of the Fracture Classification and Characterisation Project (FCC), a joint undertaking of Nagra (Switzerland) and SKB (Sweden), are

- to classify water-conducting features occurring in the Äspö tunnel system
- to characterise and conceptualise these features with respect to radionuclide transport properties (e.g. structure, mineralogy, distribution of flow and matrix porosity)
- to develop and apply a methodology for the characterisation of water-conducting features in crystalline rocks.

The investigation methodology involves a stepwise procedure:

- Compilation of an inventory of existing data (geology, hydrogeology, hydrochemistry) and of the boundary conditions for exploration of water-conducting features (e.g. in boreholes, open tunnel). Definition of the scale which the investigation should target.
- Preliminary characterisation of a limited number of typical water-conducting features, with the objective of understanding the processes governing the evolution of water-conducting features and thus defining a set of geological parameters that adequately describe the features.
- Full characterisation of a large number of water-conducting features and development of a database containing all relevant parameters that can be observed or measured.
- Database analysis (which parameters are common to all features, which vary systematically ?) and derivation of a fracture classification scheme.
- Derivation of simplified conceptual models of all types of water-conducting features, including geometric and lithological (mineralogical, porosimetric) information required for transport modelling.
- Transport modelling and sensitivity analysis of parameters from the conceptual models.

The preliminary characterisation stage indicated that, on an observation scale of metres to decametres, all water-conducting features are related to faults. The fault geometries

are consistent with the mechanistic principles of fault nucleation, propagation and linkage derived by MARTEL et al., POLLARD (1988). This model characterises the anatomy of faults as interconnected systems of shear fractures (master faults) and tensile fractures (splay cracks).

The full characterisation included 88 water-conducting features whose traces cross-cut the entire tunnel cross-section (smaller features were not included in the study). Most of the faults dip steeply and strike directions are NW-SE (dominant) and NE-SW (subordinate). Many of the faults follow pre-existing structural inhomogeneities, such as ductile shear zones or lithified cataclastic shear zones.

Fault geometries and other parameters are indistinguishable between the Småland Granite and the Äspö Diorite. Fracture frequencies are higher in the Fine-grained Granite, and other fault characteristics contributing to transport properties (e.g. lithology, mineralogy, pore-space distribution) are also different. However, Fine-grained Granite was never observed to be the dominant host rock of any of the features because it occurs as small intrusive bodies or dykes measuring several metres to a few decametres in size. It is concluded that, because (within the database of 88 water-conducting features) this rock type does not host faults over more than a few metres, it is not relevant for the larger-scale transport properties of the faults.

In the review of this report, it was pointed out that the possibility exists that large bodies of Fine-grained Granite could exist even if they were not observed in the part of the unnel system on which this report is based. It is a topic of planned future investigations to explore and characterise faults hosted by Fine-grained Granite.

The only striking difference between individual water-conducting features is the internal fault geometry; no other distinguishing criteria (such as the arrangement of lithological domains, mineralogy of fracture infills, transmissivity, etc.) were identified and probably do not exist. On the basis of the geometric arrangement of master faults and splay cracks in faults, 5 types of water-conducting features are distinguished:

- Type 1 - single fault
- Type 2 - swarm of single faults
- Type 3 - fault zone
- Type 4 - fault zone with rounded geometries
- Type 5 - parallel fault zones with long connecting splays.

Both direct observations and theoretical principles indicate that the internal geometry on which the classification is based is not a unique characteristic of a fault, i.e. the type may vary along the strike of a fault. The length of segments with constant properties (i.e. same type) is in the range of metres to many decametres. The application of the classification scheme is limited to smaller-scale considerations. In the case of large-scale transport, the results of the study indicate that, due to the common genetic history, water flow in the underground environment of Äspö is dominated by one single family of water-conducting features.

Conceptual models of fault geometry are derived on the basis of the field database and laboratory analyses of mineralogy, porosity and pore-space distribution. Flow within

faults occurs within the master faults and/or in the splay cracks. The lithological domains adjacent to the flow porosity are

- fault gouge/breccia
- lithified cataclasite
- fracture coating
- mylonite (altered or unaltered)
- granite (altered or unaltered).

The brittle fault rocks (i.e. fault gouge / breccia) are expected to interact strongly with radionuclides or tracers transported in the flow porosity by means of sorption (presence of sorbing phases such as clay minerals and Fe-oxyhydroxides) and matrix diffusion (large interconnected porosity). These processes are weaker in mylonites due to the low porosity and the scarcity of low-temperature alteration products.

1. Introduction

1.1 Overview

The Fracture Classification and Characterisation Project (FCC) is a joint venture of Nagra (Switzerland) and SKB (Sweden). In order to provide a better link between geological site characterisation and conceptual geological models on the one hand and geosphere transport modelling that builds directly on site-specific geological input on the other, it was considered worthwhile to share previous experience and use the Äspö Hard Rock Laboratory (HRL) as a test case for fracture characterisation based on tunnel evidence. Some of the results, in the form of comparisons with other sites as well as with other sets of information (e.g. derived on the basis of borehole or surface outcrop data), have already been synthesised and published in MAZUREK (2000).

This report documents the third and final phase of the FCC project. Phase I, documented in MAZUREK et al. (1995), provided preliminary information on fracture patterns and mechanistic principles of fracture formation in the Äspö HRL. In phase II, documented in MAZUREK et al. (1996), a fracture classification scheme was developed and fracture anatomy was characterised in detail. The geometry of the flow porosity and the flow-wetted surface was addressed, and rock domains in contact with flowing water were characterised with regard to connected porosity (matrix diffusion) and mineralogy (sorption). Simplified conceptual models were developed for contaminant transport and were used successfully e.g. by HEER & JAKOB (1999) and JAKOB & HEER (2000).

This report documents phase III of the FCC project. While the previous phases addressed only mesoscale water-conducting features that cross-cut the whole tunnel diameter, small-scale fracture patterns are a major topic in this report. In addition, fracture patterns on a large (regional) scale are addressed. Information on water-conducting features over a wide range of scales provides the basis for a conceptual description of the flowpath of contaminants leached from a hypothetical waste repository through different hierarchies of fractures and faults to the potential exfiltration areas in the biosphere.

1.2 Goals of the phase III work

The main objectives of this report include:

– Characterising the flowpath between a hypothetical repository at Äspö and the biosphere (large-scale conceptual model).

– Providing a geological background (structure, mineralogy, flow and matrix porosity) as input to predictive modelling of experimental sites such as TRUE-1 (small-scale conceptual models).

– Providing "illustrative examples", i.e. conceptual models closely representing natural observations that can be used for calculation of solute transport properties of the geosphere.

– Developing and illustrating an investigation methodology ("How can conceptual models for flow and transport be developed on the basis of geological information?").

1.3 Specific notation

Linear and planar orientations are given as azimuths of dip / dip angles throughout this report.

2. Derivation of a structural / hydraulic conceptual model on the metre - decametre scale (TRUE-1 block)

2.1 Introduction

For the characterisation of small-scale fracture patterns, the so-called "TRUE-1 block" was chosen. The reason for this was mainly the wealth of information available for this zone from work related to the Tracer Retention Understanding Experiment (TRUE-1, WINBERG 1996). The first stage of the TRUE-1 block is penetrated by 5 boreholes and abundant hydrogeological data are available on which the FCC work could be based. Moreover, it is planned to excavate parts of the TRUE-1 block once the hydraulic and tracer experiments are completed. This will present an opportunity to test the structural concepts and predictions discussed in this report and thus to obtain some idea of the extent to which a rock volume can be characterised by the methods applied.

The TRUE-1 block is bounded by the fracture zones NW-2, NW-3 and NWW-4 (WINBERG et al. 2000). Despite dense fracturing, there are no major faults within the TRUE-1 block volume. It can be conceived as a rock volume that occurs between decametre-size faults with an average spacing of metres to tens of metres, as described by MAZUREK et al. (1996).

2.2 Database

The conceptual structural model of the TRUE-1 site is based on geological, structural and geometric information from the tunnel between tunnel metres 2930 and 3020 and from boreholes KXTT1, KXTT2, KXTT3, KXTT4 and KA3005A. An overview of the database is shown in Table 2-1.

Table 2-1. Overview of database.

Data	Description of data base	Reference
Tunnel geometry	Map with reference points	WINBERG et al., 1996
Borehole orientation	Excel data base	HESBÖL & HERMANSON (1997)
Structural data base from drillcore mapping	Excel data base	HESBÖL & HERMANSON (1997)
Structural data base from Borehole Image Processing (BIP)	BIP images and ASCI data base an CD-ROM	Received from WINBERG
Tunnel mapping	Maps of tunnel wall	This report
Line countings in the tunnel	Field mapping notes	This report

Methods of data acquisition included drillcore mapping, digital imaging of the borehole walls (BIP), mapping of the tunnel walls and line counting of structures on the tunnel

walls and roof. An important difference to other Äspö databases is the fact that planar orientations are given in azimuth of dip (instead of strike direction) and dip angle. This leads to a simpler presentation of orientations in the stereoplots: azimuth of dips and dip angles can be presented directly as poles in stereonets.

2.2.1 Tunnel and borehole geometry

The tunnel section of interest has a NW-SE orientation. At 2944 m and 3005 m, two niches on the NE side of the tunnel contain the borehole mouths of KXTT1, KXTT2, KXTT3, KXTT4 and KA3005A **(**Figure 2-1). Borehole KA3005A differs in orientation from KXTT1 to 4. It is also the longest of the analysed cores. The KXTT holes are located close to one another, with only slight variations in orientation. The positions of the borehole mouths, as well as the orientations and the lengths of the boreholes, are summarised in Table 2-2 (data from WINBERG 1996).

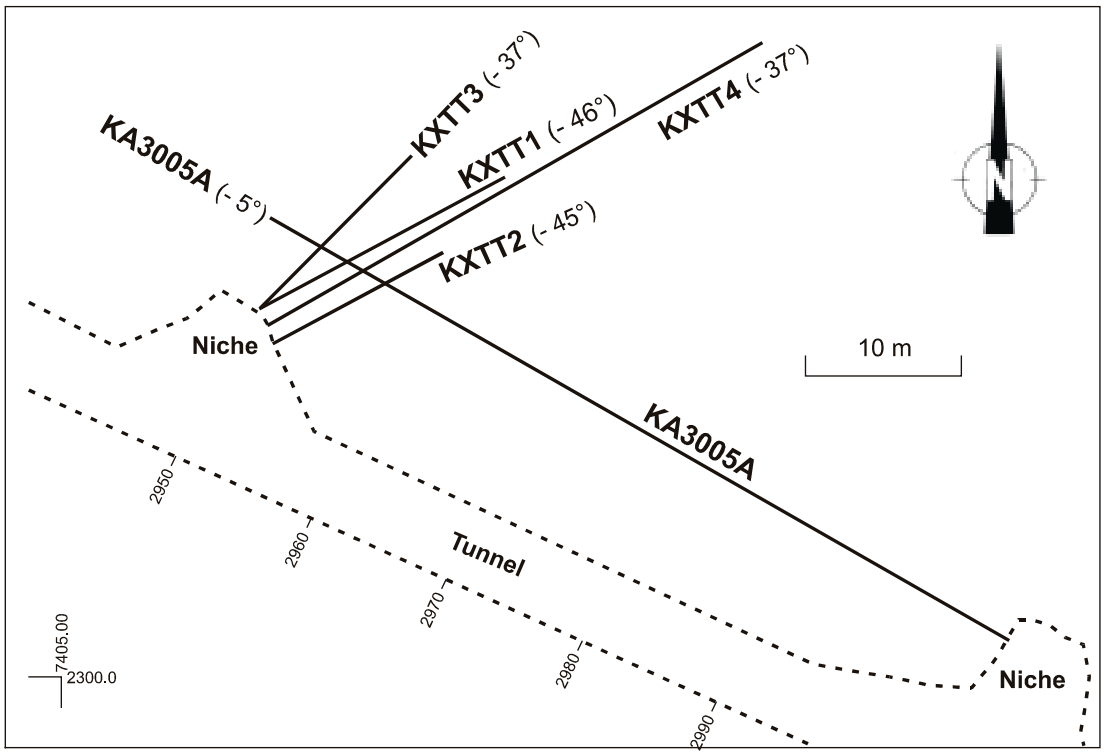

Figure 2-1. *Overview of borehole and tunnel geometry in the TRUE-1 block. Horizontal section. The values in parenthesis indicate borehole inclinations (negative value means that borehole dips downwards).*

In the following, the boreholes are defined as straight lines, calculated from the location of the borehole mouth and the orientation of the borehole. The deviation of the boreholes from these idealised lines is very small and can be ignored. A maximum deviation of 31 cm has been found in borehole KA3005A, which is clearly less than 1%.

Table 2-2. Positions of borehole mouths, orientation and length of boreholes KXTT1, KXTT2, KXTT3, KXTT4 and KA3005A.

Borehole	*Eastings [m]	*Northings [m]	*Z [m.a.s.l.]	Azimuth [degrees]	Inclination [degrees]	Length [m]
KXTT l	2313.56	7430.00	-392.12	61.53	-45.64	28.76
KXTT2	2314.38	7427.63	-392.42	61.21	-44.52	18.30
KXTT3	2313.55	7429.95	-391.07	44.32	-36.90	17.43
KXTT4	2313.86	7428.80	-391.14	60.05	-36.37	49.31
KA3005A	2363.82	7408.09	-399.86	299.05	-4.50	58.11

* based an the Äspö coordinate system

2.2.2 Geological and structural drillcore logging

Detailed geological mapping of the cores from KXTT1, KXTT2, KXTT3, KXTT4 and KA3005A has been performed with the following objectives:

- to provide detailed structural and lithological data for a general conceptualisation of the characteristics of water-conducting fractures in the Äspö HRL
- to provide data for updating the existing structural model of the TRUE-1 site.

The geological mapping included data not normally covered in SKB core mappings, such as degree of ductile and cataclastic deformation and alteration. A large effort has been made to quantify subjective geological parameters in order to produce a database that can be used as valid input to numerical models.

Methodology of data acquisition

An adjustable frame for positioning of the cores was constructed and oriented parallel to the in-situ orientation of the cores. All measurements, including foliation and fracture orientations, were performed directly as *dip* and *strike* in the lab with a Silva compass. The strike values were transformed to azimuth of dips in the database, which allows straight-forward presentation of the orientations in the stereoplots (see Chapter 2.3.2). The vertical up of the examined core material was determined by correlation with BIP (Borehole Image Processing) images (the database of the BIP images is presented in Chapter 2.2.3). The first 3 m of the cores were drilled with a core diameter of 86 mm, and thereafter with a diameter of 56 mm, using a double core barrel. The cores were examined starting from the 56 mm onset, with the exception of core KA3005A where the whole borehole length was examined. Major emphasis was placed on deformation and alteration around fractures compared to the unfractured host rock. Deformation, alteration and mineralogy are parameters that are not easily quantified as they are mainly descriptive and are subject to variation. An effort was made to quantify them

using a subjective scaling based on the geological mapping. The scaling and its limitations are described later. Table 2-3 shows the applied mapping protocol. The BIP images were either attached to the protocol or viewed separately during the mapping. Each page of the log covers a core length of 0.5 m. The subjectively scaled descriptive parameters (e.g. degree of cataclastic or ductile deformation) were mapped graphically and later converted to numerical values in the database.

Table 2-3. Example of the mapping protocol.

Detailed core-log of the TRUE-1 volume							Sheet no: 3
Length: 3 - 3,5 (m)				Date: 961122	Sign:		RH
BIPS	Dip dir/dip	Catacl. def. 1 2 3	Ductile def. 1 2 3	Foliation	Alteration 1 2 3	Lithology	Re-marks
	337/48 51 /82			51 /74			Open Tight

Database parameters

A spreadsheet-type database was produced on the basis of the core logging protocol and includes the following parameters:

1. Fracture location (borehole depth, [m])
2. Fracture orientation (strike/dip, Äspö local north). Strike value was transformed to azimuth of dip in the database.
3. Foliation orientation (strike/dip, Äspö local north). Strike value was transformed to azimuth of dip in the database.
4. Fracture mineralisation (9 columns)
5. Ductile deformation (subjective scale 0-3)
6. Cataclastic deformation (subjective scale 0-3)
7. Alteration (subjective scale 0-3)
8. Open or tight (as observed on the core)
9. Rock type
10. Rock contacts (borehole length, [m])
11. Rock texture.

The database consists of two spreadsheets, one recording parameters that relate to a specific depth along the core, such as fracture location and orientation (see Table 2-4), and the other to depth ranges, such as degree of deformation (see Table 2-5). The whole database is contained in Appendix 1. In the following, the most important attributes of these tables are explained in more detail.

Table 2-4. Example of the drillcore database. Orientation and mineralisation of fractures. F means fracture and V stands for foliation. Abbreviations: Ep Epidote, CHL Chlorite, Ca Calcite, Fe Iron Oxide, Qz Quartz, Py Pyrite, T tight fracture, O open fracture.

Fracture/ Foliation	BH depth	Orientation		Mineralogy					Open/ Tight	Remarks
	(m)	Azimuth of dip	Dip	EP	CHL	CA	FE	PY		
F	27.18	246	85	X	X				T	4 mm width
V	27.20	161	74			X			O	Fine gr. Granite
F	27.48	10	73	X					T	3 mm, 20 mm displaced
F	27.75	163	68			X			O	2 mm width
F	27.82	36	77	X					T	3 mm width
V	27.92	44	72							
F	28.05	54	84		X				O	
F	28.16	48	90		X		X		O	Qz vein
F	28.20	13	72	X		X			T	Qz vein
F	28.26	125	54		X				O	

Table 2-5. Example of the drillcore database (borehole KXTT1); Deformation, alteration and texture on a subjective scale. Cat is cataclastic, Duc ductile and A alteration. Rock type:, AD is Äspö Diorite, AG Äspö Granite and MYL mylonite. Length scale in metres. The drillcore database is shown in Appendix 1.

Type	From	To	Degree	Rocktype	Fabric/Texture	Remarks
CAT	2.17	2.22	1	AG	Medium grained	Lots of epidote veins
ROCK	2.22	2.40	-	AG/AD	Medium grained	Transitional
DUC	2.4	2.43	1	AG/AD		Epidote in upper contact
DUC	2.43	2.6	3	MYL		
A	2.42	2.43	1.5	AG/AD		Hematite impregnation
A	2.43	2.60	1.5	MYL		Hematite impregnation
DUC	2.60	2.70	2	MYL/AD		Transitional
DUC	2.70	2.76	1	AD	Medium grained	
CAT	3.19	3.22	1	AD	Medium grained	

Fracture location: Noted as the depth where the fracture intersects the core axis (column borehole depth in Table 2-4). This depth is correlated with the BIP images.

Fracture orientation: The measured orientation is given by its strike and dip (right hand rule). All measurements are presented relative to the Äspö local north axis. The strike values are transformed to azimuth of dip values in the database (see Table 2-4).

Deformation: The definitions used in the subjective scale for deformation are based on a classification diagram of fault rocks (SIBSON 1977). Plastic or ductile and cataclastic deformations are separated into two columns. When deformation is ductile, the scale ranges from 0 (background foliation in the rock) to 3 (mylonite). When deformation is

brittle (cataclastic), the cohesive rock contains fragments of randomly oriented grains and brecciated rock in a fine-grained matrix. The degree of cataclasis is recorded on a scale from 0 (rock with few fragments and microfractures) to 3 (fully brecciated). The deformation values are listed in the column denoted “degree of deformation” in Table 2-5.

Foliation orientation: When there is a parallel orientation of minerals, or mineral banding in a rock, it is said to be foliated. The foliation orientation (strike and dip, the strike values transformed to azimuth of dip values in Table 2-4) is given at regular intervals along the drillcore, with more measurements in locations of varying orientation. The foliation fabric is indicated with a “V” in the column “type” of Table 2-4.

Alteration: The degree of alteration is judged by the parameters colour, grain size and epidotisation/chloritisation and is quantified on a subjective scale from 0 to 3. Rock colouring ("staining") associated with fractures may vary from very light to very dark. The visible colouring is dependent on mineral precipitation combined with grain size and type of host rock. Because of the correlation of these parameters, it is difficult, by visible inspection of the core, to eliminate the factor of subjectivity.

Lithology: Traditionally, three granitoid rock types and one greenstone have been mapped at Äspö. The granitoids are the Fine-grained Granite, the Äspö Diorite and the Småland Granite. Transitions between these rock types are smooth but noticeable. This classification has been maintained throughout the database. Lithological unit thickness and location of rock contacts are given for each rock type. The rock types are listed in Table 2-5.

Fabric and texture: The following attributes have been used for the fabric and texture (see Table 2-5):

1. Phenocryst-bearing (idiomorphic crystals, mainly feldspars)
2. “Augen”-bearing (deformed felsic crystals)
3. Grain size (fine-, medium- and coarse-grained)
4. Fabric (massive, foliated)
5. Fragmented phenocrysts or “Augen”

The grain size is defined as follows: fine-grained < 2 mm, medium-grained 2-5 mm and coarse-grained > 5 mm.

Tight and open fractures**:** On the basis of visual inspection of the core, sealed or tight (T) and open (O) fractures have been separated (see Table 2-4, last column). It has to be emphasised that this is a biased parameter as an unknown proportion of originally tight fractures was possibly opened during drilling and handling of the core, creating artificial open discontinuities.

Remarks: Contains additional comments which were not quantified. Important information is the confirmation of fault gouge as fracture infill (see also Chapter 2.5).

Limitations in the database

Length measurements along the drillcores based only on drill rod uptake are often incorrect due to core loss or human factors. Thus, correlation of the cores with BIP images is preferable. However, it should be noted that the BIP system has its own limitations with extension or lack of extension of wires in vertical or horizontal holes. In horizontal holes, the BIP camera has to be pushed along the length of the borehole, causing the cable to respond. In vertically oriented holes, the cable falls freely along the length of the hole. When mapping the cores from KXTT1 to 4, correlation of length measurements to BIP images proved more reliable than for core KA3005A. As a result, the locations of mapped features in the KXTT holes are more reliable (estimated error of ± 2 cm) than in KA3005A (estimated error of ± 8 cm).

Interpreting subjective geological scaling is beset with constraints. Deformation and alteration of the host rock vary, with gradual transitions, along the length of the investigated core. As mapping the drillcore is tedious work, judgement of the minimum degree of deformation or alteration that it is possible to map may change slightly with time and mapped drillcore metres, even when the mapping geologist is the same person.

2.2.3 Borehole Image Processing System (BIP)

Images of the borehole walls were available in digital form for all boreholes drilled at the TRUE-1 site. They were accompanied by a database in which a set of parameters was recorded on the basis of the images. Table 2-6 shows the attributes of the BIP fracture-foliation database. These parameters consist mainly of the orientation, type, width, form and special conditions of structures.

Table 2-6. The BIP database and its attributes. The BIP database is shown in Appendix 2.

No	Depth	Azimuth of dip	Dip	Sort	Width	Form	Condition	Remarks
	[m]	**[°]**	**[°]**	**Primary structure**	**[mm]**	**Planar**	**Weathered**	**Quartz**
1				Fracture		Undulating	Dull	Chlorite
2				Vein		Stepped	Cavities	Calcite
3				Fracture zone		Irregular	Open	Epidote
4				Contact		Network	Oxidised	Hematite
5				Structure		Breccia	Chloritised	Pyrite
6				(foliation)		Shear	Epidotised	Hybride rock
7				Alteration		Crushed	Tectonised	Clay
8						Flowstructure		Granite
9						Foliation		Pegmatite
10								Fine-grained Granite
11								Mylonite

From this BIP database, a new sub-database was produced that is formally compatible with data derived from drillcore mapping. First, only *fractures* and *mylonites* were chosen. Then, the distinction between open and closed fractures was made by allocating "weathered", "dull", "cavities" and "open" structures from the "condition" column to open structures and "oxidised", "chloritised" and "epidotised" fractures to tight (closed) fractures. The columns "depth", "strike" (strike values were transformed to azimuths of dip values), "dip" and "width" were also selected. The column "form" was not used.

For the derivation of the conceptual models, three types of structures were finally distinguished: mylonites, open fractures and tight (closed) fractures. The modified BIP database is shown in Appendix 2.

2.2.4 Tunnel mapping

Detailed small-scale mapping along the tunnel wall was carried out on the south-west boundary of the TRUE-1 block, between tunnel metres 2944 and 2995. In addition to lithologies and fracture traces, the map includes information on the orientation of selected structures. These can be divided into water-conducting features, dry fractures and ductile shear zones (mylonites).

2.2.5 Line counting in the tunnel

Line counting of fractures was carried out on the south-west boundary of the TRUE-1 block, between tunnel metres 2950 and 2980. The positions, orientations and trace lengths of fractures intersecting the lines were recorded. Line countings were performed in two orthogonal directions, along the tunnel roof parallel to the tunnel axis and normal to the tunnel axis. In Table 2-7, the attributes of the line counting database are shown. The complete line counting database is presented in Appendix 3.

Table 2-7. Example of the line counting database. Line counting was carried out on the tunnel roof, parallel and normal to the tunnel axis of the TRUE-1 section between 2950 and 2980 m. FGG is the Fine-grained Granite, FA is azimuth of dip and FW is angle of dip.

Interval from	To	Lithology	Amount of fractures	Orient.		Trace length
				FA	FW	
Line counting parallel to tunnel				[°]	[°]	(m)
Start at 2950 m						
2950	1	Diorite	0	0	0	0.00
2951	2	Diorite	1	50	50	0.30
		Diorite	2	90	40	0.30
2952	3	FGG	1	90	20	0.20
		FGG	2	210	30	0.20
		FGG	3	210	30	0.20
		Diorite	4	220	85	0.30
2953	4	Diorite	0	0	0	0.00
		TOTAL	13			1.50

2.3 Results

2.3.1 Lithologies and structures in the TRUE-1 block

The dominant lithology in the cores is a granitoid, referred to as Äspö Diorite (Figure 2-2). The initial section of all the cores is made up of fairly homogeneous diorite, sometimes merging into granite. The diorite then changes character as it becomes fine-grained and dark, containing felsic phenocrysts at approximately 10 m depth. The lighter, medium-grained granites, sometimes distinctly more reddish in colour, are called Ävrö or Småland Granites. There are two varieties of this phenocryst-bearing Äspö Diorite; one in which the phenocrysts are small and fragmented with an overall cataclastic appearance, but with no apparent loss of cohesion in the rock (illustrated in KXTT1 at a depth of 20.8 m, KXTT2 at 17.6 m and in KXTT3 at 12.7 m).

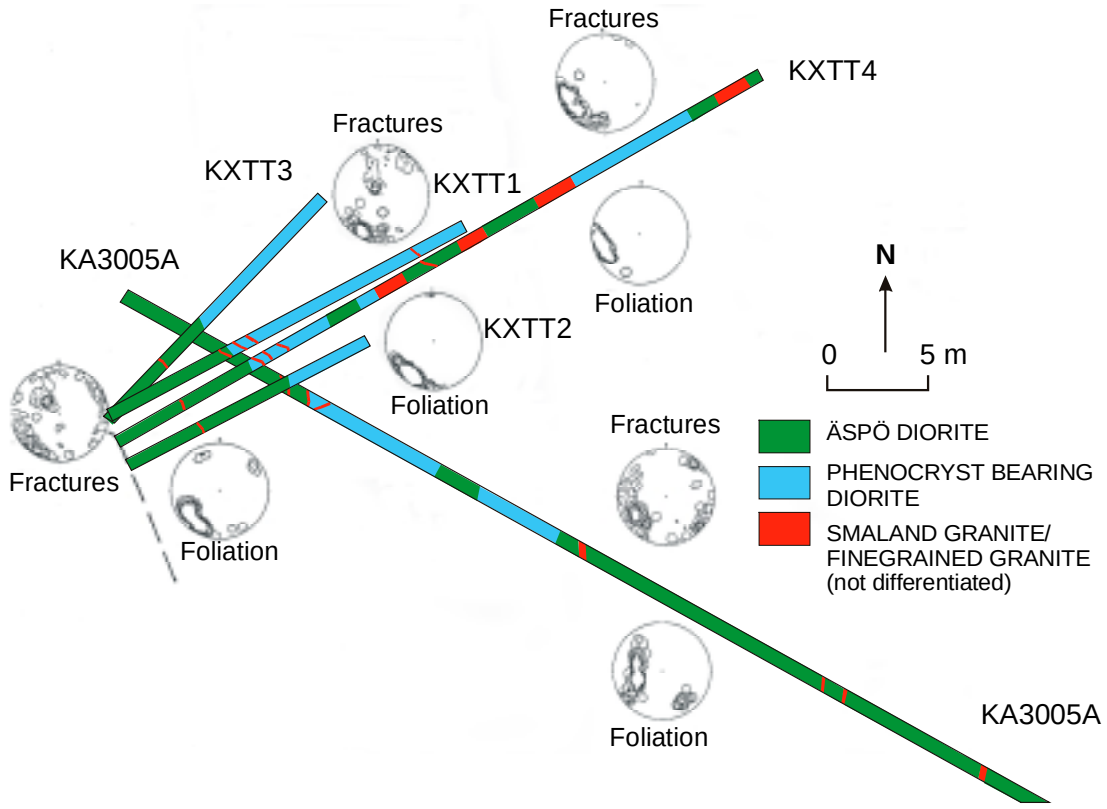

Figure 2-2. *Top view of the lithology in cores KXTT1, KXTT2, KXTT3, KXTT4 and in KA3005A, with stereoplots of poles to fracture and foliation planes.*

The other variety contains large phenocrysts, sometimes merging into very coarse diorite (in KXTT1 at approximately 17 m). In general, the diorite is often rich in epidote. In core KA3005A, the diorite is generally more massive than in cores of the KXTT1-4 boreholes. Sometimes it is heavily hematite-impregnated, which can make it hard to

distinguish from granite, and this is commonly the case in fractured areas (for example KXTT4, between 21-26 m and after 46 metres, associated with faulting, brecciation and alteration). Part of the phenocryst-bearing diorite in the KXTT4 borehole, between 18 and 19.5 m, is different from the phenocryst-bearing diorite found in the other cores. The contrast between the dark, fine-grained groundmass and light coloured, fractured and fragmented phenocrysts is more pronounced, giving it the appearance of a starry sky. It is not notably more fractured than the common diorite. Aplite or red porphyritic veins occasionally cut through the diorite. However these veins play a subordinate role in the TRUE-1 rock volume and are thus not considered further in the conceptual models.

Geological structures used for the conceptual models of the TRUE-1 block can be divided into ductile and brittle structures. Ductile structures are mainly mylonites[*)] linked to ductile shear zones. These mylonitic shear zones are usually epidote-rich and hematite-impregnated and are quite frequent in the first 20 metres of the KXTT boreholes. Brittle structures are mainly composed of the numerous joints and faults mapped in the drillcores, summarised in the following under the term fractures. Of importance for the conceptual model was not the precise tectonic classification into joints and different types of faults, but the distinction into closed and open fractures, the latter being important for flow and solute transport in the TRUE-1 block. With the aid of BIP images, it becomes clear that many of the sections affected by ductile and brittle deformation also show signs of chemical alteration, with rims of reddened host rock. A special type of brittle deformation is cataclasis[**)], producing fault gouge[***)] as a type of fracture infill. Fault gouge was not observed frequently in drillcores due to the fact that this rather cohesionless material has been washed out during the drilling process. However, the presence of fault gouge in the fractures of the TRUE-1 block has to be clearly postulated and has to be taken into account when deriving conceptual models for solute transport (see Chapter 2.8).

An overview of fracture orientations based on the drillcore database is shown in Figure 2-2. In all domains, steeply inclined fractures dominate over moderate and flat ones. As the stereoplots clearly show, the major part of fractures trend in a NW-SE direction. A minor part of fractures is E-W and NW-SE oriented.

---

*) A mylonite is a rock produced by ductile deformation. The term is used for a rock whose fabric has been partly or fully re-crystallised during metamorphism and/or progressive deformation. Macroscopically, mylonites are characterised by small-scale banding, and the cleavage intensity is often high. Microscopically, a considerable reduction of the grain sizes can be observed.

**) Cataclasis is a process of brittle shear deformation. Shear stress is accommodated by frictional sliding and grain rotation. Cataclasis can be localised to discrete horizons where the rock may be ground to a very fine-grained powder. Such focused cataclasis, together with mechanical mixing of the particles, leads to the formation of fault gouges which are incoherent and cohesionless planar horizons in fractures and reactivated shear zones.

***) Fault gouge as fracture infill material may be affected by subsequent low temperature alteration, which changes the initial mineralogy. Thus fault gouges in the TRUE-1 block may have higher contents of chlorite and clay minerals compared to the adjacent wall rocks.

There is no major faulting in the whole TRUE-1 block volume, except at its north-west boundary. This can be seen in a fracture zone at the end of borehole KXTT4, which may coincide with the regional structure called “NW2”. The rock here is faulted, brecciated and heavily hematite-impregnated.

2.3.2 Database analysis of the TRUE-1 core logs and Borehole Image Processing System (BIP)

The acquired database (see Chapter 2.2) has now been used for the analyses of the lithologies and structures of the TRUE-1 block. One method of analysing such a database is the cross-correlation of geological parameters. The analysis aims at evaluating the coupling of ductile and brittle structures to the hydraulic behaviour in the TRUE-1 block (see also Chapter 2.7).

The geological analysis was performed by investigating how pairs of parameters correlate along a borehole or a group of boreholes. Table 2-8 shows the resultant correlation matrix and its parameters. The ranking between 1 (relevant) and 4 (limited relevance) indicates which parameter combinations are deemed important for the objectives of this study. Mainly parameter combinations ranked as 1 have been subjected to a more detailed analysis. A limited number of parameter combinations ranked as being of less importance have been included to investigate the correlation of the deformation history in the rock to the current flow situation. Possible parameter combinations are the relationships between **orientation** and ductile deformation (mylonites), rock alteration, foliation, open and tight fractures or the relationships between **fracture frequency** and ductile deformation (mylonites), rock alteration, open and tight fractures.

Table 2-8. View of the parameter analysis performed on the geological database. Grey fields indicate the parameters considered most useful for cross-correlation rated on a scale from 1, critical parameter, to 4, considered not important for this study.

	DUC	ALT	CAT	ROCK	ORI	FREQ	FOL	MIN	O-T	FLOW
DUC		2	2	4	1	1	4	4	1	2
ALT	2		1	2	1	1	2	2	1	4
CAT	2	1		3	1	4	3	2	4	3
ROCK	4	2	3		2	1	3	3	2	1
ORI	1	1	1	2		4	1	3	2	1
FREQ	1	1	4	1	4		4	4	1	1
FOL	4	2	3	3	1	4		4	3	4
MIN	4	2	2	3	3	4	4		3	3
O-T	1	1	4	2	1	1	3	3		1
FLOW	2	4	3	1	1	1	4	3	1	

No correlation between lithologies and fracture orientations was found, most likely due to the fact that the occurrence of Fine-grained Granite is very subordinate (less than 10%) and the Småland Granite and Äspö Diorite behave rheologically in a similar way. Comparing the core-derived orientations with those from BIP imaging indicates an even more pronounced NW-SE maximum and a second maximum with NE-SW orientations

can be identified. Special attention has been paid to flat-lying fractures in the boreholes, because they cut the steeply inclined fractures and thus contribute to the connectivity of the fracture network. These fractures seem to form an individual group with distinct properties:

- Borehole KXTT2: Flat fractures are mostly open, with calcite or epidote coatings.
- Borehole KXTT3: Gently dipping fractures are again open and contain, with one exception, calcite. The column „condition“ in the database often indicates cavities (Table 2-6).
- Borehole KXTT4: Only open fractures contribute to the group of the gently dipping fractures. They are all filled with calcite, with one exception, and often have cavities.

Results of the orientation analyses of mylonitic, cataclastic and altered zones: all highly mylonitic, cataclastic (fault gouge) and altered sections are dominated by steep NW-SE fracture orientations. Cataclastic deformation (that often occurs in sections previously affected by ductile deformation) tends to be parallel to the ductile structures. Orientations in sections where both ductile and cataclastic deformation is low scatter widely in all directions. Approximately 1/3 of the highly deformed ductile sections also show signs of cataclastic (>1.5) deformation and the associated fractures most probably contain fault gouge.

Results of orientation analyses of open and tight fractures: open fractures have a dominant steep NW orientation, whereas tight fractures show a wider spread in orientations, in particular in the NW-SE, N-S and NE-SW directions. Sub-horizontal fractures occur in both samples but do not form a distinct set.

Results of orientation analyses of fractures in foliated and non-foliated zones: how brittle structures are affected by foliation has been tested by correlating the change in orientation of brittle fractures and ductile foliation along KXTT4. As most fractures are steep, it is considered justified to ignore the angle of dip. Similarly, foliation is steep and has a constant NW trend throughout the TRUE-1 block. The slight variation of foliation along the borehole has little effect on the orientation of fractures. This may be explained by the fact that both foliation and fracturing are sub-parallel and do not change much throughout the borehole.

Table 2-9 shows the results for *all* TRUE-1 boreholes. A weak positive correlation is found between sections of ductile deformation, cataclastic deformation and alteration, which indicates that several generations of deformation have reactivated the same structures. The best correlation is achieved when looking at cataclastic deformation (fault gouge) and its coupling to sections of high ductile deformation. This coupling supports the theory of brittle reactivation of ductile precursors as proposed by MUNIER (1995).

Reliability of drillcore and BIP databases when deriving fracture frequencies and orientations: fracture frequencies and orientations are basic parameters for deriving a conceptual structural model for the TRUE-1 block. Both parameters have been evaluated from two independent databases, one from the drillcore database and the other from

the BIP imaging. The question now is which data are more reliable for frequencies and orientations and which are most suitable for the derivation of conceptual models.

Table 2-9. Summary of results of the orientation analysis of the critical geological parameters.

Parameter	Orientation	Character
Open fractures	Dominating NW trend.	Fairly regular clustering, trending steeply towards NW.
Tight fractures	NW-SE, N-S and NE-SW fracture sets. Dominating NW trend.	Wider spread in the fracture orientation compared to open fractures. Three identifiable sets.
Rocktypes	No preferred direction of rock contacts with FGG.	There is no difference between open and tight fracture orientation in different rock types.
Ductile deformation	Follows the NW trendof the fracturing.	Open fracture orientations do not differ from tight fractures. The proportion of open fractures is higher in sections with a high degree of ductile deformation.
Cataclastic deformation	Follows the NW trend of dominating fracturing.	Often reactivates sections of highly deformed ductile structures. Approx. 1/3 of the cataclastic sections have ductile precursors. Open fracture orientations do not differ from tight fractures. The proportion of open fractures is higher in sections with a high degree of cataclastic deformation. Fault gouge as a fracture infill in the cataclastic deformded sectionshas to be cleary postulated. (occasionally observed in drillcores, most probably removed during drilling process).
Alteration	Occur in NW-SE, N-S and in NE-SW directions. Dominating NW trend.	Approx. 1/3 of the highly altered sections have ductile precursors. Open fracture orientations do not differ from tight fractures. The proportion of open fractures is higher in highly altered sections.

The fracture frequencies of drillcores and BIP imaging are shown in Figure 2-3. Starting with the BIP structures (Figure 2-3b), their frequencies indicate a very low variation. Borehole KA3005A shows the lowest value of 3.8 fractures per metre. Boreholes KXTT1-4 have frequencies of about 4.8 fractures per metre. The low value of KA3005A can be explained by the sub-parallel orientation of KA3005A to the NW-SE, resulting in a too low and biased value for fracture frequency. The mean value has been calculated as 4.5 fractures per metre, taking into account the frequency bias of borehole KA3005A. The fracture frequencies of the drillcores show significantly higher values and vary between 8 and 10 fractures per metre (Figure 2-4a). This high frequency can mainly be explained by artificial, drilling-induced discontinuities which have been mapped as tectonic discontinuities on the cores. On the other hand, BIP fracture frequencies might be slightly underestimated due to the fact that tight fractures with apertures less than 0.5 mm might be invisible in the BIP images. Finally, BIP data are preferred for the derivation of conceptual models since they result in more realistic fracture frequencies.

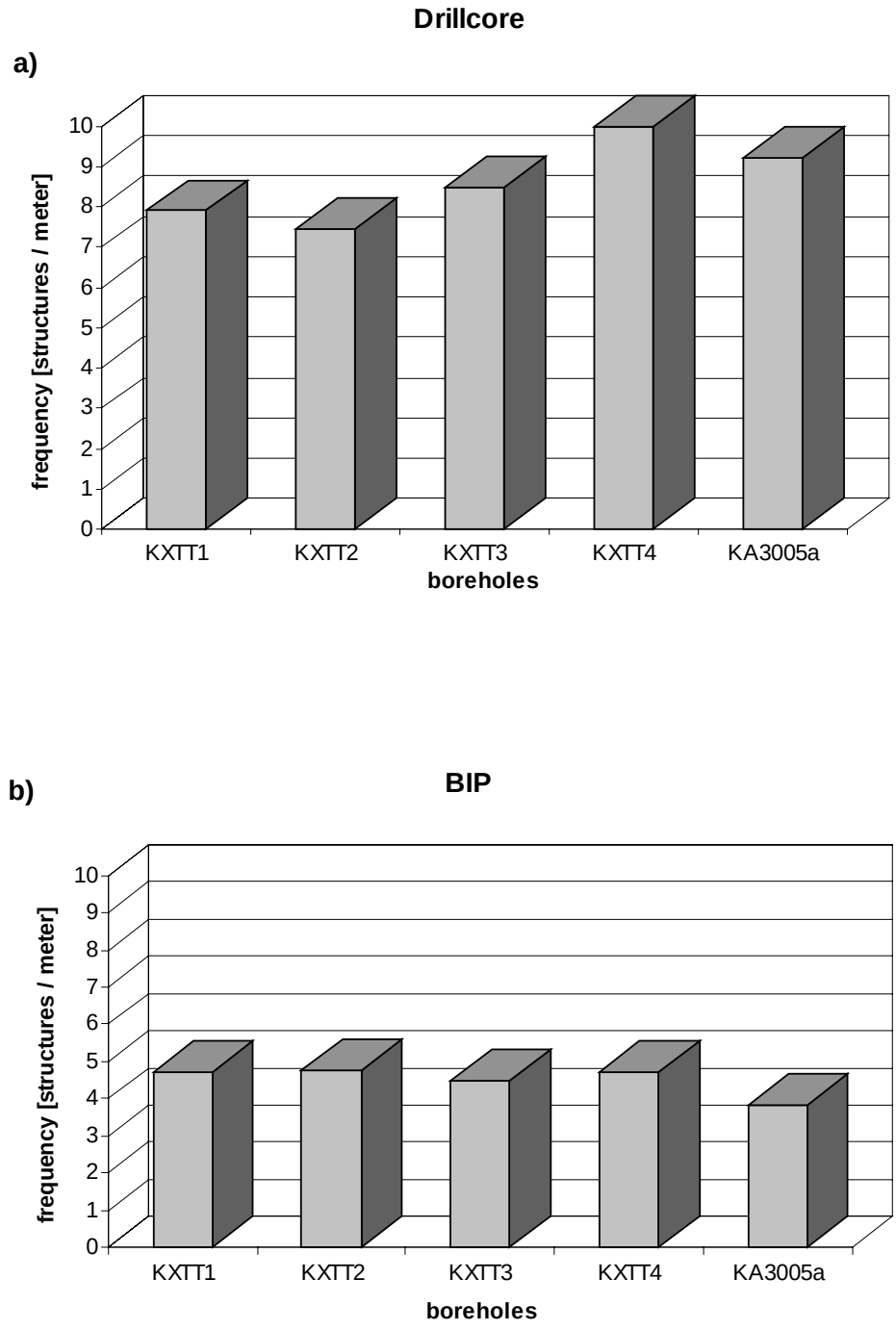

Figure 2-3. *Fracture frequencies in the TRUE-1 boreholes (a) derived from the drillcore database and b) derived from the BIP database.*

Another notable aspect of fracture frequencies is the scale effect. Figure 2-4 presents the mean fracture frequency derived using the BIP database (4.5 fractures per metre) and compares it to that derived by the line counting on the tunnel roof (2 fractures per metre parallel to tunnel and 3 fractures per metre normal to tunnel, for details see Appendix 3). This difference is mainly due to the different detail of mapping. The truncation level for fractures in the BIP database is less than one borehole diameter (< 5.6 cm), whereas the truncation level for the tunnel roof mapping has been set at 10 centimetres. This scale effect has to be taken into account when deriving conceptual structural models in the TRUE-1 block.

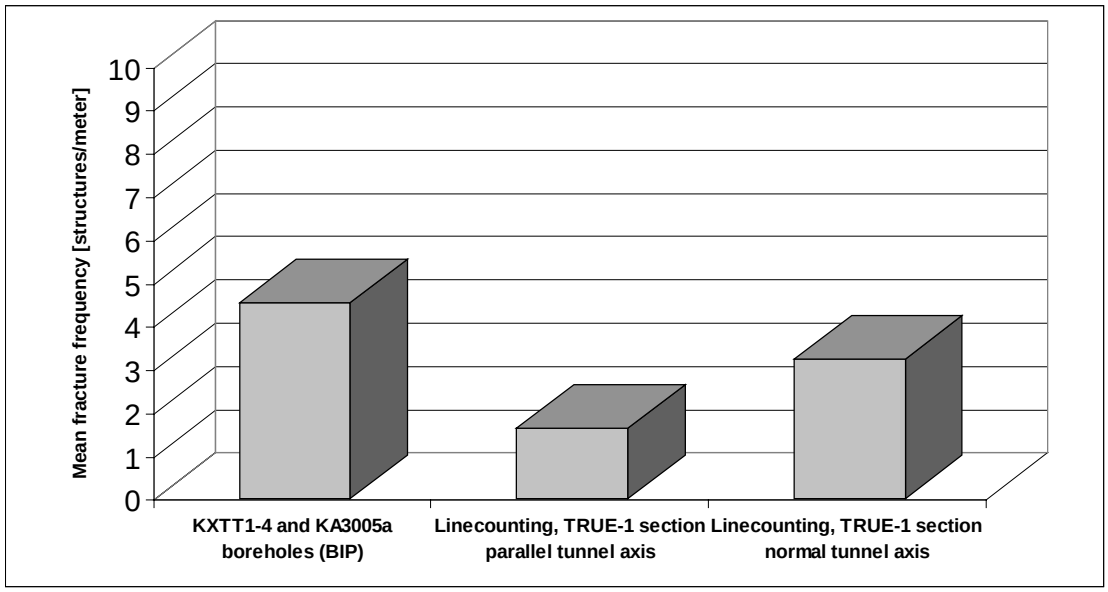

Figure 2-4. *Comparison of fracture frequencies derived from line countings and the BIP database.*

The fracture orientations of the drillcore and the BIP databases are shown in Figure 2-5, where the poles of the fractures are plotted in the lower hemisphere of an equal area stereonet. The BIP data (Figure 2-5b) contain only 552 fractures, compared to 1589 fractures recorded in the drillcores (Figure 2-5a). The fracture scattering is clearly smaller in the BIP plot. The stereogram with the drillcore fractures (Figure 2-5a) shows a very wide scatter of fracture orientations, with a maximum of poles representing NW-SE trending, steeply inclined fractures. Finally, BIP imaging results in fracture orientations that seem to be more suitable for the derivation of the conceptual models.

BIP orientations of open and closed fractures are shown for every borehole in Figure 2-6. Based on these plots, the following three fracture sets are estimated for the TRUE-1 block: steeply dipping NW-SE fractures (**first fracture set**, about 85% of whole set). A set of poles dispersed on a great circle NW-SE with a maximum at 340/30 (about 15% of whole set). These 15% can be split into a **second fracture set** (10% of whole set) characterised by steeply dipping NE-SW trending fractures and a **third fracture set**

(5% of the whole group) with sub-horizontal fractures. The three fracture sets are also presented in Figure 2-11.

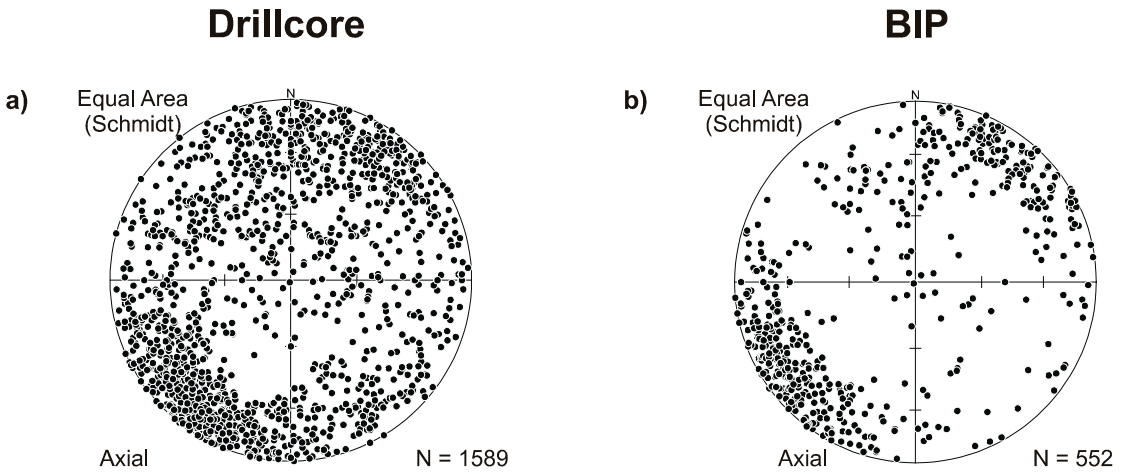

Figure 2-5. *Poles to fracture planes shown on equal area lower hemisphere plots. All data (open and closed fractures), a) fractures from the drillcore database and b) fractures from the BIP database.*

2.3.3 Comparison of tunnel maps and line countings at the TRUE-1 site with SKB standard tunnel mapping data

When excavating the tunnel system at Äspö, a team of geologists mapped the whole area with respect to rock types, fracture orientations, trace lengths etc. The collected data can be accessed through SICADA, the SKB **SI**te **C**h**A**racterisation **DA**tabase. Fractures mapped on the tunnel walls are stored both as numerical data and maps of the individual traces. The mapping was performed simultaneously with the excavation of the tunnel, which placed constraints on how long the geologists could spend mapping each section. Only traces longer than 1 m were measured in order to minimise the mapping time.

Traces of individual fractures were measured over the whole tunnel perimeter as shown in Figure 2-7a. Figure 2-7b shows the northern wall of the tunnel, i.e. comparable to the detailed tunnel wall map given in Figure 2-8, which gives an overview of the small-scale mapping along the tunnel wall of the TRUE-1 block. The detailed maps related to Figure 2-8 are shown in Appendix 4.

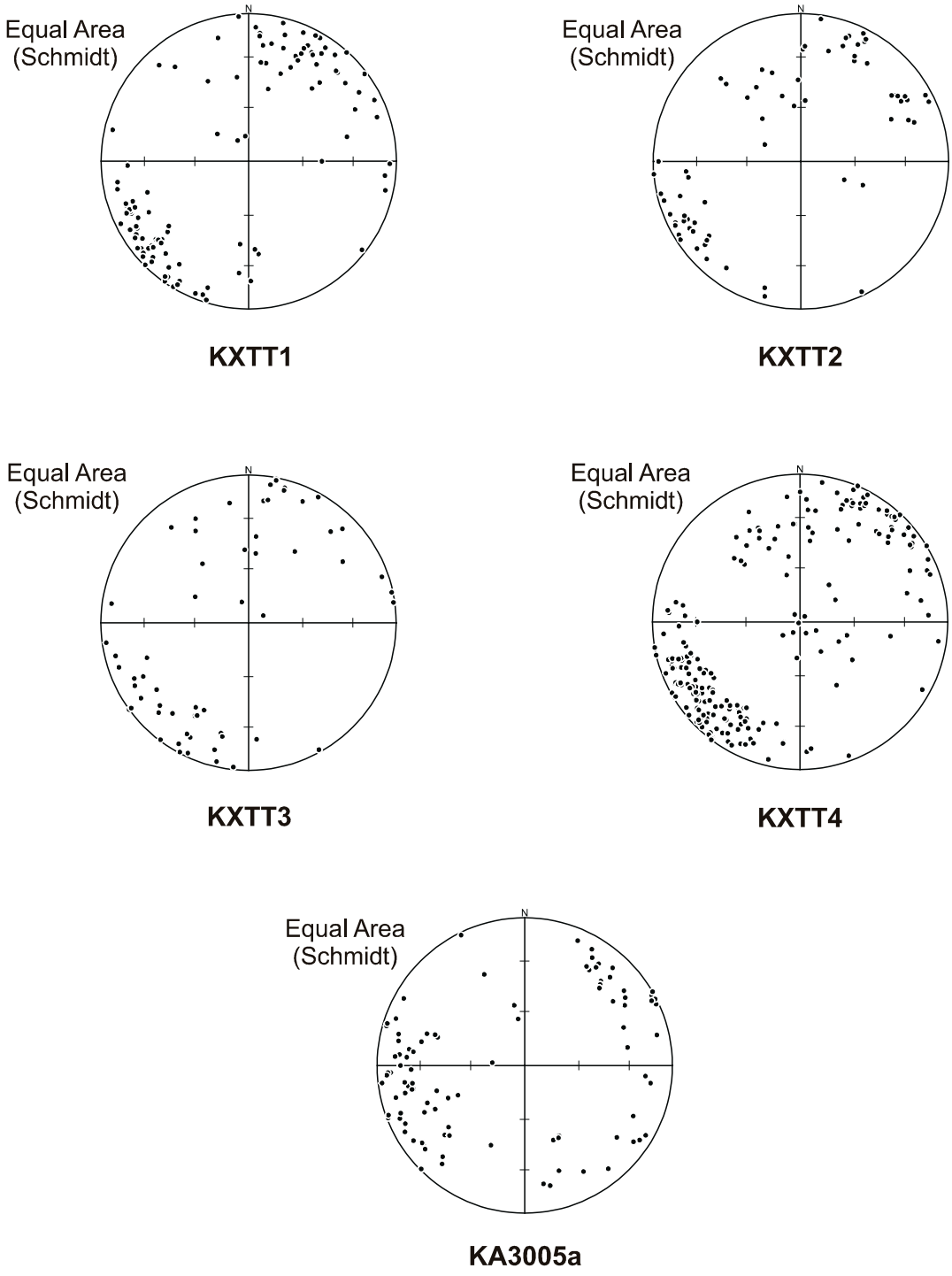

Figure 2-6. *Poles to fracture planes shown on equal area lower hemisphere plots, open and closed fractures derived from the BIP database a) borehole KXTT1, b) borehole KXTT2, c) borehole KXTT3, d) borehole KXTT4 and e) borehole KA3005A (for Situation see Figure 2-1).*

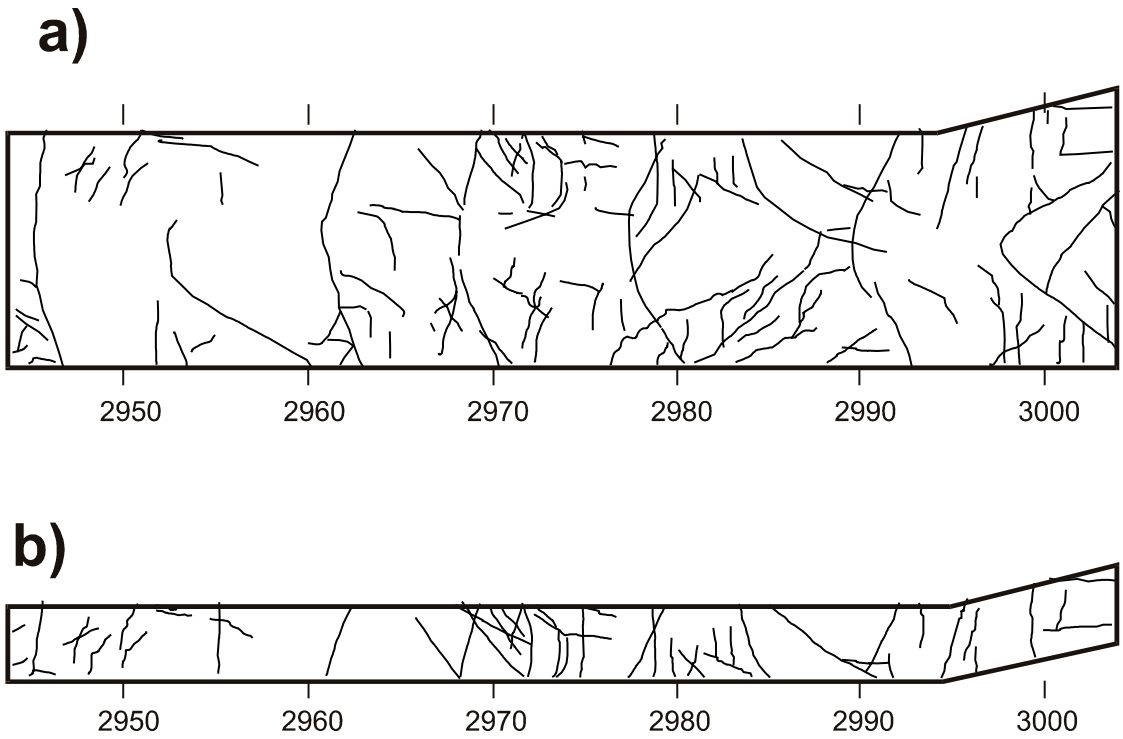

Figure 2-7. *Trace maps of the tunnel section 2944 –3044 m. a) shows the whole tunnel map while b) shows only the northern tunnel wall, which is comparable to the map produced by Mazurek et al. (1996).*

The total fracture trace length derived from Figure 2-8 is about twice that based on Figure 2-7b (see also Table 2-10). This is mainly due to the different degrees of detail underlying the two maps (truncation levels for fractures: ca. 0.3 - 0.5 m for Figure 2-8,

Table 2-10. Summary of the standard mappings of the Äspö tunnel section close to the TRUE-1 block and the detailed tunnel wall map.

	Whole tunnel (both walls and roof)	**Northern tunnel wall (equivalent to MAZUREK et al. 1996)**	**Detailed tunnel wall map**
Section	2944 – 3004 m	2944 - 3004 m	2944 – 3004 m
Number of fracture traces	104	48	229
Total trace length (m)	429.3	149.5	304.8
Mean trace length (m)	3.98	3.12	1.33
Standard deviation	0.72	1.60	1.21
Tunnel surface area (m^2)	779	Approx. 240	Approx 240
Fracture intensity , P_{21}, (m^{-1})	0.55	0.62	1.27

1 m for Figure 2-7). Fractures mapped as single features during standard mapping have occasionally been mapped as several separate traces during the detailed mapping.

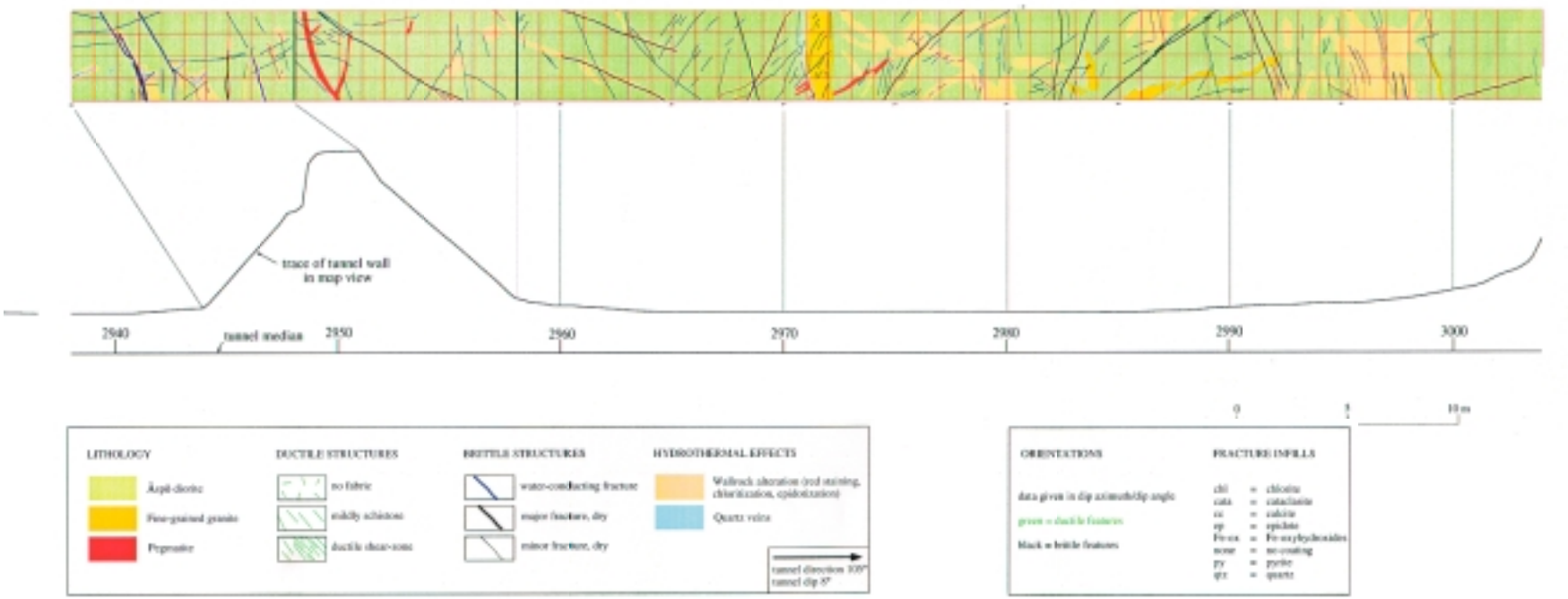

Figure 2-8. *Overview of the TRUE-1 tunnel wall fracture trace map. The detailed small-scale maps can be found in Appendix 4.*

Fracture orientations exist in the standard mapping data (SICADA) and partly also in the detailed mapping.

A qualitative comparison between the two mapping campaigns shows the degree of detail. Fractures interpreted as one single trace in SICADA actually consist of several smaller traces. It is not always clear whether each individual trace is a separate fracture or if they can be treated as one fracture plane with an uneven trend.

2.4 Deterministic Conceptual Structural Model of the TRUE-1 site

A number of boreholes penetrate the TRUE-1 volume and provide deterministic information on the spatial distribution of rock types and fracture patterns. However, other parts of the volume have not been accessed by boreholes and deterministic information is thus lacking. These regions are represented by stochastic methods as described in Chapter 2.5.

2.4.1 Methodology

The methodology for deriving the deterministic part of the conceptual structural model is shown in Figure 2.9.

The basic idea behind this methodology is to first compile the whole structural database from the TRUE-1 block, then to select appropriate data, exclude inappropriate data and finally to integrate, synthesise and, if necessary, to abstract the remaining information. Database management in spreadsheet format and fracture visualisation programmes (Autocad) are the two basic tools which have been used. The methodology for deriving the conceptual structural model can be divided into three steps: 1) selection and updating of the database, 2) analysis and visualisation of the data and 3) derivation of the conceptual structural model. These three steps are now explained in more detail.

1) Selection and updating of the database: from the fracture-foliation spreadsheet of the drillcore database (Table 2-4), the exact position along the borehole (depth), the azimuth of dip and the dip values for every structure were selected. The mineralogical information (from *EP* to *PY* in Table 2-4) has not been taken into account due to the fact that no cross-correlation between fracture orientation and mineralogy exists (MUNIER 1993).

The column *"Open/Tight"* is very important for the interpretation of the model and was therefore also selected. Structures without an entry in the T/O column have been counted as open structures. From the column "Remarks", the number of fractures was used (numbers >1 were treated as fracture zones). In addition, information about fault gouge infills and ductile deformation (mylonites) was selected from this column.

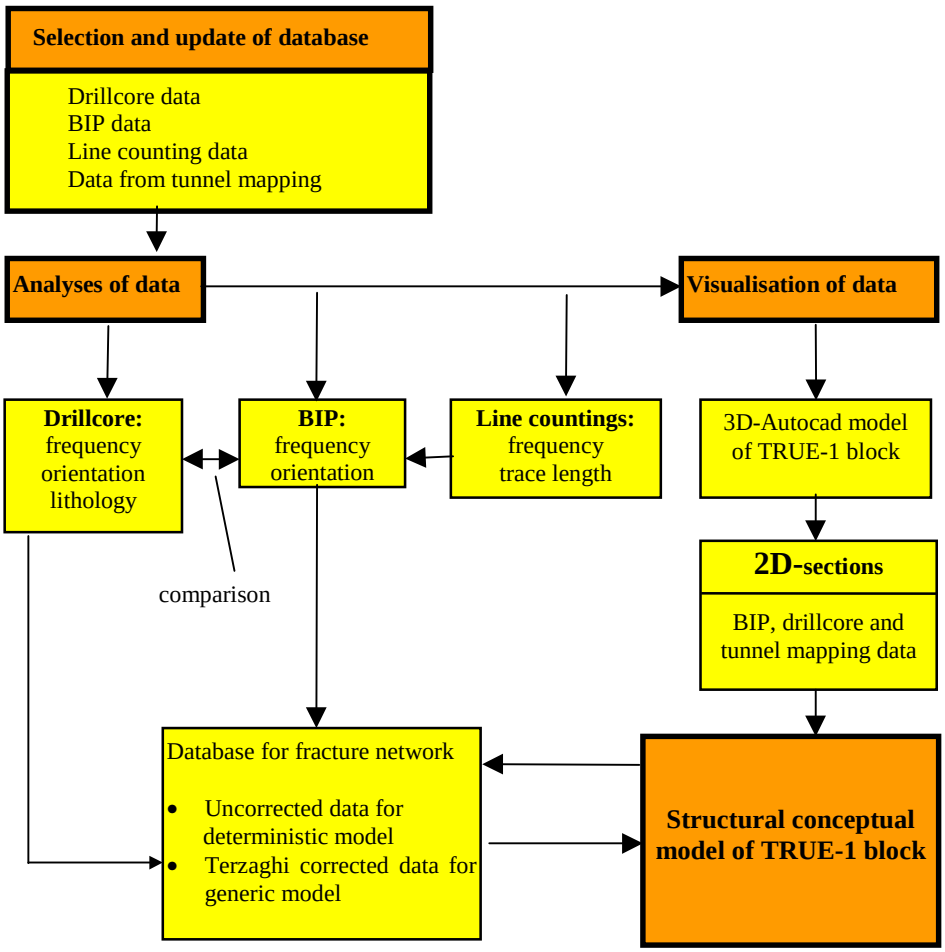

Figure 2-9. *Flow chart illustrating the methodology for deriving the structural conceptual model.*

Information from the fracture-foliation spreadsheet was then combined with the deformation-alteration-rock spreadsheet of the core logging database (Table 2-5). The latter contains information that refers to finite sections of the core, whereas the fracture-foliation database refers to specific points in the core.

With all this information, a new database was generated which allowed the data to be imported directly into the Autocad visualisation programme. In this database the following types of structures are distinguished:

- mylonites (single structures or zones with mylonitic deformation).
- open fractures.
- open fractures with fault gouge (only a few structures are confirmed by the database).
- tight fractures
- zones[*)] of open fractures
- zones of tight fractures
- zones of open fractures with fault gouge (only a few structures are confirmed by the database).

As outlined above, the BIP data define the fracture patterns better than the drillcore data (artificial discontinuities in drillcores). Drillcore data are more reliable when lithologies, ductile deformation or the classification of fractures are addressed. This leads to a combined selection of BIP and drillcore data (the fractures were first located in the BIP database and then combined with the drillcore database; the common attribute of both databases was the borehole depth).

The line countings performed on the tunnel roof close to the TRUE-1 block (see Appendix 3) were used to derive the trace lengths.

2) Analysis and visualisation of the data: The modified database of step 1 is now used to analyse and visualise the fracture pattern. The fracture frequency derived from core mapping is much higher than that in the BIP data. The core data are affected by artefacts (single and double core-barrel drilling frequently generates artificial fractures) and the BIP data are thus considered to represent fracture frequencies and orientations more accurately. On the other hand, drillcore data are more reliable when the lithologies and the classification of fractures (e.g. mylonites, open fractures, fractures filled with fault gouge) are addressed and the two methods were therefore combined for the analysis of the borehole-derived data. Line countings were very useful for deriving the trace lengths, especially lines acquired on the tunnel roof. The synthesis of drillcore, BIP and line counting data is quite important and leads to the conclusion that ductile precursors (e.g. mylonites) influence the orientation of the fractures and that the fracture network is better interconnected in these areas than elsewhere. A special projection technique was then applied to visualise the lithologies and fractures along the boreholes. This technique is explained in more detail in Chapter 2.4.3.

3) Derivation of the conceptual structural model: The data selection of steps 1 and 2 results in a fracture network database (including mainly frequencies, trace lengths and orientations). The analysis of fracture orientations shows that 3 sets of fractures can be distinguished (see Chapter 2.3.2 and Figure 2-11c). All these data are compiled in the

---

[*)] A fracture zone is defined as a location in a borehole of increased fracture frequency (e.g. >10 fractures per metre). When fracture zones are then correlated between different boreholes, the resulting structure can be defined as a fracture cluster.

form of “non Terzaghi corrected” data (contained in the raw database) and “Terzaghi corrected” data. The Terzaghi correction accounts for the lower probability of fractures running sub-parallel to the boreholes being intersected compared with fractures that are perpendicular to the borehole. The non Terzaghi corrected data can now be used for the derivation of a deterministic model. The corrected data are useful for the derivation of generic models (see Chapter 2.8.2).

2.4.2 The fracture network

Fracture frequencies

As discussed in Chapter 2.3.2, the BIP data are thought to best represent in-situ conditions with regard to fracture frequencies, and an average value of 4.5 fractures per metre is chosen as being representative for the TRUE-1 block (see Figures 2-4b and 2-11a).

There is a clear anisotropy of fracture frequencies when fracture counting is performed in different directions. Fracture frequencies along the KXTT boreholes (NE-SW oriented) are higher than those along the KA3005A borehole (NW-SE oriented). The frequency along vertical lines can be derived from fracture maps of the tunnel walls and is <1 fracture per metre. This anisotropy is consistent with the dominance of steeply dipping, NW-SE oriented structures.

No clear distinction between fracture frequencies and different rock types such as Fine-grained Granite, Äspö Diorite and Småland Granite has been found. Fine-grained Granite is subordinate in the TRUE-1 block and seems to form isolated patches. Äspö Diorite and Småland Granite behave rheologically in a similar way. However, an increased fracture frequency occurs in zones with ductile precursors. This relationship is shown in Figure 2-10, where fracture frequencies from the drillcore database are related to zones of ductile precursors. These ductile precursors are divided into zones affected by different degrees of ductile deformation. The highest ductile deformations result in mylonites (see also Chapter 2.3.1). The mylonites also have the highest fracture frequencies, followed by the zones affected by moderate and lower ductile deformation. It is concluded that the interconnectedness of the fracture network is more developed in zones of ductile precursors than in areas without ductile precursors (see also Chapter 2.3.2).

Orientations

The BIP orientation data are taken as the basis for deriving the deterministic conceptual model. The total dataset was split into 3 sets, as shown in Figure 2-11c. Set 1, which contains 85% of all fractures, is defined by steeply NW-SE trending fractures. Set 2 (10% of all fractures) is defined by steeply and moderately ENE-WSW trending fractures. Set 3 (5% of all fractures) is defined by sub-horizontal fractures.

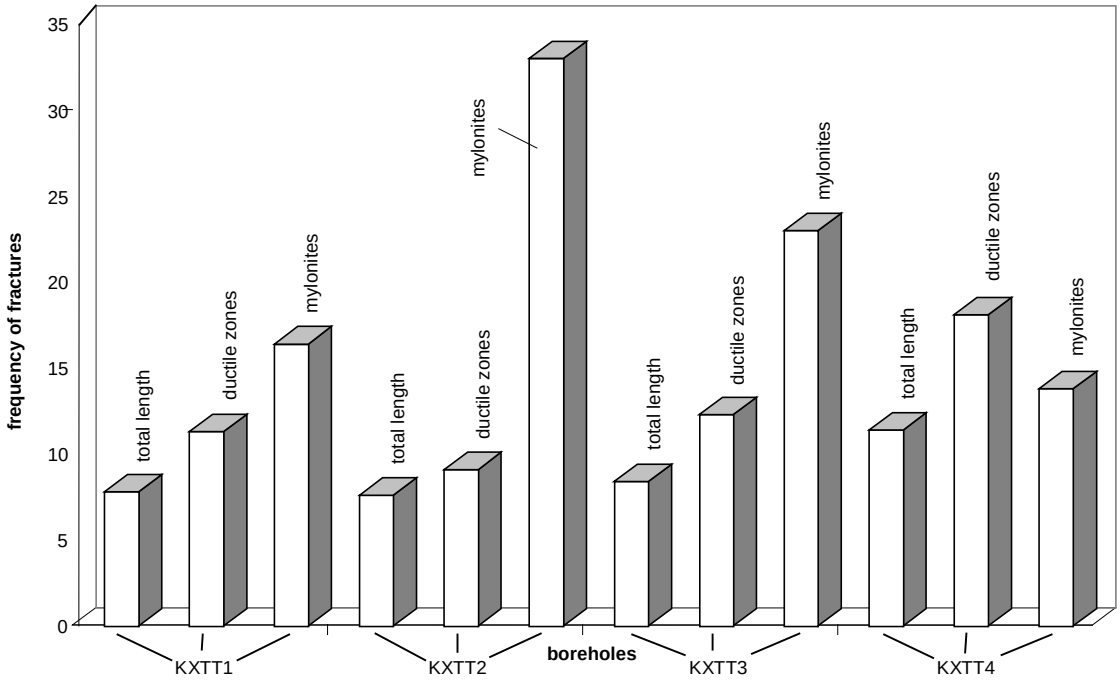

Figure 2-10. *Fracture frequencies in different lithologies.*

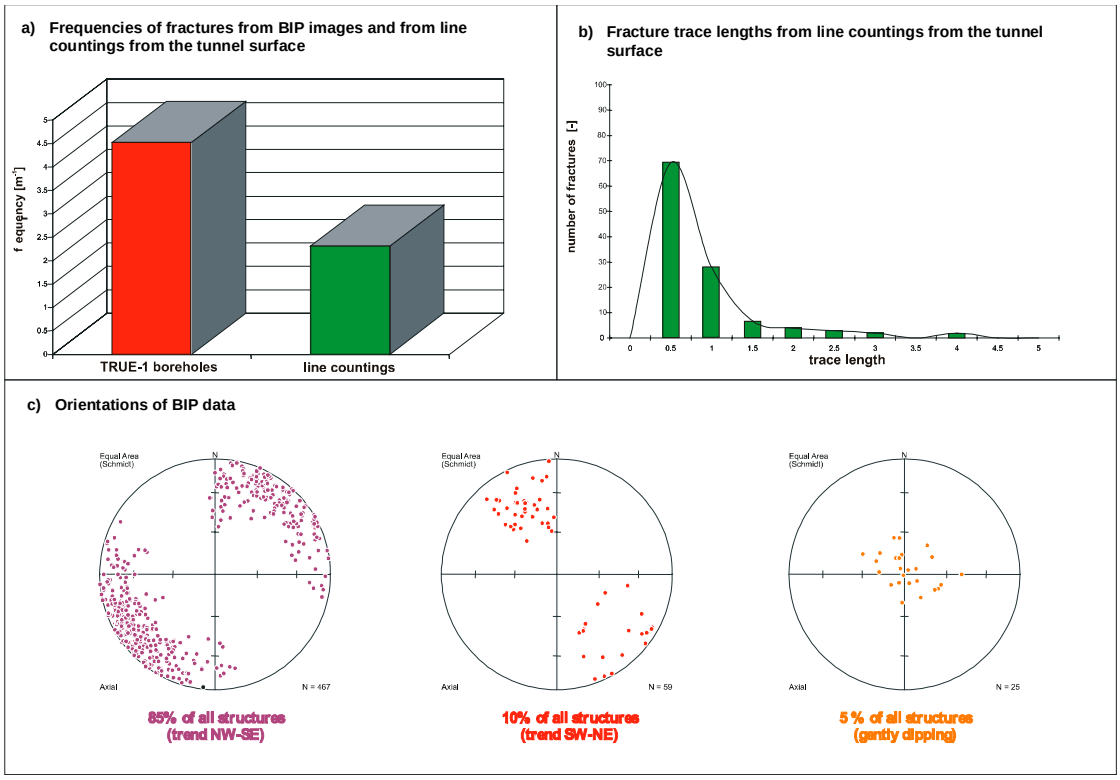

Figure 2-11. *Compilation of frequencies, trace lengths and orientations.*

Fracture trace lengths

All data are based on line countings on the tunnel roof at the SW boundary of the TRUE-1 block. The line counting database is explained in Chapter 2.2.5 and documented in Appendix 3. Figure 2-11b shows the resulting fracture trace length distribution. In this figure, fractures between 0.5 and 4 m are considered. Fractures longer than 4 m were not observed (truncation effect, size of the observation window). The majority of the fractures have trace lengths between 0.2 m and 1 m. For further analyses, a log-normal distribution of the field data is used. However, it cannot be clearly demonstrated that the distribution is really log-normal, and a negative exponential distribution may also be possible (see Chapter 2.5.3).

The quantitative dominance of rather small fractures is an important finding for the TRUE-1 block. It can be concluded that there are only very few fractures with trace lengths larger than the tunnel diameter and that faults or fault zones as defined in MAZUREK et al. (1996) are not present.

2.4.3 Visualisation of core logging and BIP data

Figure 2-12 shows the procedures that underlie the visualisation. A borehole, shown in red, is projected onto the chosen projection plane (yellow). A fracture plane intersected by the borehole is shown in red. The representation of this fracture in the projection plane is its intersection trace (black line) with the projection plane (i.e. the fracture plane is extrapolated along the strike and its representation is NOT just a projection of the intersection point with the borehole). The consequence of this procedure is that structures that are sub-parallel to the borehole may have positions on the projection plane far away from the projected borehole trace. Moreover, the relative positions of fractures on the projection plane may be different from those observed in the borehole.

With increasing distance of the projection plane to the borehole, the distance for the extrapolation of the structural elements increases. Due to the limited size of the fractures and to uncertainties inherent in linear extrapolation, only fractures with extrapolation distances less than 5 m have been represented in the projection planes.

Three types of projection planes have been used:

- A horizontal plane at -400 m a.s.l. This map view just about intersects with the mouths of the KXTT boreholes (see also Table 2-1).

- A plane with dip azimuth of 60° and angle of dip of 40°. This plane runs sub-parallel to the four KXTT boreholes and lies within the array of these boreholes: KXTT1 and KXTT2 lie beneath, and KXTT3 and KXTT4 above, this plane.

- The third type of plane has variable orientations and runs along the boreholes. In these planes, no extrapolations are needed for the representation of fractures.

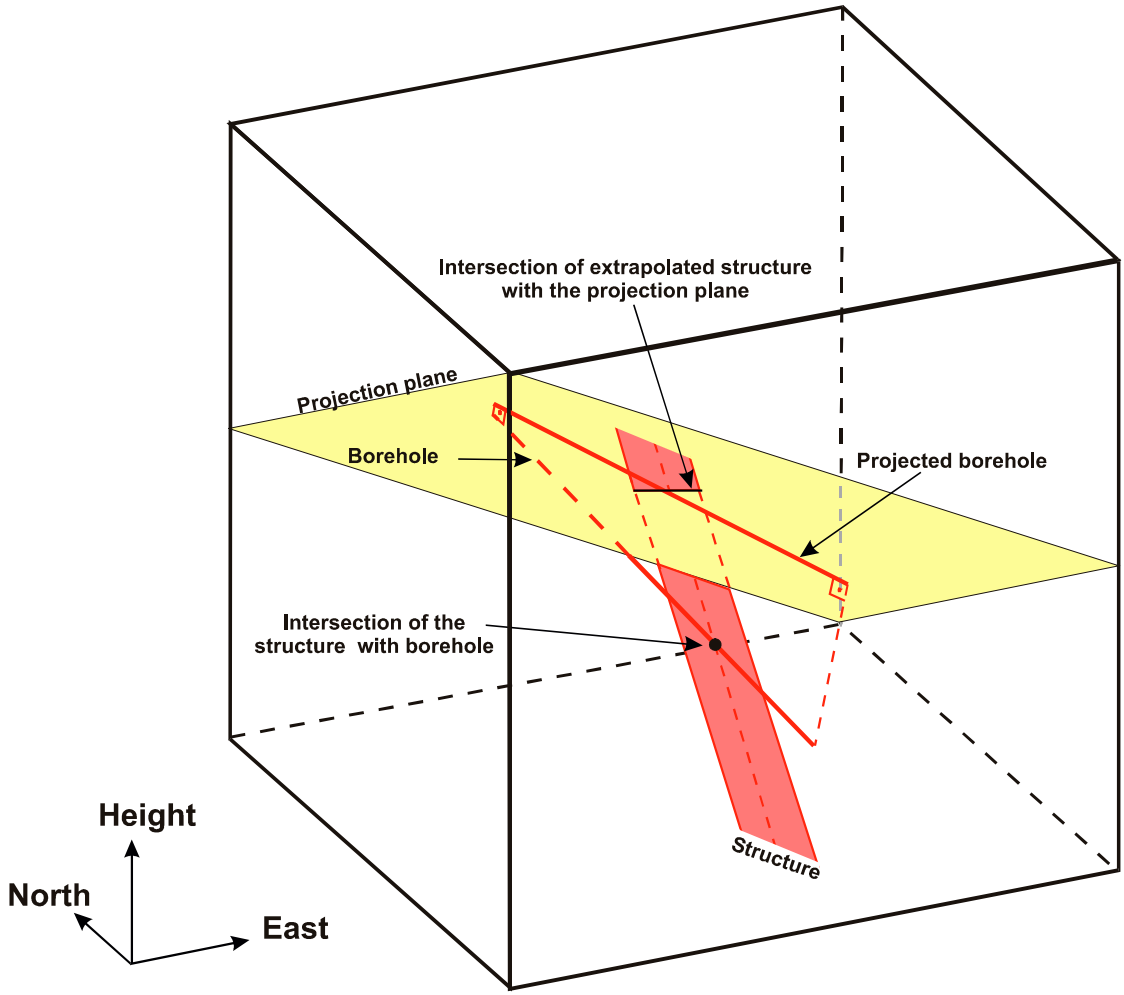

Figure 2-12. *Transparent cube showing how boreholes and structures are projected and extrapolated to the 2D planes.*

Two examples of plots are presented in Figures 2-13 (fractures and lithologies along the boreholes based on the **drillcore database** in the 060/40 plane) and Figure 2-14 (fractures and mylonites based on the **BIP database**, same plane). The drillcore plot of Figure 2-13 shows a much higher fracture frequency than the BIP plot of Figure 2-15 due to the fact that artificial discontinuities are included in the drillcore database, but excluded in the BIP database. On the other hand, the mylonites are fully included in the drillcore plot of Figure 2-13, but only partially included in the BIP plots. Thus, both types of plots are needed for deriving the conceptual structural model.

All other plots are shown in Appendices 5.1 to 5.19. These appendices are now briefly explained:

– Appendices 5.1 to 5.10 (drillcore structures): In the horizontal and 060/40 projection planes, the number of fractures is very high and therefore the information is very dense. However, the clustering of fractures around the mylonites can be seen very clearly (e.g. end of KXTT3 and intersection of KXTT4 with KA3005A). In addition to this increased fracture frequency in mylonites, fracture clustering has also been observed outside the mylonites (e.g. end of KXTT1). It is obvious that,

in borehole KA3005A, NE-SW trending structures (fractures and mylonites) are more prominent than in the KXTT boreholes. This effect can be related to the orientation of the borehole. The mylonites in Appendix 5.4 generally show a clear NW-SE trend.

– Appendices 5.11 to 5.19 (BIP structures): Due to the fact that only 3 mylonites exist in this dataset, mainly open fractures were plotted. The orientation of most of the fractures indicates a dominant NW-SE trending system, with clustering of the fractures at different depths of the boreholes. The derivation of the conceptual structural model below is mainly based on these BIP structures. Of special interest is Appendix 5.17, where only every fifth open fracture is plotted. Such plots with a systematic reduction of fractures along the borehole are of great help when fracture zones have to be correlated among boreholes (e.g. it becomes difficult to make a correlation in Figure 2-14, where all open BIP fractures are plotted and the resulting fracture pattern is too dense for a correlation).

2.4.4 Prerequisites for the deterministic structural model

The logic behind the derivation procedure for the deterministic model is presented in Figure 2-15. The basis is the selection of three structural subsets from the database.

Selection 1: in Appendix 5.17, every fifth open fracture[*)] from every borehole is plotted on the basis of the BIP database. The selection was made to achieve a better readability of the graphical fracture patterns.

– Orientation: In the chosen 060/40 projection plane, only the two main orientation sets are shown, i.e. the dominant NW-SE set and the subordinate NE-SW set (the third set containing flat fractures has been excluded, because projected flat fractures would mostly lie outwith the extrapolation distances of 5 m around the borehole and thus bias possible correlations). In the NW-SE set, a slight rotation of the fractures from a more NNW-SSE orientation in borehole KXTT2 to WNW-ESE in borehole KXTT3 can be observed.

– Frequency: The selected fractures represent quite clearly the zones of high fracture frequency and are thus representative for the complete dataset presented in Figure 2-14 (e.g. between 18 and 24 m in KXTT1, at the end of KXTT3 and around 12 m in KXTT2 and 13 m in KXTT4).

*) Different starting points in the database were used. The different realisations are very similar. Thus, different starting points seem not to affect the resulting structural pattern.

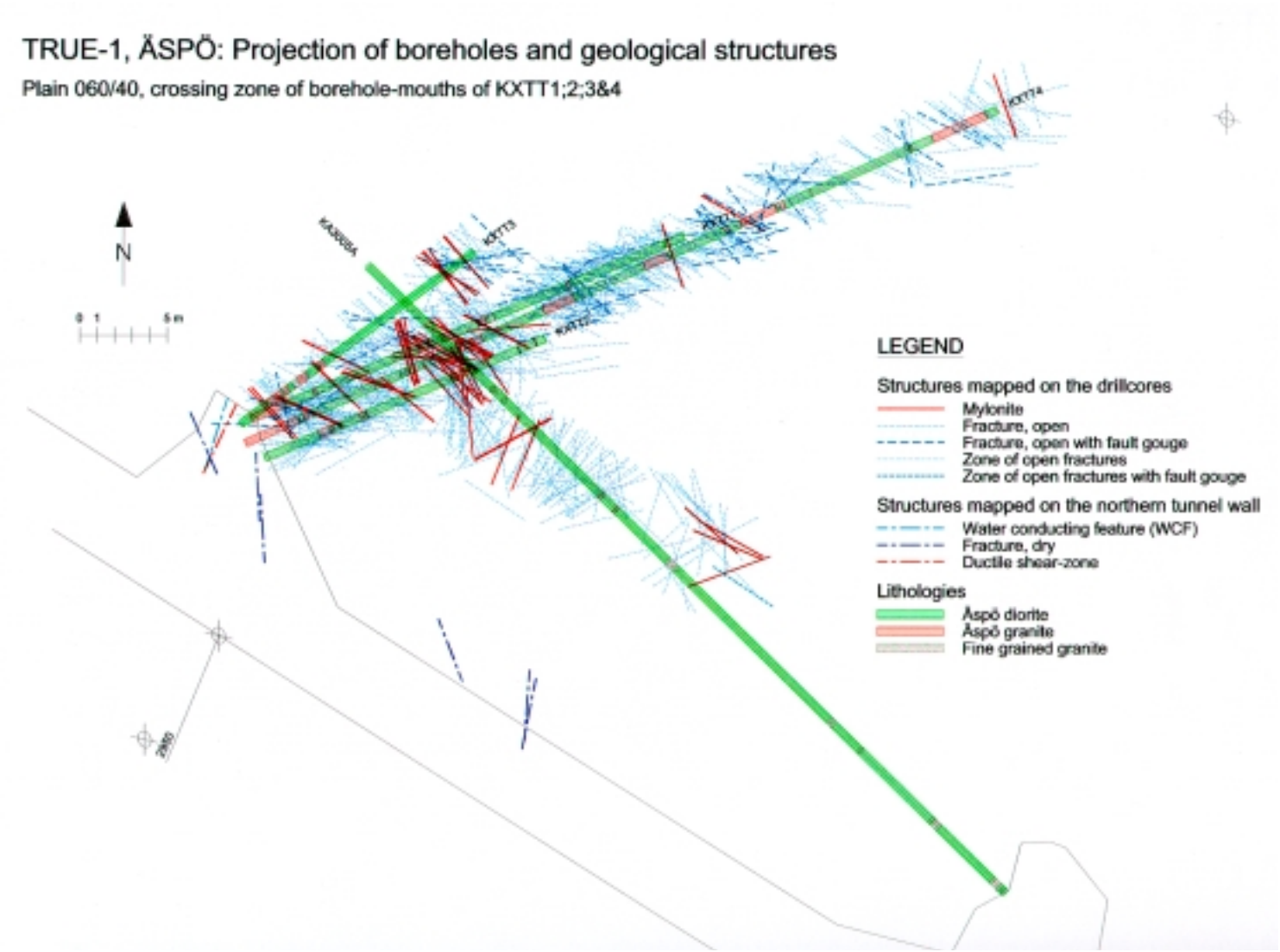

Figure 2-13. *Visualisation of fractures from the drillcore database: 060/40 plane: all open structures, mylonites and lithologies.*

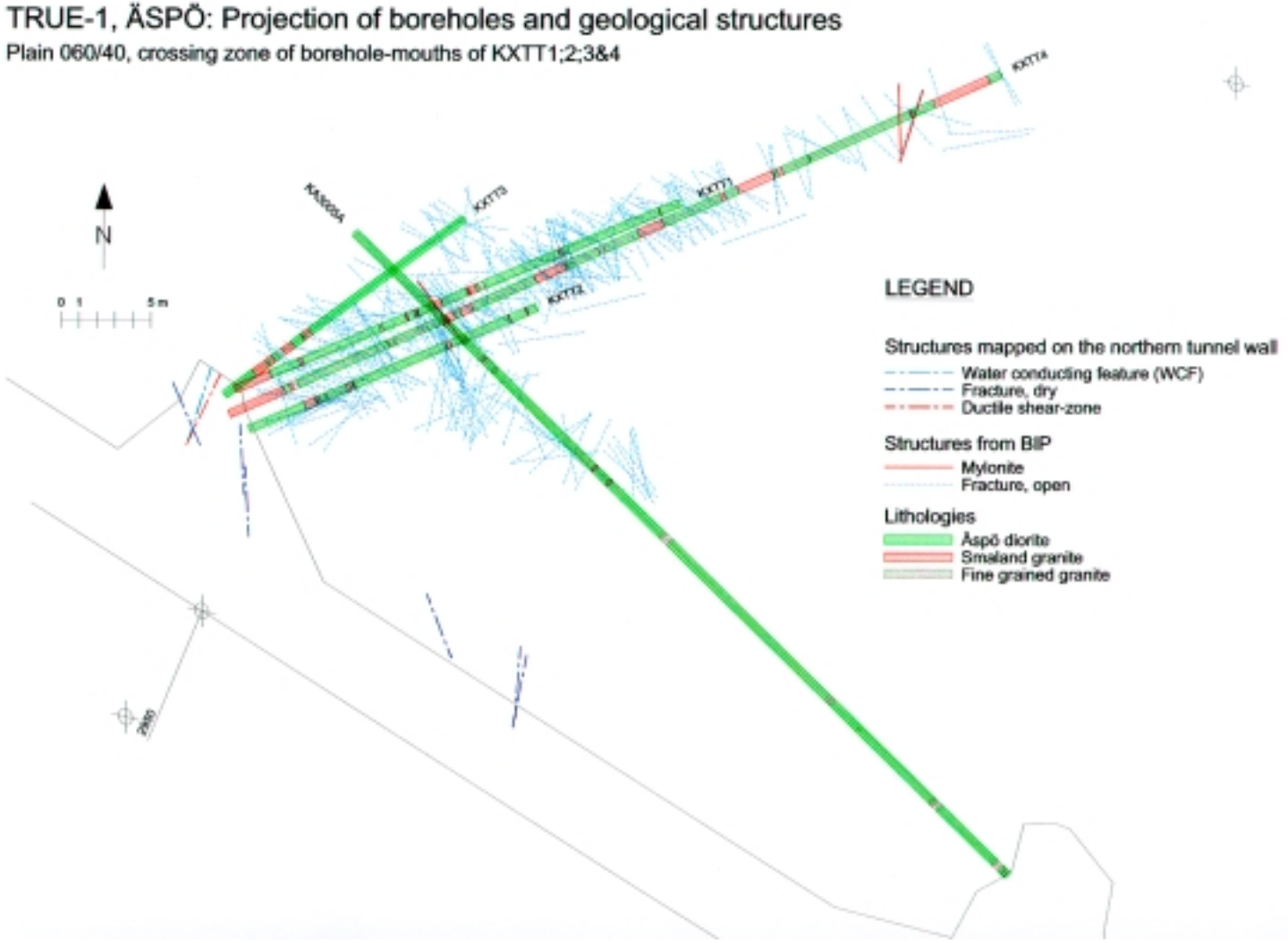

Figure 2-14. *Visualisation of fractures from the BIP database: 060/40 plane: all open structures and mylonites.*

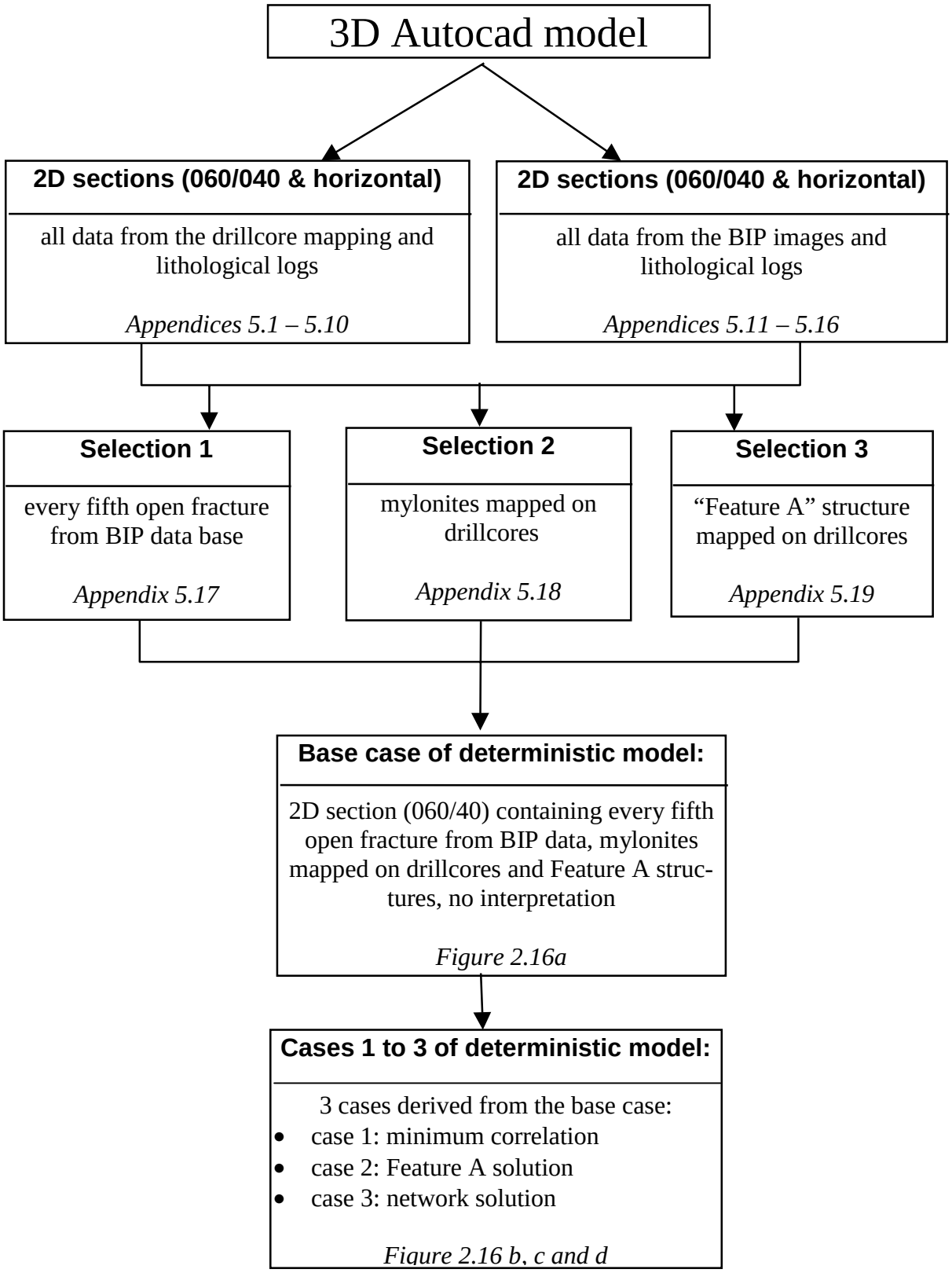

Figure 2-15. *Flow chart illustrating the logic behind the deterministic structural model.*

Selection 2: Appendix 5.18 shows mylonites from the core logging database.

- Orientation: The same orientation sets as in selection 1 are also present in the mylonites, but with a much higher dominance of the NW-SE directions over NE-SW trends (only very few NE-SW oriented mylonites occur along KA3005A). Again, a slight curvature of the mylonites from a NW towards a WNW direction is visible.

- There is a concentration of mylonites at the intersection of KA3005A with the KXTT boreholes. Every borehole except KXTT3 shows several mylonites in this area. KXTT3 contains some mylonites at the borehole end, where a very high fracture frequency is also observed.

Selection 3: Appendix 5.19 shows the mylonites in the so-called "Feature A[*)]" structure.

- Orientation: "Feature A" in KXTT1, KXTT3 and KXTT4 trends in a NW-SE direction, whereas NNW-SSE trends are seen in KXTT2 and KA3005A. Overall, "Feature A" follows the general curvature already described in selections 1 and 2. Thus, the "Feature A" structure cannot be described as a simple planar fracture structure over a distance of about 10 metres.

2.4.5 The deterministic model

For the deterministic model, the three selections of Appendices 5.17, 5.18 and 5.19 were synthesised to form the base case of the deterministic model, as shown in Figure 2-17a. From this base case, a total of three further model cases were elaborated. These three model cases are shown in Figures 2-16b (case 1), 2-17a (case 2) and 2-17b (case 3). In deriving cases 1-3, the strategy was NOT to interpolate and connect individual fractures among boreholes but to add new, separate but interconnected fractures that build up a *fracture array*. This procedure is justified because trace lengths of individual fractures are mostly shorter than 1 m (see Figure 2-11b). Borehole spacings (KXTT1-4, KA3005A) are clearly larger than 1 m. Thus, the majority of single fracture planes cannot intersect 2 or more boreholes.

[*)] Feature A is the target structure of the TRUE-1 project. WINBERG (1996) defines Feature A as a planar fracture structure (azimuth of dip: 61^{o}, dip angle: 79^{o}) of an extent of about 10 m, crossing the KXTT1-4 and KA3005 boreholes (KXTT1 at 15.72 m, KXTT2 at 15.04 m and KXTT3 at 14.10 m, KXTT4 at 12.10 m and KA3005A at 44.97 m). In Feature A, numerous hydraulic and tracer tests were carried out.

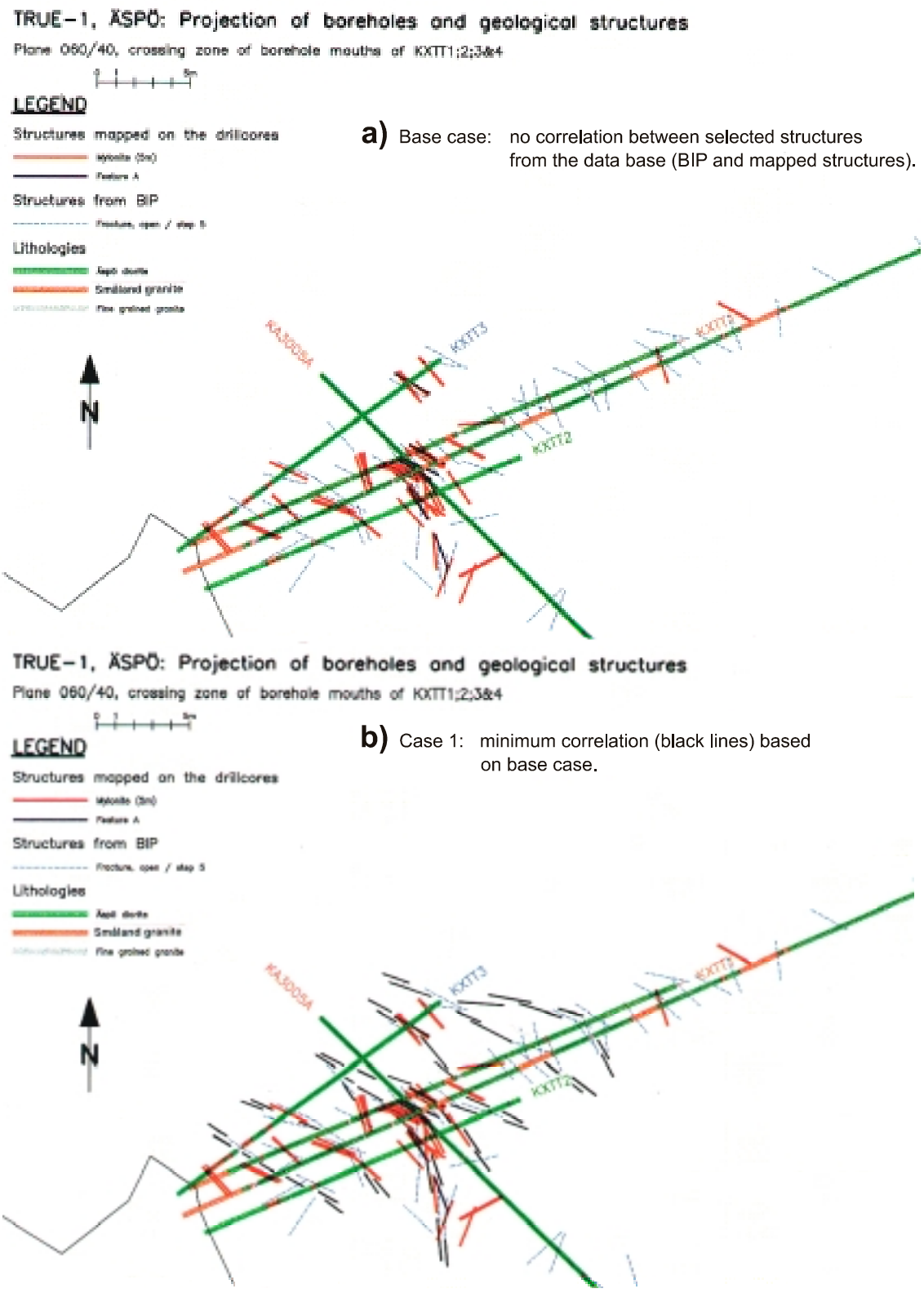

Figure 2-16. *The deterministic structural model in the 060/40 plane.*
a) base case, and b) case 2, minimum correlation..

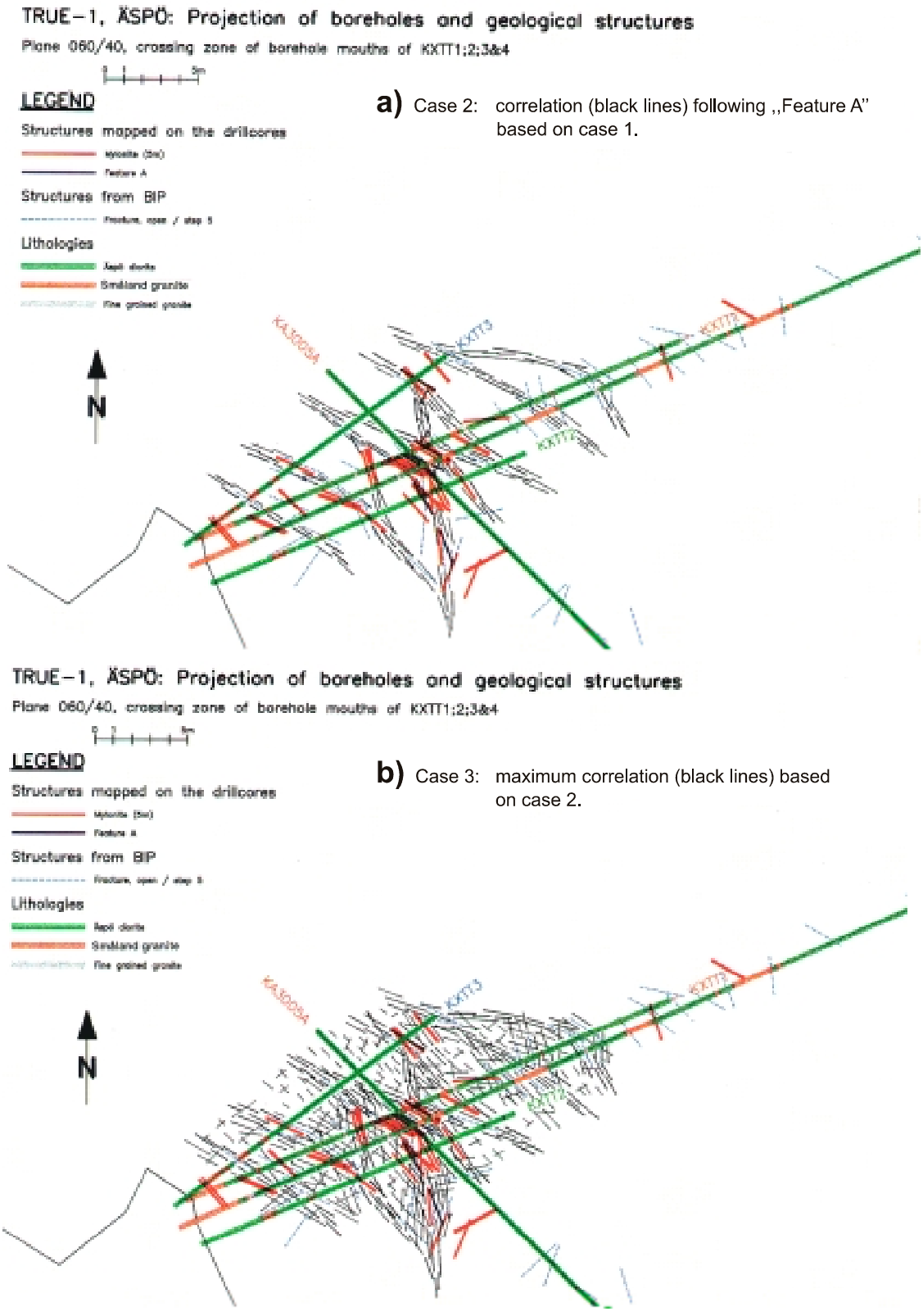

Figure 2-17. *The deterministic structural mode, in the 060/40 plane a) case 2, „Feature A" solution, and b) case 3, network solution .*

- **Base case** (Figure 2-16a): The base case is derived directly from the Autocad model, without any additions. Every fifth open fracture from the BIP data, the mylonites from the drillcore data and the selected structures of "Feature A" have been plotted. This combination of structures clearly demonstrates that "Feature A" correlates with areas of increased mylonite and ductile shear zone densities. The fact that fracture frequency is increased in mylonitic shear zones (see Figure 2-10) is further corroborated. However, there are also highly fractured zones outside mylonites (e.g. KXTT1, 18-24 m). The orientations of all structural elements (ductile shear zones, mylonites, fractures) are very similar: steeply inclined structures with a main NW-SE striking trend.

- **Case 1** (Figure 2-16b**:** minimum correlation): This case can simply be described as the base case of Figure 2-16a plus the connection of obviously related deterministic structures from neighbouring boreholes. Case 1 takes into account that zones containing mylonites show higher fracture frequencies (see Figure 2-10), and that these zones are slightly curved. Such zones of mylonitic shear zones, with increased fracture frequencies, intersect borehole KXTT4 at 8, 11 and 12 m. Zones with a high fracture frequency (KXTT4 between 20 and 28 m: around 11 fractures per metre) can easily be correlated through the whole investigated area. It must be emphasised that the minimal fracture network is mainly related to the existence of ductile shear zones. Certainly, there are additional fractures between these zones not drawn in this case, but with a considerably lower frequency (e.g. KXTT4 between 28 and 45 m: around 4 fractures per m). Due to the fact that only the most “obvious” fractures (high fracture frequencies which are linked to mylonitic shear zones) are inter- and extrapolated, case 1 is also termed the “highway solution”.

- **Case 2** (Figure 2-17a: "Feature A" solution): Case 2 can be defined as case 1 containing two major additions: 1) individual fractures are combined to elongated fracture zones with higher fracture frequencies and 2) "Feature A" is represented explicitly as a highly fractured zone. The fractures defining "Feature A" all lie in zones with ductile precursors (mainly mylonites in ductile shear zones). However, “Feature A” as defined by WINBERG (1996) is not an obvious planar structure which could easily be drawn between the boreholes. To create “Feature A” in case 2, additional NNW-SSE oriented fractures have to be introduced, as shown in Figure 2-17a.

  The existence of one single planar fracture that would constitute "Feature A" as defined in WINBERG (1996) cannot be proven or rejected on the basis of existing data. Arguments favouring the interpretation of "Feature A" as one single fracture include:

  - All fractures related to "Feature A" are found along reactivated ductile precursors and thus reflect a corridor of increased fracture frequency. This fact allows correlations over longer distances than for fractures outside the mylonites.

  - The projected "Feature A" intersections in the boreholes can be arranged into a 10 m long corridor with a width of only 0.80 m.

- Analyses of porewater in the packed-off “Feature A” indicate a different geochemical evolution when compared to other porewaters in the TRUE-1 block (WINBERG et al. 2000).

Arguments against the interpretation of "Feature A" as one single fracture include:

- The orientations of "Feature A" intersections in the boreholes cannot be lined up into one planar structure.
- Planar features with an extent of about 10 m were not observed at the TRUE-1 site and also do not agree with the observed trace-length distributions (see Figure 2-11b).
- "Feature A" is not unique; there are some other situations in the TRUE-1 block where structures such as "Feature A" could be constructed.

- **Case 3** (Figure 2-17b: “network solution”): The network solution acknowledges the observation that fracture frequency is generally very high, and thus one single network could exist connecting the vast majority of all fractures in the TRUE-1 block. Areas with high fracture frequencies follow the fracture zones shown in case 2 but are much more extended and therefore build a network over the whole block. The remaining space between these fracture zones is covered by a less dense fracture network. Case 3 now overlaps with the stochastic part of the structural model (Chapter 2.5).

2.5 A stochastic geometric model of the fracture network in the TRUE-1 volume

2.5.1 Principle

The geometric properties of the fracture network in the TRUE-1 volume can be simulated using a stochastic discrete fracture network code such as FracMan®. The rationale behind using a 3D network approach is that statistics from 1D (boreholes, scanlines) and 2D (surface outcrops) fracture data can be used for estimating the 3D properties of the fractures in a rock volume. The stochastic approach ensures that the statistics in the simulated network follow the observed statistics, but the locations of individual fractures are random.

Generating realistic stochastic fracture networks requires the existence of relevant fracture information. The fracture network model can be used for several purposes, such as simulating the mechanical behaviour around underground openings, flow properties in a rock block or transport properties of flowpaths in the rock, depending on the input data. The most basic fracture network model requires knowledge of the fracture orientation, trace length and location, and this is sufficient input to produce a geometric model which can reproduce the observed geometries in boreholes and in outcrops.

Based on information on fracture orientations, trace lengths and frequencies along boreholes, it is possible to estimate fracture size[*)] and fracture intensity in the 3D network. Fracture spacing along boreholes or the pattern of fracturing in outcrops can be used to estimate the distribution of fractures in 3D.

2.5.2 Previous work

A previous stochastic network model for the TRUE-1 site was developed by DERSHOWITZ et al. (1996). These authors used geological and hydraulic data to represent conductive fractures and fracture orientations derived from BIP logging in the TRUE-1 boreholes. Fracture trace information for estimating areal intensity was taken from the regular SKB mapping (SICADA) in the TRUE-1 tunnel section and from the detailed fracture trace map of this section given in Figure 2-8 and Appendix 4 in this report. Fracture-size distribution is based on an investigation of 890 conductive structures in the whole tunnel system (LA POINTE et al. 1995). The evaluated parameters of the DERSHOWITZ et al. (1996) geometric network are listed in Table 2-11.

Table 2-11. Summary of the TRUE-1 DFN model of Dershowitz et al 1996.

Parameter	Stochastic model	Reference
Location model	Baecher Model	from WINBERG et al., (1996) trace map
Orientation distribution	Bootstrap	from BIPS measurements in KXTT l-4 and KA3005A
Size distribution	Lognormal, Mean = 6 m and Std Dev = 2 m	from 890 conductive fractures in the Äspö HRL
Conductive feature intensity	P_{32c} = 2.45 m^{-1} T_{min} = 5x 10-9 m^2/s	Oxfilet analysis of flowlogs and from geological mapping

To derive a stochastic model containing all fractures, both conductive and non-conductive, it is necessary to perform a new analysis of the geometric properties of the fracture network in the block. This study presents a new, refined fracture *size estimate* performed on the detailed fracture trace maps presented by MAZUREK et al. (1996) from the TRUE-1 tunnel section, on new line counting data from the roof in the same tunnel section (see Chapters 2.2 and 2.3) and on BIP and borehole fracture data. This refined analysis is performed to derive a more realistic stochastic conceptual model containing realisations of fracture networks in the TRUE-1 block.

[*)] Fracture size can be described as an equivalent radius of a circular disk with the same area as a fracture independent of shape.

2.5.3 Fracture size estimation

Fracture size cannot simply be derived directly from fracture trace length because of the complex and non-unique relationship between the length of the traces, the fracture orientation and the orientation of the sampling plane. A trial and error method was used, where stochastic fracture network realisations are calculated assuming different fracture size distributions. The trace length statistics from a number of tunnel wall simulations were then compared to the observed trace length statistics derived from the tunnel wall map (Figure 2-8 and Appendix 4). The best estimate of fracture size distribution was achieved when the observed and simulated trace length statistics match. In this type of size analysis it is generally not necessary to make assumptions regarding fracture traces that intersect the border of the observation window as long as there are enough traces present and unless the observed trace map contains a large number of fractures that have traces longer than the size of the observation window. If the above criteria are fulfilled and a good match is achieved, both simulated and observed trace maps will have similar proportions of fracture traces extending beyond the observation window.

A similar procedure can be performed with the fracture line counting data. After generating a number of DFN models with different size distributions, each realisation is sampled with a plane identical in scale and orientation to the roof of the TRUE-1 tunnel section. Trace length statistics are then calculated for all traces intersecting a scanline within this plane. Again, by comparing the simulated distributions with the observed trace length distribution, it is possible to backtrack which DFN model matches best. The procedure is performed on the available trace map data from both the detailed trace map (Figure 2-8 and Appendix 4) and from the scanline data (Table 2-12).

Table 2-12. Statistics for the Äspö tunnel section near the TRUE-1 block.

	Mazurek et al., (1996)	**Scan line mapping data**
Section	2944 - 3004 m	2950 - 2980 m
Total section length	60 m trace map	30 m scan line
Approx. mapped perimeter	4 m	-
Total trace length	304.8 m	31.20 m
Number of fracture traces	229	49
Mean trace length	1.33 m	0.64 m
Std Dev of trace lenth	1.21 m	0.67 m
Approx. mapped tunnel surface area	240 m^2	-
Approximate Fracture intensity P_{21} or P_{10}	P_{21} = 1.27 m^{-1}	P_{10} = 1.63 m^{-1}

Fracture size distributions based on the TRUE-1 tunnel map

The size of the model domain was chosen as 80 x 20 x 20 m^3. The aim was to evaluate size for each of the fracture sets, but observations on the tunnel wall and scanlines were too scarce to be subdivided into separate sets. Therefore, fracture orientation data were taken directly from the BIP observations in the TRUE-1 boreholes. Each generated fracture was drawn from the observed orientation distribution so that the final model exactly reflected this distribution (bootstrapping). Parameters for network models with different size distributions and bootstrapped orientations inside the model domain are shown in Table 2-13. A number of stochastic realisations were performed for each DFN model to ensure valid statistics.

Table 2-13. Different size distributions in DFN models based on tunnel wall map traces (MAZUREK et al., 1995).

Powerlaw	**Min**	**Exponent**	# of realisations
	0.1 - 0.4 (m)	3.05 - 3.5	7
Lognormal	**Mean**	**Std Deviation**	# of realisations
	0.125 - 2.0 (m)	0.1 - 2.0	10
Exponential	Mean		# of realisations
	0.125 - 1.0 (m)		4

On the basis of the tunnel wall map of Figure 2-8, 229 fracture traces could be observed. Another 49 traces were observed by line counting on the tunnel roof (Appendix 3). The observed traces on the tunnel wall map are truncated by a lower measurement limit of approximately 0.5 m and those of the line counting were truncated by a lower measurement limit of 0.1 m. The latter is important as it implies that fracture sizes smaller than 0.1 m are excluded. To mimic this measurement truncation, sampled trace maps and line counting observations from the simulated networks were subjected to the same truncation as the observed trace map and line countings.

Results from the simulated size estimations show that the observed fracture trace data can be matched very well, as shown in Figure 2-18 and Table 2-14. The cumulative density function (CDF) graph shows the distribution of trace lengths for a certain simulated fracture size distribution. The steeper the curve of the CDF the less spread there is in various fracture sizes. Actually, simulations of different size distributions all match well with the observed data. The parameters that best fit the observed data are summarised in Table 2-15. It can be argued that models with power law size distributions better mimic the behaviour of both the large and rarely occurring fractures as well as the dominant small fractures than do the other models. However, in the particular trace map (Figure 2-8), the size of the observation window is limited so that the large (usually steep) fractures are extensively eliminated. This effect works in favour of the two other models, log-normal and exponential size distributions. This is in fact a windowing effect and is described in detail by LAPOINTE et al. (1999). He shows that a truly power law distributed trace map sampled in successively smaller observation windows will have a better logarithmic match when the fracture size distribution becomes larger than the size of the observation window.

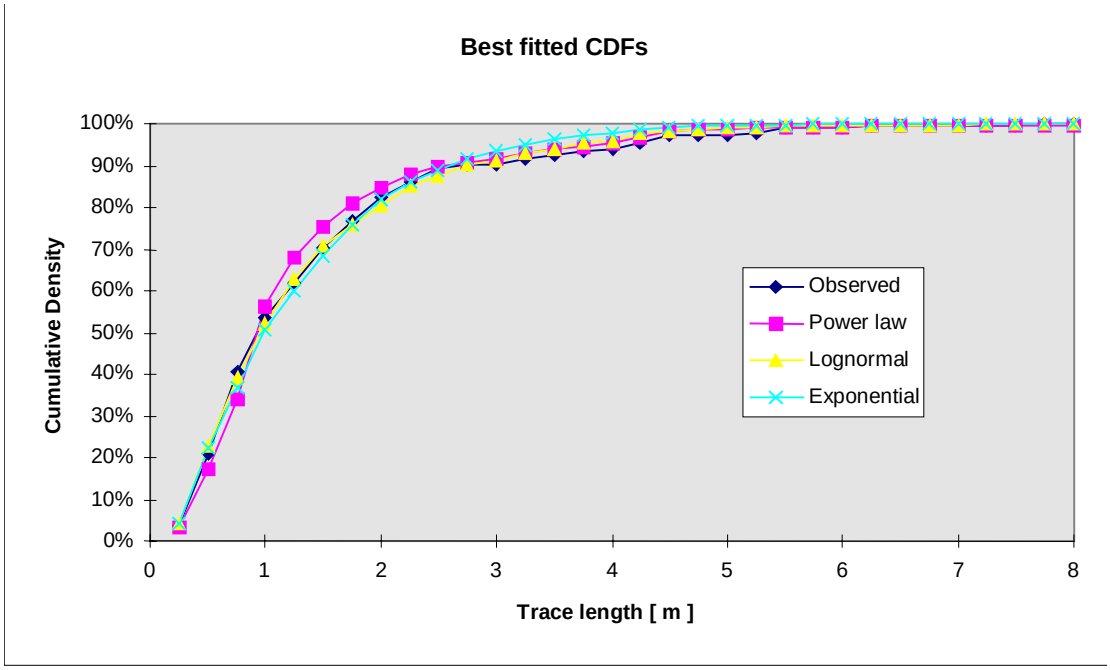

Figure 2-18. *Cumulative density functions of observed trace length data from the TRUE-1 tunnel wall and simulated trace lengths generated with three different DFN models for the tunnel wall map analysis.*

Table 2-14. Correlation between the observed trace length CDF and the simulated trace length CDF's.

	Correlation	Σ absolute difference
Powerlaw	99.6 %	0.477
Lognormal	99.9 %	0.300
Exponential	99.7 %	0.496

Fracture size distributions based on line counting observations

The data from the line countings consist of 126 trace segments, of which only 49 have been oriented. This investigation is more detailed and measures traces down to 0.10 m. Although the mapping campaigns were performed in the same tunnel section, the trace mean differs significantly, from 1.33 m for the trace map data to 0.64 m for the scanline data. The reason for this deviation must be the different mapping techniques and levels of truncation.

Results of the DFN size estimates show that it is possible to simulate traces using any of the three simulated size distributions (Figure 2-19). The parameters for each distribution are given in Table 2-16. The match between simulated and observed line counting traces is less clear than in the trace map analysis. This is attributed to the small oriented sample of only 49 traces and to the fact that most of these fractures are very short.

Table 2-15. Best fit size estimates (trace map) for all three tested models based on the tunnel wall map traces.

Powerlaw	**Min** 0.4	**Exponent** 3.5
Lognormal	**Mean** 0.5	**Std Deviation** 0.5
Exponential	**Mean** 0.5	

Table 2-16. Best fit size estimates (scan line) for all three tested models based on line counting measurements.

Powerlaw	**Min** 0.1 (m)	**Exponent** 3.5
Lognormal	**Mean** 0.15 (m)	**Std Deviation** 0.1
Exponential	**Mean** 0.125 (m)	

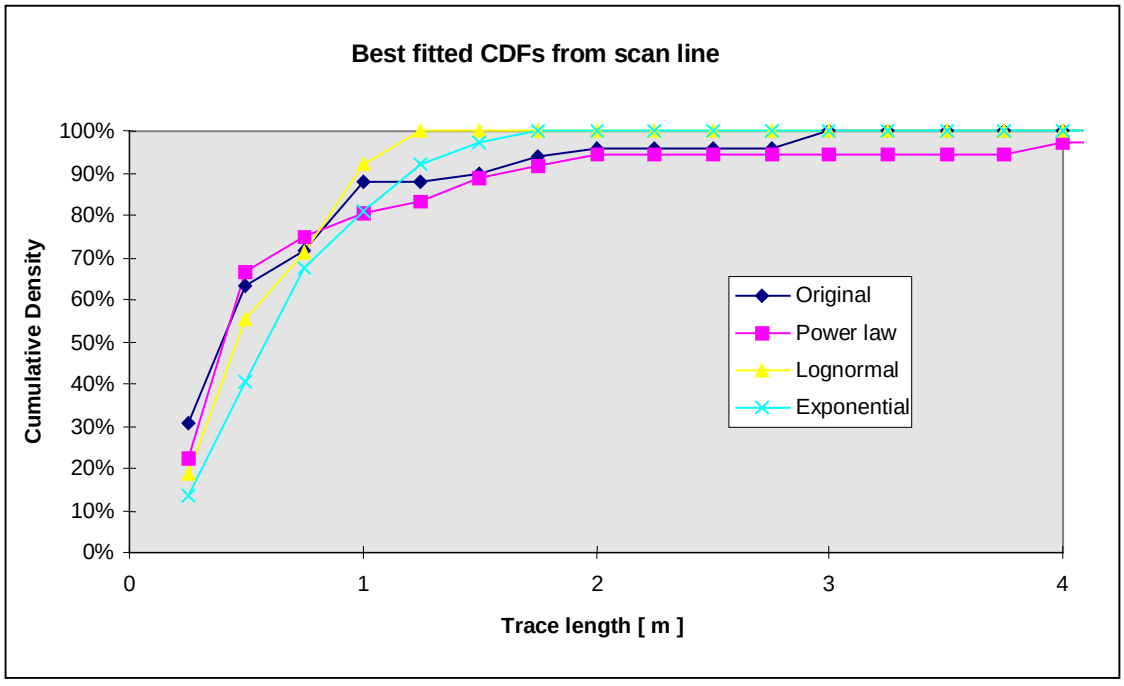

Figure 2-19. *Cumulative density functions of observed trace length data from the scanline measurements and simulated trace lengths generated with three different DFN models based on the scanline measurements.*

Conclusions

A comparison between Tables 2-15 and 2-16 shows that fracture sizes are in the order of three to four times smaller if the size estimate is based on the line counting data

rather than on trace map data. This is the effect of a different, more detailed mapping technique revealing shorter fractures when performing the scanline mapping than when mapping the whole tunnel wall. The results may also be influenced by the fact that there are different levels of truncation between the two datasets. It is also interesting to note that steep fractures parallel to the tunnel are only seen on the roof and not on the wall. Furthermore, 85% of all fractures strike in a NW-SE direction, just sub-parallel to the tunnel.

It is worth noting that another DFN model study performed by HERMANSON et al. (1998), based on a trace map from part of the ZEDEX tunnel in the Äspö Hard Rock Laboratory, shows almost identical results to the TRUE-1 trace map analysis in terms of fracture size estimation. The trace statistics from this study, with a mean trace length of 1.03 m, are similar in trace length to what is mapped in the TRUE-1 tunnel section. However, the areal intensity of fracturing on the surface of the ZEDEX tunnel section is significantly higher, with a P_{21} of 2.6 m^{-1}.

2.5.4 Fracture intensity

Fracture intensity is defined as the fracture area per unit volume of rock (m^2/m^3). In FracMan®, this entity is given the **symbol P_{32}**. This intensity is directly proportional to the total trace length per outcrop area, P_{21}, or to the number of fractures intersecting a scanline (e.g. a borehole), P_{10} (fracture frequency). P_{21} and P_{10} depend both on orientation and size distribution of the fractures as well as the orientation and shape of the outcrop. P_{32}, however, does not depend on the number of fractures or on the size distribution (DERSHOWITZ 1984).

The fracture intensity P_{32} cannot be measured directly in the field. However, DERSHOWITZ and HERDA (1992) have shown that P_{21} and P_{10} are linearly correlated to P_{32} according to the equations:

$$P_{32} = C_{21} * P_{21} \text{ or } P_{32} = C_{10} * P_{10}$$

where *C* is an unknown constant of proportionality. This constant depends only on the orientation and size distribution of the fractures in the rock mass and the orientation of the surface (P_{21}) or along the line (P_{10}) in which the fractures have been mapped. Applying its linear relationship with P_{21}, P_{32} can be calculated from tunnel trace maps by means of generating a DFN model based on the orientation and size distributions derived in the previous chapters with a hypothetical $P_{32,sim}$. The methodology is as follows: a number of realisations of each DFN model are generated, and simulated P_{21sim} values are calculated by sampling a simulated drift, equivalent in size and orientation to the TRUE-1 trace map. The fracture intensity value for the simulation, $P_{32,sim}$ is then varied until the ratio $P_{21,sim}$ to $P_{21,obs}$ is equal (ratio=1). This method requires that the fracture orientation and size distribution be determined previously to provide an estimate of the true 3D fracture intensity in the rock mass.

Fracture intensity based on the trace map of Figure 2-8 has not been analysed by DERSHOWITZ et al. (1996). Following the methodology just described, a P_{32} of 2.1 can be derived from the tunnel wall map. This value is lower than the intensity based on the borehole flow log analysis calculated by DERSHOWITZ et al. (1996). Those authors report that the conductive fracture frequency (P_{10c}) is 1.55 m^{-1} in the KXTT cores. Based on this estimate, they calculate P_{32c} at 3.17 m^2/m^3. WINBERG et al. (1996) report that there are few if any conductive structures on the mapped tunnel wall next to the TRUE-1 volume. This discrepancy may be explained by the fact that the measurable inflow into a packed-off borehole interval is different from that observed on a tunnel wall, where visible inflows also depend on the evaporation rate in the tunnel and on skin effects (stress redistribution).

The estimated fracture frequency along ten simulated scanlines over the tunnel wall trace map shows that P_{10} is in the order of 0.8 fractures per metre, i.e. less than the open fracture frequency of 1.3 to 2.0 m^{-1} in the KXTT boreholes. This means that 1) all fractures mapped on the tunnel wall would be water-conducting in the boreholes, and 2) additional fractures with trace lengths <20 cm (that were not mapped) also contribute to flow in the boreholes.

If fracture intensity is based instead on the average fracture frequency of open and closed fractures based on BIP evidence (4.5 m^{-1}, see Figure 2-3b), simulations reveal a P_{32} of 6.7 m^2/m^3. However, this frequency includes fractures with sizes below the measurement cut-off used for trace map analyses along the tunnel walls and roof. Furthermore, it is likely that more fractures are sampled from the BIP images than are really water-conducting. This leads to the assumption that BIP data for fracture frequency may represent an overestimate of the conductive fracture frequency.

2.5.5 Summary of the stochastic geometric DFN model

Three different stochastic models are presented that are consistent with the information extracted from the TRUE-1 boreholes (BIP data), the tunnel wall map and line counting measurements. Tables 2-17 to 2-19 summarise the geometric parameters necessary for generating these models and Figure 2-20 shows horizontal sections through each of these models. The first parameter defines the spatial model used for generating the fractures in the volume. DERSHOWITZ et al. (1996) carried out a spatial analysis showing that there are no other hypotheses than that fracture locations are purely random (in FracMan called the Baecher model). The orientation distribution is constrained to what is observed in the BIP images of the boreholes, i.e. bootstrapped orientations. Fracture size and intensity are varied according to the three model descriptions below:

Table 2-17. Summary of DFN model A with fracture intensity based on borehole data and size based on scan line measurements.

Parameter	Stochastic model	Reference
Location model	Baecher Model	DERSHOWITZ (1996)
Orientation distribution	Bootstrap	From BIP measurements in KXTT 1-4 and KA3005A (this report, see Appendix 2).
Size distribution	Lognormal mean = 0.15 m Std Dev = 0.1 Power law = 0.1 Exponent = 3.5 Exponential = 0.125	From scan line measurements in tunnel section between 2950 m and 2980 m (this report, see Appendix 3).
Fracture intensity	P_{32} = 6.7 P_{1o} = 4.5	From all fractures in the BIPS logs of theTRUE-1 boreholes (this report, see Appendix 2).

Table 2-18. Summary of DFN model B with fracture intensity based on borehole data excluding fractures inside clusters (see text on conceptual model of the TRUE-1 block below) and size based on scan line measurements.

Parameter	Stochastic model	Reference
Location model	Baecher Model	DERSHOWITZ (1996)
Orientation distribution	Bootstrap	From BIP measurements in KXTT 1-4 and KA3005A (this report, see Appendix 2)
Size distribution	Lognormal mean = 0.15 m Std Dev = 0.1 Power law = 0.1 Exponent = 3.5 Exponential = 0.125	From line counting measurements in tunnel section between 2950 m and 2980 m (this report, see Appendix 3)
Fracture intensity	P_{32} = 5.1 P_{1o} = 2.6	From all fractures in the BIP logs of the TRUE-1 boreholes (this report, see Appendix 2)

Table 2-19. Summary of the DFN model C with fracture intensity and size based on trace map data.

Parameter	Stochastic model	Reference
Location model	Baecher Model	Dershowitz (1996)
Orientation distribution	Bootstrap	From BIP measurements in KXTT 1-4 and KA3005A boreoles (this report, see Appendix 2).
Size distribution	Lognormal mean = 0.5 m Std Dev = 0.5 Power law = 0.4 Exponent = 3.5 Exponential = 0.5	From small scale fracture trace map (this report, see Figure 2-8 and Appendix 4).
Fracture intensity	P_{32} = 2.1 P_{10} = 0.8	From small scale fracture trace map (this report, see Figure 2-8 and Appendix 4).

DFN model A is based on all scanned BIP fractures (open and closed) for estimates of fracture intensity and orientations. The size distribution is deduced from the line counting measurements. Figure 2-20 (DFN model A) shows the traces that intersect a planar section through the model.

DFN model B is like model A (open and closed fractures), but with a less dense fracture intensity (P_{32} as well as P_{21}). DFN model B can be defined as model A minus the observed fracture clusters[*)]. These fracture clusters are considered to form part of the deterministic structural model and stochastically generated fractures within these domains are thus removed from the model (the removed fracture clusters are the zones of increased fracture frequency visualised in Figure 2-17a).

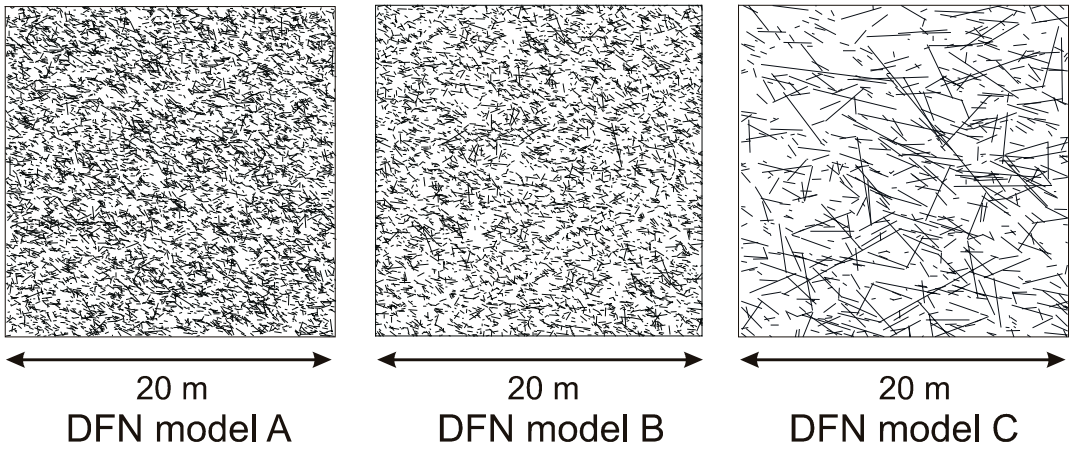

Figure 2-20. *A horizontal section through a realisation of the DFN models A, B and C.*

*)] Fracture clusters are elongated zones several metres in extent where fracture frequency is increased (i.e. along ductile shear zones or mylonites).

Thus DFN model B can be considered as a background fracturing in the block excluding deterministically selected sections with clustered fractures. The model is based on sizes drawn from line counting measurements and fracture intensities deduced from all fractures along the boreholes by BIP images. The resulting trace map of this DFN model is shown in Figure 2-20 (DFN model B).

DFN model C shows a representation of the block-scale network, which is based on data from the tunnel wall trace map (open and closed fractures). Figure 2-20 shows a horizontal section through one realisation of the DFN model C.

The choice of a suitable DFN model which is representative for the TRUE-1 site depends on the purpose of the project. The present analyses are focused on the characteristics of fracture networks with scales ranging from hundreds of metres down to single fractures such as those tested in the TRUE-1 volume (which extend over a few metres at least). However, the tested fractures in the TRUE-1 volume (e.g. the "Feature A" structure) can be interpreted as being a cluster of smaller fractures closely connected to build up a single structure, as has been observed along mylonitic shear zones. The conceptualisation of how these structures should be presented depends on the purpose.

DFN model A (Figure 2-21) represents mainly fractures on the small scale of the TRUE-1 block. Only a few longer fractures exist in this simulation and larger fractures as observed on the tunnel wall are missing. In the absence of any deterministic fracture information, this realisation would best describe the fracture pattern in the TRUE-1 block. However, DFN models are not able to represent discrete fracture clusters as observed along the boreholes. DFN model A could be used as a conceptual structural model for flow and transport in the absence of any deterministic information on the small scale, as is the case in rock volumes where no borehole information is available.

DFN model B (Figure 2-22) shows a realisation where the observed fracture clusters along ductile precursors do not contribute to the areal fracture intensity P_{21}. This was done by subtracting the intensities of these clusters from DFN model A, resulting in a fracture network for DFN model B which is obviously less dense than model A. This representation is also unable to simulate fracture clusters as observed along ductile precursors, and larger fractures as observed on the tunnel wall are also missing. However, DFN model B, when combined with the deterministic fracture clusters, would result in an appropriate conceptual model for flow and transport on the small scale of the TRUE-1 block. Such a combined model could be used for flow and transport when independent information on fracture clustering is available (e.g. BIP images along boreholes).

DFN model C (Figure 2-23) is mainly based on the fracture network mapped on the tunnel wall of the TRUE-1 block. The larger fractures are taken into account in this model. However, the really small-scale fractures are virtually absent due to the fact that small-scale fractures were not mapped on the tunnel wall. In DFN model C, fracture clusters with very dense and interconnected fractures could be conceptualised as one single straight and extended fracture.

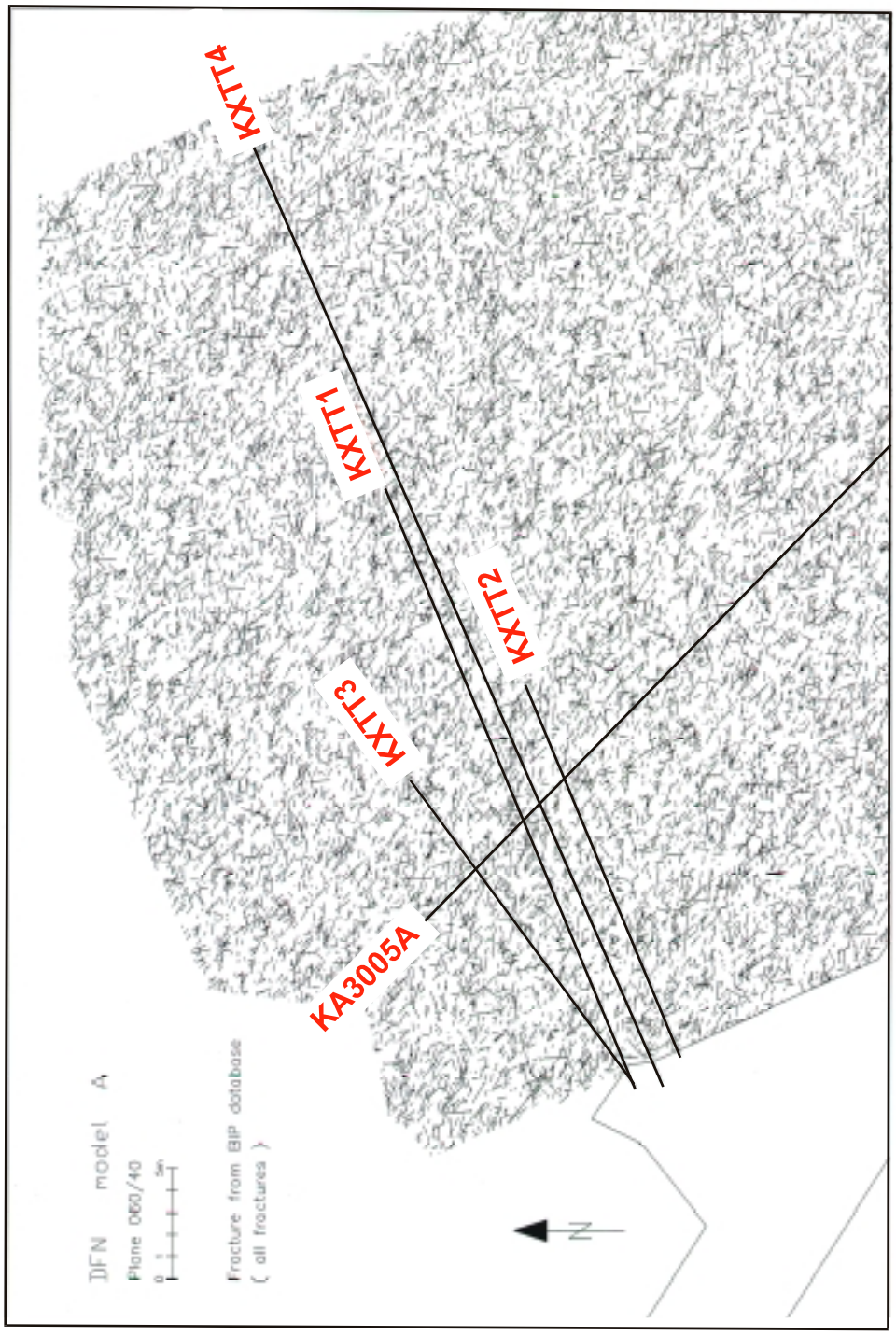

Figure 2-21. *Realisation of DFN model A (all fractures). Fracture traces are shown in a plane with azimuth 60 and dip 40, which is oriented sub-parallel to the TRUE-1 boreholes.*

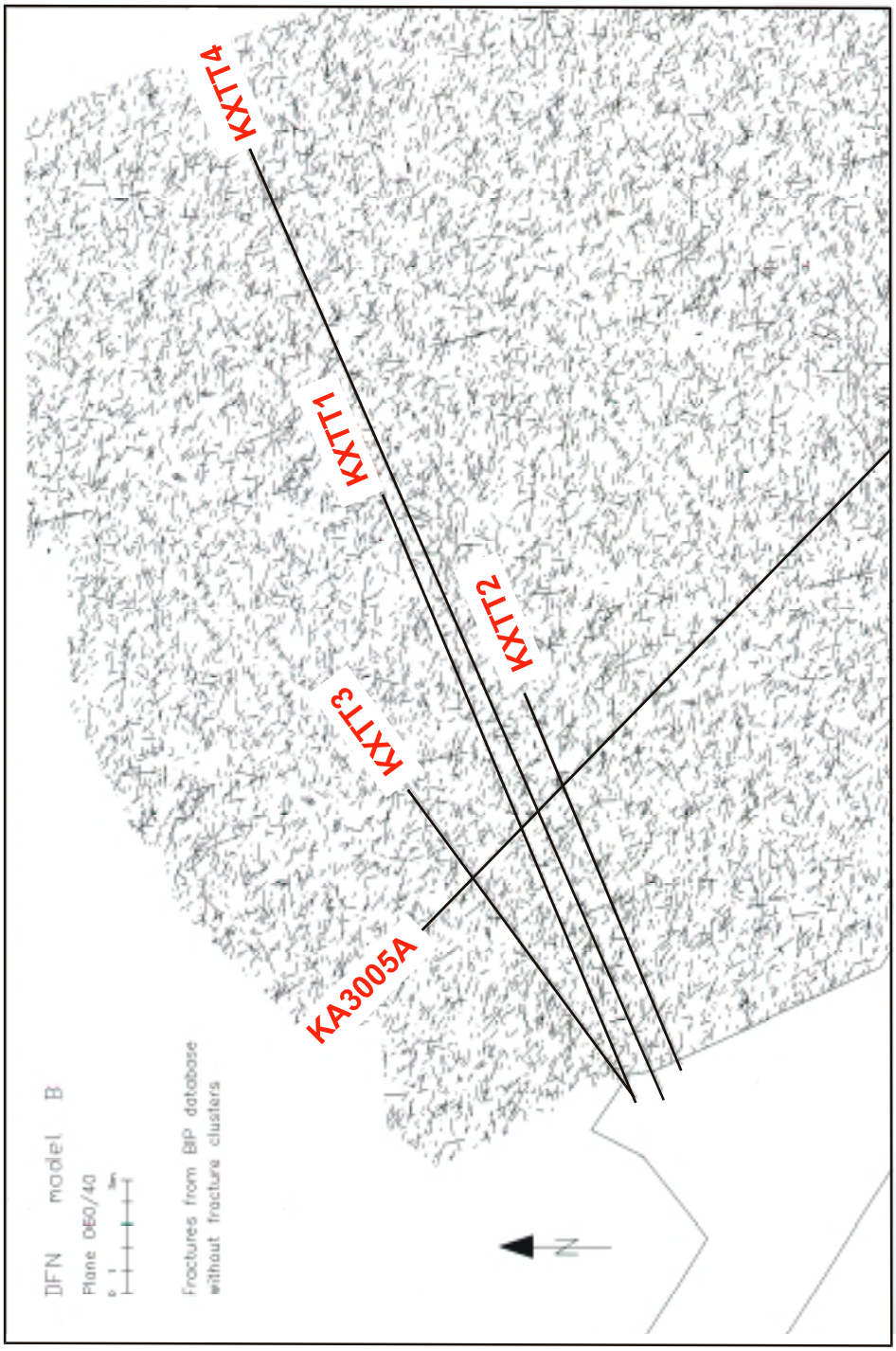

Figure 2-22. *Realisation of DFN model B (background fracturing). Fracture traces are shown, as in model A, in a plane with azimuth 60 and dip 40, which is oriented sub-parallel to the TRUE-1 boreholes.*

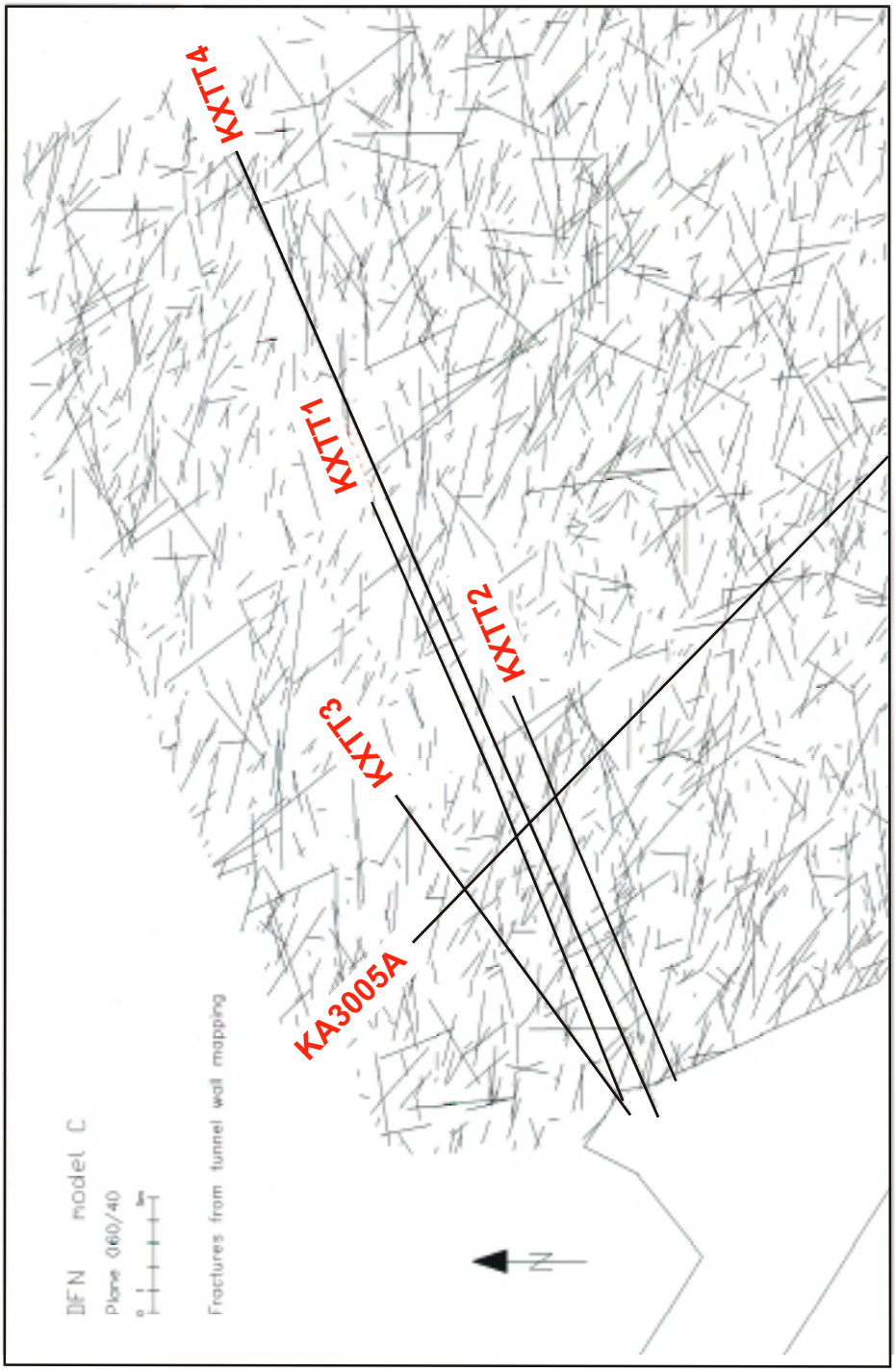

Figure 2-23. *Realisation of DFN model C (block-scale network). Fracture traces are shown, as in model A and B, in a plane with azimuth 60 and dip 40, which is oriented sub-parallel to the TRUE-1 boreholes.*

This upscaling (fracture clusters are summed into one large fracture) is a conceptual approach and is not based on observations. It results in a fracture network with lower fracture intensities compared to that on the small scale of the previous two model cases. DFN model C is believed to best represent the whole TRUE-1 volume on the experimental scale as data are drawn from a wall of approximately the same size as a section through the experimental volume (50 x 50 x 50 m volume). It has, on the other hand, to be clearly stated that the long fractures do not represent the deterministic fracture clusters as observed at distinct coordinates along the boreholes. DFN model C could be further modified and improved conceptually by moving the large fractures to those locations where fracture clusters have really been observed. This process is also termed model conditioning.

Models B and C are used for the integrated structural model. They are based on different scales, model B being small scale and model C block scale.

2.6 Derivation of the integrated structural model

The basic idea of a synthesis of the deterministic and the stochastic models is to present a concept for fracturing in the whole TRUE-1 block which obeys the integrated results of fracture geometry (fracture intensity, trace length, orientation) and structural geology (ductile precursors, deformation, alteration etc.) in the rock mass.

The deterministic structural model and the stochastic structural model have been derived separately above. The database and the logic of the derivation procedure have been discussed in detail. Both models rely on fracture statistics from drillcore mapping and BIP images, line countings along the tunnel roof and fracture mapping of the tunnel wall. Both models take into account the existence of an interconnected fracture network with a pronounced anisotropy (short fracture trace lengths, preferred fracture orientations and high fracture frequencies). However, the major difference in the conceptualisation of the two types of models is how the fracture data are presented. The deterministic model treats structural data as observed and highlights deterministic structures located at specific positions in the rock volume, whereas the DFN model presents data according to a number of statistical distributions generated as stochastic fracture networks. Both models have advantages; the deterministic model explains features that can be observed directly, and the stochastic model provides a means of representing parts of the rock mass that are only indirectly observed.

In detail, the deterministic model combines the geometry of ductile precursors such as mylonites (from the drillcore database) with the mapped fractures (from the BIP database). This results in an interconnected deterministic fracture array along the boreholes, consisting of zones of higher frequencies (mainly associated with the mylonites) which are connected to zones of lower frequencies outside the mylonites.

The fact that fracture trace data are derived with two different length truncations and with different degrees of detail makes conceptualisation of fractures in the whole block difficult. The large size difference between the two datasets, (log-normal size mean of DFN models A and B is 0.15 m and of DFN model C is 0.5 m, respectively) indicates that there are at least two different ways to conceptualise the rock block. One way is to

explain the size difference as a matter of observation scale. The other way to explain the fracturing is that only small fractures exist, some which are clustered and form connected highways. The problem with the latter conceptualisation is how to explain the observation of larger fractures. Larger fractures do exist (e.g. trace lengths > 5 m), but their intensity is fairly small ($P_{32} < 1$). Their existence could be explained using the mechanical principle, as was done in FCC Phase 2 (fault zones, single fractures).

DFN models A to C, presented in Figure 2-20, show the type of information that comes from borehole and BIP data, focused line countings and tunnel wall maps. The level of detail of the observed data that underlie the DFN models is different, with the most detailed borehole-scale data in models A and B and tunnel-scale data in model C. Zones of increased fracture frequency such as fracture clusters, as observed and shown in the deterministic model, cannot be simulated with DFN models.

2.6.1 Integration of deterministic and stochastic models

The basic idea of an integrated structural model is to combine the geometry of the deterministic structural model with that of the stochastic structural model. Both models give complementary information: the deterministic model fixes zones of increased fracture intensities, mainly along mylonites, and suggests the most likely correlations of these zones among boreholes. The stochastic model was able to specify fracture sizes which are in agreement with the observed fracture network (orientations, trace lengths and frequencies).

The integration of deterministic and stochastic models is done on two scales, namely the "small scale" and the "block scale". The "small scale" is defined here as a range between several centimetres and a few metres, where fracture data were derived from the detailed drillcore and BIP mapping but also from the line counting. The "block scale" is defined here as a range between a few metres and several decametres, where fracture data were derived from the fracture trace mapping performed along the tunnel walls (i.e. Figure 2-8).

The DFN models B and C, which are based on the two different fracture size estimates, can now be related to the small scale (Figure 2-22) and the block scale (Figure 2-23). The same has to be done for the deterministic (DET) models. However this is not so straight-forward, because the DET models were only derived on the small scale, where three model cases have been distinguished (Figure 2-16b, 2-17a and 2-17b). Of these three model cases, the deterministic model of Figure 2-17a is selected as the deterministic small-scale model (termed model DET C in the following) due to the fact that it contains the most likely fracture clusters and also the "Feature A" structure (the model in Figure 2-16b has been disregarded because "Feature A" is not included and the model in Figure 2-17b already contains fractures between the clusters). The small-scale DET C model is now shown in Figure 2-24, where "Feature A" is especially highlighted.

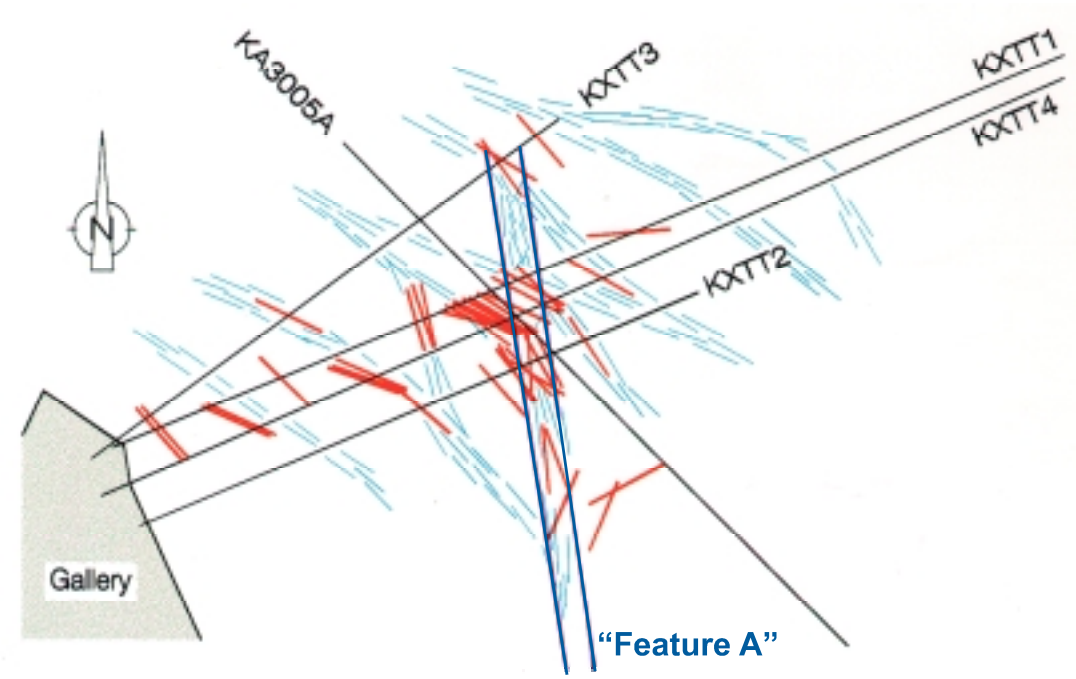

Figure 2-24. *Deterministic model C on the small scale, taking into account Feature A and the mylonites. The "highways" are characterised as zones of increased fracture intensities (fracture clusters), which are bound to ductile precursors such as mylonites.*

What is still missing is the deterministic model on the block scale. The small-scale arrangement of fractures (fracture clusters) in Figure 2-24 can now be upscaled in such a way that a number of interconnected deterministic fractures are transformed into larger features on a scale comparable to that observed on the tunnel wall (Figure 2-8). This procedure is visualised in Figure 2-25, where both the small-scale fracture clusters and the upscaled single fractures are drawn. The block-scale DET C model is now the resulting fracture network of the extended single fractures in Figure 2-25, where the small-scale fracture clusters are omitted. "Feature A", which has undergone this upscaling, is no longer interpreted as a curved fracture cluster, but rather as a straight single fracture.

Both the DFN models and DET models are now available on the small and the block scale, resulting in four model cases: models DFN B "background fracturing" and C "block scale network" and models DET C "fracture cluster " and DET C "single fracture".

The integration or synthesis procedure is now shown in Figure 2-26; it relies on the DET models from Figures 2-24 and 2-25 and its coupling to the two scales of fracture data as shown in DFN models B and C (Figures 2-22 and 2-23). Space filling between the fracture clusters of DET C (small-scale) and DET C (block-scale) is done with the stochastic realisations of DFN models B (small-scale) and C (block-scale), respectively.

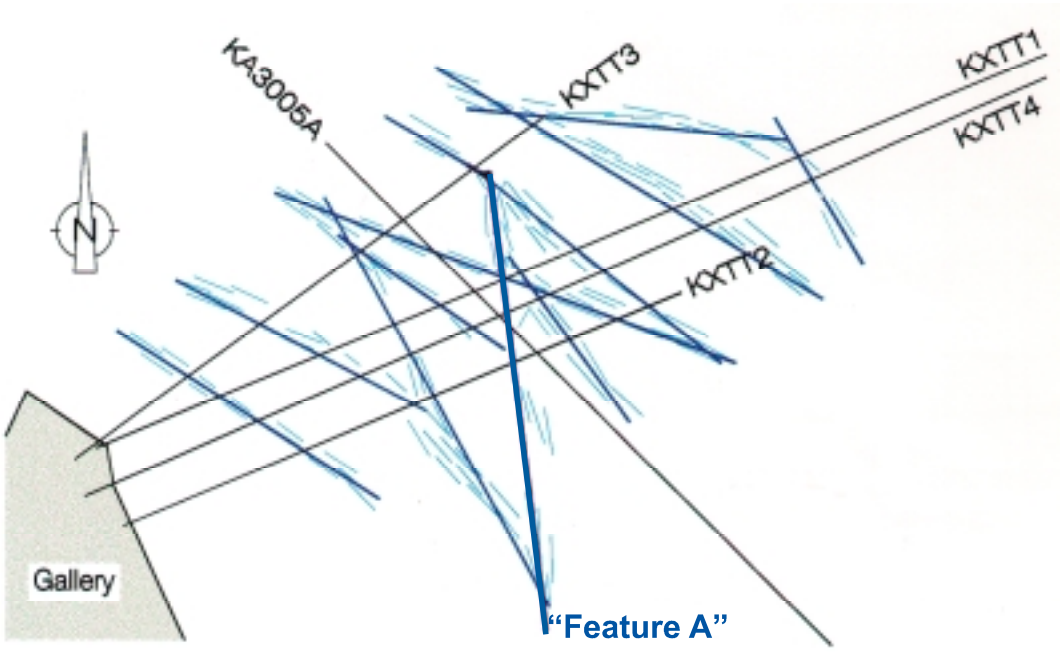

Figure 2-25. *Deterministic model C (highways) on the block scale, taking into account Feature A. The small-scale fracture clusters are conceptualised as single straight fractures on the block scale (see also Figures 2-43 and 4-1).*

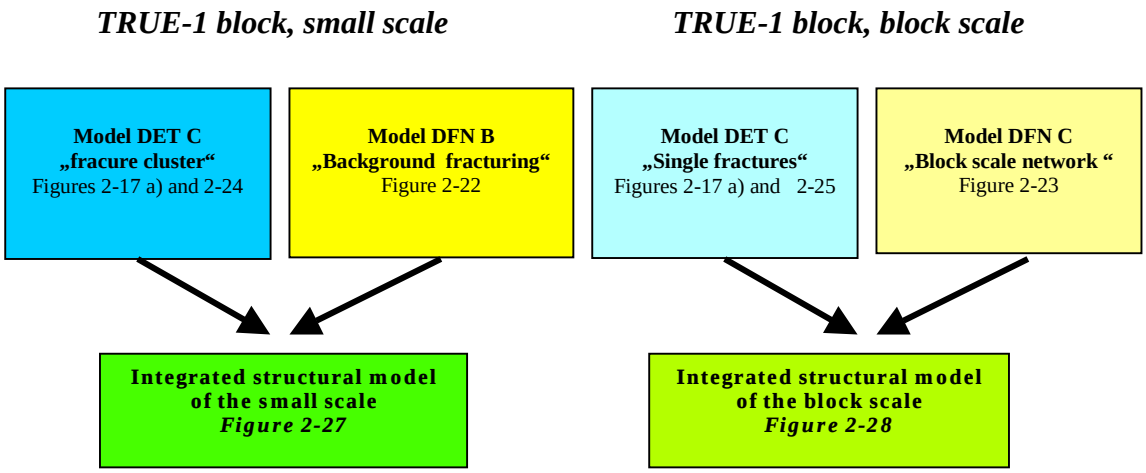

Figure 2-26. *Integration procedure for deterministic and stochastic models on the small and block scales.*

2.6.2 Visualisation of the results

The visualisation of the integration of deterministic and stochastic structural models is shown in Figures 2-27 and 2-28, where the resulting fracture network is shown in a 2D-plane containing the KXTT boreholes (orientation of plane 060/40, the same as in Figures 2-16 and 2-17). In Figure 2-27, the small-scale integrated structural model is shown, where the deterministic fracture clusters along the ductile precursors are combined with the stochastic background fracturing. In Figure 2-28, the block-scale integrated structural model is shown, where the deterministic, upscaled single fractures along the ductile precursors are combined with the stochastic block-scale network.

From the visualisation of these fracture networks, it is quite evident that both fracture networks are highly interconnected, even when fracturing is now presented on different scales. On both scales, the interconnection is more pronounced in the NW-SE direction than in the normal direction. The two integrated model cases clearly demonstrate that the fracture networks look different when fracture data of different degrees of detail are considered. The densest fracture network with the smallest fracture trace lengths is obtained in the small-scale model. Another less dense network results on the block scale with still interconnected fractures due to larger fracture trace lengths, which have been observed on the tunnel wall.

Neither of these two cases provides all the information. Fracture geometry derived from borehole data (BIP and drillcore) lacks trace length data, while fracture geometry derived from tunnel wall mapping suffers from insufficient orientation data and from ignoring small-scale fractures. The most appropriate model relies on a combination of borehole (drillcore and BIP) and tunnel wall information. Thus, the most likely fracture network seems to be a compromise between the small-scale structural model of Figure 2-27 and the block-scale model of Figure 2-28.

2.7 Constraints on the structural model based on hydrogeological observations

2.7.1 Available hydraulic data

In the TRUE-1 block, an extensive hydraulic test programme was carried out (WINBERG et al. 1996). The aim of these tests was the hydrogeological characterisation of the TRUE-1 block, mainly to assess hydraulic parameters such as transmissivity and storativity of identified structures and the connectivity among the structures.

Two types of tests performed in the TRUE-1 block are used here:

– **Flow logging tests:** A packer is moved from the borehole end to the borehole mouth and the integrated outflow of the borehole is measured. This flow logging has been performed in all 5 boreholes. Assuming steady-state conditions, the transmissivity can be calculated for every logging interval, which is normally 1 m long. The test evaluation is documented in WINBERG (1996).

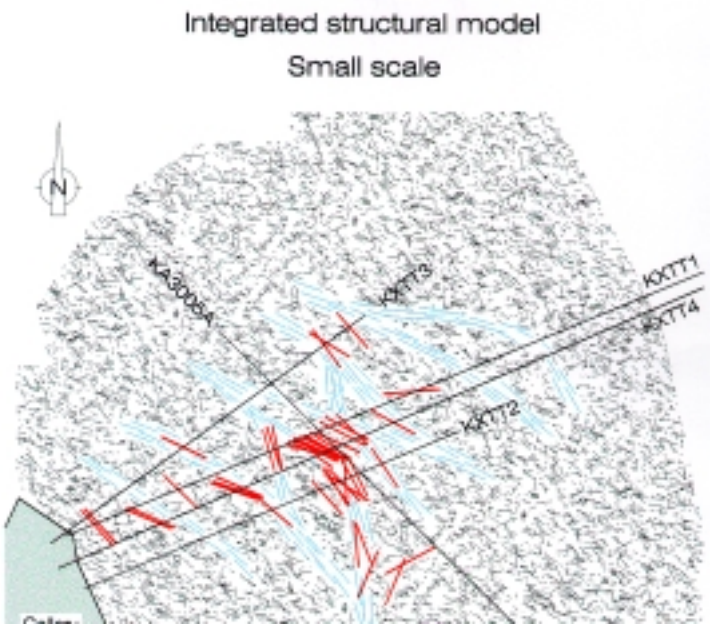

Figure 2-27. *Integrated structural model* ***(small-scale****), showing the deterministically derived fracture clusters (blue) and mylonites (red) together with a stochastically derived realisation of the background fracturing.*

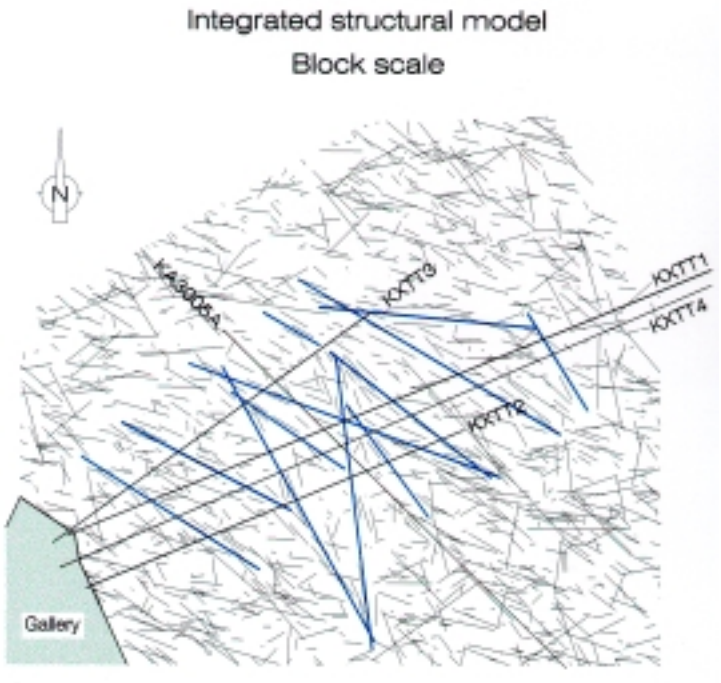

Figure 2-28. *Integrated structural model* ***(block scale****), showing the upscaled single fractures together with a stochastically derived realisation of the block scale fracturing..*

– **Interference tests:** In total, 14 test sequences in the 5 boreholes of the TRUE-1 block were performed. Each sequence consisted of a constant head withdrawal test in a selected borehole interval. The pressure in the withdrawal interval was set to zero and the flow rate was measured together with the pressure responses in the surrounding boreholes. The test evaluation is documented in WINBERG (1996), where transmissivities and storativities of all test intervals are reported. Additionally, the connectivity of the different observation intervals was evaluated by comparing and indexing the pressure responses among individual intervals.

The raw data from flow logging and interference tests are revisited here. The main objective is to further constrain the structural model by integration of hydraulic information. The interference tests were used to re-evaluate hydraulic parameters of a single test by applying different estimation methods (Chapter 2.7.2) and to derive a hydraulic conceptual model for the TRUE-1 block (Chapter 2.7.3). The flow logging tests have been used to correlate zones with inflows with the BIP images of the borehole walls (see Chapter 2.7.4) and thus to check if highly transmissive zones correspond to high fracture frequencies.

2.7.2 Evaluation of hydraulic tests

The evaluation procedure for selected interference tests is shown in Figure 2-29. In the following, the four steps shown in Figure 2-29 are presented.

Step A involves the selection of one test sequence out of the 14 tests. The main selection criterion was steady-state outflow, such that the assumption of a homogeneous, infinite radial flow system with a flow dimension of 2 is justified. This assumption is necessary when classical test evaluation methods are applied, such as straight-line methods. Diagnostic plots are appropriate tools to check the early time periods of a test (e.g. wellbore storage effects), middle time periods (e.g. linear, radial or spherical flow) and late time periods (e.g. effect of a boundary). Several diagnostic plots have been checked on the basis of the withdrawal intervals of the 14 tests. Finally, test 5 has been selected (Figure 2-30) due to the existence of a radial flow period and of clear and high pressure responses in the observation intervals, together with a low steady-state outflow in the test interval (borehole KXTT2, interval 2) of only 350 ml/min. Figure 2-30 clearly shows that the wellbore storage period is quite short (less than 10 s). The infinite radial flow period ends after ca. 1 h (graph in Figure 2-30 is no longer horizontal at later times).

Step B consists of estimating hydraulic parameters on the basis of test 5 with the classical straight-line method. Altogether, 6 intervals from 3 boreholes have been chosen to derive transmissivity and storativity (intervals 3 and 4 in KXTT1, intervals 3 and 4 in KXTT4 and intervals 1 and 2 in KA3005A). Borehole KXTT3 was not used because its intervals were too far away from the withdrawal interval 2 of borehole KXTT2. The locations of the boreholes and their test and observation intervals are shown in Figure 2-31. An overview of test 5 (pressures in observation intervals and outflows in withdrawal interval) is shown in Figure 2-32. The straight-line regressions and the evaluated

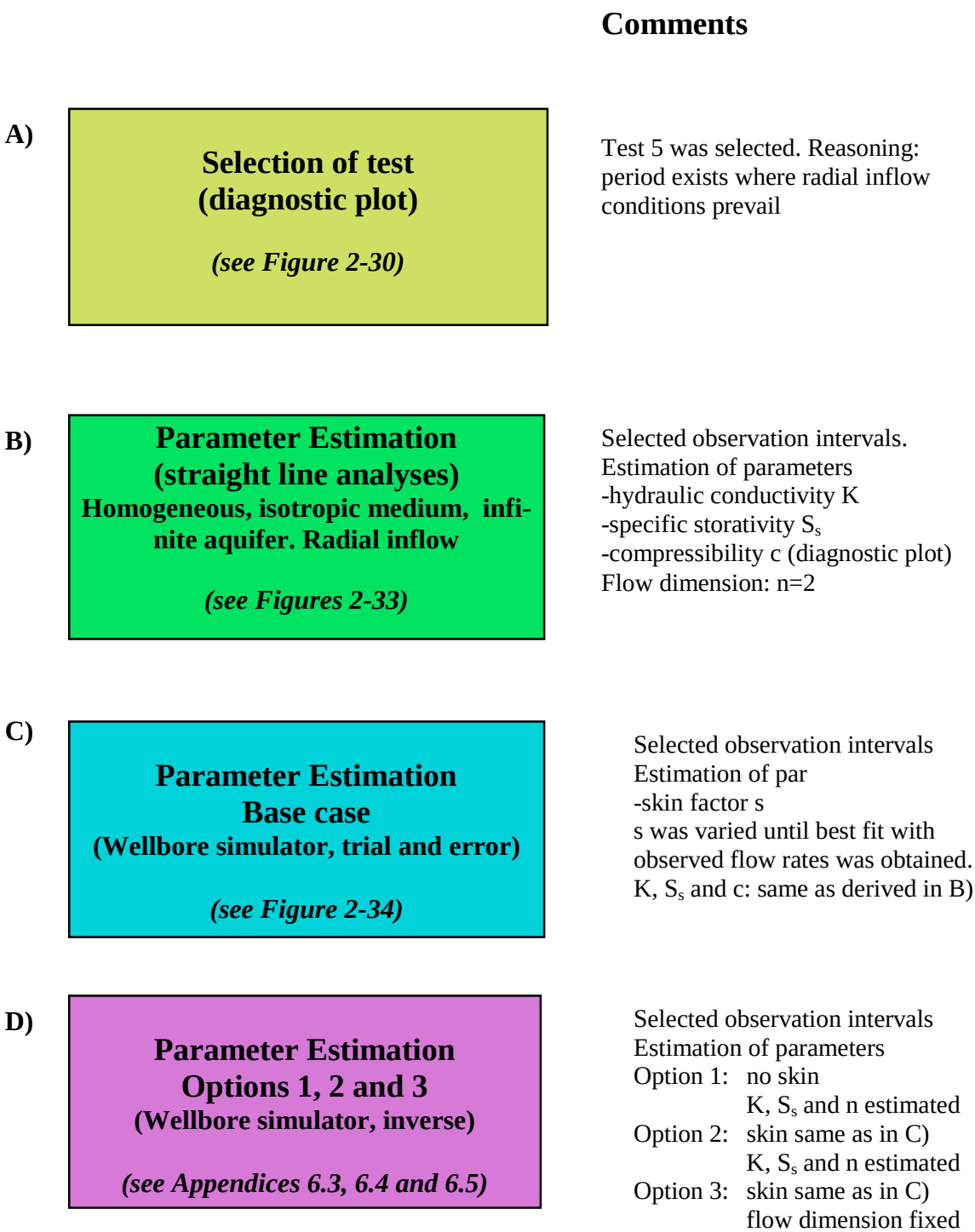

Figure 2-29. *Parameter estimation: approach.*

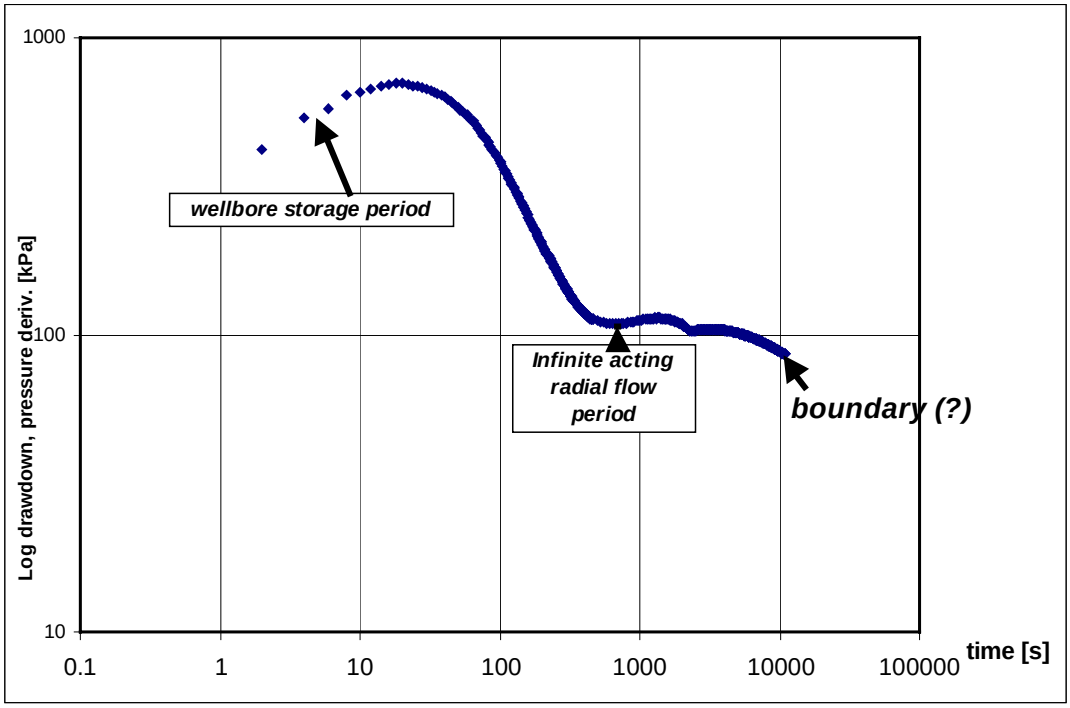

Figure 2-30. *Diagnostic plot of borehole KXTT2, withdrawal interval 2 (Test 5).*

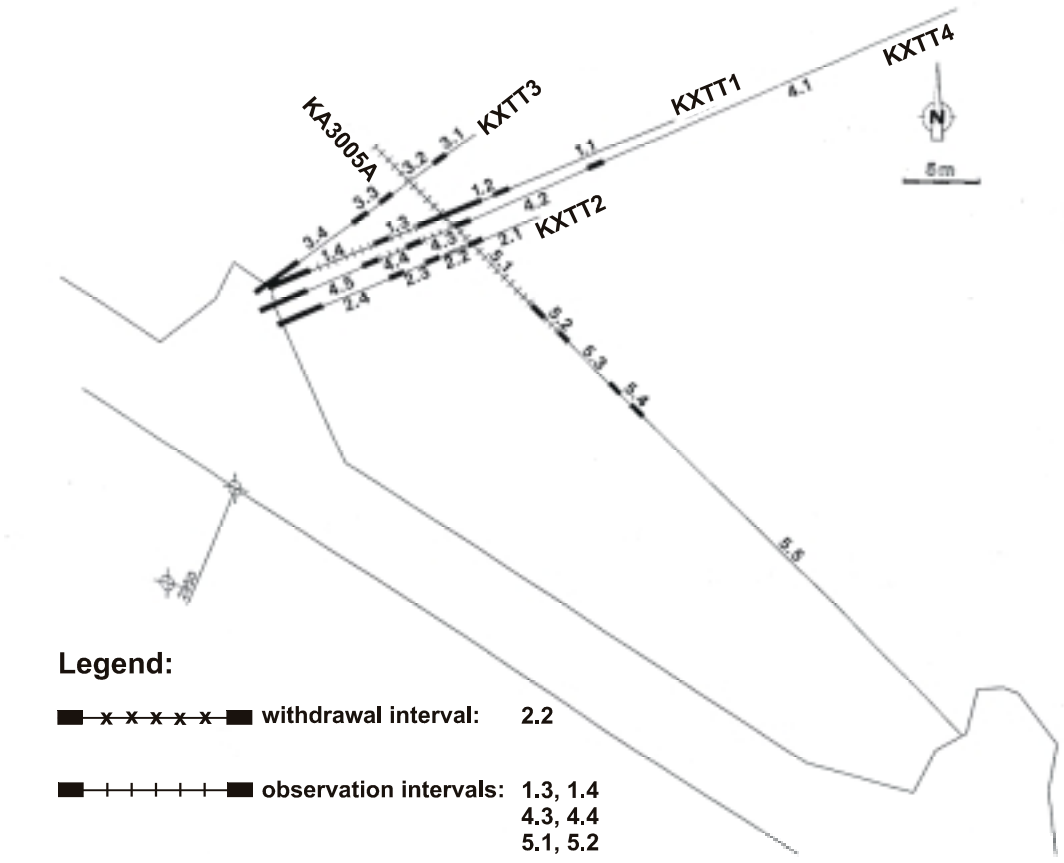

Figure 2-31. *Locations of boreholes and observation intervals.*

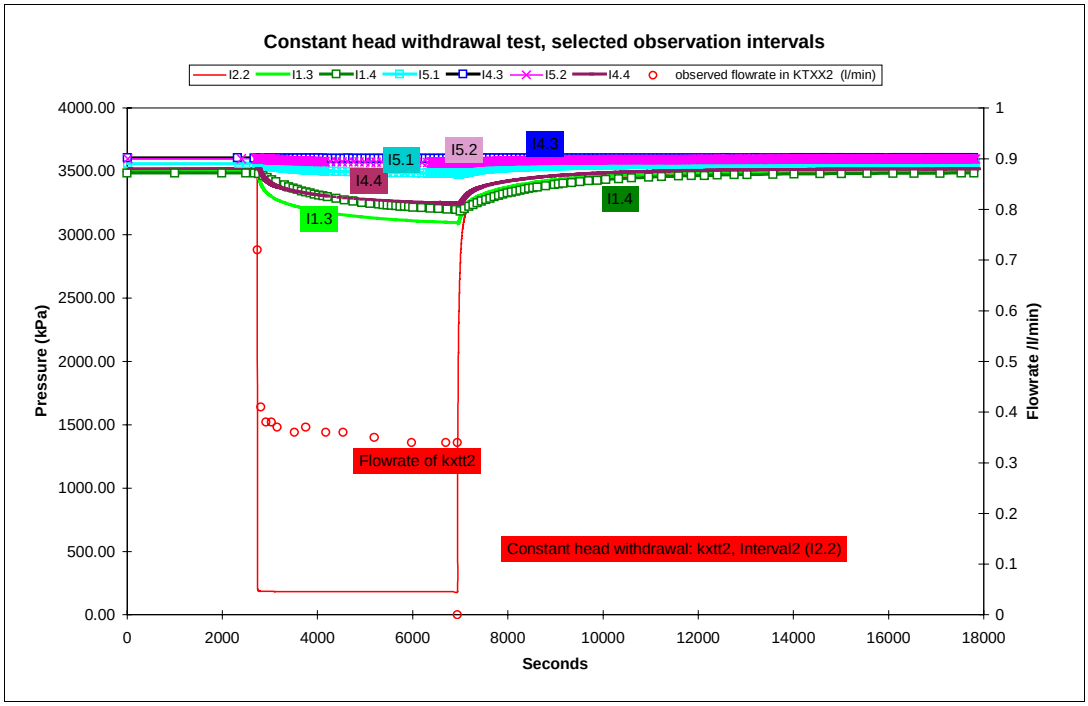

Figure 2-32. *Overview of interference test 5.*

transmissivities and storativities are presented in Figure 2-33 and in Appendices 6.1 and 6.2. Transmissivity values vary between $2 * 10^{-6}$ and $4 * 10^{-8}$ m^2/s and the storativities between $9*10^{-6}$ and $3 * 10^{-7}$ (storativites are dimensionless). These parameter values are comparable with those derived from the test evaluations by WINBERG (1996).

Step C consists of estimating hydraulic parameters by simulating test 5 with the well-bore simulator GTFM. Again interval 2 of borehole KXTT2 is chosen as the withdrawal interval, and intervals 3 and 4 in KXTT4 are the observation intervals. The first parameter estimates of step B were used as input values and were then subsequently varied until a best fit between measured and simulated pressures and flow could be obtained. The flow dimension was fixed as 2 (radial flow). A hydraulic conductivity of $2.5 * 10^{-8}$ m/s and a specific storativity of $5 * 10^{-7}$ m^{-1} were obtained (the corresponding transmissivity and storativity can be obtained by multiplying conductivity and storativity by the length of the observation interval). The results are shown in Figure 2-34. The surprising result was that measured and simulated values could only be fitted by introducing a positive skin factor s of nearly 12, even though such a skin appears difficult to justify on the basis of independent evidence. One reason could be a reduced hydraulic conductivity in the surroundings of the borehole wall.

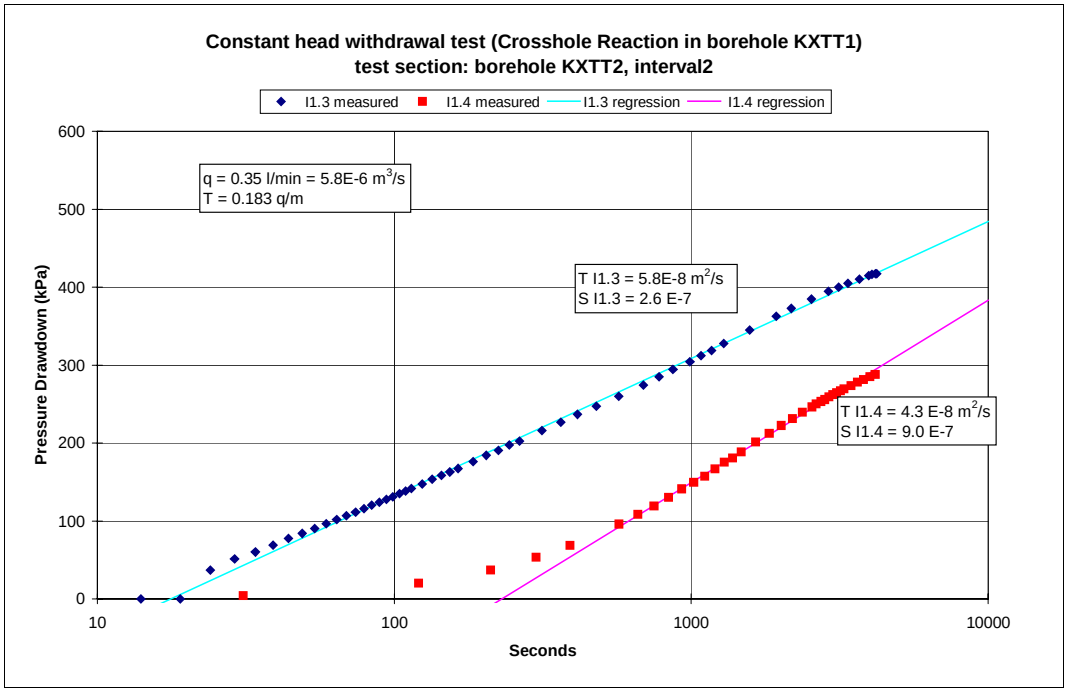

Figure 2-33. *Crosshole reactions in borehole KXTT1 and estimation of parameters.*

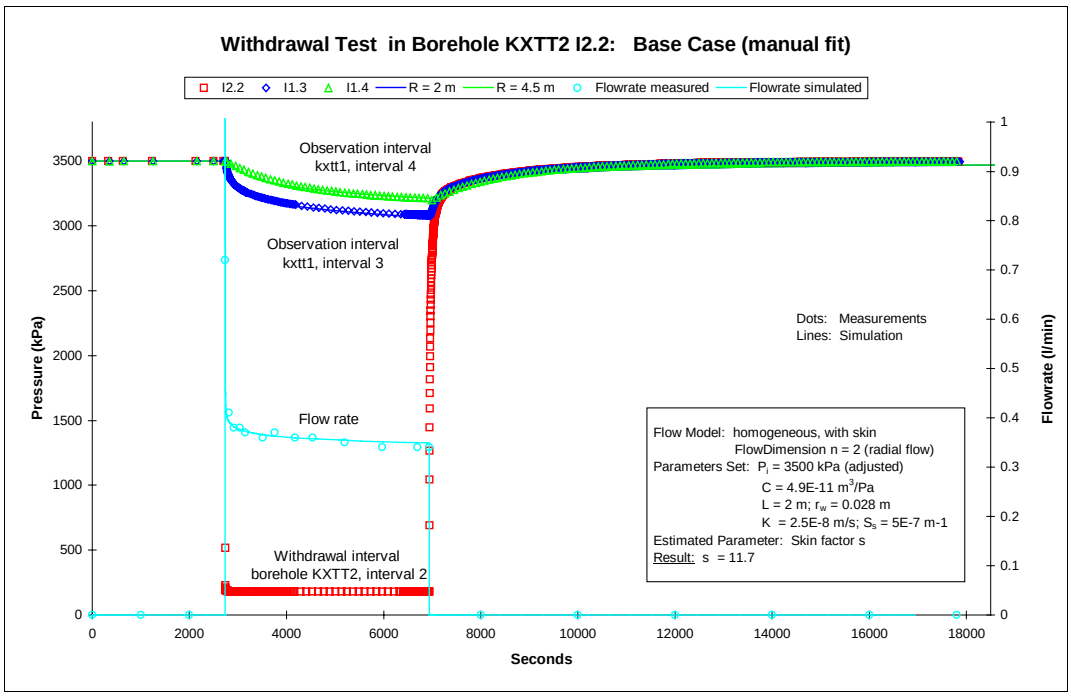

Figure 2-34. *Trial and error modelling of withdrawal test in borehole KXTT2, base case. Best fit is obtained with a positive skin factor. Inverse model options: see Appendices 6-3 - 6-5.*

Another, possibly more plausible argument might be a non-radial flow-field around the borehole, caused by fractures that intersect the borehole at acute angles (a radial flow-field would require at least fractures which are perpendicular to the borehole axis). The fracture network derived for the conceptual structural model also supports the idea of non-radial, highly tortuous flowpaths in the TRUE-1 block.

Step D consists of automatically estimating the parameters by an inverse (maximum likelihood) method. The trial and error estimations of hydraulic parameters of step C were used as the base case.

- In the first estimation (option 1, Figure 2-29), the skin factor was fixed to zero and the flow dimension, hydraulic conductivity and specific storativity were automatically estimated. However, it was not possible to adequately fit measured and simulated values. In particular, as shown in Appendix 6.3, measured and simulated flow rates largely disagree. A flow dimension of 2.35 has been estimated (tendency towards spherical flow). It is concluded that, without the introduction of a positive skin factor, no good fit is possible even with an inverse method.

- Option 2 (simulation shown in Appendix 6.4) considers a skin factor of 11.7 (as obtained in step C), but with an inverse estimation of the flow dimension, hydraulic conductivity and specific storativity. Although the fit is better than that of option 1 (especially the pressures), there is no satisfactory fit of measured and simulated values. A flow dimension of 1.85 has been estimated (tendency towards linear flow).

- In option 3 (simulation shown in Appendix 6.5) the flow dimension was fixed to 2.55, a value which has also been suggested by WINBERG et al. (1996). A value between 2 and 3 for the flow dimension means that pseudo-spherical flow occurs. The fit of the flow rate turned out to be better. On the other hand, the pressure fit becomes worse.

It is concluded that the hydraulic parameters obtained from the base case (step C, Figure 2-34) are the best parameter estimations (i.e. this case provides the best fit). This base case assumes a flow dimension of 2 and a positive skin factor of almost 12. The need to introduce a high positive skin factor (that is difficult to justify independently) may be an indication that the borehole wall is less transmissive than the rock. However this seems not to be the case because borehole-disturbed zones in granitic rocks normally exhibit a higher transmissivity than the undisturbed rock. Also, artificial borehole sealing before or during the hydraulic testing seems to be very unlikely. Another explanation could be that this positive skin factor is an indication that the homogeneous, infinite-acting radial flow system may not be the appropriate conceptual model for simulating flow in the fracture network of the TRUE-1 block. The next section explores whether the underlying assumptions for the calculations presented above have a sound basis or whether alternative sets of assumptions need to be considered.

2.7.3 Connectivity of the fracture network

In addition to the estimation of hydraulic parameters, the connectivity of the fracture network is another important parameter for deriving the conceptual hydrogeological

model. The interference tests ideally serve to check which test and observation intervals are connected (on the basis of measured drawdowns). To estimate this connectivity more quantitatively, WINBERG et al. (1996) derived a connectivity matrix, where measured drawdowns in observation intervals are normalised to the steady-state outflow in the test interval. The results of this connectivity matrix (see Tab. 4-15 in WINBERG et al. 1996) are visualised in Figure 2-35. The colour codes of the lines connecting the intervals indicate a ranking of connectivity, ranging from blue (excellent response) through green and red to yellow (poor response). The conclusions from this connectivity pattern include:

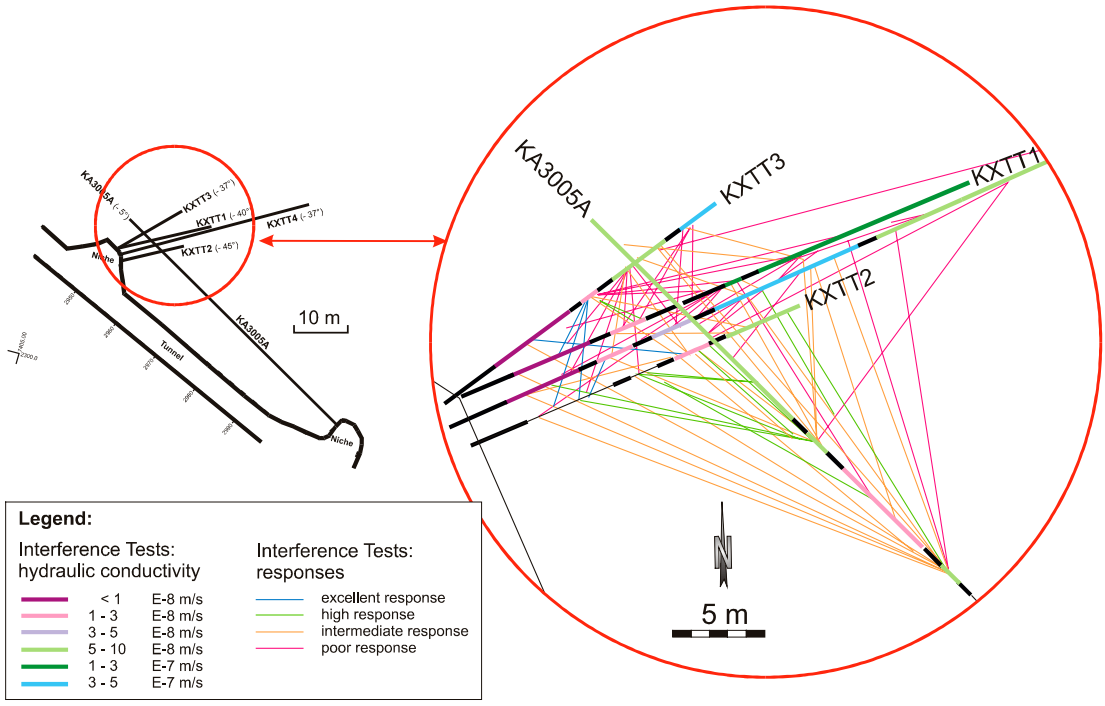

Figure 2-35. *Interval responses from interference tests (lines connecting test intervals indicating excellent, high, intermediate or poor responses). The colour of the test interval reflects hydraulic conductivity.*

- There is a clear spatial anisotropy of the responses. In spite of a possible bias from the geometry of the borehole array, most good connections trend in a NW-SE direction, whereas NE-SW connections tend to be poor.
- The highest responses are found between intervals with short separation distances. These are mainly the intervals 3 and 4 of the KXTT boreholes.
- The weakest responses can be observed between intervals with long distances in a NE-SW direction.

– Within the KXTT boreholes, intervals with higher responses appear to have lower hydraulic conductivities, and vice-versa (the hydraulic conductivities of most test intervals are also shown in Figure 2-35).

In order to evaluate and understand these findings, a conceptual question needs to be answered: what is the relationship between transmissivity and pressure response (drawdowns) in the TRUE-1 block? Figure 2-36 and Figure 2-37 visualise the problem. There are two basic alternatives:

– In a „classical" aquifer (porous continuum, homogeneous and infinite aquifer), high responses correspond to low conductivities, and vice-versa. This means that the highest pressure responses trend in a NW-SE direction, as observed, and are linked with the lowest fracture transmissivities (Figure 2-36b). The highest fracture transmissivities would trend in a NE-SW direction. All parameters derived in Chapter 2.7.2 are based on this concept.

– The alternative case is shown in Figure 2-37: The direction of highest transmissivities corresponds to that of highest pressure responses.

The flow logging data may be used to discriminate between the two concepts. Four boreholes (KXTT1-4) are oriented towards the NE, thus intersecting mainly the NW-SE trending fractures. One borehole (KA3005A) is oriented towards the NW, thus intersecting mainly the NE-SW trending fractures. The average inflow per metre in the KXTT 1-4 boreholes is higher by a factor 4 to 70 than that found in the KA3005A borehole (see Table 2-20). When the inflow is normalised to fracture frequency, then inflows in boreholes KXTT1, 3 and 4 are about 3 times higher than in KA3005A[*)]. Thus, the NW-SE oriented fractures seem to be clearly more transmissive than the NE-SW oriented ones and therefore the approach of Figure 2-37b, suggesting that the highest transmissivities are directly proportional to the highest pressure responses (drawdowns), seems to be plausible.

Table 2-20. Total inflows from TRUE-1 boreholes, derived from flow logging.

Borehole	Total inflow Q [litre/min]	Borehole length L [metre]	Flow per meter (Q/L) [litre/min*metre]
KXTT 1	77.20	28.76	2.68
KXTT2	2.39	18.30	0.13
KXTT3	11.50	17.43	0.66
KXTT4	84.0	49.31	1.70
KA3005A	1.90	50.50	0.04

[*)] This statement is not true for borehole KXTT2, where an unexpected small inflow of only 2.4 l/min has been measured. The inflow normalised to its fracture frequency is thus clearly smaller than the corresponding value for KA3005A.

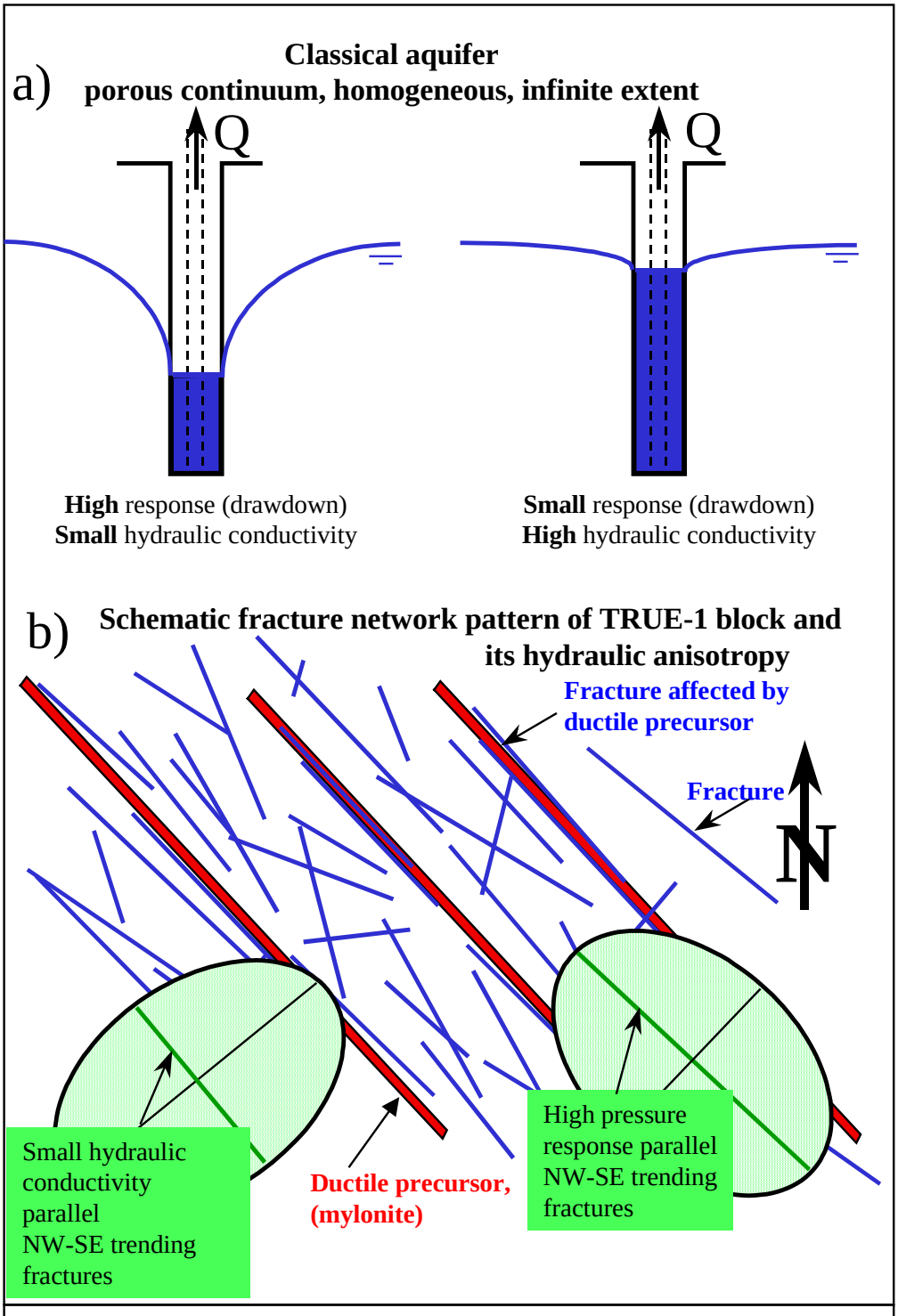

Hydraulic responses versus hydraulic conductivity: The hydraulic anisotropy (K-ellipse) does not coincide with the NW-SE trending fractures.

Figure 2-36. *Hydraulic responses vs. hydraulic conductivity: the* ***continuum*** *approach a) for a classical aquifer b) schematic fracture network and its hydraulic conductivity.*

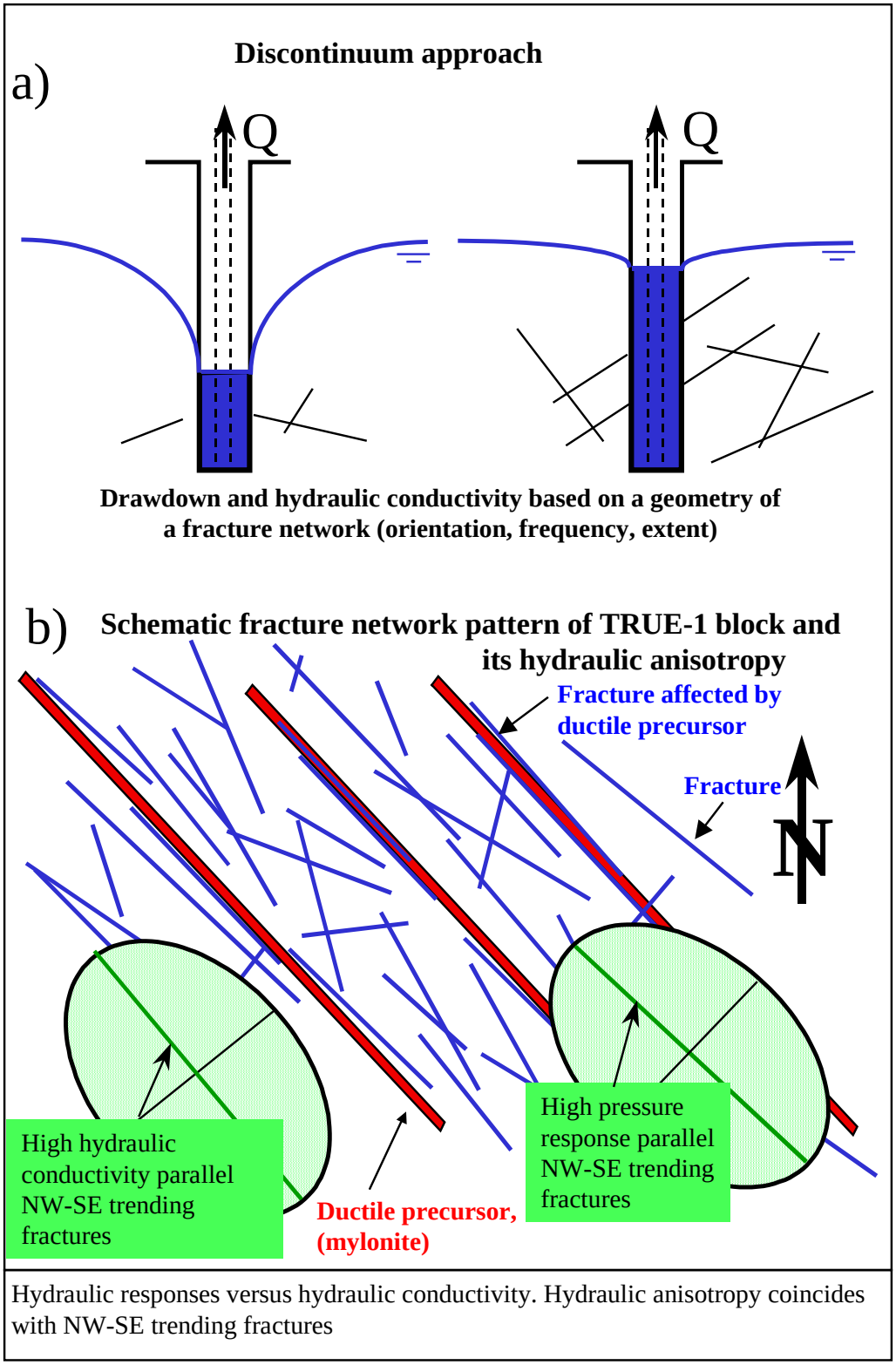

Hydraulic responses versus hydraulic conductivity. Hydraulic anisotropy coincides with NW-SE trending fractures

Figure 2-37. *Hydraulic responses vs. hydraulic conductivity: the* ***discontinuum*** *approach. a) for a fracture network b) schematic fracture network and its hydraulic conductivity.*

If this is the case, then the whole parameter estimation carried out in Chapter 2.7.2 is not valid: the underlying assumption of the borehole simulator is the validity of the Darcy law in a porous continuum, which would result in high transmissivities together with small drawdowns and vice versa (compare Figure 2-36a with Figure 2-37a).

Thus, the poor fit between observed and calculated drawdowns (and the introduction of an unlikely high, positive skin factor) is due to the application of the porous continuum model which seems to be inadequate in a fracture network such as the TRUE-1 block.

2.7.4 Relationships between structures and hydraulics in the TRUE-1 boreholes

In Figure 2-38, the inflows along selected TRUE-1 boreholes are cross-correlated with fracture frequency derived from BIP imaging. Inflow measurements relate to interval lengths of 0.5 m, and they thus clearly represent more than one single fracture. Additionally, in Appendix 6.6, inflows >0.5 l/min are shown for every borehole, together with the fracture logs. Inflows >5 l/min are indicated with precise values. The following conclusions can be drawn on the basis of these analyses:

- There is a very high variability of inflows along the boreholes (see also Table 2-20). The highest inflows have been measured in borehole KXTT4 where, at a depth of 20 m, an inflow of 33.4 l/min has been observed (Appendix 6.6d). In the deep part of borehole KXTT1 (Appendix 6.6a), 63 l/min were recorded over a distance of only 5 metres. The smallest inflows are recorded in borehole KA3005A, where inflows are always less than 1 l/min (Appendix 6.6e).

- Zones of high inflows in a borehole generally correspond with zones of increased fracture frequencies, but NOT vice versa. Zones of high fracture frequency may show very small or even unmeasurable inflows.

- The measured inflows demonstrate that the transmissivities of NW-SE directed fractures are higher than those of NE-SW directed fractures. In the NW directed borehole KA3005A, inflows are associated with zones where NW-SE striking fractures occur (Appendix 6.6e).Assuming steady-state conditions, transmissivity can be calculated from the flow logs. The highest value of $2 * 10^{-6}$ m^2/s (hydraulic conductivity = $4 * 10^{-6}$ m/s) was obtained in KXTT4 at 20 m. The smallest transmissivities are $<1 * 10^{-9}$ m^2/s and are found preferentially in KA3005A. Some of these transmissivity values are in clear contradiction to those derived from the interference tests (see Chapter 2.7.2). This discrepancy between measured and modelled results again casts some doubt on the validity of the conceptual assumptions underlying the evaluation of the interference tests (e.g. borehole simulator with continuum approach should not be applied in the fracture network of the TRUE-1 block).

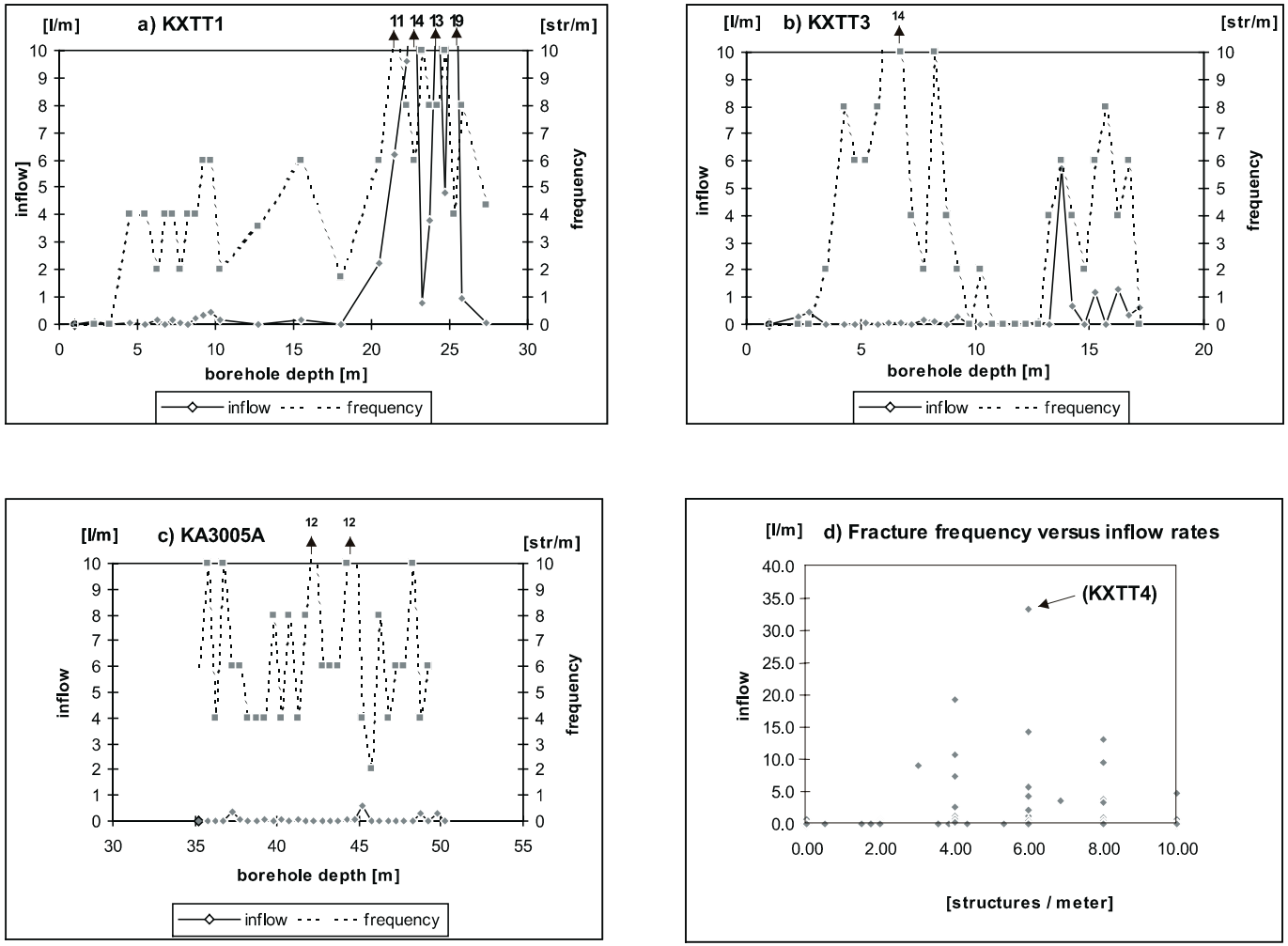

Figure 2-38. *Flow logging (withdrawal rates) compared with fracture frequency a) for borehole KXTT1, b) for borehole KXTT3, c) for borehole KA3005A, d) plot demonstrates that fracture frequency doesn't well correlate with inflow.*

Borehole inflows seem not to correlate well with fracture frequency (Figure 2-38 d), or any geological parameter, when analysing all boreholes together. By carrying out a correlation analysis as described in Chapter 2.3.2 for every borehole, different behaviours appear for different boreholes. Fracture and flow cross-correlation suggests that the frequency of open fractures has a weak positive correlation with inflows in boreholes KXTT1, KXTT2 and KXTT3. KXTT4, on the other hand, does not show a positive correlation with open fractures, but a negative correlation with tight fractures, i.e. many tight fractures in "dry" sections. Hydraulically active structures (i.e. water-conducting fractures) seem to intersect the boreholes both as single features and in swarms. Furthermore, rock types are not in any case correlated to flow. This shows that the Fine-grained Granite in the TRUE-1 volume is not more conductive than other rock types or that the flow logging resolution is too rough to reflect the relatively small volume of Fine-grained Granite in the TRUE-1 block.

The analysis of the correlation of fracture orientations with water inflows suggests that more than one orientation set of water-conducting fractures is present (3 orientation sets are defined for the TRUE-1 block, see Figure 2-11c), although the NW trending set is proportionally most abundant. However, the pattern of fractures in high inflow sections is still similar to the total sample of fractures. Furthermore, the correlation analysis of fractures and borehole inflow shows that the highest discharges are associated with altered fractures. Average inflows from fractures associated with ductile and cataclastic deformation cannot be distinguished from the total sample. Plotting the orientations of fractures characterised by high alteration in sections of high inflow reveals one steep NW trending set. This indicates that the largest conductors are often highly altered, with a fairly constant orientation towards the NW. This finding is in perfect agreement with the hydraulic anisotropy in the fracture network of the TRUE-1 block, with the highest transmissivities of fractures trending NW-SE.

2.7.5 Specific constraints on hydrogeological testing and conceptual structural models

In general, the hydraulic tests performed in the five boreholes support the idea of an interconnected fracture network in the TRUE-1 block. The hydraulic tests are in agreement with the fracture network outlined in the integrated structural model (Figure 2-27): the relatively short fractures are highly interconnected. This is supported particularly by the interference tests, demonstrating fairly quick drawdown reactions in all directions. Thus, a "Feature A" structure could be located at several places in the TRUE-1 block. Important for such a "Feature A" is only its orientation, which is the direction of the highest hydraulic conductivity (see also hydraulic anisotropy below) and the increased fracture frequency, the latter being linked to ductile precursors such as mylonites. In the following, the consequences for the conceptual structural model, as well as some recommendations for testing and modelling, are briefly outlined.

– **Consequences for the conceptual structural model:** The structural anisotropy fits well with the hydraulic anisotropy in the TRUE-1 block. NW-SE striking ductile precursors are responsible for the orientation of the fracture network, where NW-SE striking, steeply dipping fractures occur preferentially and thus define a structural anisotropy within the TRUE-1 block. These preferred fracture

orientations correlate directly with the highest transmissivities (see also hydraulic anisotropy below). On the other hand, only a part of these NW-SE striking fractures show high water inflows. One possibility could be that not all of these fractures are „sufficiently“ transmissive (>10^{-7} m^2/s) and that transmissivities may be highly variable, even in a single fracture.

- **Hydraulic anisotropy**: a rather pronounced anisotropy of hydraulic conductivity seems to exist in the TRUE-1 block. Hydraulic conductivities in NW-SE directions are clearly higher than in the NE-SW direction. This hydraulic anisotropy is mainly supported by the flow logging method, where inflows have been measured in differently oriented boreholes drilled into the TRUE-1 block (from the flow logging, an aspect ratio of 3 is expected). The parameter evaluation of the crosshole tests, based on a continuum approach, did not take account of this anisotropy.

- **Recommended tests for hydraulic parameter estimation in an environment such as the TRUE-1 block:** Crosshole tests in a fracture network as observed in the TRUE-1 block are of limited use when a homogeneous, isotropic continuum model is used to estimate parameters such as hydraulic transmissivity. Crosshole tests are more relevant when the connectivity of such a fracture network has to be qualitatively derived. To derive hydraulic conductivities, flow logging is a much quicker and also cheaper method.

- **Implications for solute transport experiments (tracer dipoles):** Advection-dispersion are assumed to be the relevant transport processes in the TRUE-1 fracture network. Diffusion may play an important role in the altered rock sections and in the fault gouges and fault breccias. The hydraulic and structural anisotropy suggests that NW-SE directed dipoles reveal quicker breakthroughs than the corresponding NE-SW ones. Breakthrough curves may become very complicated (multiple peaks) due to the fact that tracers are using all three fracture sets in the 3D network. To achieve 100% tracer recovery, very strong dipole fields may be necessary.

- **Implications for flow modelling:** The high skin factor derived by the fitting of observed and simulated pressures and flows may be an indication that porous continuum models are not appropriate for simulating flow in a 3D fracture network such as in the TRUE-1 block. It is recommended to use a discontinuum model for the flow modelling. The parameters derived in the conceptual structural model (fracture orientations, frequencies, and extents) should be used to discretise the fracture network (deterministic and stochastic, as was done in the integrated structural model, see Chapter 2.6). The hydraulic anisotropy can be assessed by taking into account the structural anisotropy (e.g. NW-SE striking fractures show higher transmissivities than NE-SW ones). A problem might be the assignment of the (expected) highly variable transmissivities to the fracture network itself, but also to individual fractures.

2.8 Conceptual model for tracer transport in "Feature A" and a generic block model of the TRUE-1 site.

The so-called "Feature A" is the target structure of the TRUE-1 project. WINBERG et al. (1996) define "Feature A" as a planar structure, dipping steeply towards ENE, with an extent of about 10 m and crossing the KXTT1-4 and KA3005 boreholes at well defined depths. Numerous hydraulic and tracer tests were carried out in "Feature A". It is visualised in several Figures of this report, i.e. Figures 2-17a, 2-24 and 2-25.

The analysis of the fracture network in the previous chapters has shown that "Feature A" is NOT a water-conducting fault in the sense of MAZUREK et al. (1996), where 5 types were distinguished (1. single fault, 2. swarm of single faults, 3. fault zone, 4. fault zone with rounded geometries and 5. parallel fault zones with long connecting splays). One common property of these water-conducting faults is a geometry persisting over several metres to decametres and an increased permeability (i.e. T > 1E-6 m^2/s). This is not the case for "Feature A", although this structure is also water-conducting. The "Feature A" structure was discussed in Chapter 2.4.5, resulting in the deterministic conceptual model shown in Figures 2-17a and 2-24.

In this Chapter, "Feature A" will be conceptualised taking into account the results from previous chapters, namely the geometry of the fracture network in the TRUE-1 block. Special emphasis is placed on the mineralogy of the structural units in "Feature A" and the fracture infill such as fault gouge. This is an important prerequisite for a conceptual model of solute transport.

The conceptualisation of "Feature A" will be performed on different scales. For solute transport, the conceptualisation is concentrated mainly on the small scale, not exceeding the range of one borehole diameter (< 0.1 m). On the other hand, it is of vital importance to have an idea of how "Feature A" looks on a larger scale such as the TRUE-1 block scale. This will be achieved by introducing a generic model of the TRUE-1 block. This generic block-scale model also takes into account the results of the previous chapters, namely the geometry of the fracture network in the TRUE-1 block.

2.8.1 Conceptualisation of "Feature A"

"Feature A" can be defined as an elongated zone of increased fracture frequency, with values between 5 and 25 fractures per m. This elongated zone is several metres long, with a varying width between 10 and 50 cm and mean width of about 25 cm. The individual fractures are short in extent, with fracture radii normally less than 0.50 m. Important for "Feature A" is the coincidence of structural and hydraulic anisotropy in the TRUE-1 block. NW-SE striking ductile precursors containing mylonites are responsible for the orientation of the fracture network, where NW-SE striking, steeply dipping fractures persist preferentially and thus define a structural anisotropy within the "Feature A" structure.

These preferred fracture orientations directly correlate with the highest hydraulic conductivities. Hydraulic conductivities in NW-SE directions are up to a factor of 3 higher than in NE-SW directions (see Chapter 2.7.4). Thus, the two prerequisites for any other structure similar to "Feature A" in the TRUE-1 block are 1) an increased fracture fre-

quency, which is linked to ductile precursors and 2) the "right" orientation, which is NW-SE.

According to WINBERG (1996), the "Feature A" structure crosses the KXTT1-4 and the KA3005 boreholes at defined depths[*)]. The method for conceptualising "Feature A" is now firstly to define the structural units which envelope this structure and then to define the mineralogy. In a second step, a conceptual model for solute transport on the small scale can be derived, taking into account the mineralogy of "Feature A".

The structural units are defined in Figure 2-39 and include undeformed and unaltered granitic matrix, mylonites, cataclasites, fractures with mineral coatings and open fractures, the latter initially filled with fault gouge material and mostly flushed out by the drilling operations. The mineralogy is now related to these structural units. The analytical results of this mineralogy are presented in Figure 2-39 and are based mainly on the findings of the classification and characterisation of water-conducting features at Äspö (MAZUREK et al. 1996). It is postulated that the fault gouge in fractures of the TRUE-1 block has the same overall mineralogy (mainly high contents of chlorites and a clay fraction) as the fault gouge in water-conducting faults.

The conceptualisation of "Feature A" is presented in Figures 2-40 – 2-42, which are based on the drillcore and BIP database of boreholes KXTT3 and KXTT4. The visualisation of "Feature A" is shown as a 40 centimetre long borehole log containing the structural units, together with the corresponding BIP images. Clearly visible are the ductile fabrics in the BIP logs (Figures 2-42a and 2-42b), acting as ductile precursors for the fractures. On this small scale, "Feature A" can be clearly described as a zone of increased fracture frequency. Over a zone of 40 centimetres, there are 8 fractures in KXTT3 and 5 fractures in KXTT4, leading to a fracture frequency of 20 m^{-1} and 12 m^{-1}, respectively. This is clearly higher than the average fracture frequency of 4.5 m^{-1} (see Figure 2-11a). Thus, a width for "Feature A" varying between 10 and 50 cm can be estimated. The conceptualisation of "Feature A" by WINBERG (1996) is also shown in Figures 2-40 and 2-41. The most prominent open fracture is chosen in the corresponding BIP logs and then correlated to one single planar structure. The pro and cons if "Feature A" fits more readily to a single planar structure or to a fracture cluster have been discussed previously (i.e. Chapter 2.4.5).

The conceptual model for solute transport is now shown in Figure 2-43. This conceptual model defines "Feature A" on the block scale as a NNW-SSE trending zone of increased fracture intensity. A single fracture from this fracture cluster is now selected and conceptualised on the microscopic scale (i.e. millimetre scale). The aperture width of the fracture varies between 1 and 5 mm. Of vital importance for this conceptual model is the existence of fault gouge material, filling the single fracture of "Feature A". While no gouge was observed in the cores, we assume by analogy with other fractures investigated by MAZUREK et al. (1996) that it was originally there and was flushed out during drilling.

[*)] Feature A crosses the KXTT1-4 and KA3005 boreholes at the following borehole depths: KXTT1 at 15.72 m, KXTT2 at 15.04 m and KXTT3 at 14.10 m, KXTT4 at 12.10 m and KA3005A at 44.97 m. These data were used to define a "Feature A" plane with an azimuth of dip of 61^{o}and a dip angle of 79^{o}.

Mineralogy of structural units of 'Feature A'

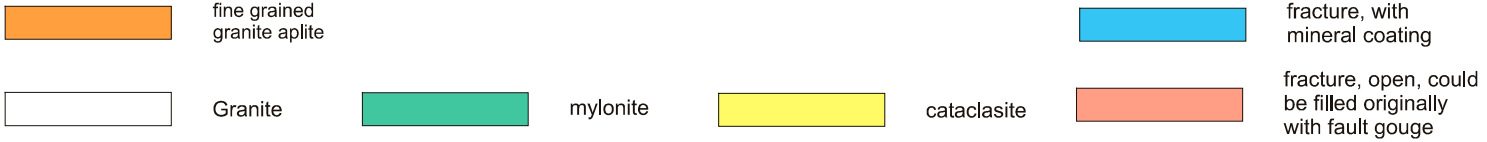

Granite (undeformed, unaltered)	
Mineralogy	[wt%]
Quartz	17
Plagioclase	44
K-feldspar	13
Biotite	13
Titanite	3
Opaques	2
Epidote	5
Chlorite	+
Sericite	+
Fe-Oxides	0
Calcite	+
Clay fraction:	minor or
Illite	absent
Ill/Sm ML	
Chlorite	
Chl/sm ML	
Porosity	0.3 [vol %]

Mylonite (foliated rock, unaltered):	
Mineralogy	[wt%]
Quartz	15
Plagioclase	30
K-feldspar	21
Biotite	23
Titanite	3
Opaques	+
Epidote	5
Chlorite	+
Sericite	+
Fe-Oxides	0
Calcite	+
Clay fraction:	minor or
Illite	absent
Ill/Sm ML	
Chlorite	
Chl/sm ML	
Porosity	0.05 [vol %]

Cataclasite:	
Mineralogy	[wt%]
Quartz	10
Plagioclase	14
K-feldspar	14
Biotite	+
Titanite	2
Opaques	+
Epidote	45
Chlorite	14
Sericite	+
Fe-Oxides	+
Calcite	+
Clay fraction:	minor
Illite	+
Ill/Sm ML	+
Chlorite	+
Chl/sm ML	+
Porosity	1.3 [vol %]

Fracture filled with fault gouge:	
Mineralogy	[wt%]
Quartz	12
Plagioclase	7
K-feldspar	11
Biotite	0
Titanite	3
Opaques	+
Epidote	4
Chlorite	44
Sericite	+
Fe-Oxides	+
Calcite	4
Clay fraction:	
Illite	+
Ill/Sm ML	+
Chlorite	8
Chl/sm ML	4
Porosity	10 - 20 [vol %]

"+" = occurence in trace amounts

Figure 2-39. *Definition of structural units and mineralogy of "Feature A".*

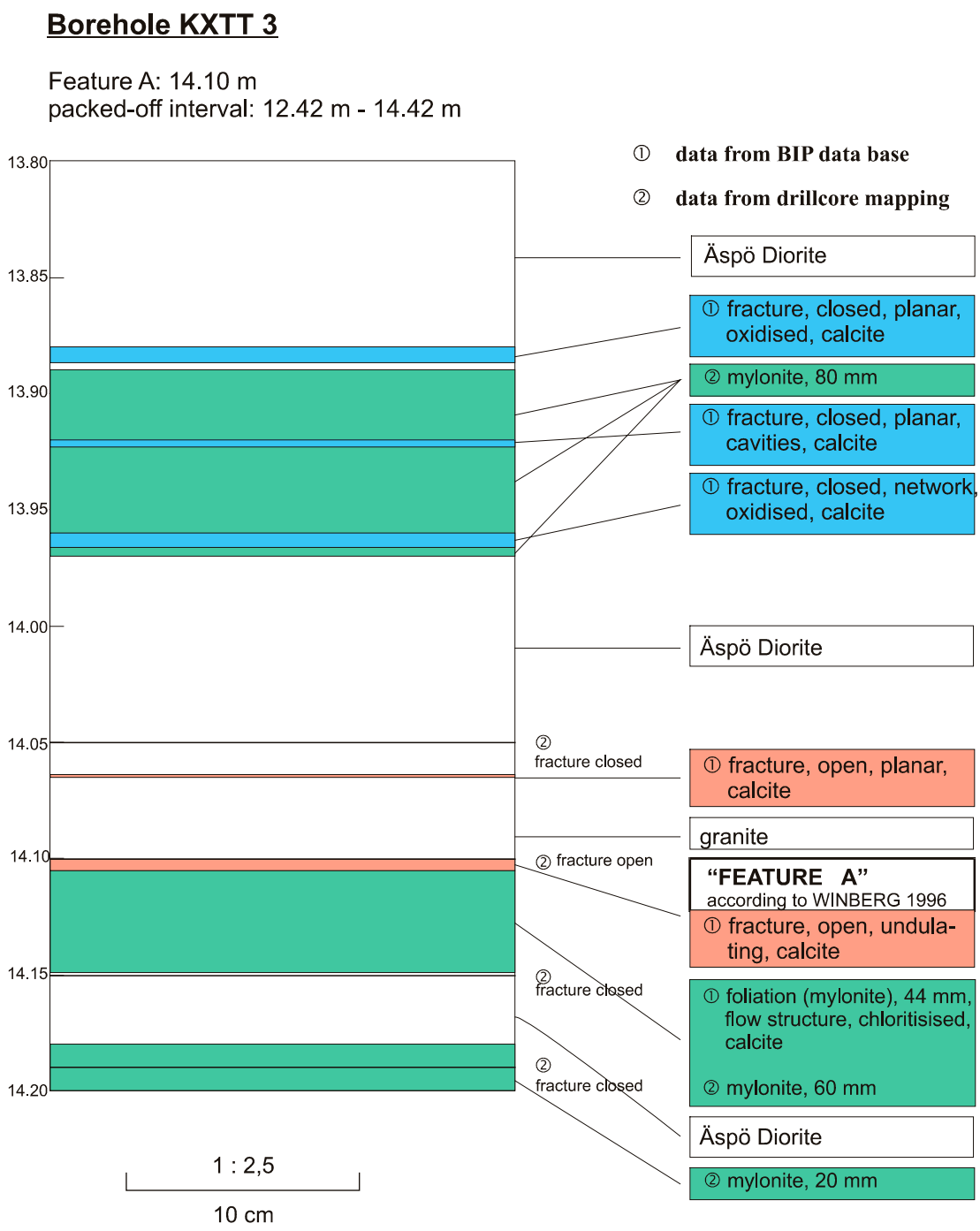

Figure 2-40. *Structural units of "Feature A", based on BIP images (see Figure 2-42a) and drillcore mapping in borehole KXTT3. The present report defines"Feature A" in borehole KXTT3 as the whole drillcore section between 13.80 and 14.20 m, whereas WINBERG (1996) relies only on the fracture at 14.10 m.*

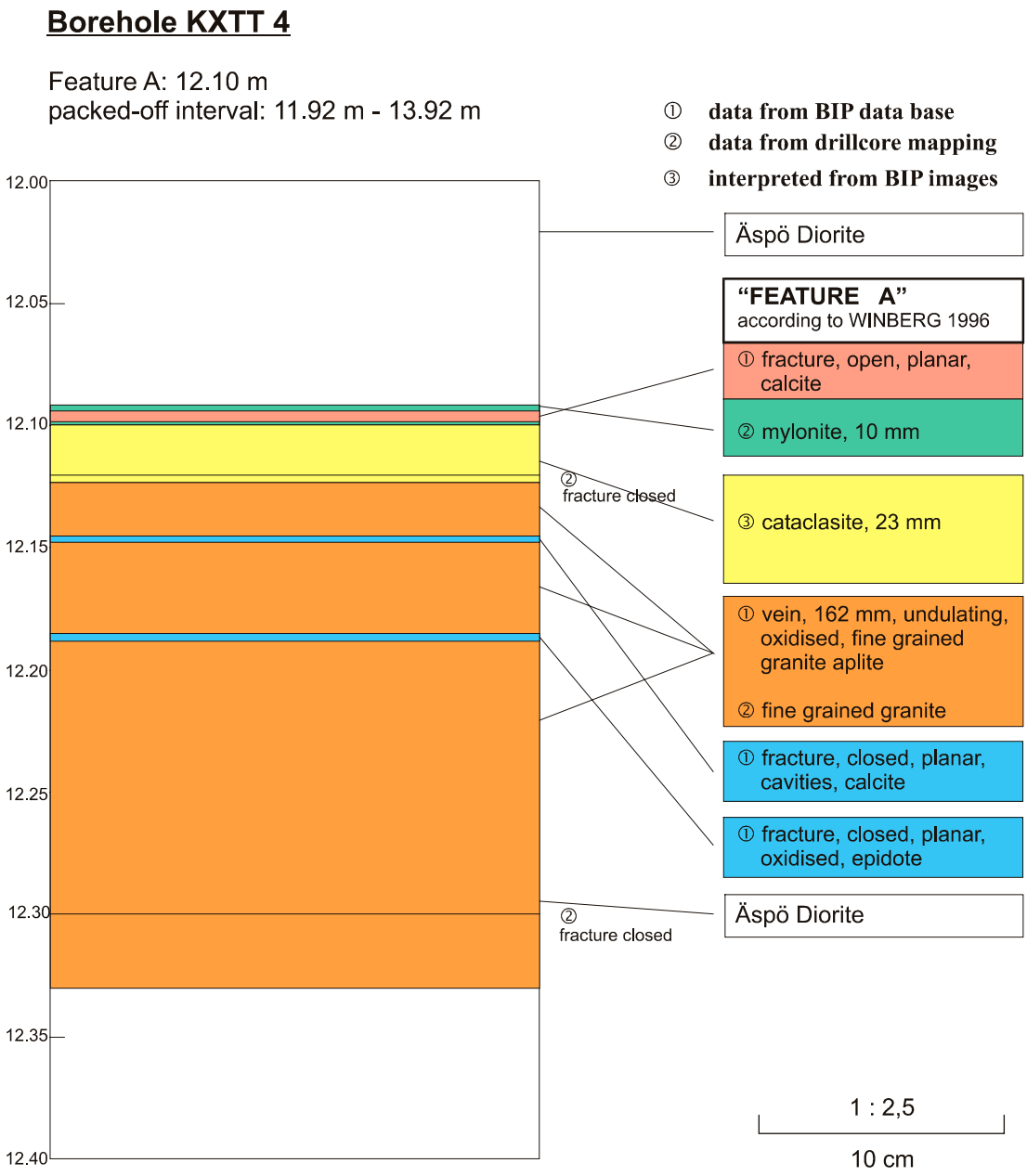

Figure 2-41. *Structural units of "Feature A", based on BIP images (see Figure 2-42b) and drillcore mapping in borehole KXTT4. The present report defines "Feature A" in borehole KXTT3 as the whole drillcore section between 12.00 and 12.40 m, whereas WINBERG (1996) relies only on the fracture at 12.10 m.*

Borehole KXTT3

a)

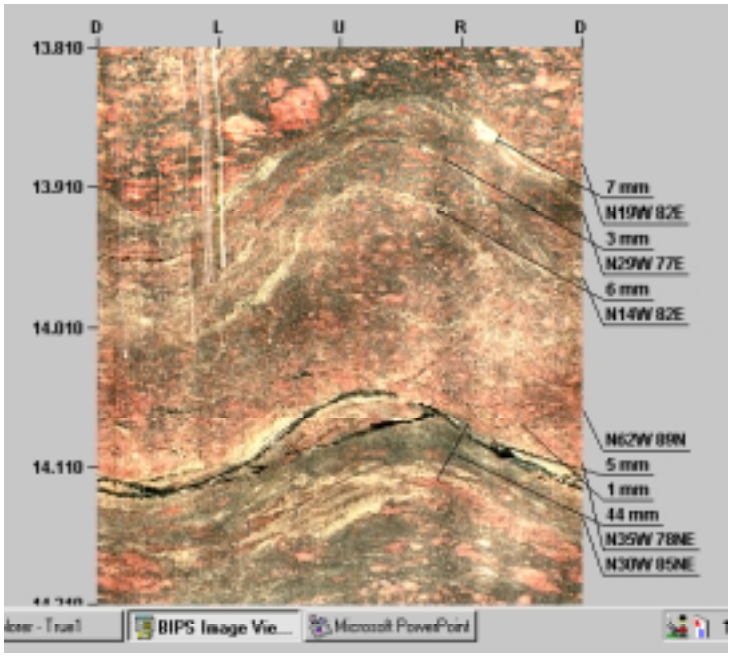

Feature A: 14.10 m

Borehole KXTT4

b)

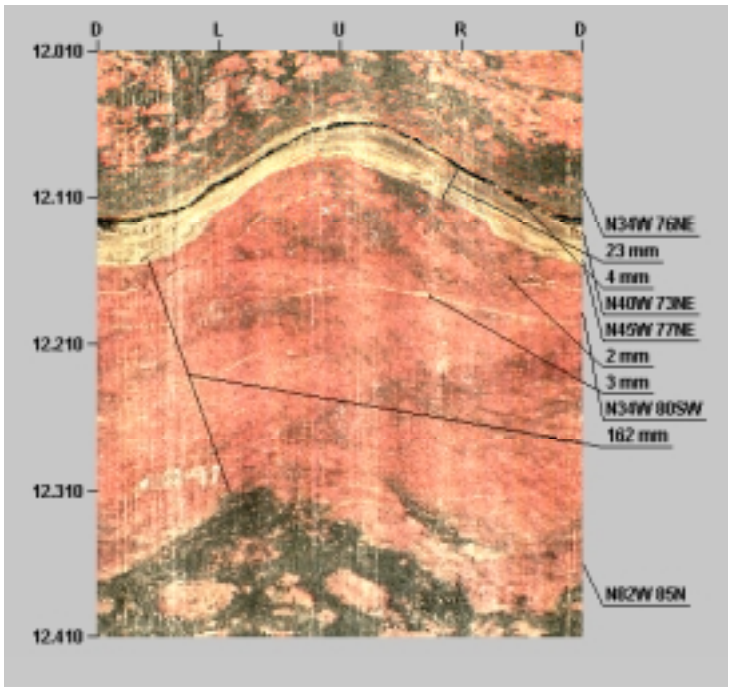

Feature A: 12.10 m

Figure 2-42. *BIP image of "Feature A", borehole KXTT4.*
a) borehole KXTT3 b) borehole KXTT4.

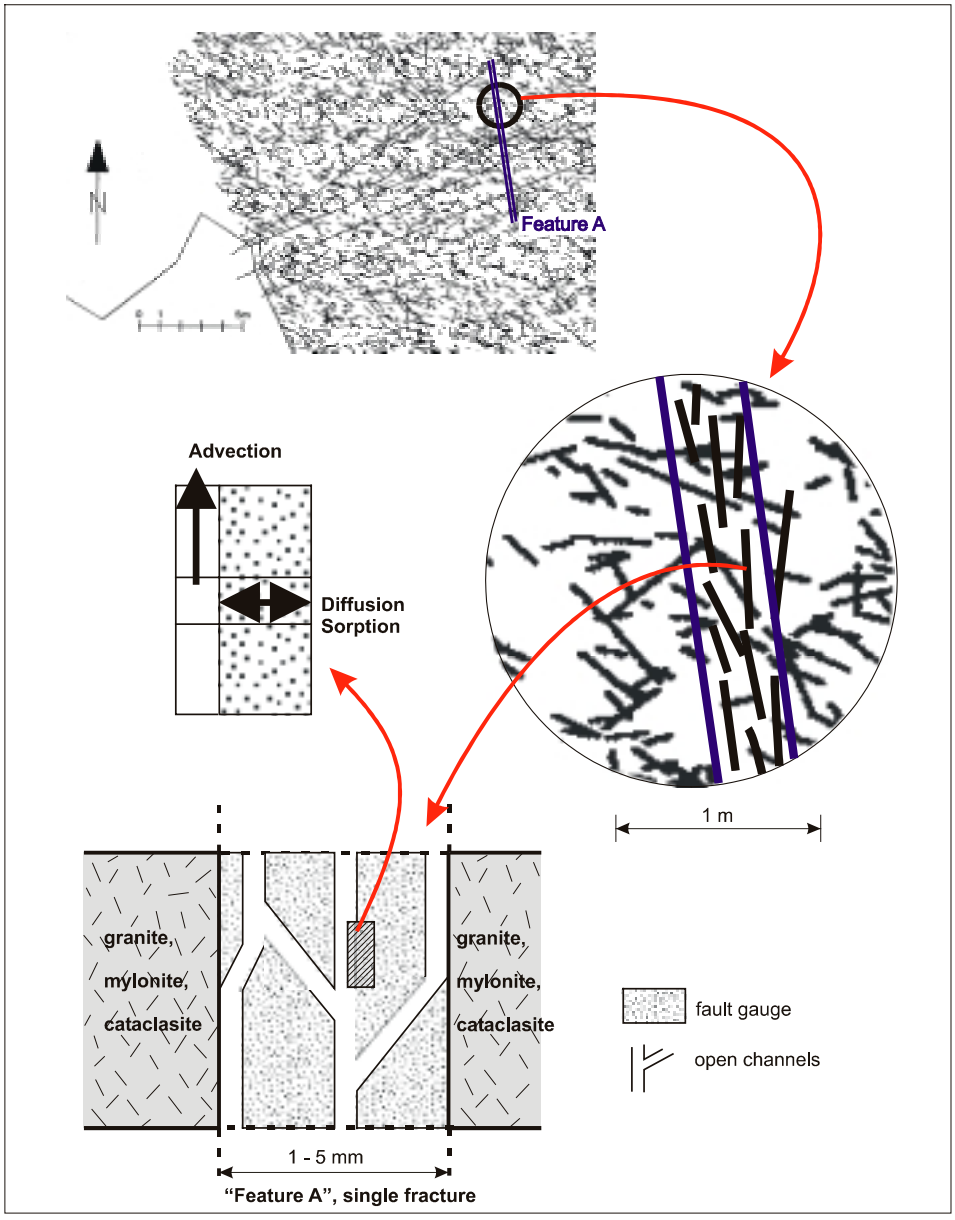

Figure 2-43. *Conceptual model of transport in "Feature A" (see also Figures 2-25 and 4-1).*

This conceptual model further assumes that the fault gouge is truncated by more or less parallel and open channels, especially at the interface of fracture and wallrock. The transport process in the parallel channels is mainly advection. The fault gouge itself has a quite high porosity (10-20 vol.%, see Figure 2-39), enabling diffusion into the fault gouge. During a tracer pulse test, this may be forward diffusion from the parallel channels into the fault gouge and later backward diffusion from the fault gouge into the parallel channels. Due to the extremely high specific surface of the clay fraction in the fault gouge, sorption is another key process to be taken into consideration when modelling solute transport. As a conclusion, the fault gouge in "Feature A" may highly retard tracer breakthroughs during solute transport experiments.

2.8.2 Generic block model of the TRUE-1 block

The TRUE-1 block, as an example of a block containing mainly small-scale discontinuities, has been described by an integrated conceptual structural model (Chapter 2.6). The visualisation of the 3D network was done mainly in 2D sections. One important aim of the generic model is to visualise the existing structures of the TRUE-1 block in 3 dimensions, taking into account the results of the fracture network study derived in the previous chapters. This generic block model can also be described as a "hand-made stochastic" realisation which is consistent with the database.

The generic block model is also of importance for understanding the “Feature A” structure. In the previous chapters, it has been concluded several times that “Feature A” is not composed of a single fracture, but more likely a zone of increased fracture frequency. Furthermore, similar structures to “Feature A” can be found elsewhere in the TRUE-1 block. These statements can be visualised readily in a generic block model.

The generic block model is presented in Figure 2-44. The model is a schematic visualisation containing all the results from the database analysis and the three-dimensional fracture network. Figure 2-44 presents, at the top, a cube of 25 m side length (similar to the scale of the TRUE-1 block). From this cube, two smaller cubes with side lengths of 5 m are isolated (scale of crosshole tests). These two cubes show the deformation pattern with and without ductile deformation, the latter resulting in an increased fracture frequency along ductile precursors. Finally, from these two cubes of intermediate scale, four further cubes are isolated with side lengths of 0.2 m, containing the full structural information (trace length, width, frequency, see data boxes at the bottom of Figure 2-44).

Special emphasis has been placed on deriving the geometric data of the fractures and the structural units in the small cubes. The ranges and means are consistent with the database. Note that the fracture frequencies in the 25 m and 5 m cubes are still too low, but drawing the fractures with the same density as defined in the database would lead to an unreadable black cube. All the other characteristics such as fracture orientations and trace lengths are consistent with the database.

The major conclusions of this generic model are:

- The fracture pattern is mainly influenced by ductile precursors, leading to zones of increased fracture frequencies.

- The fracture network is very dense and well interconnected in three dimensions in the whole TRUE-1 block, both within and outside regions with ductile precursors.

- Fracture trace lengths are generally small. Water-conducting faults as described in MAZUREK et al. (1996) were not observed in the TRUE-1 block and thus not implemented in the generic block model.

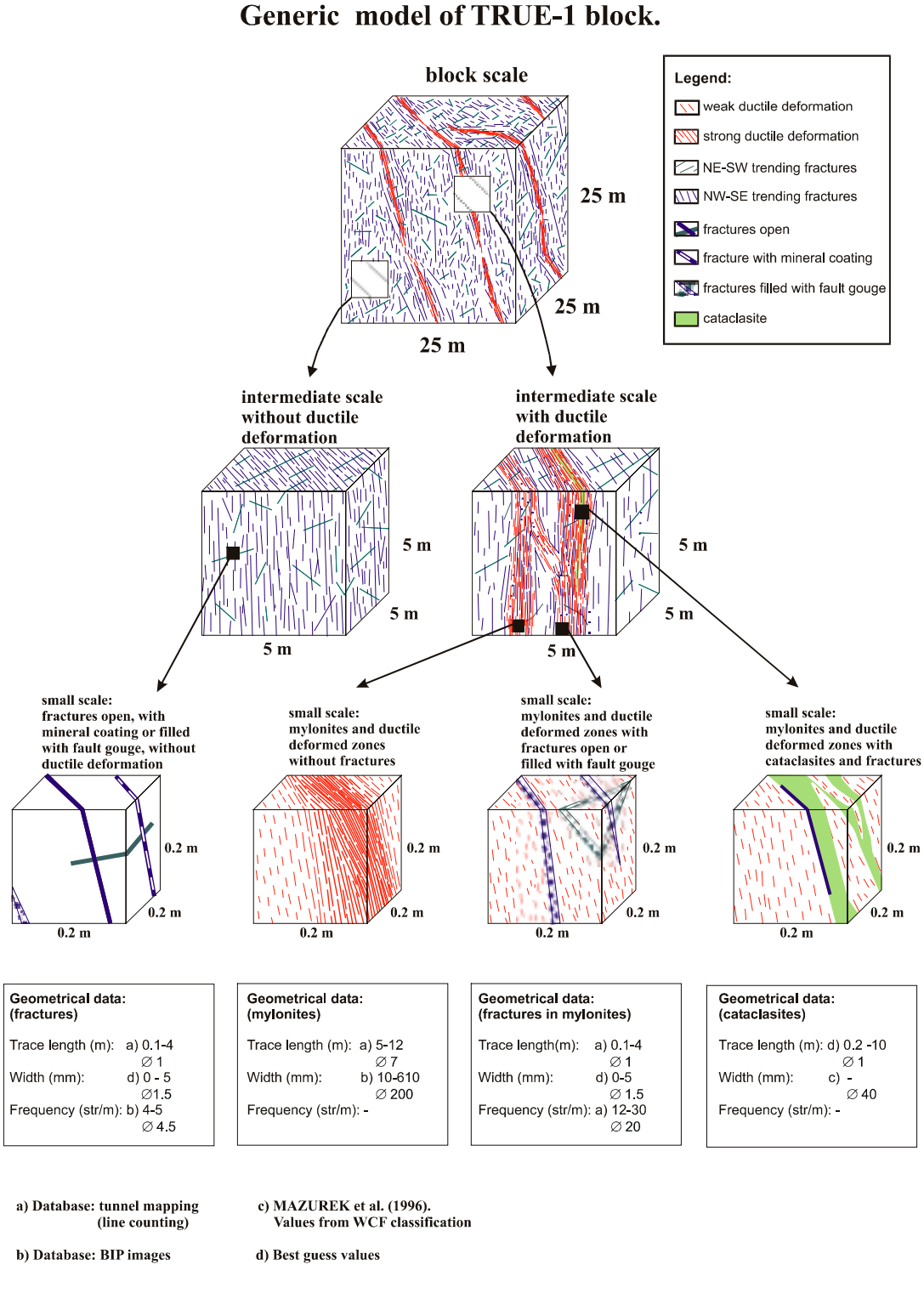

Figure 2-44. *The generic model of the TRUE-1 block.*

3. Large-scale structures and flowpaths, scaling relationships

3.1 Introduction

Chapter 2 focused on the characterisation of the 3-dimensional structure of the TRUE-1 block, i.e. a small rock volume devoid of major water-conducting features. The size of the block is that of a cube with side lengths in the range of several metres. Previously, MAZUREK et al. (1996) characterised the medium-scale structures, i.e. those that visibly discharge into the tunnel, cross-cut the entire tunnel diameter, and are thus longer than approx. 5 m. The transmissivities of these structures exceed those measured in the TRUE-1 block. Even larger structures, such as major faults that are also mappable at the surface, were penetrated by the tunnel and often have transmissivities exceeding those of the medium-scale structures described by MAZUREK et al. (1996). These findings suggest that hydraulic parameters are scale-dependent, as suggested previously by several authors.

While the available dataset is insufficient for defining an explicit relationship between scale and hydraulic properties, the derivation of scaling relationships appears feasible for the geometry of the fracture network. Geometric/structural data from the Äspö region are available on a wide range of scales. This chapter presents these data and addresses the question whether small-scale fracture networks are self-similar to large-scale fault zones. If so, any fracture network on a larger scale could be derived (modelled) from a small-scale network or vice versa. Together with the conclusions from regional hydraulic data (mainly hydrotesting results in and around the Äspö Hard Rock Laboratory), and the integration of hydrochemical data, the structural and hydraulic interconnectedness of the Äspö fracture and fault network on any scale is highlighted.

3.2 Database

Twelve fracture maps were used as the basis for geometric analysis, and the main characteristics are summarised in Table 3-1. Three maps are taken from MAZUREK et al. (1996), two maps are from a Swedish Nuclear Power Inspectorate study (SKI, 1996) and the remaining maps have been produced specifically for this report. The scales of the maps vary between 1 : 25 and 1 : 100'000, and the mapped areas range between ca. 2 m^2 and about 1200 km^2. All maps are based on geological/structural mapping, with the exception of the two large-scale maps taken from SKI (1996) that result from the analysis of lineaments. Maps of both horizontal and vertical sections are available. All maps are shown in Figure 3-1 to Figure 3-8. The localities of the maps are indicated in Table 3-1. The five surface maps correspond mainly to Äspö and Ävrö islands and the seven tunnel maps were elaborated at different locations along the tunnel and in niches of the Äspö Hard Rock Laboratory. All maps were digitised, resulting in a database of fracture orientations and traces. The database consists of 2382 fracture data. The elaboration and evaluation of this database was done in collaboration with the University of Freiburg/Germany and the detailed stochastic analyses will be presented in a diploma

thesis (GLÜCK 2001, in preparation). This report presents a part of these analyses (Figures 3-9 - 3-11 and Appendix 7) and gives the main conclusions.

Table 3-1. Overview of structural surface and tunnel maps.

No	Figure number	Title	Location in tunnel	Observation window	Scale	Reference	Remarks
Surface maps							
1	Figure 3-1 a	Äspö regional		30 km x 30 km	1: 10'000	SKI, 1996	
2	Figure 3-1 b	Äspö local		1 km x 1.5 km	1:500	SKI, 1996	
3	Figure 3-2 a	Äspö West		85 m x 30 m	1:50	This report	
4	Figure 3-2 b	Äspö village		6 m x 7 m	1:250	MAZUREK et al., 1996	
5	Figure 3-3	Avrö		30 m x 60 m	1:100	This report	
Tunnel maps							
6	Figure 3-4	Äspö HRL	Tunnel metre 1978 - 2003	6 m x 25 m	1:100	MAZUREK et al., 1996	Fault zone, tunnel roof
7	Figure 3-5 a	Äspö HRL	Tunnel metre 3580	2 m x 2 m	1:25	This report	
8	Figure 3-5 b	Äspö HRL	Tunnel metre 2050	1.5 m x 1.75 m	1:100	This report	Fine-grained Granite
9	Figure 3-5 c	Äspö HRL	Tunnel metre 2963	2.5 m x 2.75 m	1:25	This report	TRUE-1 site
10	Figure 3-6	Äspö HRL	Tunnel metre 2232 - 2260	2 m x 28 m		This report	Fine-grained Granite
1 1	Figure 3-7	Äspö HRL	Tunnel metre 2944 - 3004	4 m x 60 m	1:100	WINBERG et al., 1996 and this report (see also Figure 2.9 and Appendix 4)	TRUE-1 site
12	Figure 3-8	Äspö HRL	Tunnel metre 3124	2 m x 4 m	1:25	MAZUREK et al., 1996	Single fault, Assembly Hall

The hydraulic responses of the fracture and fault network during and after the construction of the Äspö Hard Rock Laboratory have been measured in great detail and documented in numerous SKB reports. Thus, our database consists mainly of these reports. The important ones, covering our aim, are:

PR 25-92-18, where large-scale hydraulic interference reactions were recorded during the excavation of the Äspö HRL. Of special interest is the hydraulic response when crossing the NE-1 and NE-3 major fault zones (PR 25-92-18 is not listed in the references).

- PR 25-92-18c, where rather high transmissivities of interference tests were calculated (see Table 5.1 of that report). It has to be emphasised that the network of test and observation boreholes covers Äspö, Ävrö, Bockholem and Laxemar (PR 25-92-18c is not listed in the references).

- PR 25-94-39, dealing with the hydraulic response in one borehole during the drilling of other (remote) boreholes through water-conducting faults. (PR 25-94-39 is not listed in the references).

- RHEN and FORSMARK (2000), where highly transmissive fractures and faults of Southern Äspö are documented. The evaluated data are based on observations during the construction phase and post long-term hydraulic monitoring.

Of special interest for our purpose are extended fault zones with high transmissivities (high permeability features), discharging into the tunnel during the construction of the rock laboratory, and their related hydraulic pressure drawdowns in neighbouring areas.

3.3 Methodology

All fractures shown on the twelve structural maps of Figures 3-1 to 3-8 were numbered for unique identification. Data acquired from the maps included

- fracture trace length

- fracture orientation (e.g. azimuth of dip for horizontal maps)

- junction type

For the comments, the attributes “contained”, “dissecting” and “transsecting” have been distinguished:

- *contained:* both ends of the fracture trace are within the observation window

- *dissected:* one end of the fracture is within the observation window, the other end is beyond the mapped area

- *transsected:* the fracture cuts through the entire observation window, with both ends beyond the mapped area.

Trace lengths and azimuths of dip were digitised in Autocad, resulting in a database of fracture orientations, trace lengths and junction types of all maps.

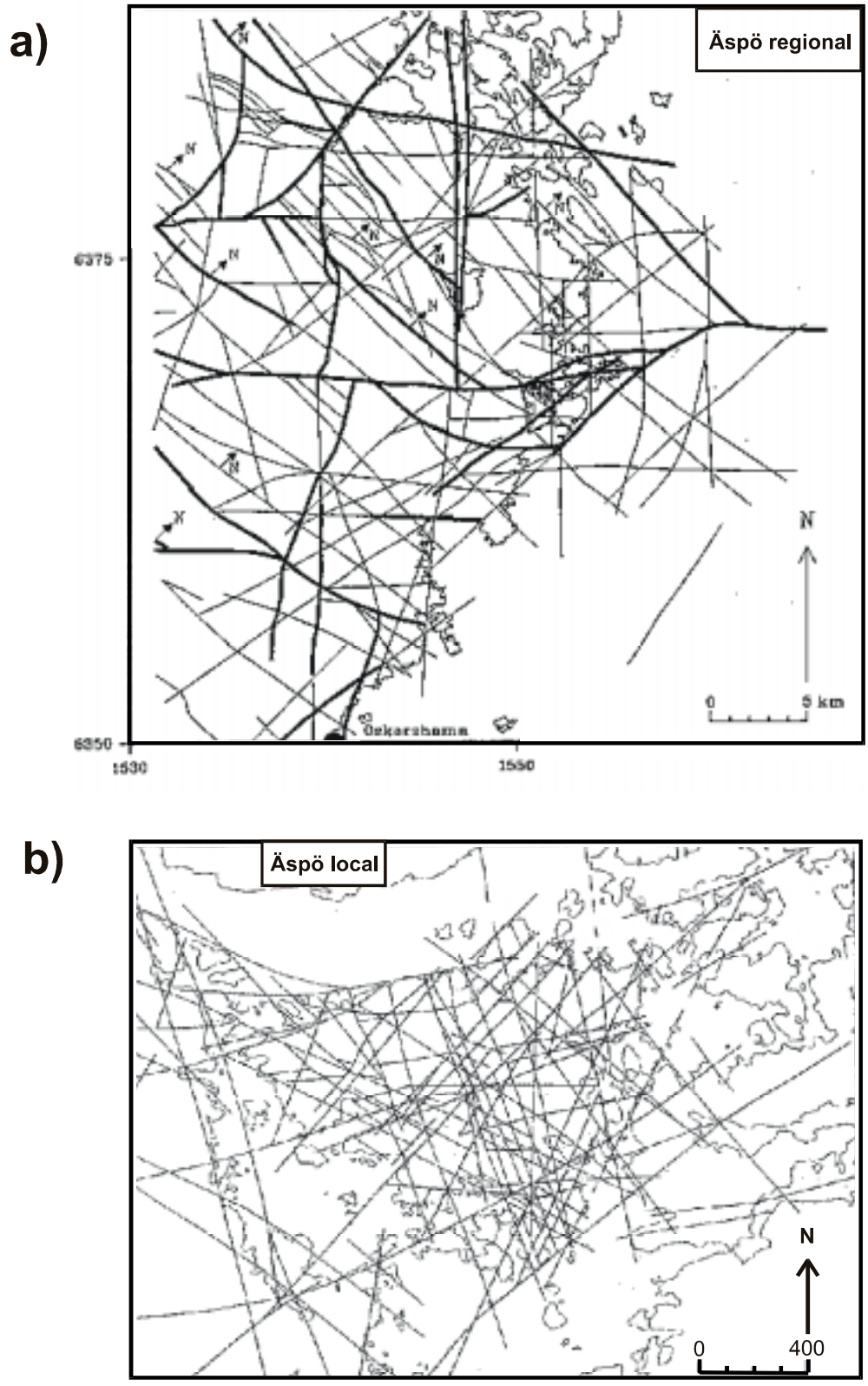

Figure 3-1. *Major structural surface discontinuities in horizontal sections a) Äspö regional scale b) Äspö local scale.*

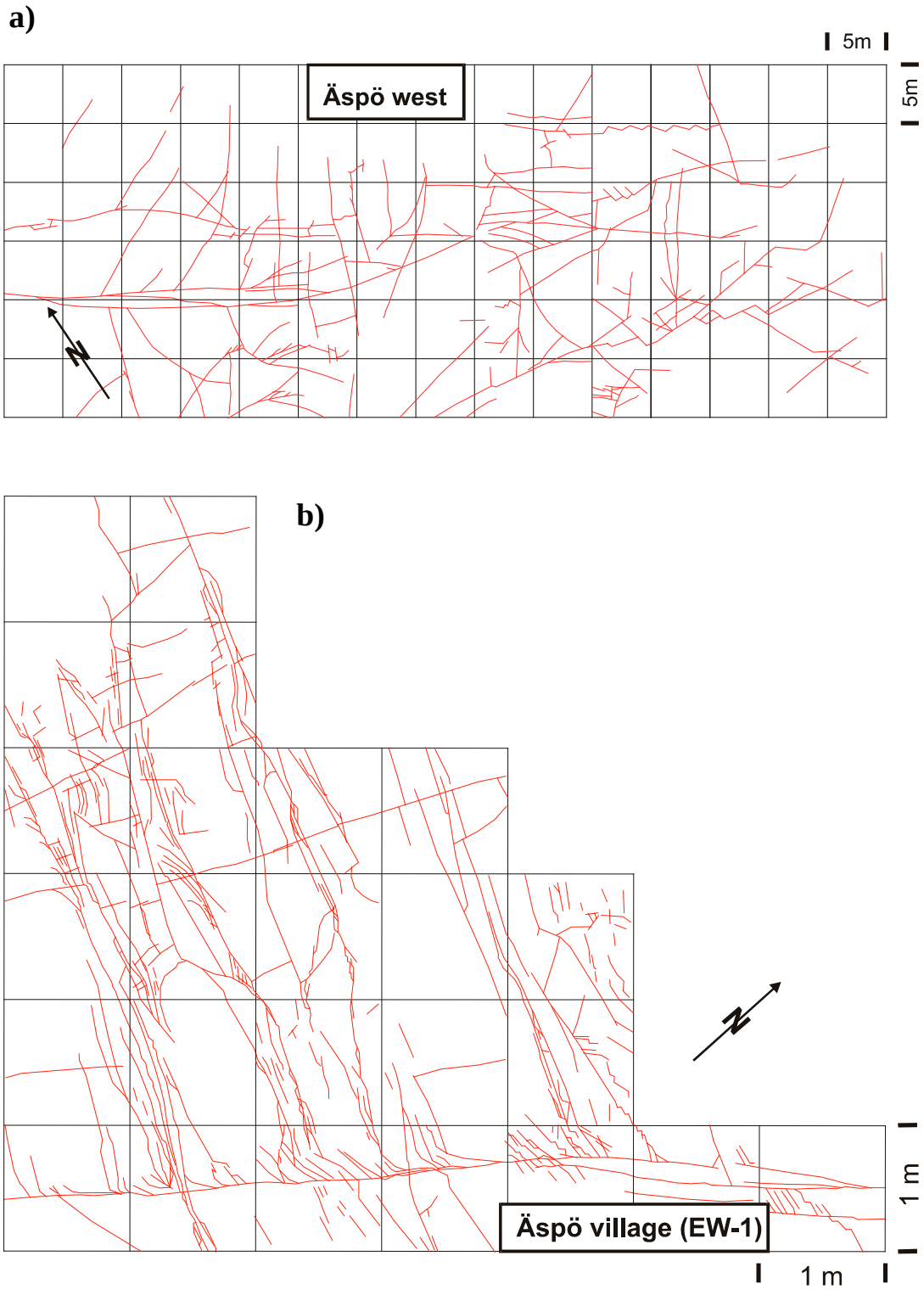

Figure 3-2. *Structural surface maps in horizontal sections a) Äspö West and b) outcrop at Äspö village.*

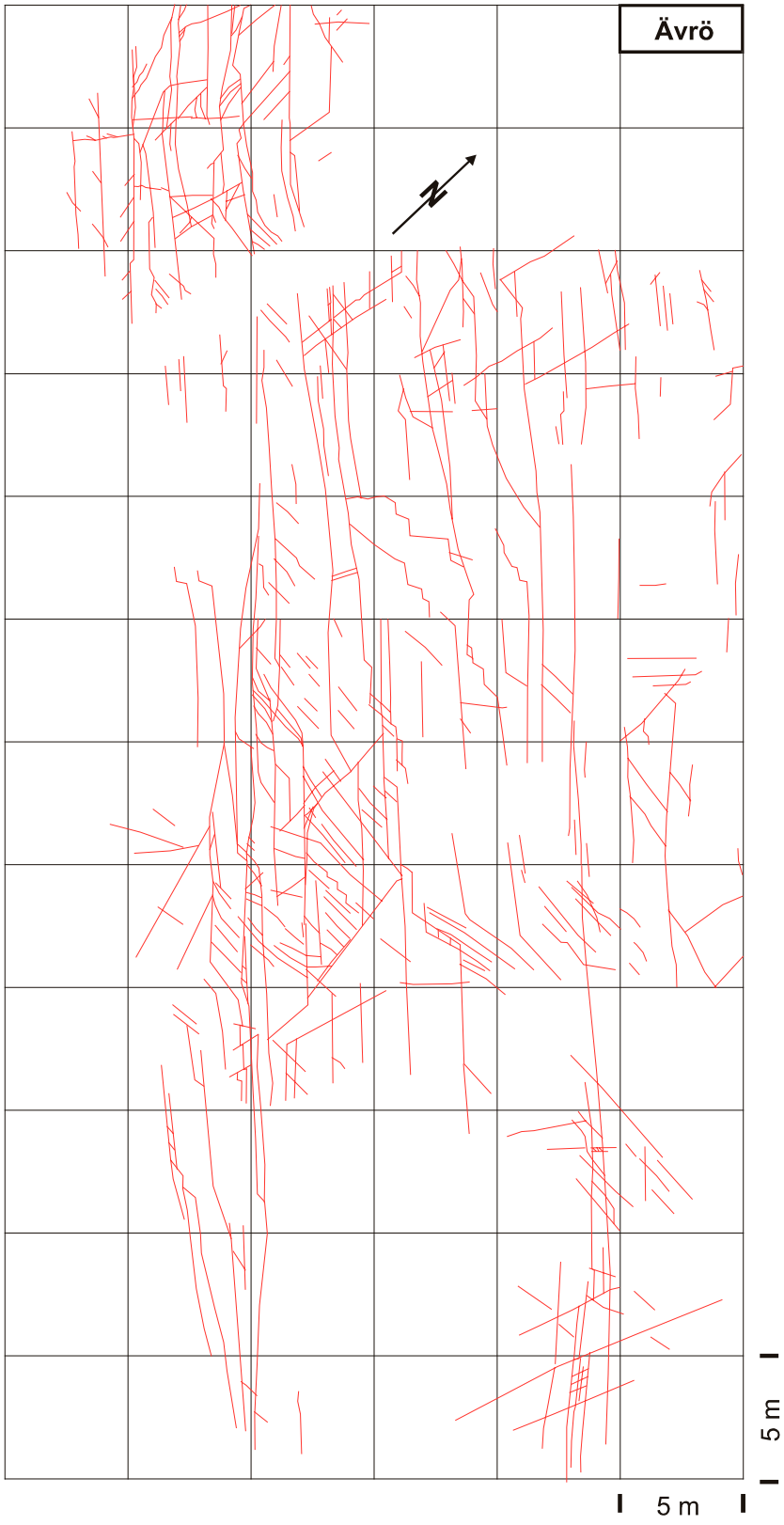

Figure 3-3. *Structural surface map in horizontal section. Outcrop at Ävrö island.*

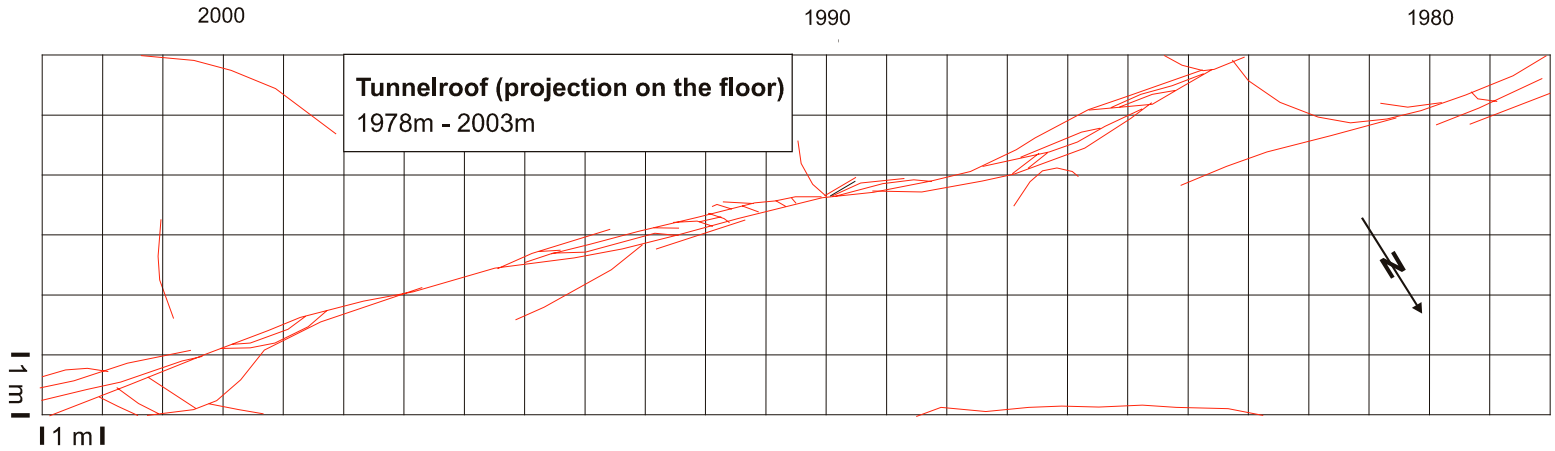

Figure 3-4. *Structural map at Äspö rock laboratory, tunnel metre 1978 – 2003. Projection of tunnel roof onto horizontal section.*

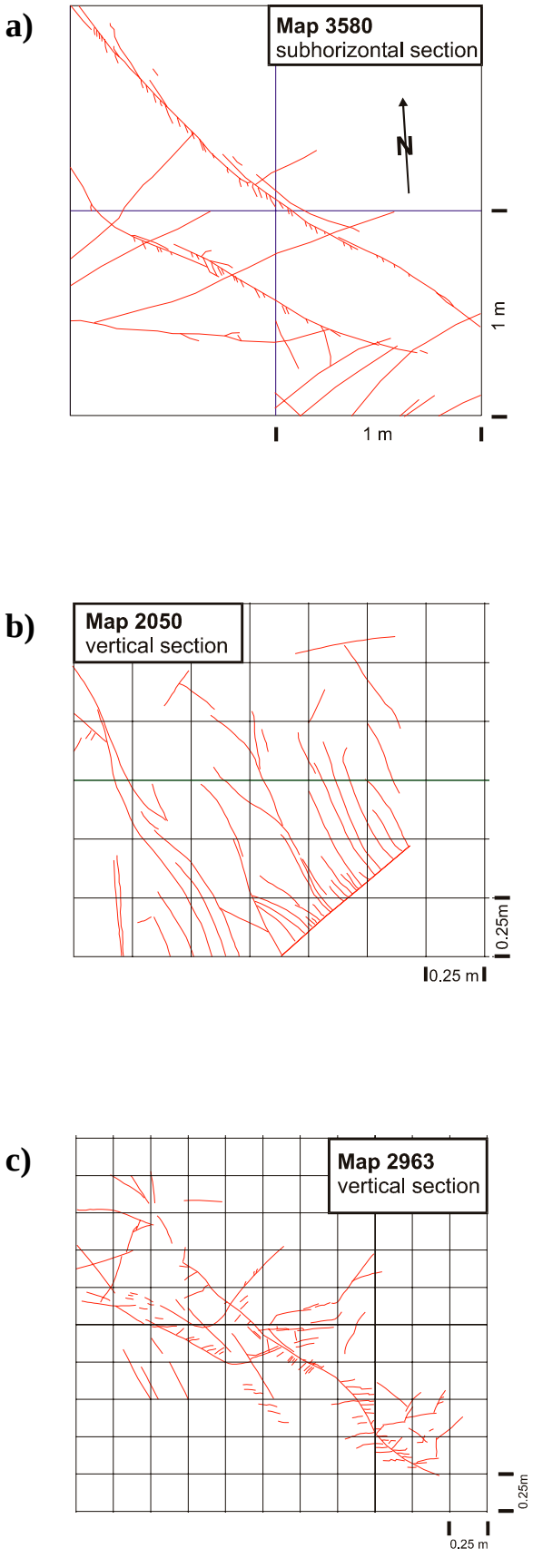

Figure 3-5. *Small scale structural maps at Äspö rock laboratory, all vertical sections a) tunnel metre 3580, b) tunnel metre 2050 and c) tunnel metre 2963.*

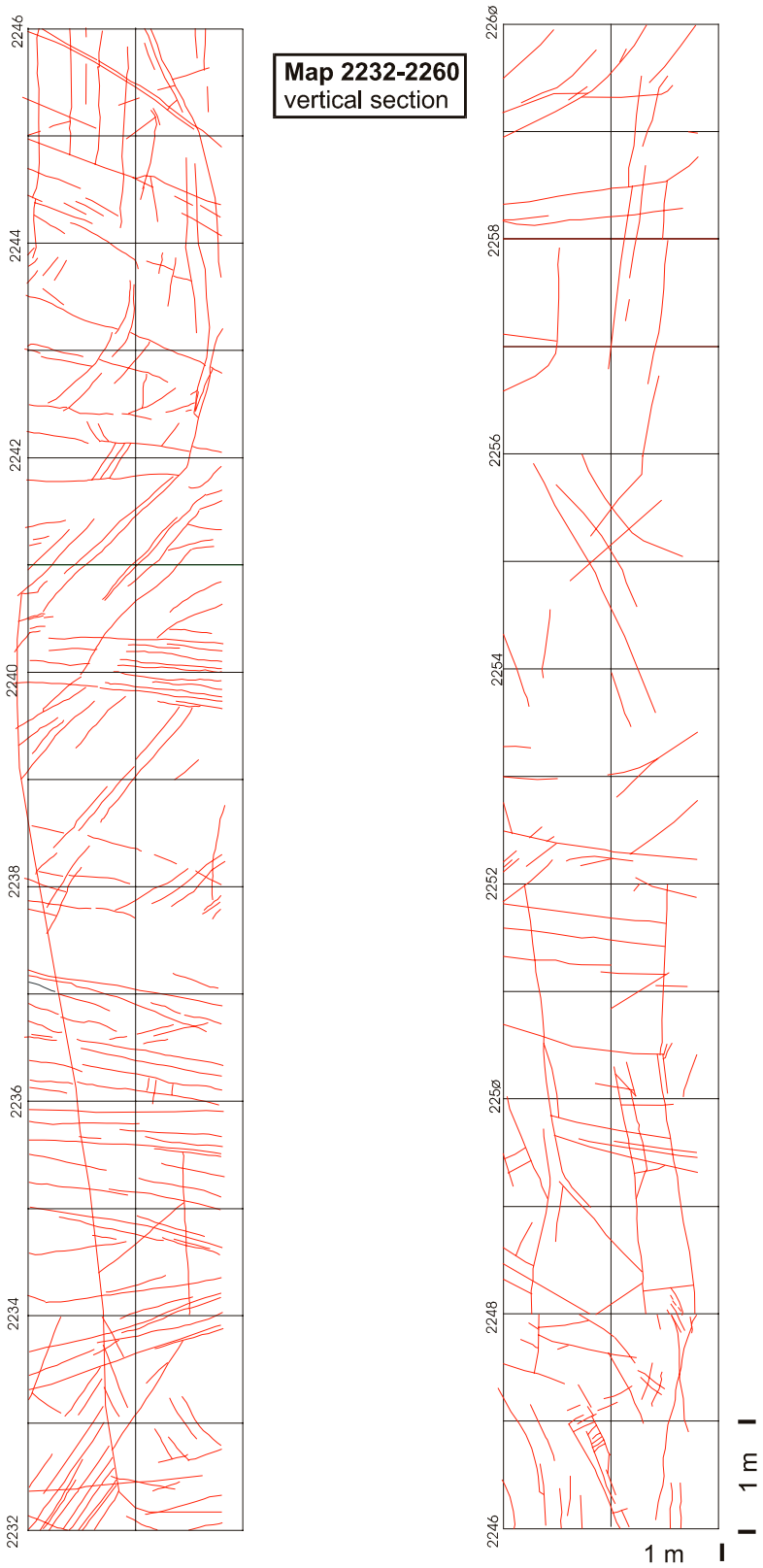

Figure 3-6. *Structural mapof tunnel wall at Äspö rock laboratory, vertical section. Tunnel metre 2232 - 2260.*

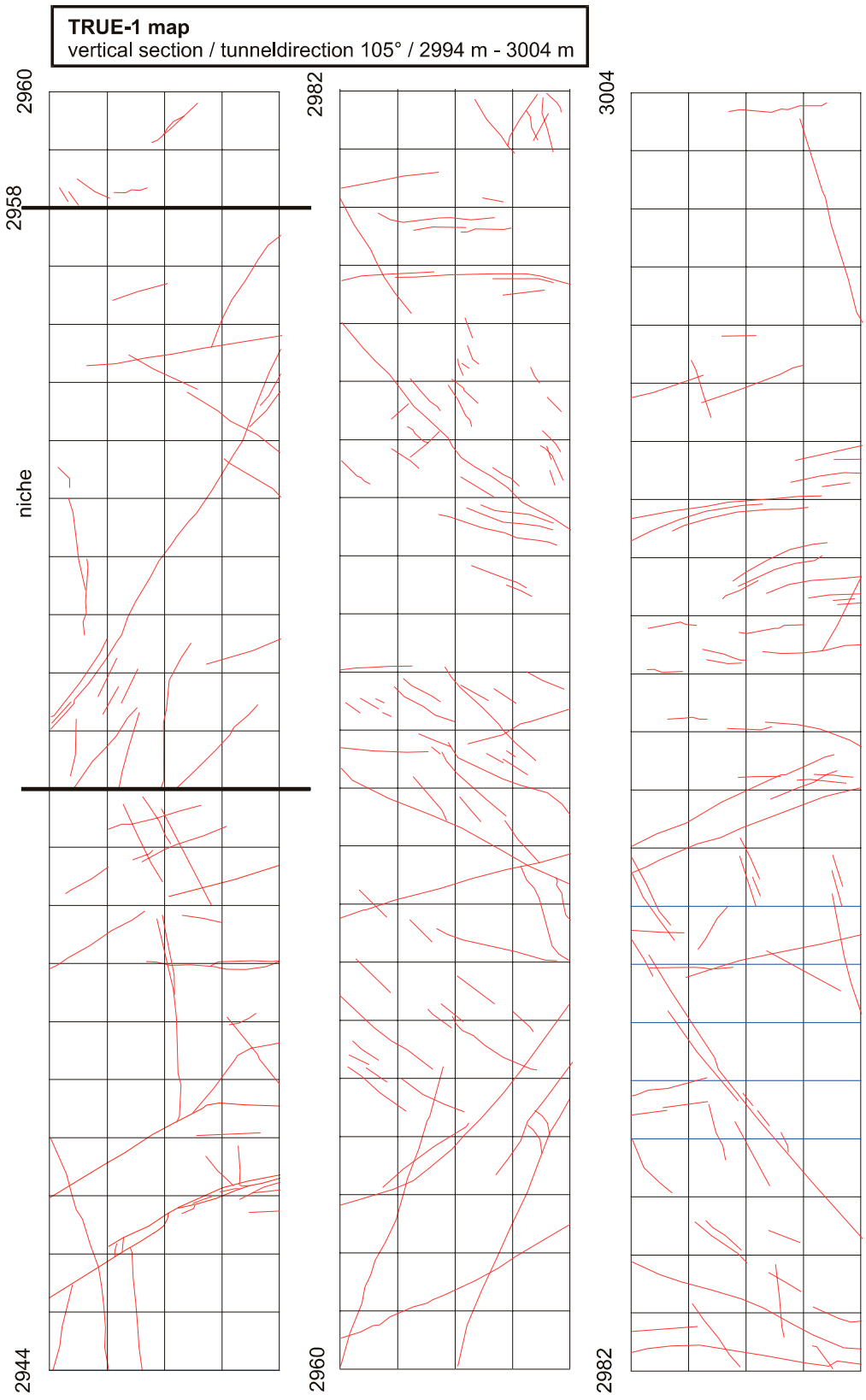

Figure 3-7. *Structural map along the tunnel wall of the TRUE-1 block at Äspö rock laboratory, vertical section. Tunnel metre 2944 – 3004. The detailed maps are shown in Appendix 4.*

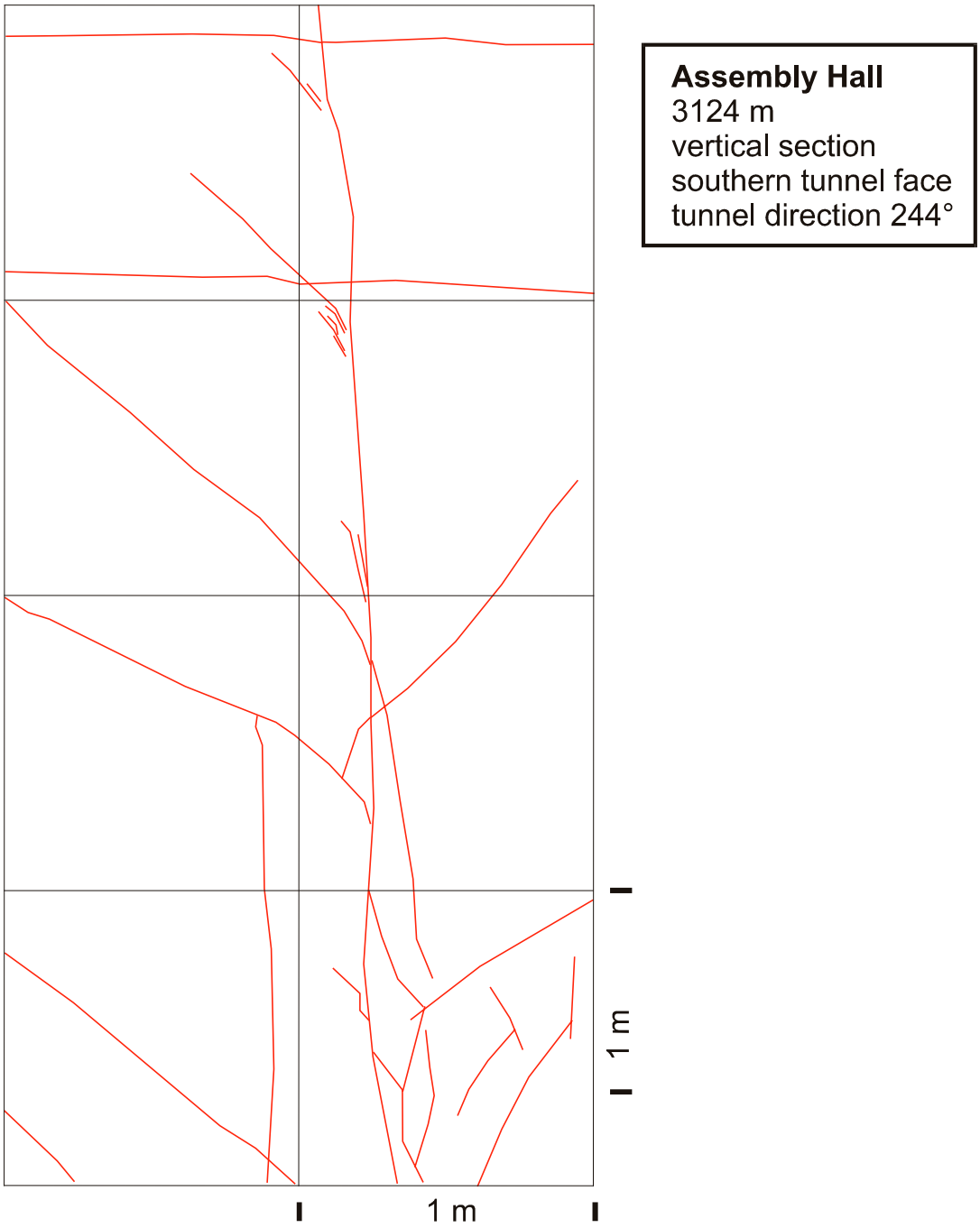

Figure 3-8. *Smale scale structural map of a water conducting feature at the Äspö rock laboratory, vertical section. Tunnel metre 3124.*

a)

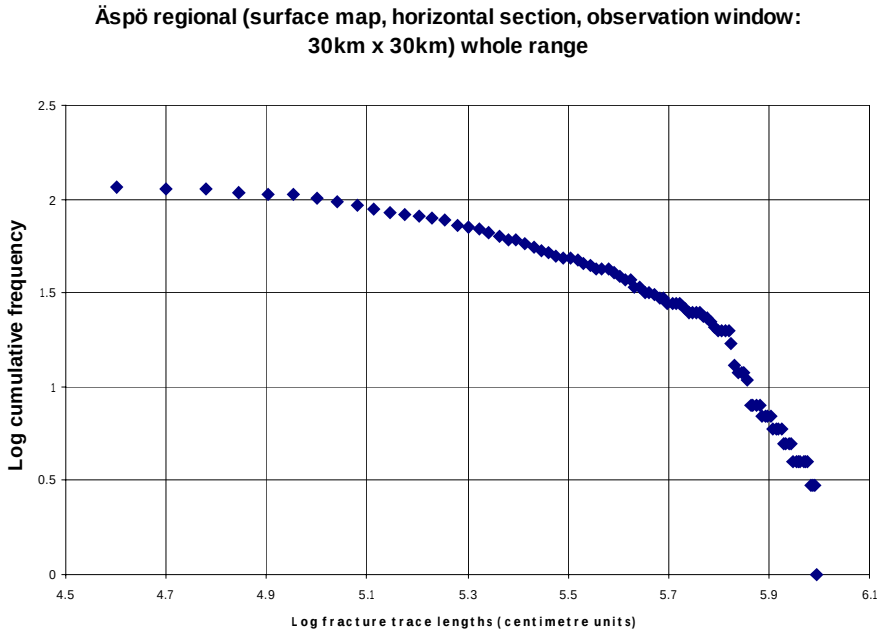

b)

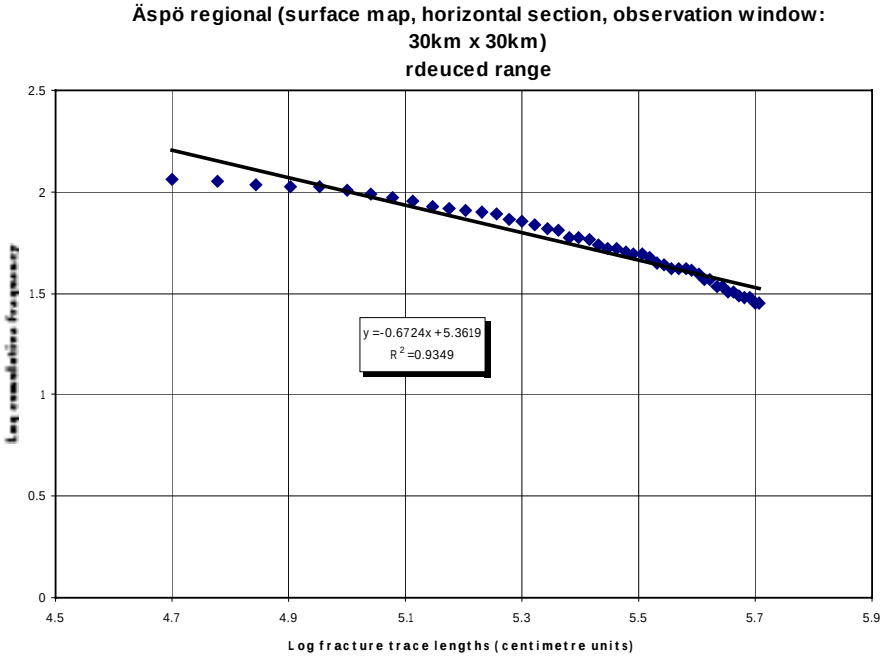

Figure 3-9. *Cumulative frequency plots of large scale discontinuities. Äspö regional scale (map is shown in Figure 3-1), a) whole range of data and b) reduced range, linear segment.*

a)

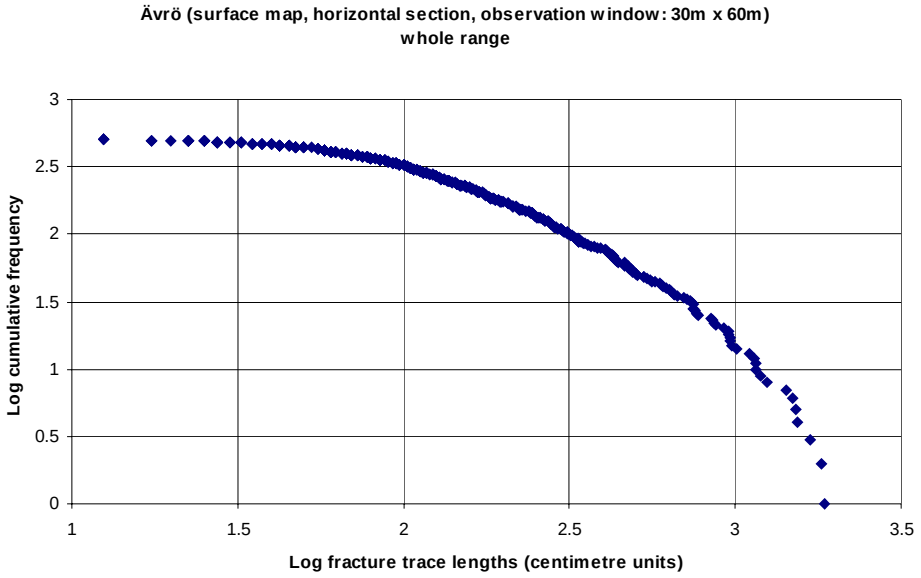

b)

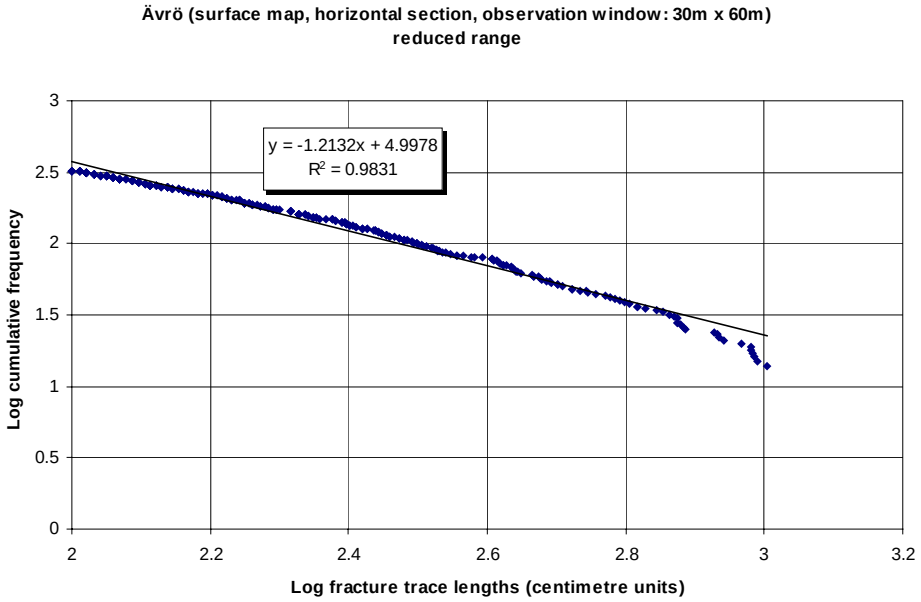

Figure 3-10. *Cumulative frequency plots of fractures mapped on outcrop at Ävrö island (map is shown in Figure 3-3), a) whole range of data and b) reduced range, linear segment.*

a)

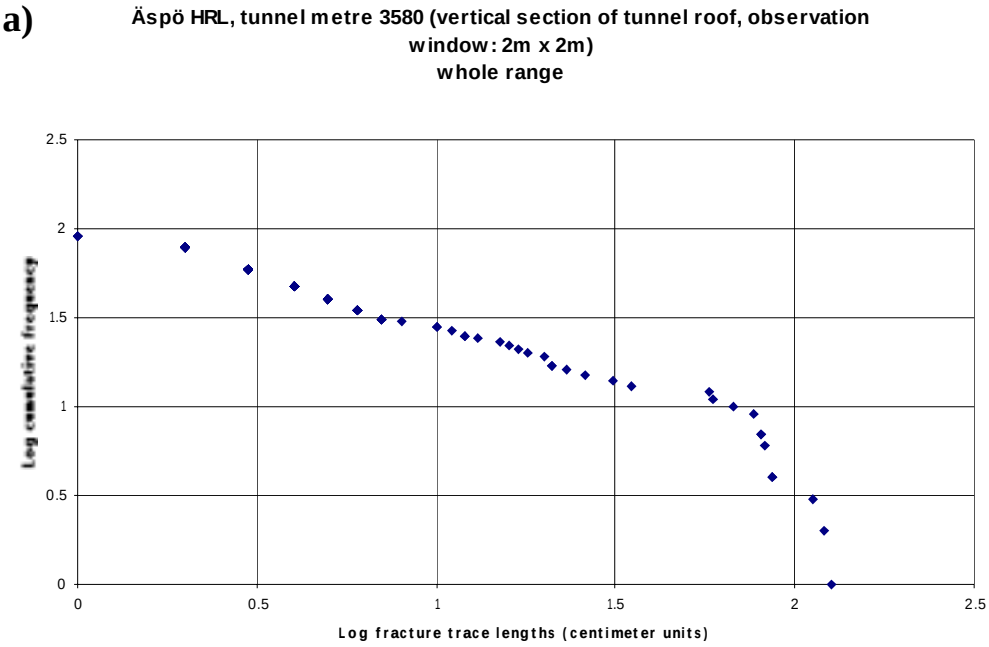

b)

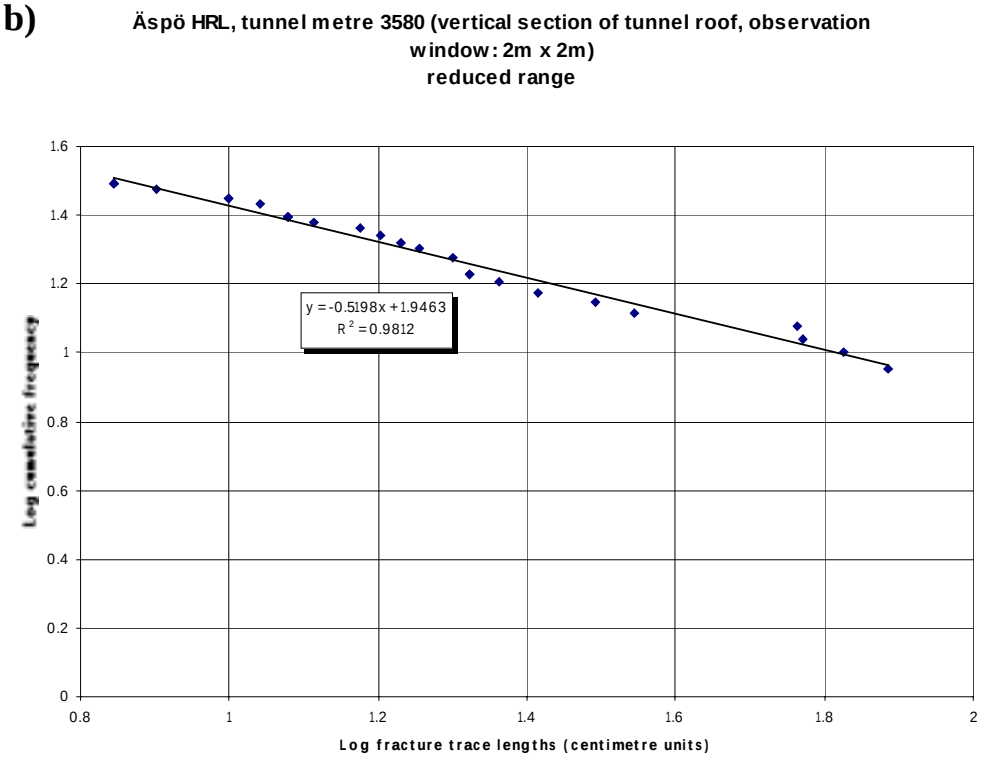

Figure 3-11. *Cumulative frequency plots of fractures mapped in the small scale, Äspö rock laboratory (map is shown in Figure 3-5a), a) whole range of data and b) reduced range, linear segment.*

From this database, the absolute and relative cumulative frequencies of trace lengths were evaluated. This results in a dataset on the basis of which the fracture trace lengths can be plotted versus their relative cumulative frequencies. The fractal dimension, which is the important parameter for deciding whether fracture networks are self-similar over a wide range of scales or not, is then calculated from the slope of the central linear segments of each plot.

3.4 Results

The results for the twelve fracture and fault networks are shown in Figures 3-1 to Figures 3-8, where the fracture network is visualised (digitised map). Figures 3-9 to 3-11 show trace lengths versus cumulative frequencies in a log-log plot (for background see e.g. WALSH and WATTERSON 1992, WATANABE and TAKAHASHI 1995).

The graphs of these cumulative frequency plots are, if simple monofractal scaling is indicated, composed of a central linear segment on the left (smaller trace lengths) and a steep segment on the right (larger trace lengths). The flattening of the curve on small scales is due to the *truncation bias*, i.e. due to the limited spatial resolution of the observation method. The steepening of the large-scale curve (right side) is due to the *censoring bias (or finite range effect)*, i.e. the fact that the scale exceeds the size of the observation window. Provided the range of scales that were observed is sufficiently wide (1 order of magnitude at least), a linear curve segment appears in the central part of the curve. The slope of this segment directly yields the fractal dimension of the fracture network.

The slope or fractal dimension of each of the twelve fracture networks can now be derived on the central linear segment, provided that the observation window is large enough (non-linearity can be due to a too small observation window). This has been done for every fracture network (GLÜCK 2001) and is shown in the plots of Figures 3-9, 3-10, 3-11 and Appendices 7.1 – 7.10. The compilation of all values is done in Table 3-2 and Figure 3-13. Quite unexpected is the fact that fractal dimensions vary over a rather wide range, from –0.52 (as a low negative value) to –1.21 (as a high negative value). The reason for this large variation lies in the geometry of the fracture network. If the ratio of small to large trace lengths is high, then the slope (or fractal dimension) of the middle segment is also high (identical with a high negative value). If the ratio of small to large trace lengths is moderate or low, which means that a fairly uniform distribution of trace lengths exists, then the slope of the middle segment is also moderate or small. High slope values generally indicate a relatively good interconnectedness of fractures and small slope values the opposite, i.e. a poorer interconnectedness. This relationship of fractal dimension and interconnectedness can be seen on many examples (i.e. compare Figure 3-10b with Figure 3-11b. Figure 3-10b reveals a high negative slope with a well interconnected fracture network and in Figure 3-11b a low negative slope corresponds with a reduced interconnectedness). Applied to the fault classification scheme (MAZUREK et al. 1996), there is no clear rule. However, it can generally be stated that a fault zone with a relatively small amount of splay joints and a relative high amount of master faults will result in a smaller fractal dimension than a single fault (some “stepping” master faults) with a considerable amount of diverging splays.

Table 3-2. Statistics and fractal dimensions of surface and tunnel maps. Tm stands for tunnel metre.

Map	Figure	Number of fractures	Correlation coefficient R^2	Dimension
Äspö regional	Figure 3-9	134	0.9349	-0.6724
Äspö local	Appendix 7-1	112	0.9184	-0.8277
Äspö West	Appendix 7-2	214	0.9561	-0.7206
Äspö village	Appendix 7-3	475	0.9821	-1.0112
Ävrö	Figure 3-10	502	0.9831	-1.2132
Tm 1978 - 2003	Appendix 7-4	50	0.9108	-0.8457
Tm 3580	Figure 3-11	93	0.9812	-0.5198
Tm 2050	Appendix 7-5	54	0.8954	-0.5511
Tm 2232 - 2260	Appendix 7-6	360	0.9127	-0.7610
Tm 2963	Appendix 7-7	133	0.9459	-1.1090
Tm 2944 - 3004	Appendix 7-8	227	0.9343	-1.0283
Tm 2950 - 2980	Appendix 7-9	49	0.9108	-0.8457
Tm 3124	Appendix 7-10	28	0.9690	-0.6368

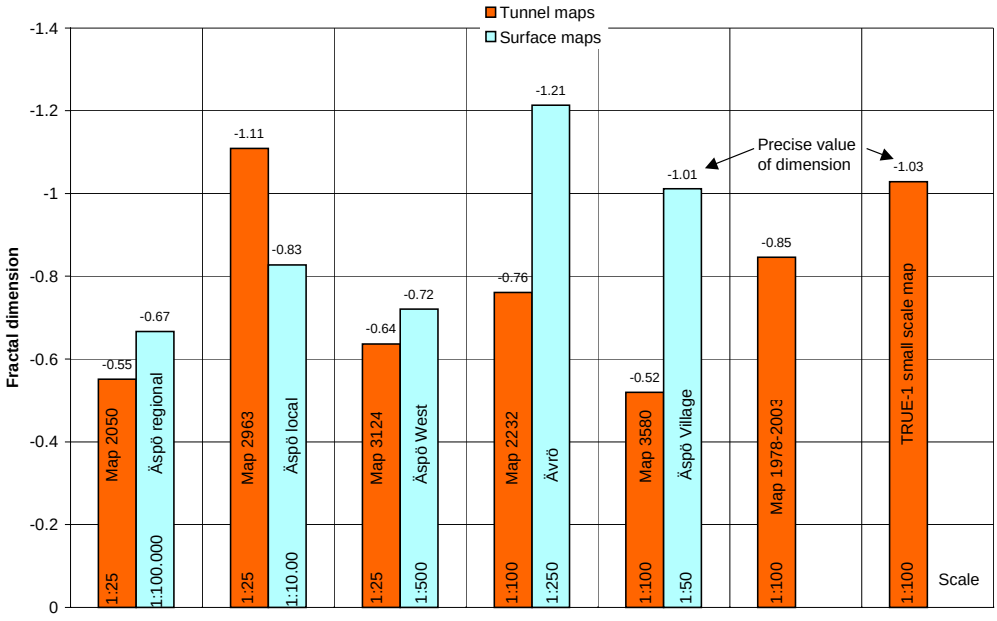

Figure 3-12. *Overview of fractal dimensions of surface and tunnel maps.*

The three basic requirements for self-similarity of fracture networks are now 1) the linearity of the central segment where a rather high correlation factor is required ($R^2 > 0.95$), 2) this linearity has to persist over at least one order of magnitude of trace lengths and 3) the slopes (=fractal dimensions) of this middle segment for different fracture networks has to be, with regard to statistical fluctuations and sampling errors, nearly identical.

The plots in Figures 3-9b, 3-10b and 3-11b show, at a first glance, a quite good linearity of the central segment; at least 50% of the plots have correlation factors >0.95. However, when the central segments of these plots are studied and compared in more detail, then most of the plots show a slightly convex rather than a linear form. A perfect linear form never exists even when the correlation factor is nearly 1. Furthermore, the slopes or the fractal dimensions of the twelve fracture networks are not identical (see Table 3-2). As a result, the twelve fracture networks do not satisfy at least one of the three basic requirements for self-similarity mentioned above. Thus, it can be concluded that the analysed fracture networks are not self-similar. This conclusion is most probably valid for the whole Äspö region, which may also be evident given the geological setting: a geological environment like Äspö, with a multiphase deformation history where many deformation phases have contributed to the final fracture network, is not a likely candidate for a self-similar fracture network. This would tend more to be the case in a more simply deformed region, where e.g. only one brittle deformation phase has occurred.

This rather clear and negative result also has implications for fracture network modelling, i.e. a fracture network on the 10 km scale cannot be derived from a fracture network on the 100 m scale (this would certainly be the case if the fracture network at Äspö were self-similar). Thus, fracture networks on any scale have to be derived independently, e.g. using the methodology proposed in Chapter 2.

3.5 Structural and hydrogeological constraints

Water-conducting features have been characterised and classified in the Äspö HRL (MAZUREK et al. 1996). This study was mainly limited to the tunnel scale, i.e. a scale equal to one tunnel diameter (ca. 5 m), where the major water-conducting features in the tunnel were structurally analysed and classified. In the previous chapter, twelve fracture networks derived on different scales and geological-structural units in the Äspö crystalline, ranging from 1 m to 30 km, were presented, resulting in a high structural interconnectedness of discontinuities on all scales. This fact is further corroborated by the integrated structural model of the TRUE-1 block, suggesting a high structural and also hydraulic interconnectedness of fractures in a rock mass ("matrix") lying between major water-conducting faults. The main question of interest is now if this fracture network in the rock mass is hydraulically interconnected with the main fracture and fault zones and what the hydraulic properties of the whole, large-scale network are.

The large-scale interference data available for Äspö confirm that pressure responses can extend up to several hundred metres away from the tunnel, especially when highly permeable fractures and faults have been cross-cut during the construction of the tunnel. The corresponding drawdowns were measured in numerous observation boreholes

drilled and instrumented in Äspö, Ävrö, Bockholmen and Laxemar. Thus, it can be concluded that at least the network of highly permeable fractures and faults in the Äspö HRL is hydraulically connected over distances of at least 100 to 400 m.

RHEN and FORSMARK (2000) carried out a statistical analysis of high-permeability features (termed HPF) and also compiled results for the lower permeability rock mass, the latter lying between the HPFs. These results are of considerable importance to answering the question whether HPFs and the lower permeability rock mass are hydraulically interconnected.

High-permeability features (HPF):

RHEN and FORSMARK (2000) define a HPF as a water-conducting feature having a transmissivity T of ≥1E-5 m^2/s. The Äspö database contains 79 such features. Only about 50% of these HPFs are correlated to major fracture and fault zones that were identified deterministically (hydrogeological, geophysical and geochemical investigation methods) and have hydraulic radii of influence extending over several hundred of metres. The remaining 50% of HPFs consist of joints and faults between the deterministic zones with a hydraulic radius of influence of 30 – 100 m. The frequency of these HPFs is quite high: the mean distance between two HPFs varies between 73 – 106 m. RHEN and FORSMARK (2000) attempted to relate HPFs to the geology. They found that HPFs are most frequent in Fine-grained Granite, with frequencies twice as high as in the Äspö Diorite and Småland Granite. HPFs are preferentially associated with rock contacts or mineral veins. Furthermore, there is a hydraulic anisotropy: HPFs with the highest water discharge are steeply inclined and strike towards NW-SE.

Lower permeability rock mass between HPFs:

A good example of a lower permeability rock mass is the site of the TRUE-1 block. No HPFs are present in this block and transmissivities vary mainly between 1E-7 and 1E-9 m^2/s. The hydraulic and structural anisotropies of lower permeability rock masses also seem to be similar to those in the TRUE-1 block. Generally, steeply inclined and NW-SE directed joints and fractures have higher transmissivities than those in other directions. This is mainly supported by the numerous interference tests carried out during and after construction of the Äspö HRL, at different levels in the tunnel. Of special interest is the Fine-grained Granite: although its structural geometry is not clear (i.e. deterministic 3D geometry of Fine-grained Granite bodies in and around Äspö), fracture frequency and transmissivity in the Fine-grained Granite are increased compared to those of Äspö Diorite and Småland Granite. Thus, the Fine-grained Granite increases the structural and hydraulic interconnectedness of fracture networks lying outside it. RHEN and FORSMARK (2000) conclude that Fine-grained Granite may effectively interconnect fracture systems even if its volume is quite small.

Conclusion:

HPFs are hydraulically interconnected with rock masses of lower permeability. All fractures observed and mapped on the different scales (maps of Figures 3-1 – 3-8) are structurally and hydraulically interconnected and may act as hydraulic pathways. This means that a non-sorbing conservative tracer, which is injected at any location in the Äspö crystalline, may reach an important hydraulic conductor such as a high-permeability feature.

3.6 Integration of hydrochemical evidence

At Äspö, SMELLIE *et al.* (1995) used structural and hydrochemical information from boreholes to derive a groundwater flow pattern. Chemical compositions of borehole-derived groundwater samples are consistent with mixing of surface-derived components (fresh/brackish water, seawater) and a deep saline groundwater component in different proportions. Combining the knowledge of the subsurface fault network at Äspö with limited hydraulic information (basically the distinction between recharging and discharging faults) yields a rough subsurface flow pattern. This conceptual model was substantially refined by integrating the chemical compositions of groundwaters. The relative proportions of the surface-derived and deep components in each groundwater sample were calculated, and the spatial distribution of mixing ratios was used to constrain the flow directions and the penetration depth of surface-derived waters. It was shown that in spite of the modest surface topography, the penetration depth of surface-derived waters is in excess of 500 m along some of the steeply dipping faults.

In retrospective, some revisions are needed to this model which was proposed before the excavation of the tunnel system. In specific, the flat-lying water-conducting features which are present in SMELLIE et al.'s (1995) model could not be corroborated by more recent studies on the basis of tunnel observations.

Whereas the work of SMELLIE et al. (1995) was based on data derived from a limited number of boreholes, LAAKSOHARJU et al. (1999a,b) investigated a much larger dataset that was available after the construction of the underground laboratory. In spite of a seemingly simple pattern of increasing salinity with depth, they distinguished at least 3 major groundwater components, namely meteoric fresh water, different types of Baltic sea water and stagnant brines. On the basis of a substantial number of hydrogeochemical tracers, they provided block models of the rock volume underlying Äspö on a scale of ca. 1 km^3. The observations are consistent with thorough mixing of groundwaters that penetrated the underground at different times. Such mixing events require the existence of a fracture system that is connected in 3 dimensions. On the scale of 1 km^3, spatial heterogeneity due to the existence of different fracture hierarchies and systems is not evident, and this means that three-dimensional connectivity is achieved on a scale smaller than 1 km^3.

In the TRUE-1 and TRUE Block Scale experiments, hydrochemical differences between different structures were observed (WINBERG 1996, WINBERG et al. 2000). "Feature A" in the TRUE-1 block has been shown to contain groundwaters whose compositions are consistently different from other fracture waters in the block. Thus from a

hydrochemical point of view, a full connectivity within the TRUE-1 block cannot be shown on the basis of hydrochemical signatures. This means either that such connectivity does not exist, or that a chemical homogenisation of all fracture waters was not achieved due to the limited permeabilities and timescales available for homogenisation. Because hydraulic interference tests (Fig. 2-35) show a fairly good connectivity in 3 dimensions throughout the investigated volume, the latter alternative is preferred.

3.7 Conclusions

Based on the analyses of fracture networks on different scales, an important finding is that fracture networks at Äspö are NOT self-similar. This clear negative statement has implications for fracture network modelling: i.e. a large-scale fracture network cannot be derived from a small-scale fracture network.

Another important conclusion is the structural interconnectedness of tectonic fractures on all scales. We assume that the findings for the TRUE-1 block are also valid at other sites in the Äspö crystalline: fracture networks between major tectonic faults seem to be highly interconnected and also connected to the major tectonic fault zones. This implies that, on a larger (kilometre) scale, the Äspö crystalline could be considered as a porous continuum.

Hydrogeological tests carried out on different scales and hydrochemical data clearly confirm this interconnectedness.

4. Summary of concepts: water flowpaths between waste canisters and the biosphere

4.1 Fracture geometries of different scales

In a hypothetical waste repository at Äspö, waste canisters would be located away from major water-conducting features. Contaminants leached from the engineered barrier system would therefore be transported through low-permeability fractures of limited size. Due to the good interconnection of fracture systems on all scales, the contaminants would subsequently exfiltrate into larger-scale and higher-permeability networks and finally into high-permeability features, according to the definition of RHEN and FORSMARK (2000). The succession of fracture hierarchies through which transport between the repository and the biosphere is achieved includes:

1. Small-scale fracture network (e.g. the background fracturing within the TRUE-1 block, fracture size in the range of dm to a few m)

2. Fracture clusters within the small-scale fracture network, typically along ductile precursors (e.g. "Feature A")

3. Mesoscopic network of decametre-size faults (i.e. the 5 types of water-conducting features described by MAZUREK et al. 1996)

4. High-permeability features (HPFs), including deterministically known regional faults.

The water flowpaths on the whole range of scales are illustrated in Figure 4-1. The basis for this figure is this report (sketches a-d), MAZUREK et al. (1996) (sketch e-f) and RHEN and FORSMARK (sketch f).

One important result of this report is that structures on different scales are not necessarily self-similar with regard to fracture geometry and mechanistic principles. Most larger-scale structures (HPFs, mesoscopic faults, fracture clusters such as "Feature A") are faults, i.e. products of brittle shear deformation. Fault gouges are frequently fracture infills. These structures have, at least episodically, also been water-conducting throughout geological evolution, which is shown by different types of fracture mineralisations and wallrock alterations. All these structures have been reactivated recurrently (e.g. highlighted by the existence of fully cemented cataclasites and younger, uncemented fault gouges) and often have ductile precursors. In spite of these similarities, fault geometries are different on different scales. Regional features (Figure 4-1f) are largely linear and can often be mapped over several kilometres. In contrast, the mesoscopic fault system (Figure 4-1e) shows a typical pattern of master faults and connecting splay systems. MAZUREK et al. (1996) distinguished 5 types of faults on this scale. However, faults on the small scale (fracture clusters in Figure 4-1d) do not show these geometries at all, so there appears to be a scale limitation for such faults.

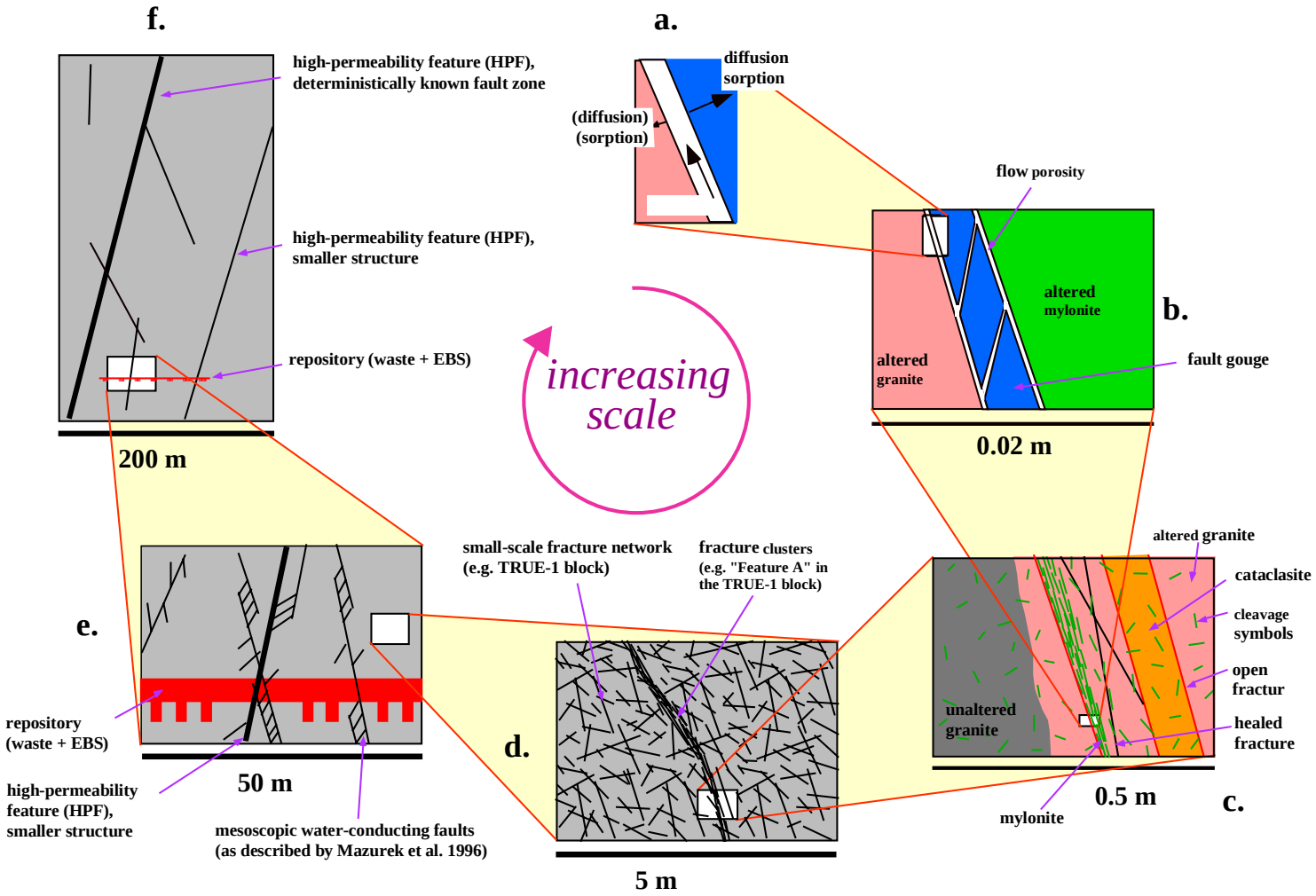

Figure 4-1. *Series of conceptual models showing fracture geometries and water flowpaths on a range of scales (see also Figures 2-25, 2-27, 2-28 and 2-43).*

The small-scale fracture network outside fracture clusters (Figure 4-1d) is somewhat chaotic and patternless, i.e. its geometry is in sharp contrast to the highly organised structures on the larger scales. Individual fractures are mostly short (<1 m), and a majority do not show clear evidence of shear deformation; positive evidence of fault gouges is not available. Fracture mineralisations, if any, are very thin.

4.2 Implications for contaminant transport between the repository and the biosphere

Waste canisters in a hypothetical repository at Äspö would be placed away from larger-scale water-conducting features such as HPFs (Figure 4-1f) or mesoscopic faults (Figure 4-1e), and the following conclusions can thus be drawn on the basis of Figure 4-1:

1. An emplacement tunnel in the repository system with a nominal length of 100 m would cross at least 1 HPF, and this would most likely require some engineering measures (e.g. reinforcements, grouting, tunnel seals / plugs).

2. The same tunnel would cross-cut several mesoscopic faults (whose mean spacing is in the range 10 - 20 m). These would present less technical challenges, but some "respect distance" would have to be considered between the fault and the nearest canister. This means that canisters cannot be emplaced at a regular distance in the tunnel, but there would be gaps due to the existence of water-conducting faults.

3. The size of the "respect distance" depends on design and safety considerations. In a typical safety assessment, the first part of the flowpath of contaminants leached from the engineered barriers is thought to occur through "good rock", i.e. a low-permeability block with well constrained transport and retardation characteristics. The length of this part of the flowpath varies as a function of repository design and system properties, a typical value being 10 m. This length also determines the "respect distance" to higher-permeability features into which the contaminants may exfiltrate.

In geosphere transport calculations, the contribution of the "good rock" block to radionuclide retardation typically dominates over the contribution of the downstream flowpaths through higher hierarchies of fractures. This is partly due to the expected higher permeability in the larger structures, but also to the more limited possibility for full hydrogeological characterisation of the large structures (and therefore the need for conservative assumptions which minimise retardation). Thus, the characterisation of the size and properties of the blocks of "good rock" is one of the most important issues of a site investigation.

Acknowledgements

The authors are grateful to Peter Wikberg, SKB, for initiating the project and for his technical advice and motivation to during the investigations. Andreas Gautschi from Nagra is thanked for his technical and financial support. We would like to thank Anders Winberg, Conterra AB, for the critical and fruitful discussions and his encouraging support at the Äspö site. Anders Winberg and Ingvar Rhén also reviewed this report. Linda McKinley from Nagra is acknowledged for linguistic support, and Eva and George Horal, both GI, were responsible for the final layout of this report.

References

Bossart, P., Mazurek, M. and Hermanson, J., 1998. Structural conceptual models of water-conducting features at Äspö. In Characterisation and Evaluation of Sites for Deep Geological Disposal of Radioactive Waste in Fractured Rocks. Proceedings of the 3rd Äspö International Seminar, June 10-12, 1998. SKB TR-98-10.

Dershowitz, W.A., 1984. Rock Joint Systems. PhD Dissertation, Massachusetts Institute of Technology, Cambridge, MA, USA.

Dershowitz, W.A., Lee, G., Geier, J., Foxford, T., LaPointe, P. and Thomas, A., 1995. FracMan, interactive discrete feature data analysis, geometric modelling and exploration simulation. User documentation, version 2.5. Golder Associates Inc. Seattle, Washington.

Dershowitz, W.A. and Busse, R., 1996. Discrete fracture network analysis in support of the Äspö Tracer Retention Understanding Experiment (TRUE-1), SKB ICR 96-05, Swedish Nuclear Fuel and Waste Management Company, Stockholm.

Follin, S. and Hermanson, J., 1996. A discrete fracture network model of the Äspö TBM Tunnel Rock Mass, SKB AR D-97-001, Swedish Nuclear Fuel and Waste Management Company, Stockholm.

Geosigma, 1997. BIP images of the TRUE-1 block. Data available on CD.

Glück, M., 2001. Fraktale Geometrie und deren Interpretation in spröd deformierten Kristallin (Beispiel Äspö Granit). Diplomarbeit an der Universität Freiburg i. Br. (in preparation).

Heer, W. and Jakob, A., 1999. Structural geology and transport modelling for Grimsel and Äspö. In: Water-Conducting Features in Radionuclide Migration, Proc. Intern. Geotrap Workshop, Barcelona (Spain), 10-12 June 1998, NEA/OECD

Hermanson, J. and Stigsson, M., 1998. A discrete fracture network model of the Äspö ZEDEX tunnel section. Äspö Hard Rock Laboratory Progress Report, HRL-98-29. Swedish Nuclear Fuel and Waste Management Company, Stockholm.

Hesböl, R. and Hermanson, J., 1997. Detailed structural core logging of cores KXTT1-KXTT4, KA3005A at Äspö HRL (FCC-1 project, not published).

Jakob, A. and Heer, W., 2000: Summary of work done by the PSI modelling team for the Äspö migration experiments, Tasks 4e and 4f. PSI Technical Note TM-44-00-01, Paul Scherrer Institute, Würenlingen, Switzerland.

Laaksoharju, M., Tullborg, E.L., Wikberg, P., Wallin, B. and Smellie, J., 1999. Hydrogeochemical conditions and evolution at the Äspö HRL, Sweden. Appl. Geochem. 14, 835-860.

Laaksoharju, M., Skårman, C. and Skårman, E., 1999. Multivariate mixing and mass balance (M3) calculations, a new tool for decoding hydrogeological information. Appl. Geochem. 14, 861-872.

LaPointe, P., Wallmann, P. and Follin, S., 1995. Estimation of effective block conductivities based on discrete network analyses using data from the Äspö site, SKB TR 95-15, Swedish Nuclear Fuel and Waste Management Company, Stockholm.

LaPointe, P., Cladouhos, T. and Follin, S., 1999. Calculation of displacements on fractures intersecting canisters induced by earthquakes: Aberg, Beberg and Ceberg examples. SKB Technical Report, TR-99-03. Swedish Nuclear Fuel and Waste Management Company, Stockholm.

Martel, S.J., Pollard, D.D. and Segall, P., 1988. Development of simple strike-slip fault zones, Mont Abbot quadrangle, Sierra Nevada, California. Geol. Soc. Am. Bull., v.100, 1451-1465.

Mazurek, M., 2000. Geological and hydraulic properties of water-conducting features in crystalline rocks. In: Stober, I. and Bucher, K. (eds.): Hydrogeology of crystalline rocks, Kluwer Scientific Publishers, 3-26

Mazurek, M., Bossart, P. and Eliasson, T., 1996. Classification and characterization of water-conducting features at Äspö: Results of investigations on the outcrop scale. SKB International Cooperation Report ICR 97-01, Swedish Nuclear Fuel and Waste Management Co, Stockholm, Sweden.

Mazurek, M., Bossart, P. and Eliasson, T., 1995. Classification and characterization of water-conducting features at Äspö: Results of phase I investigations. SKB Äspölaboratoriet Progress Report 25-95-03, Swedish Nuclear Fuel and Waste Management Co, Stockholm, Sweden.

Munier, R., 1993. Segmentation, Fragmentation, and Jostling of the Baltic Shield with Time. PhD-Thesis, Acta Universitatis Upsaliensis. University of Uppsala, Sweden.

Munier, R., 1995. Studies of geological structures at Äspö - Comprehensive summary of results, SKB PR 25-95-21, Swedish Nuclear Fuel and Waste Management Company, Stockholm.

Rhén, I. and Forsmark, T., 2000. Äspö Hard Rock Laboratory. High-permeability features (HPF). International Progress Report IPR-00-02

Sibson, R.H., 1977. Fault rocks and fault mechanisms. J. Geol. Soc. Lond. 133, pp. 191-213.

SKI, 1996. SKI Site-94. Deep repository Performance Assessment project. Volume I. ISSN 1104-1374. ISRN SKI-R—96/36—SE.

Smellie, J. A. T., Laaksoharju, M. and Wikberg, P., 1995. Äspö, SE Sweden: a natural groundwater flow model derived from hydrogeochemical observations. J. Hydrol. 172, 147-169.

Stanfors, R., Rhén, I., Tullborg, E.L. and Wikberg, P., 1999. Overview of geological and hydrogeological conditions of the Äspö hard rock laboratory site. Appl. Geochem. 14, 819-834.

Terzaghi, R.D., 1965. Sources of error in joint surveys. Geotechnique 15, pp. 287-304.

Walsh, J. J. and Watterson, J., 1992. Populations of faults and fault displacements and their effects on estimates of fault-related regional extension. J. Struct. Geol. 14, 701-712.

Watanabe, K. and Takahashi, H., 1995. Fractal geometry characterization of geothermal reservoir fracture networks. J. Geophys. Res. 100, 521-528.

Winberg, A. (Ed.), 1996. First TRUE Stage- Trace Retention Understanding Experiments. Descriptive structural-hydraulic models on block and detailed scales of the TRUE-1 site. SKB International Cooperation Report ICR 96-04. Swedish Nuclear Fuel and Waste Management Company, Stockholm.

Winberg, A., Andersson, P., Hermanson, J. and Stenberg, L., 1996. Results of the SELECT Project- Investigation Programme for Selection of Experimental Sites for the Operational Phase. Swedish Nuclear Fuel and Waste Management Company. Äspö Hard Rock Laboratory Progress Report PR HRL-96-01.

Winberg, A., Andersson, P., Hermanson, J., Byegård, J., Cvetkovic, V. and Birgersson, L. 2000. Final report of the first stage of the Tracer Retention Understanding Experiments. Swedish Nuclear Fuel and Waste Management Company (SKB), Technical Report TR-00-07.

Appendices

SKB TR-01-21

Appendix 1

The drill core database

1-1 Fracture-foliation data

1-2 Deformation-alteration-rock data

Appendix 1.1
Fracture-foliation data

Legend:

F	fracture
V	foliation
T	tight
O	open
FG	fault gouge
QZ	quartz
Ep	Epidote
Chl	Chlorite
Ca	Calcium
Fe	Iron-hydroxides
Py	Parite
Fl	Fluorite
Mu	Muscovite
Lau	Laumontit

Drillcore KXTT1

Type	BH depth	Azimuth of dip	Dip	EP	CHL	CA	FE	PY	FL	MU	LAU	T/O	Remarks
F	2.12	180	53		X	X						T	
F	2.18	248	72			X						O	FG
F	2.16	228	68		X	X						O	
F	2.36	227	80		X							O	
F	2.38	74	76	X								T	
F	2.40	222	78		X							O	
F	2.43	76	76	X								T	Contact
F	2.51	58	62	X								T	3 mm
F	2.55	86	64	X								T	4 mm
F	2.56	224	72		X							O	
V	2.61	46	64										
F	2.74	201	47		X	X						O	
V	2.81	60	66										
F	2.90	196	55		X	X						O	FG
F	2.98	181	54		X	X						O	
F	3.20	52	80	X	X							T	
F	3.32	28	90			X						O	
F	3.38	164	68		X							O	
V	3.35	48	64										
F	3.55	164	50	X								T	
F	3.64	208	80			X						O	
V	3.67	51	62										
V	3.83	56	68										
F	4.11	180	77		X	X						O	
F	4.16	129	51		X	X						O	FG
F	4.18	142	75		X	X						O	FG
F	4.21	162	50		X	X						O	FG
F	4.26	46	68	X								T	Contact
V	4.28	34	68										
F	4.62	18	73	X								T	Trippel
V	4.64	30	65										
V	4.93	42	66										
F	5.02	166	57									O	Empty
F	5.04	163	57									O	Empty
F	5.07	26	71	X								T	2 mm
F	5.18	40	71	X								T	
V	5.22	42	67										
F	5.27	156	39		X							O	
V	5.43	41	66										
V	5.55	25	62										Mylonite with Epidote
V	5.65	25	62										Mylonite with Epidote
F	6.05	358	86		X	X						O	
F	6.12	203	50		X	X						O	
V	6.16	60	72										

Type	BH depth	Azimuth of dip	Dip	EP	CHL	CA	FE	PY	FL	MU	LAU	T/O	Remarks
F	6.28	134	33	X	X							T	
F	6.29	193	72			X						O	
F	6.37	161	46				X					O	
V	6.44	48	70										
F	6.49	200	50		X	X	X					O	
F	6.54	183	34	X								T	
V	6.58	38	67										
F	6.72	42	76	X								T	Qz, 15 mm
F	6.75	43	76	X								T	3 mm
V	6.86	39	69										
V	7.13	28	68										
F	7.21	173	69			X						O	
F	7.26	170	86			X						O	
V	7.31	36	66										
F	7.35	14	75	X								T	2 mm
F	7.56	203	65									T	
V	7.74	44	72										
V	7.93	50	72										
F	8.04	244	74		X	X						O	
V	8.14	48	70										
F	8.22	27	83	X								T	4 mm
F	8.24	42	88			X						O	
V	8.63	25	66										
F	8.78	39	73	X								T	
V	8.87	46	70										
F	8.91	11	89			X						O	
F	9.03	208	76	X								T	3 mm
F	9.12	38	76										
F	9.18	24	68	X								T	1 mm
V	9.15	56	74										
F	9.25	207	73		X	X						O	
F	9.33	46	77	X								T	2 mm
V	9.42	51	64										
F	9.52	31	78	X	X							T	
F	9.57	184	70			X						O	
F	9.64	209	88	X								T	4 mm
F	9.85	28	85		X	X						O	
F	9.7	35	77		X	X						O	
F	10.36	183	77		X	X						O	Minerali-zation
F	10.58	201	68		X	X						O	
F	10.64	64	71			X						T	
F	10.91	49	61										
F	11.25	213	73		X							O	
V	11.31	42	66										
F	11.42	232	77		X							O	
F	11.48	355	85			X						O	
V	11.45	54	68										
V	11.71	81	52										

Type	BH depth	Azimuth of dip	Dip	EP	CHL	CA	FE	PY	FL	MU	LAU	T/O	Remarks
F	11.92	32	68	X								T	
V	12.05	65	72										Mylonite
V	12.07	70	76										Mylonite
F	12.08	261	72		X	X						O	
F	12.17	188	52		X							O	
V	12.15	64	74										Mylonite
F	12.34	182	36		X			X				O	
V	12.35	65	72										Mylonite
F	12.47	252	62	X		X						T	2 mm
F	12.63	148	48		X	X		X				O	FG, 3 mm
F	12.665	258	84		X			X				O	3 mm
F	12.91	198	89	X	X							T	3 mm
F	13.03	172	74				X					T	
F	13.12	6	83			X						O	
V	13.13	38	66										
F	13.23	214	77		X	X						O	FG
V	13.36	44	70										
F	13.46	220	84	X	X							O	
F	13.55	234	70		X	X						O	
F	13.64	148	14			X						T	1 mm
V	13.65	49	64										
V	13.85	42	64										
F	13.91	144	22				X					T	
V	14.12	48	70										
F	14.21	21	81		X	X						O	
V	14.31	42	70										
F	14.32	25	76		X	X						O	
F	14.39	113	78			X						T	1 mm
F	14.51	335	77			X						T	Subpar-allell
V	14.51	79	82										
V	14.63	80	83										
F	14.71	38	53		X							O	Planar, rough
V	14.72	81	80										
V	14,80	90	87										
F	15.02	340	74			X						T	Subpar-allell
F	15.10	148	78		X	X						O	Rough, subpar-allell
F	15.25	32	83	X								T	
V	15.25	32	83										
F	15.31	226	64		X							T	Set 1, planar
F	15.32	228	62										Set 1, subpar-allell
F	15.35	330	53		X								Planar
F	15.36	234	55										Set 1,

Type	BH depth	Azimuth of dip	Dip	EP	CHL	CA	FE	PY	FL	MU	LAU	T/O	Remarks
													subpar-allell
F	15.39	229	55										Set 1, tight
V	15.32	36	80										
V	15.38	40	80										
F	15.41	226	50		X								Set 1, planar
F	15.45	356	60									T	Subpar-allell
F	15.46	214	60		X								Set 1, planar
V	15.49	46	83										
F	15.51	216	60										C-Feature
F	15.52	212	68										
F	15.55	216	62										
F	15.57	214	60										
F	15.59	234	78										
F	15.61	172	32										C-Feature
V	15.61	28	76										
F	15.76	30	78										A-Feature
V	15.76	30	78										Mylonite
F	15.78	25	75	X								T	Mylonite
V	15.80	29	78										Mylonite
F	15.805	25	70										A-Feature
F	15.90	33	80			X							Fault
V	15.90	31	76										
F	15.99	162	50										Rough
F	16.01	72	40	X								T	
V	16.55	32	78										
V	16.15	34	78										
V	16.25	30	80										
V	16.35	30	78										
V	16.45	26	70										
V	16.65	36	68										
F	16.74	183	69			X						O	
F	17.27	151	17		X			X				O	
F	17.33	196	54		X	X						O	
V	17.42	42	64										
F	17.72	67	62			X						O	1 mm, subpar-allell
F	18.20	57	79		X							O	Fault, slickenl 37 to 014
V	18.24	38	70										
F	18.32	52	16			X		X				O	
F	18.41	42	67										
F	18.47	35	76		X							O	Slicken-lines 40to356
F	18.86	38	78		X	X						O	Rough

Type	BH depth	Azimuth of dip	Dip	EP	CHL	CA	FE	PY	FL	MU	LAU	T/O	Remarks
V	18.99	52	74										
F	19.08	25	84	X								T	
F	19.17	186	74	X		X						T	2 mm
F	19.25	40	86	X								T	5 mm
F	19.30	128	13	X								T	3 mm
F	19.35	35	74		X	X						O	Planar
V	19.34	38	72										
F	19.43	216	10		X	X						O	Planar
F	19.49	171	42	X								T	8 mm
V	19.75	48	70										
V	20.11	46	70										
F	20.13	246	41	X								T	15 mm
F	20.15	107	23		X	X						O	
F	20.17	171	70									T	
F	20.20	161	80		X	X						O	Rough
F	20.25	161	76									O	
F	20.32	41	78		X							T	
V	20.38	32	68										
V	20.61	30	68										
F	20.65	161	76									O	FG
F	20.74	7	89			X		X				O	Mineralization, Ca-crystals
V	20.81	36	70										
F	20.86	21	89			X			X			O	Partially tight
F	20.88	232	58	X								T	
F	20.89	14	85	X		X						O	
F	20.97	24	76			X						T	
V	21.02	39	64										
F	21.1	159	85	X								T	
F	21.17	34	79		X							O	
F	21.22	47	70			X						T	
V	21.30	39	64										
F	21.36	20	84			X						O	2 mm
F	21.47	152	88		X							O	FG
F	21.49	341	65			X						O	FG
F	21.57	195	82									O	FG, 2 mm
F	21.6	179	84									O	FG, 2 mm
F	21.7	220	69	X								T	3 mm
V	21.81	24	67										
F	21.85	11	85		X	X						O	
F	21.88	353	88		X	X						O	
F	21.91	283	70		X	X						O	2 mm
F	21.99	13	79		X	X						O	
F	22.05	124	90		X	X						O	FG
F	22.15	176	53										
V	22.22	34	68										

Type	BH depth	Azimuth of dip	Dip	EP	CHL	CA	FE	PY	FL	MU	LAU	T/O	Remarks
F	22.25	12	86			X	X					O	
V	22.33	22	65										
F	22.38	44	75	X								T	8 mm
F	22.5	227	81		X							O	
F	22.54	39	65	X								T	
F	22.65	44	76		X							O	
F	22.69	44	76		X							O	
F	22.82	48	79			X						O	
F	22.85	315	22			X				X		T	
V	22.89	34	68										
F	23.005	342	47										
F	23.02	198	61		X							O	
F	23.08	191	69			X						O	FG
F	23.3	180	59									O	
F	23.305	47	77		X	X						O	
F	23.51	180	67			X						O	
F	23.58	43	79		X							O	
V	23.63	57	64										
F	23.73	187	73			X						O	
F	23.8	32	82			X						O	
F	23.96	36	82										
V	23.89	81	76										
F	24.02	279	84									T	Qz, partly open
F	24.14	44	72		X							O	
F	24.32	27	59		X	X						O	
F	24.45	332	50		X	X						O	Subpar-allell
F	24.48	33	76		X							O	
F	24.77	182	74		X	X						O	
F	24.83	336	70		X	X						O	FG, sub-parallell
F	24.85	354	79			X						O	
F	24.96	190	77										
F	25.05	336	15				X					T	K-fsp, 2 mm
V	25.01	68	65										
F	25.22	182	70			X						T	1 mm
V	25.35	42	66										
F	25.45	6	86										
F	25.51	172	78										
F	25.56	186	86										
F	25.81	184	86										
F	25.87	182	65										
F	26.17	200	74			X						O	2 mm
F	26.12	54	80	X								T	
F	26.15	36	19		X							O	
F	26.24	41	86			X						O	
F	26.27	42	88			X						T	
F	26.28	118	70		X	X						T	

Type	BH depth	Azimuth of dip	Dip	EP	CHL	CA	FE	PY	FL	MU	LAU	T/O	Remarks
F	26.32	46	78			X						T	
F	26.48	281	26				X					T	K-fsp
F	26.64	194	85			X						O	
F	26.86	148	66		X							O	
V	26.81	68	68										
F	27.16	167	70			X						O	
F	27.18	246	85	X	X							T	4 mm
F	27.20	161	74			X						O	FG
F	27.48	10	73	X								T	3 mm, 20 mm dis-place-ment
F	27.75	163	68			X						O	2 mm
F	27.82	36	77	X								T	3 mm
V	27.92	44	72										
F	28.05	54	84		X							O	
F	28.16	48	90		X		X					O	Qz
F	28.20	13	72	X		X						T	Qz
F	28.26	125	54		X							O	

Drillcore KXTT2

Type	BH depth	Azimuth of dip	Dip	EP	CHL	CA	FE	PY	FL	MU	LAU	T/O	Remarks
F	2.12	24	68	X								T	10 mm, micro-fractures
V	2.23	34	66										
V	2.44	42	70										
F	2.51	203	62	X								T	micro-fractures
F	2.71	356	26	X								T	micro-fractures
V	2.75	32	58										
V	2.88	38	62										
F	2.91	90	22				X					T	
F	2.93	38	78	X								T	3 mm
F	3.07	181	56			X						O	
F	3.13	180	61			X						T	
F	3.135	236	36	X								T	4 mm
F	3.15	186	63			X						O	
F	3.155	140	56			X						O	2 mm
V	3.16	40	72										
F	3.19	228	70	X								T	5 mm
F	3.21	171	50		X	X						O	
F	3.35	126	38									T	
F	3.42	176	82			X						O	
V	3.39	42	70										
F	3.42	176	82			X						O	
F	3.55	211	85	X								T	4 mm
F	3.62	5	86	X								T	3 mm
V	3.52	34	70										
F	3.70	172	80	X								T	2 mm
V	3.74	26	72										
F	3.84	102	26	X	X							T	2 mm
V	3.88	28	68										
F	3.96	152	50		X							O	
F	3.99	138	52		X							O	
F	4.07	190	78										
F	4.09	206	76			X						O	
F	4.11	138	53		X	X						O	
F	4.15	227	70	X								T	5 mm
F	4.16	116	47		X	X						O	
V	4.14	58	70										
F	4.34	40	74	X			X					T	
F	4.35	133	52		X							O	
F	4.31	40	84	X								T	4 mm
F	4.44	125	49										
V	4.45	26	72										
F	4.48	32	64	X								T	
F	4.55	16	26				X					T	K-fsp
F	4.60	51	76	X	X							T	

Type	BH depth	Azimuth of dip	Dip	EP	CHL	CA	FE	PY	FL	MU	LAU	T/O	Remarks
V	4.61	56	66										
F	4.65	267	37	X								T	
V	4.81	32	73										
F	4.96	43	60	X								T	3 mm
F	5.14	170	66			X						T	
F	5.22	156	65			X						O	
F	5.27	158	67			X						O	
F	5.29	158	67			X						O	
F	5.40	149	31	X								T	3 mm
F	5.48	221	57	X								T	3 mm
F	5.61	188	70			X						O	Coating
F	5.69	83	39	X	X							T	
V	5.81	44	68										
F	6.04	130	45	X								T	2 mm
F	6.06	156	44	X								T	2 mm
F	6.13	60	16	X								T	
F	6.20	165	18	X								T	4 mm
F	6.3	160	34	X								T	20 mm
F	6.39	176	72			X						O	Coating
F	6.44	94	14	X								T	1 mm
F	6.58	225	67	X								T	5 mm
F	6.65	269	26	X								T	15 mm
F	6.78	52	70	X								T	
F	6.89	10	82	X								T	2 mm
V	6.82	30	74										
V	6.93	28	64										
F	7.01	20	81	X								T	7 mm
F	7.10	352	78			X						O	
F	7.12	284	28	X								T	2 mm
F	7.23	182	77									O	Empty
V	7.19	32	66										
F	7.30	184	66									O	Empty
F	7.35	32	60	X	X							T	
V	7.43	32	79										
V	7.64	45	68										
V	7.85	35	70										
F	7.94	233	73									O	Empty
F	8.00	178	70		X							O	Hem, fibrous chlorite
V	8.05	41	62										
F	8.09	112	62		X							O	Rough
F	8.51	216	62		X							O	
F	8.54	164	87									O	Empty
F	8.62	92	64	X								T	Qz, CON-TACT
F	8.96	164	24		X							T	
V	9.05	48	62										
F	9.12	223	67		X	X						O	Rough

Type	BH depth	Azimuth of dip	Dip	EP	CHL	CA	FE	PY	FL	MU	LAU	T/O	Remarks
F	9.15	26	81		X							O	
F	9.19	211	67		X							O	Planar
V	9.25	60	63										
F	9.29	216	72		X							O	Planar
F	9.30	184	81		X							O	Planar
F	9.38	236	70		X							O	Fibrous chlorite
F	9.40	226	70		X							O	
F	9.49	210	76		X	X						O	
F	9.59	61	67	X								T	2 mm
V	9.71	65	70										
F	9.76	25	75	X	X							T	17 mm
V	9.90	71	68										
F	9.94	39	75	X	X							T	2 mm
F	10.08	27	69	X								T	6 mm
F	10.14	182	86			X						O	Planar
V	10.14	54	74										
F	10.25	184	83			X						O	
V	10.35	53	70										
F	10.43	50	86	X								T	6 mm
V	10.60	63	70										
F	10.79	39	85	X	X							T	21 mm, mylonitic
V	10.85	56	70										
V	11.11	56	70										
F	11.12	39	78	X								T	1 mm
V	11.20	58	68										
V	11.43	66	72										
F	11.55	36	72	X								T	6 mm
F	11.63	221	85	X								T	
F	11.65	66	86	X								T	
V	11.74	38	70										
V	11.91	42	70										
V	12.12	44	71										
F	12.17	177	81		X	X						O	2 mm
F	12.205	214	72			X						O	2 mm
F	12.21	238	74				X					O	
V	12.24	44	70										
V	12.30	30	78										
F	12.56	351	84	X								T	6 mm
V	12.51	38	67										
F	12.66	230	72			X		X				O	
F	12.69	212	68		X	X		X				O	Planar
V	12.76	20	64										
V	12 89	18	68										
F	12.91	216	69			X						O	Coated
F	13.09	210	65		X	X						O	Planar
V	13.12	20	74										
F	13.16	24	77	X	X							T	

Type	BH depth	Azimuth of dip	Dip	EP	CHL	CA	FE	PY	FL	MU	LAU	T/O	Remarks
V	13.29	24	74										
V	13.41	22	75										
V	13.60	20	74										
V	13.76	20	76										
V	13.94	28	76										
F	14.12	35	86	X								T	
V	14.05	30	80										
V	14.12	35	86										
F	14.21	226	82		X							O	Rough
V	14.20	31	80										
F	14.25	234	35			X						O	Planar
F	14.27	238	40			X						O	Planar
F	14.28	210	88			X						O	Planar
F	14.30	140	38										JOKER
V	14.35	26	83										
F	14.42	194	80										
V	14.42	28	80										
V	14.55	32	80										
F	14.62	190	69										
V	14.65	38	78		X								Rough
F	14.7	198	56		X	X							
F	14.92	76	80									T	Mylonite
V	14.92	76	80										
F	14.98	66	90		X								
F	15.05	55	74	X									Mylonite
V	15.05	50	74										
V	15.10	44	77										
F	15.12	35	77										
V	15.20	46	68										
V	15.30	33	76										
F	15.55	138	85			X						T	
F	15.61	58	80	X									Mylonite
V	15.61	58	80										
V	15.78	48	84										
F	15.90	260	45			X							
F	15.95	291	82			X							
V	16.14	71	74										
V	16.25	65	76										
F	16.34	61	90	X								T	2 mm
V	16.39	62	70										
F	16.46	228	70			X						O	Coated
F	16.53	53	87	X								T	6 mm
V	16.60	66	70										
V	16.75	66	74										
V	16.94	58	75										
V	17.11	47	68										
F	17.27	235	64		X	X		X				O	Slicken-lines 39to354
V	17.31	56	66										

Type	BH depth	Azimuth of dip	Dip	EP	CHL	CA	FE	PY	FL	MU	LAU	T/O	Remarks
F	17.36	174	20		X							O	
V	17.41	50	64										
F	17.48	194	66					X	X				
V	17.55	54	70										
F	17.69	33	87	X								T	9 mm
V	17.68	52	74										
F	17.76	218	85	X								T	3 mm
V	17.86	42	76										
V	18.12	44	66										Ep in foliation planes
V	18.17	44	68										
F	18.24	14	88		X							O	

Drillcore KXTT3

Type	BH depth	Azimuth of dip	Dip	EP	CHL	CA	FE	PY	FL	MU	LAU	T/O	Remarks
F	2.05	163	40	X								T	2 mm
V	2.19	103	30										
F	2.31	235	84		X							O	
V	2.38	295	26										
V	2.61	305	38										
F	2.63	264	28			X						T	
F	2.64	217	47	X								T	2 mm
F	2.65	221	24		X	X						O	
F	2.70	187	46		X							O	
F	2.84	146	60	X								T	4 mm
F	3.01	39	82	X								T	4 mm
F	3.05	33	84	X								T	3 mm
V	3.12	4	80										
F	3.21	191	56			X						O	
F	3.28	156	28		X							O	Black oxide
F	3.30	72	77	X								T	
F	3.37	140	10	X								T	1 mm
F	3.41	34	88	X								T	1 mm
F	3.67	46	74	X								T	1-2 mm
V	3.68	59	70										
V	3.85	52	68										
F	3.90	28	70			X						O	Coating
F	3.93	153	62	X	X	X						O	Coating
F	4.05	220	09		X	X						O	Planar, 2 mm
F	4.12	198	72		X								Rough
V	4.17	26	74										
F	4.21	206	67				X					O	
V	4.29	43	67										
F	4.41	130	60		X	X						O	
F	4.45	118	42		X							O	Planar
F	4.02	332	68	X								T	2 mm
V	4.69	23	68										
F	4.64	268	14	X								O	Coated
V	4.70	23	70		X							O	
F	4.73	114	48		X							O	
F	4.82	74	69		X							T	
V	4.86	16	74										
F	4.88	126	61		X							O	Planar
V	5.09	38	66										
F	5.18	146	56		X							O	Black oxide
F	5.22	234	89	X	X							T	
V	5.27	42	66										
F	5.39	134	49			X						T	
V	5.41	30	76										
F	5.45	1	87			X						O	Rough

Type	BH depth	Azimuth of dip	Dip	EP	CHL	CA	FE	PY	FL	MU	LAU	T/O	Remarks
F	5.46	46	64	X	X							T	
F	5.56	185	87			X						O	Rough
V	5.58	52	74										
F	5.65	118	44	X								T	4 mm
F	5.66	213	65	X								T	8 mm
F	5.68	126	60	X								T	
F	5.70	30	90	X								T	5 mm
V	5.77	31	75										
F	5.84	185	76	X								T	Contact
F	5.90	150	82	X								T	
F	5.97	117	72		X							O	
V	5.95	25	78										
F	6.00	160	61		X							O	Planar
F	6.05	350	66	X								T	8 mm
F	6.12	138	12		X	X				X		T	
V	6.15	30	76										
V	6.12	26	66										
F	6.14	3	76	X								T	
V	6.33	24	78										
F	6.34	171	84		X	X						O	Rough, undulat-ing
F	6.38	167	88			X						O	Undu-lating
F	6.46	171	82	X								T	3 mm
V	6.48	23	66										
F	6.56	161	49		X	X						O	FG
V	6.65	34	72										
V	6.84	26	74										
F	6.89	163	72	X	X							T	5 mm
F	6.905	349	86			X						O	Coated
F	6.94	342	88			X						O	
V	7.10	26	74										
F	7.15	201	79			X						O	Coated
V	7.24	16	72										
V	7.39	24	72										
F	7.48	5	75	X								T	3 mm
F	7.51	320	80			X						O	1/2-tight, subpar-allel
F	7.515	27	80	X	X							T	Qz
V	7.55	26	61										
V	7.67	30	66										
F	7.71	37	70	X								T	
F	7.76	51	78	X	X	X						O	
V	7.84	60	70										
F	7.90	227	30	X	X							O	
F	7.905	33	76	X								T	
F	7.98	30	66	X								T	3 mm
F	8.005	351	78			X						O	
F	8.03	16	69	X								T	

Type	BH depth	Azimuth of dip	Dip	EP	CHL	CA	FE	PY	FL	MU	LAU	T/O	Remarks
V	8.15	27	71										
V	8.26	26	68										
F	8.35	23	71	X								T	
V	8.45	25	67										
F	8.48	147	71		X	X		X				O	FG, 2 mm
V	8.53	44	65										
F	8.59	62	64	X								T	4 mm
F	8.61	182	77			X			X			O	Fl-coated
F	8.64	60	54	X	X							T	
V	8.68	30	62										
F	8.82	45	66	X									
V	8.89	28	68										
V	9.07	42	62										
F	9.14	35	68		X	X						O	
F	9.18	42	64		X	X						T	Qz
F	9.195	200	24		X	X						O	Planar, chl-coated
F	9.27	40	74		X	X						O	
F	9.34	21	75		X	X						O	FG, rough
V	9.42	48	62										
F	9.47	224	36		X								
V	9.59	38	62										
F	9.66	30	74	X								T	
V	9.70	29	78										
F	9.93	191	46		X	X						O	Coated, rough
F	10.01	170	65		X	X						O	Coated, rough
F	10.08	38	66	X								T	Parallells
V	10.14	33	63										
F	10.27	358	56		X	X						O	FG, 1/2-tight
F	10:30	3	56		X	X						O	FG, slickenl. 39to358
V	10.40	44	67										
F	10.55	192	57		X							O	Break, coated
V	10.61	20	65										
F	10.63	348	84		X		X					O	
F	10.65	188	74				X					O	Break; coated
V	10.87	29	68										
F	10.90	35	67		X							T	
F	10.99	10	78		X							T	
V	11.15	32	66										
F	11.295	214	74		X	X						O	Coated
V	11.36	30	60										
V	11.55	48	60										

Type	BH depth	Azimuth of dip	Dip	EP	CHL	CA	FE	PY	FL	MU	LAU	T/O	Remarks
V	11.75	38	64										
V	11.95	45	60										
F	11.995	219	61			X	X					O	Break, coated
F	12.14	224	24			X						O	Coated, roughish
V	12.19	36	64										
V	12.39	24	68										
F	12.49	183	26		X							O	Roughish
F	12.505	230	26		X							O	Coated, planar
V	12.67	29	60										
F	12.66	32	66	X								T	
F	12.67	144	72		X	X						O	Coated
V	12.79	39	63										
V	12.92	39	64										
F	13.075	162	39		X	X						O	Fault
F	13.08	164	40									T	1 mm thick coating
V	13.15	36	70										
F	13.175	20	67	X								T	
F	13.18	334	68			X						T	
V	13.25	36	65										
F	13.39	228	88		X	X						O	Rough
F	13.41	128	44		X	X						O	Rough
V	13.65	38	70										
F	13.6	183	24		X						X		Planar
V	13.65	36	72										
V	13.75	41	74										
V	13.85	41	70										
F	13.90	47	82	X								T	Mylonite
V	13.90	47	82										
F	13.96	52	82	X									Mylonite
V	13.96	52	82										
V	14.05	41	78										
F	14.05	278	36		X								Splay?
F	14.06	4	89		X								Planar
F	14.10	31	78			X							A-Feature, large pores
V	14.13	38	80										
F	14.15	36	80										Fault
F	14.19	130	76									T	Splay?
V	14.24	39	86										
V	14.35	38	74										
V	14.46	36	75										
V	14.55	36	75										
V	14.65	40	72										
V	14.75	42	74										

Type	BH depth	Azimuth of dip	Dip	EP	CHL	CA	FE	PY	FL	MU	LAU	T/O	Remarks
F	14.795	6	62		X								Rough
V	14.84	38	78										
F	14.92	220	82		X								Rough
V	14.95	40	74										
F	15.05	180	38		X	X						O	Planar
F	15.08	307	88									O	Rough
V	15.11	46	68										
F	15.16	40	72		X							T	
F	15.20	30	88		X							O	FG, rough
V	15.25	44	62										
F	15.31	197	45		X							O	Planar
F	15.32	5	61			X						O	FG
F	15.41	12	86		X	X	X					O	Coated, planar
V	15.42	61	67										
F	15.47	232	74		X		X					O	Coated, planar
F	15.56	153	41		X	X						O	Planar
F	15.60	153	41		X		X					O	Planar, "rust"
F	15.64	330	82		X	X						O	Coated, 1/2-tight
F	15.65	39	69		X	X						O	Coated, 1/2-tight
V	15.67	067	71										
F	15.73	54	80		X	X						T	
F	15.75	227	85	X								T	5 mm
F	15.78	227	85		X	X		X				O	Coated
V	15.88	62	72										
F	15.92	40	75										
F	15.97	138	14			X			X			O	Planar
F	16.01	22	90			X			X			O	Undu-lating, roughish
F	16.28	238	89	X	X							O	Rough
F	16.33	13	89									T	
F	16.44	4	64			X			X			O	1/2-tight
F	16.57	165	84	X		X	X					O	FG
F	16.65	356	82									T	
F	16.75	25	66		X							T	
F	16.76	58	87	X								T	Qz-vein
F	16.85	285	36			X						T	1 mm
F	17.02	42	68	X	X							O	FG
F	17.13	22	71									T	
F	17.15	187	62			X						O	FG, Qz-x:tals
F	17.155	172	77		X							O	FG
F	17.20	24	84		X	X		X				O	Qz-xtals
F	17.30	231	70									O	

Drillcore KXTT4

Type	BH depth	Azimuth of dip	Dip	EP	CHL	CA	FE	PY	FL	MU	LAU	T/O	Remarks
F	3.17	313	48				X	X				T	
V	3.15	27	74										
F	3.18	27	82	X								T	2 mm
F	3.25	288	20			X	X					T	
V	3.27	33	76										
F	3.3	260	26		X		X					O	
V	3.42	20	78										
F	3.47	38	79	X			X					T	
F	3.48	294	50				X					T	
F	3.51	36	20	X									2 mm
F	3.58	194	72			X						O	
V	3.61	21	82										
F	3.65	32	85			X	X					T	Trippel
F	3.72	148	24			X						O	
V	3.74	006	80										
F	3.82	192	50			X						O	With a splay
F	3.87	208	78	X			X					T	Trippel
F	4.03	012	80	X								T	
F	4.04	191	38	X	X							O	
F	4.05	203	22	X	X	X						T	
F	4.12	214	51		X							O	
F	4.17	299	70		X							T	
F	4.20	218	51		X							O	
F	4.27	051	74			X						O	
F	4.28	237	20			X						O	
F	4.31	234	23			X						O	
F	4.315	296	24			X						O	
F	4.33	206	90	X								T	
F	4.35	192	66			X						O	
F	4.37	131	30	X	X							O	
F	4.41	157	54	X	X							O	
F	4.49	189	68			X						O	
F	4.505	188	74			X						O	
F	4.56	032	76	X								T	
F	4.60	143	42			X						O	
F	4.61	056	90			X						O	
F	4.62	161	53			X						O	
F	4.65	118	36	X	X							O	
F	4.73	339	46	X								T	3 mm
V	4.79	016	70										
V	5.10	014	75										
F	5.15	044	72	X								T	1 mm
F	5.28	134	28	X								T	
F	5.29	201	74		X							O	
F	5.35	206	72	X								T	3 mm
F	5.41	289	86	X									2 mm
F	5.44	140	29		X							O	
F	5.445	202	76	X								O	

Type	BH depth	Azimuth of dip	Dip	EP	CHL	CA	FE	PY	FL	MU	LAU	T/O	Remarks
F	5.51	193	62	X								T	1 mm
F	5.64	194	63									O	
F	5.67	219	78	X								T	5 mm
F	5.68	161	56									T	
V	5.68	047	64										
F	5.70	138	28			X						O	
F	5.77	172	66	X								T	3 mm
V	5.82	048	73										
F	5.90	030	80	X									
F	5.94	206	48									O	Empty
F	5.95	038	82									O	Empty
F	5.99	132	30										
F	6.01	205	56	X								O	
F	6.08	130	22	X	X	X						O	
V	6.05	056	67										
F	6.16	230	16	X	X		X					O	
F	6.36	066	70	X								T	
V	6.37	048	68										
F	6.43	210	70	X		X						T	
V	6.47	074	75										
F	6.48	060	72	X								O	
F	6.51	028	85	X								T	Quadruppel
F	6.60	052	84	X								T	2 mm
F	6.75	040	80	X								T	
V	6.78	066	76										
F	6.84	034	82	X	X							T	Double
V	6.87	066	72										
F	6.90	036	78	X	X							T	Trippel
F	6.95	052	86	X	X							T	Quadruppel
F	6.98	040	74	X	X							T	
V	7.09	029	78										
V	7.20	012	78										
F	7.23	344	16			X						T	
V	7.34	29	80										
F	7.45	193	72			X						O	
V	7.55	34	77										
F	7.57	215	82	X								T	
F	7.59	196	38	X								O	
V	7.67	21	73										
F	7.75	180	74	X								T	
F	7.78	206	80	X	X							T	Contact
F	7.87	51	81	X	X								
F	7.95	20	84	X								T	Qz, many parallell
F	8.02	24	78	X								T	Mylonite, 4 mm
V	8.06	34	76										
F	8.12	20	79	X								T	
F	8.15	189	78			X						O	
V	8.18	22	76										
V	8.31	22	75										
F	8.40	140	29		X							O	

Type	BH depth	Azimuth of dip	Dip	EP	CHL	CA	FE	PY	FL	MU	LAU	T/O	Remarks
V	8.46	1	88										
F	8.47	315	40		X							T	
F	8.65	183	54			X						O	
V	8.71	18	78										
V	8.84	23	76										
F	8.87	184	54		X							O	
F	8.98	44	85	X								T	Quadruppel
V	8.98	32	80										
F	9.00	49	80	X								T	
V	9.09	33	78										
V	9.20	24	78										
V	9.31	16	74										
F	9.34	311	28			X						T	
F	9.35	26	74	X								T	
F	9.38	11	80	X								T	
F	9.45	224	79		X							O	
F	9.67	354	89	X	X	X						O	Fault
V	9.73	22	73										
V	9.89	18	74										
V	10.15	16	70										
F	10.11	34	68	X									5 mm
V	10.16	12	72										
F	10.17	26	74	X									3 mm
V	10.28	13	72										
F	10.36	251	30				X					O	Black oxide
V	10.39	13	80										
F	10.44	202	78			X						O	
F	10.59	24	69	X								T	2 mm
F	10.61	264	24	X								O	
V	10.60	2	85										
F	10.72	254	20		X							O	
F	10.83	288	25		X							O	
F	10.94	10	90		X							O	
V	10.95	8	80										
F	10.98	190	47										
V	11.05	38	74										
V	11.15	36	78										
F	11.17	22	68										Mylonite
V	11.25	38	76										
F	11.28	10	64										Mylonite
V	11.35	28	70										
F	11.46	2	61										Mylonite
V	11.46	2	61										
V	11.65	38	63										
V	11.66	36	68										
F	11.73	42	58	X									Mylonite
V	11.75	46	65										
F	11.78	348	88	X		X						T	
V	11.85	41	62										
F	11.88	29	78	X									Mylonite, small

Type	BH depth	Azimuth of dip	Dip	EP	CHL	CA	FE	PY	FL	MU	LAU	T/O	Remarks
F	11.90	30	76	X									Mylonite, small
V	11.95	33	67										
F	12.11	32	76										Mylonite, A-feature
V	12.11	32	76										
F	12.12	181	14			X							Fault, with splay
V	12.15	32	62										
F	12.16	212	80	X								T	
F	12.18	214	90	X								T	
V	12.25	31	64										
F	12.30	180	58			X							
V	12.34	352	86										Contact
V	12.45	37	75										
V	12.55	33	74										
V	12.65	36	72										
V	12.75	30	75										
V	12.85	28	73										
V	12.95	26	74										Pyrite in rock
F	13.01	20	80		X								Fault, planar
F	13.02	216	80	X	X							O	
F	13.05	216	80	X	X							T	
F	13.06	216	80	X	X							T	
F	13.08	26	75	X								T	3 mm
V	13.13	24	78										
F	13.27	30	88	X								T	
F	13.32	30	88	X								T	
V	13.33	24	84										
F	13.44	200	82	X								T	4 mm
F	13.45	178	52	X								T	Double
F	13.49	144	15			X						O	
F	13.57	034	90	X								T	
F	13.58	034	88	X								T	
V	13.58	006	78										
F	13.60	038	90	X								T	
F	13.65	034	80	X								T	
F	13.70	006	78			X						T	
V	13.72	006	70										
F	13.81	226	75			X						O	
V	13.90	006	78										
F	13.92	052	82	X		X						T	
F	13.94	028	85	X		X						T	5 mm
F	14.05	226	90	X								T	
F	14.09	024	88	X								T	
F	14.17	238	70									O	
F	14.20	174	60	X								T	
F	14.21	226	15			X							
F	14.27	038	88				X	X					
F	14.33	034	85	X								T	
F	14.35	176	48			X						T	
F	14.36	041	72	X	X							T	
F	14.48	334	90										

Type	BH depth	Azimuth of dip	Dip	EP	CHL	CA	FE	PY	FL	MU	LAU	T/O	Remarks
F	14.49	354	72			X						O	
F	14.55	204	44		X							O	
V	14.62	002	90										
F	14.65	207	75		X							O	
V	14.72	032	86										
F	14.77	024	86	X	X							T	Contact
F	14.90	046	90			X							
F	14.97	056	58	X								T	
F	14.99	215	49		X							O	
F	15.00	018	70	X								T	
F	15.03	210	55			X						T	
F	15.05	052	68		X							T	
V	15.05	052	68										
F	15.07	052	68		X							T	
F	15.10	182	88		X							O	
F	15.13	008	85	X	X							T	
F	15.19	028	87	X	X							T	
F	15.205	333	67		X							O	
F	15.21	184	50		X							O	
F	15.23	196	88	X	X							O	Fault
F	15.25	196	88		X							O	
F	15.31	198	42	X								T	
F	15.32	140	27		X							O	Planar
F	15.39	188	58	X								T	
F	15.47	164	60	X								T	
F	15.50	142	90	X		X						O	
F	15.51	218	36	X	X							O	
F	15.55	218	36	X	X							O	
V	15.59	006	82										
F	15.64	164	24		X							O	
F	15.68	167	26		X	X		X				O	
V	15.71	002	86										
F	15.87	170	60										
F	15.90	206	22	X		X						O	
V	15.94	356	90										
F	16.08	260	27	X								T	
F	16.10	228	18	X		X						O	
V	16.16	016	87										
F	16.22	190	38			X						O	
V	16.30	016	85										
F	16.43	021	86	X								T	4 mm
V	16.57	006	83										
F	16.68	156	26			X						O	
V	16.87	002	85										
F	16.95	160	60	X								T	
F	17.03	170	55	X								T	
F	17.13	030	83	X	X							T	
F	17.15	086	68			X						T	
V	17.16	028	78										
F	17.20	034	79	X	X							T	Qz

Type	BH depth	Azimuth of dip	Dip	EP	CHL	CA	FE	PY	FL	MU	LAU	T/O	Remarks
F	17.21	069	67	X								T	Qz, 5 mm
F	17.28	240	65		X	X						O	
V	17.44	048	84										
V	17.53	016	81										
F	17.55	045	05	X	X							T	
F	17.63	206	80		X							T	
V	17.66	008	87										
F	17.69	164	55	X	X							T	
V	17.74	358	90										
F	17.79	216	70		X							O	
F	17.85	196	69	X								T	10-15 mm
F	17.94	242	90	X	X	X						O	
F	18.24	199	89	X								T	
F	18.35	231	64	X								T	
F	18.47	045	87	X								T	
F	18.49	029	76		X							O	
F	18.67	146	37	X	X	X						O	
F	18.87	166	40		X	X						O	
V	18.97	346	88										
F	19.07	159	72			X						O	Rough
F	19.17	013	60	X	X							T	
F	19.22	000	30		X							O	
V	19.23	090	76										
F	19.23	000	30		X							O	
F	19.30	215	82			X						T	
F	19.32	210	74		X	X						O	Ca-x:tals, idiomorphic
F	19.33	026	75		X	X						O	Ca-x:tals, idiomorphic
F	19.55	046	80	X								T	Contact
F	19.57	296	36			X						T	
F	19.60	215	72	X	X							O	
F	19.74	359	75								X	O	
F	19.75	180	75			X						O	
V	19.85	014	77										
F	19.98	240	90		X							T	
F	20.00	282	36									O	
F	20.10	035	89									O	Empty
F	20.15	036	87		X							O	
F	20.20	045	75									O	FG
F	20.22	045	75									O	FG
F	20.25	045	75									O	FG
F	20.30	035	89									O	
F	20.36	022	90		X	X						O	
F	20.41	197	84									O	FG
F	20.42	170	30			X						O	
F	20.45	056	90									O	FG
F	20.50	191	82		X							O	
F	20.58	344	71			X						T	
F	20.585	344	71	X								T	
F	20.59	344	71		X	X						O	
F	20.75	038	88			X						T	

Type	BH depth	Azimuth of dip	Dip	EP	CHL	CA	FE	PY	FL	MU	LAU	T/O	Remarks
F	20.76	038	82		X							O	
F	20.78	213	72		X							O	
F	20.81	025	70									O	FG
F	20.85	121	45			X						O	
V	20.90	000	72										
F	20.94	177	77			X			X			O	
F	20.95	211	82			X						O	
F	20.96	014	81			X						O	
F	21.00	186	60		X							O	
F	21.08	180	77		X	X						O	
F	21.10	180	77		X	X						O	
F	21.15	262	62	X	X							T	
F	21.20	210	24			X						T	
F	21.21	136	42			X						T	
F	21.25	174	40			C						O	
V	21.28	002	82										
F	21.34	037	76		X							O	
F	21.37	028	01		X	X				X		O	
V	21.41	020	70										
F	21.44	212	86				X					T	Partly open
F	21.49	039	61		X							O	Fault, slickensides 55to012
F	21.50	033	59		X							O	
V	21.56	016	78										
F	21.60	174	64			X						O	Only small amounts
F	21.65	046	80		X							O	
V	21.68	270	74										
F	21.75	031	90			X						O	
F	21.76	030	62		X							O	
F	21.83	255	52	X								T	2 mm
F	21.85	328	78		X								
F	21.87	214	23	X								T	4 mm
V	21.89	052	68										
F	21.95	040	82		X							O	
F	22.07	218	78	X								T	1-2 mm
V	22.12	014	78										
F	22.20	208	64			X						O	
F	22.25	228	54			X						O	
F	22.26	268	82	X	X							T	Contact
F	22.33	266	88	X	X							O	Fault, slickensides 0to200
F	22.43	256	80	X	X							O	Fault, slickensides 50to190
F	22.49	040	90	X	X							O	Fault, slickensides
F	22.52	254	84	X								T	5 mm
F	22.58	350	10			X						T	
V	22.63	66	58										
F	22.75	068	83	E								T	
F	22.76	202	72			X						O	
F	22.80	074	82	X								O	

Type	BH depth	Azimuth of dip	Dip	EP	CHL	CA	FE	PY	FL	MU	LAU	T/O	Remarks
F	22.83	156	64				X					T	
F	22.85	34	72		X							O	
F	22.87	118	82	X	X							T	
F	22.90	034	72		X							O	
V	22.91	029	68										
F	22.98	220	80		X							O	
F	23.03	356	62		X							O	
F	23.12	016	78									O	
F	23.15	026	82										
F	23.29	026	82										
V	23.25	025	70										
F	23.34	324	18			X						T	
F	23.48	221	66		X							O	
F	23.53	039	62		X							O	
V	23.55	026	68										
F	23.59	354	55		X							O	
F	23.65	183	74		X							O	
F	23.655	198	54	X								T	
F	23.70	186	58	X								T	
F	23.75	186	54	X								T	
F	23.82	187	78				X					O	
F	23.85	187	54	X								T	3 mm
F	23.86	187	80	X	X							T	
V	23.96	022	67										
F	24.12	013	72			X						O	3 mm
F	24.18	014	70			X						T	
F	24.24	002	69			X						O	
F	24.29	005	64			X		X				O	
F	24.32	011	81			X						O	
F	24.35	046	63		X	X						O	
F	24.38	066	59			X						O	
F	24.58	064	71	X									8 mm
F	24.65	016	72		X		X					O	
F	24.80	274	10	X	X						X?	O	2 mm
F	24.85	205	87	X	X						X?	O	3 mm
F	25.02	005	85		X							O	
F	25.24	009	59		X							O	
F	25.27	216	77		X	X						O	
F	25.31	210	50		X	X						O	
F	25.34	304	20		X	X						O	
V	25.34	036	64										
F	25.37	044	80		X	X						O	
F	25.42	030	80		X	X						O	
F	25.47	349	60			X						O	
F	25.03	198	81									O	
F	25.05	011	75									O	
F	25.61	023	76			X						T	x:tals, porous
F	25.64	214	68			X						T	x:tals, porous
F	25.71	349	85		X							O	
F	25.85	357	77		X							O	

Type	BH depth	Azimuth of dip	Dip	EP	CHL	CA	FE	PY	FL	MU	LAU	T/O	Remarks
F	26.00	331	75		X							O	FAULT
F	26.12	114	08			X						O	
V	26.16	026	62										
F	26.27	031	74		X							O	
F	26.34	014	76	X	X							O	
F	26.57	194	85		X							O	
F	26.60	010	63		X	X						T	
V	26.65	021	64										
F	26.66	178	84				X					T	
F	26.72	344	72		X	X						O	
V	26.81	041	64										
F	26.85	004	85		X							O	
F	26.94	032	69		X							O	
F	27.04	224	82	X								T	2 mm
F	27.05	224	82		X							O	
F	27.08	019	82			X						O	
V	27.09	18	72										
F	27.10	133	54			X						O	
F	27.22	122	50			X						O	
V	27.28	000	78										
F	27.40	022	85		X							O	
F	27.41	216	48			X						O	
F	27.44	025	90		X							O	
F	27.50	013	89			X						T	
V	27.63	016	75										
F	27.66	189	84				X					O	
F	27.75	009	79			X						O	
V	27.85	015	75										
F	28.05	146	27		X	X						O	
V	28.13	016	67										
F	28.14	068	82	X								T	
F	28.25	037	70		X	X						T	
V	28.25	026	73										
F	28.38	028	12			X						T	
V	28.38	028	70										
F	28.66	020	82		X							O	
V	28.67	020	72										
F	28.74	030	65	X								T	10 mm, Mylonite
F	28.85	032	65		X	X						O	FAULT
F	28.86	049	66		X			X				O	FG
F	28.92	028	64		X	X						O	FG
V	28.95	010	72										
F	29.05	209	78		X							O	
F	29.07	359	90			X						O	FG
F	29.13	021	70	X								T	3 mm
F	29.16	184	87			X						O	
F	29.24	050	82	X									4 mm
F	29.27	213	84		X							O	
F	29.30	040	83		X							O	FG
F	29.32	010	78		X	X						O	FG, ca-x:tals

Type	BH depth	Azimuth of dip	Dip	EP	CHL	CA	FE	PY	FL	MU	LAU	T/O	Remarks
F	29.34	032	80										
F	29.37	036	88			X						O	FG, ca-x:tals, slicken-sides 38to350
F	29.40	042	87			X						O	Ca-x:tals
F	29.45	010	73	X								T	25 mm
F	29.54	165	85	X								T	10-15 mm
F	29.61	063	90		X	X	X	X				O	Ca-x:tals
V	29.65	062	70										
V	29.81	084	74										
V	29.92	088	80										
F	30.02	002	81	X		X	X					O	FG, Ca-x:tals
F	30.07	180	60	X			X					T	
F	30.08	168	66		X							O	FG
V	30.09	072	79										
F	30.12	228	70				X					O	FG
F	30.14	194	26	X								T	4 mm
F	30.27	216	40				X					O	
V	30.33	081	72										
F	30.54	198	69	X								T	3 mm
F	30.55	013	89	X		X	X	X				O	FG
F	30.58	158	76	X		X	X	X				O	FG
F	30.65	216	72	X					X			O	
F	30.70	218	68		X				X			O	
F	30.74	216	70		X	X						O	
F	30.86	048	73	X								T	2 mm
F	30.90	049	73	X								T	2 mm
F	31.09	204	60			X						O	
V	31.12	039	70										
F	31.17	035	74	X								T	2 mm
V	31.25	31	72										
F	31.29	132	59			X		X				O	
F	31.37	049	68	X									9 mm
F	31.40	049	68	X	X							O	FG
F	31.44	019	75		X	X	X	X				O	
F	31.51	208	70									O	
F	31.52	027	65									O	
F	31.58	029	74									O	
F	31.62	026	78	X								T	2 mm
V	31.64	012	68										
F	31.69	050	79	X								T	3 mm
F	31.76	006	76			X						O	
V	31.81	028	76										
F	31.85	028	76	X								T	
F	31.93	038	72	X								T	1 mm
V	31.94	020	68										
F	32.10	024	66			X		X				O	
F	32.14	050	66			X						O	
F	32.29	030	76		X							T	
V	32.32	019	70										
F	32.37	018	76	X	X							T	

Type	BH depth	Azimuth of dip	Dip	EP	CHL	CA	FE	PY	FL	MU	LAU	T/O	Remarks
F	32.39	008	58		X	X		X				O	FG, slickensides 80to338
F	32.54	016	63		X		X					O	
V	32.62	050	68										
F	32.63	046	68		X							T	
F	32.75	046	62	X	X							T	
V	32.76	048	62										
F	32.82	048	54		X							T	
F	32.86	028	71			X						O	
F	32.90	013	90			X						T	
F	32.93	054	78	X	X							T	
F	33.05	049	75	X					X			O	
F	33.08	076	70		X			X				O	
F	33.13	042	64		X							O	FG
F	33.17	061	80	X		X						O	
F	33.19	028	80	X		X						O	
F	33.22	056	74	X	X		X					O	
F	33.25	006	55		X							O	
F	33.39	026	80		X	X						O	
F	33.57	014	72		X							T	
F	33.63	028	76	X								T	
V	33.66	072	62										
F	33.71	074	69	X								T	1 mm
V	33.93	060	76										
F	34.05	078	56	X								T	1 mm
F	34.07	270	41		X							O	FG
F	34.11	200	78			X						O	
F	34.22	304	60			X						O	FG
F	34.31	336	48			X						O	
F	34.36	008	65		X							O	Bad fit
F	34.45	006	73		X							O	Bad fit
F	34.51	041	78		X	X	X					O	
V	34.57	062	55										
V	34.67	050	64										
V	34.85	074	58										
F	35.00	184	80		X	X						T	
V	35.09	070	76										
F	35.15	034	78		X							T	
F	35.20	000	80			X						O	FG
V	35.28	056	74										
V	35.43	073	66										
F	35.73	042	80			X		X				O	
F	35.76	044	78			X		X				O	
F	35.90	019	68		X							T	
F	35.95	048	74	X	X							T	
F	36.03	022	80			X		X				O	
F	36.10	018	62				X						
V	36.16	077	68										
F	36.30	019	62	X	X								
F	36.38	018	86		X	X		X				O	

Type	BH depth	Azimuth of dip	Dip	EP	CHL	CA	FE	PY	FL	MU	LAU	T/O	Remarks
V	36.42	078	72										
F	36.49	236	72	X								T	
F	36.60	039	80		X							T	2 mm
V	36.65	064	66										
F	36.75	036	59	X									
V	36.78	070	65										
V	36.80	072	72										
F	36.99	041	72			X		X				O	
F	37.14	002	66	X			X					T	
V	37.16	076	74										
F	37.30	016	62	X	X							T	
V	37.34	084	66										
F	37.73	024	72	X			X					T	
V	37.78	082	74										
F	37.86	302	14			X						T	Qz, K-fsp
F	37.89	028	76	X									
V	37.93	080	70										
F	37.96	080	80	X								T	
F	38.03	038	80			X		X				O	
V	38.14	084	76										
V	38.30	082	74										
F	38.56	062	78	X								T	
F	38.76	198	85			X		X				O	
V	38.89	070	70										
F	38.95	056	78	X								T	
V	39.14	094	80										
V	39.35	084	80										
F	39.47	185	58			X						O	
F	39.52	070	78									T	
F	39.55	071	79		X	X						O	FG, bad fit
V	39.56	071	78										
F	39.59	071	78		X	X		X				O	Bad fit
F	39.77	075	74			X						T	
V	39.93	082	80										
F	39.95	062	75	X								T	
V	40.09	096	80										
F	40.07	071	78	X								T	
F	40.20	075	78	X								T	
F	40.22	073	78	X								T	
F	40.30	053	90	X			X					O	
F	40.38	041	64	X		X	X					O	
F	40.43	70	82			X						O	
F	40.55	60	86			X						O	
F	40.62	56	72	X								T	
V	40.67	62	72										
F	40.75	5	66	X								T	
V	40.89	60	62										
F	40.91	215	84			X						O	
F	40.98	54	68										
F	41.10	215	85			X						O	

Type	BH depth	Azimuth of dip	Dip	EP	CHL	CA	FE	PY	FL	MU	LAU	T/O	Remarks
V	41.15	084	74										
F	41.21	034	90			X		X				O	FG
F	41.22	206	70		X	X						O	
F	41.23	034	74			X						O	
V	41.28	067	70										
V	41.42	086	78										
F	41.75	201	77		X	X						O	
F	41.76	108	46		X	X						O	Rough, slickensides 08to047
V	41.80	076	76										
F	41.83	58	82	X								T	
V	41.89	070	64										
F	42.04	046	74		X	X						O	
V	42.19	090	73										
F	42.24	302	74	X								T	
F	42.34	309	68	X								T	
F	42.55	084	78	X								T	
V	42.64	084	78										
F	42.75	035	76			X						O	
F	42.78	172	80			X						O	
V	42.86	082	72										
F	43.05	220	86	X								T	15 mm
F	43.15	050	76	X								T	
V	43.16	058	58										
F	43.20	056	69	X				X				T	
F	43.3	028	86			X						O	FG
F	43.36	121	53			X						O	1 mm
F	43.55	068	76	X								T	2 mm
F	43.57	041	84			X						O	
F	43.60	036	84			X						O	
F	43.63	020	88									O	
V	43.71	051	54										
F	43.77	016	78	X								T	
F	43.83	054	76	X								T	
F	43.98	044	72	X		X						O	FG, bad fit
F	44.05	041	72		X	X		X				O	FG, bad fit
F	44.13	016	65	X								T	
V	44.15	054	54										
F	44.22	093	66		X							O	Slickensides 20to226
V	44.28	054	58										
F	44.45	161	54			X						O	
F	44.55	037	89			X		X				O	
F	44.59	039	82			X						O	
V	44.65	056	60										
F	44.70	170	56			X						O	FG
F	44.73	032	74	X								T	3 mm
V	44.84	052	56										
F	44.90	018	66	X								T	
F	45.15	170	34			X						O	
V	45.18	052	62										

Type	BH depth	Azimuth of dip	Dip	EP	CHL	CA	FE	PY	FL	MU	LAU	T/O	Remarks
F	45.27	054	84			X						O	
F	45.40	143	56		X							O	
V	45.43	051	56										
F	45.47	211	80		X	X		X				O	FG, 3 mm
F	45.49	128	16										
F	45.53	162	48		X							T	
F	45.56	211	82		X							O	
V	45.58	044	60										
F	45.70	154	42		X		X					T	
V	45.73	046	67										
V	45.88	029	56										
F	45.91	071	79		X	X	X	X				O	Qz, slickensides 20to014
F	46.06	168	72		X		X					T	
F	46.07	210	72		X		X					O	
V	46.11	042	60										
F	46.21	110	52		X	X	X					O	
F	46.25	035	88		X							O	
V	46.28	044	66										
F	46.34	042	70		X								
F	46.35	152	56		X								
F	46.40	132	48		X		X					O	
F	46.45	142	48		X		X	X				O	
V	46.47	056	68										
F	46.57	132	57		X	X	X					O	FG, 3 mm
F	46.65	166	52		X	X	X	X				O	
V	46.65	046	68										
F	46.69	112	48		X	X	X	X				O	
F	46.75	188	40		X	X	X					O	
V	46.76	040	58										
F	46.78	174	54				X					O	
F	46.86	218	80		X	X		X				O	
F	46.89	211	82			X						O	
F	46.91	029	86			X						T	
F	47.01	206	80			X				X		O	Slickensides
F	47.03	029	77			X						O	FG, rough
F	47.05	046	90		X	X						O	2 mm
F	47.17	142	41		X	X		X				O	Fault; FG, rough
F	47.21	226	83			X						T	
F	47.30	042	68		X		X					O	Slickens 52to012
F	47.39	160	52		X	X	X					T	Partly open
V	47.43	056	58										
F	47.45	136	40		X	X						T	
F	47.54	127	60		X	X	X					O	Rough
F	47.64	038	62		X		X					T	
V	47.67	054	54										
F	47.76	150	40		X	X	X					O	
F	47.77	030	90		X	X	X					O	

Type	BH depth	Azimuth of dip	Dip	EP	CHL	CA	FE	PY	FL	MU	LAU	T/O	Remarks
F	47.86	098	20		X							O	Tachylitic, slicken-sides 20to132. Sense of movement opposite dip direction
V	47.89	060	56										
F	48.01	066	85	X	X	X		X				O	
F	48.04	243	76	X								T	Mylonite, 2 mm
F	48.06	250	80		X							O	
F	48.14	274	32		X							O	
F	48.20	059	78		X	X	X					O	
V	48.23	042	58										
F	48.25	342	88		X	X	X					O	
F	48.36	042	70		X							O	
F	48.37	196	4		X	X						T	2 mm
F	48.55	016	82	X								T	
V	48.61	064	64										
F	48.65	186	61			X						O	
F	48.75	064	76	X								T	
V	48.76	064	64										
F	48.80	180	64		X							O	
F	48.85	076	72		X	X						O	Rough
F	48.855	146	72		X	X						O	FG, rough
F	48.95	160	63			X						O	
F	49.14	190	78			X						O	
F	49.22	050	72		X							O	

Drillcore KA3005a

Type	BH depth	Azimuth of dip	Dip	EP	CHL	CA	FE	PY	FL	MU	LAU	T/O	Remarks
V	0.30	057	78										
F	0.51	350	62		X							T	
F	0.59	016	60		X	X						O	Several parallels
F	0.73	016	60		X							T	Parallels
F	0.75	016	60		X							T	Parallels
V	0.95	072	58										
V	1.25	052	76										
F	1.56	003	62	X								T	2 mm
V	2.56	336	55										
F	2.57	076	74	X		X							
V	2.75	338	50										
V	2.96	322	90										
V	3.14	326	50										
F	3.26	166	80	X	X								
F	3.38	166	80	X	X								
F	3.30	166	80	X	X								
V	3.45	336	70										
F	3.55	170	80	X	X								
V	3.65	342	74										
F	3.70	238	78										
V	3.75	342	78										
F	3.89	270	84			X							
V	4.10	320	67										
V	4.26	319	68										
V	4.36	322	69										
V	4.46	319	62										
V	4.57	335	88										
V	4.70	328	63										
F	4.75	047	36		X								
V	4.93	336	90										
F	4.93	081	80	X								T	
F	4.95	082	82	X								T	
F	4.99	076	18		X							O	Planar
F	5.00	108	72			X						T	
F	5.15	076	88	X									
F	5.23	220	28										
F	5.25	174	33	X									
F	5.645	344	68	X	X							T	
F	5.65	080	80	X									
F	5.67	326	74	X	X								Qz
V	5.73	332	58										
F	5.75	332	40	X	X							T	
F	5.86	336	70	X	X							T	
F	5.95	322	62										Splay
F	5.955	154	58										Master
V	5.98	330	56										
F	6.06	132	86		X								Contactarea
V	6.13	326	50										

Type	BH depth	Azimuth of dip	Dip	EP	CHL	CA	FE	PY	FL	MU	LAU	T/O	Remarks
F	6.25	274	70	X								T	
F	6.28	272	68	X									
V	6.31	318	54										
F	6.35	336	42	X								T	3 mm
F	6.45	340	56	X								T	3 mm
V	6.76	150	74										
V	6.94	148	79										
V	7.11	332	84										
F	7.17	051	88	X	X							T	
F	7.36	072	72	X	X								
F	7.39	335	80	X	X								
V	7.42	336	90										
F	7.49	345	88										
F	7.55	338	65	X								T	
V	7.55	338	65										
F	7.60	218	30	X								T	
F	7.66	284	36	X	X								
F	7.68	218	22								X		
V	7.83	346	86										
F	7.85	244	64	X								T	Trippel
F	7.92	314	68		X								
V	7.98	164	60										
F	8.00	230	36		X								
F	8.04	230	38		X	X							
V	8.06	164	62										
V	8.24	346	90										
F	8.27	266	40		X	X							
F	8.29	226	25		X	X							
F	8.31	306	58		X	X							
V	8.55	168	80										
V	8.63	162	70										
F	8.66	234	34		X	X							FAULT, planar, bad fit
V	8.90	164	74										
F	9.01	028	24			X				X		T	
V	9.15	163	76										
F	9.24	344	40		X	X							
V	9.25	156	80										
F	9.30	336	64										
F	9.37	332	72	X	X								Trippel
V	9.41	336	70										
F	9.54	310	68	X	X	X							
F	9.56	330	72									T	Double
V	9.61	336	76										
F	9.65	326	74	X								T	
F	9.67	290	76	X		X							
F	9.68	302	78	X		X							
F	9.70	322	74										
F	9.73	240	76										
V	9.74	348	58										
F	9.92	326	74	X								T	

Type	BH depth	Azimuth of dip	Dip	EP	CHL	CA	FE	PY	FL	MU	LAU	T/O	Remarks
F	10.01	329	76	X								T	Double
V	10.07	164	88										
F	10.20	082	80										Qz, 1 mm
V	10.24	162	78										
F	10.37	236	42			X						T	
V	10.42	148	74										
F	10.51	210	58			X						T	
V	10.51	163	82										
F	10.65	308	78	X									2 mm
F	10.67	324	67	X								T	
F	10.69	332	74	X								T	
F	10.72	314	78	X								T	
F	10.75	216	67										
F	10.77	332	74										
V	10.77	168	82										
F	10.85	330	78	X									1 mm
F	10.92	333	82	X									2-3 mm
F	10.94	226	62										
F	10.99	222	58										
F	11.05	218	64	X								T	
V	11.14	164	78										
F	11.27	057	68									T	No visible filling
F	11.33	263	80	X									
V	11.34	161	82										
F	11.35	230	63		X							T	
F	11.40	246	78									T	
F	11.55	233	72		X							T	
V	11.56	324	80										
V	11.60	336	80										
F	11.85	060	84	X	X								
F	11.88	069	84	X		X							Double
F	11.93	308	67	X	X								
F	11.99	062	90										
F	12.03	324	76	X									1 mm
F	12.04	324	74	X								T	
F	12.045	231	74	X									
F	12.06	230	73	X									
F	12.12	243	78	X	X	X							2 mm
F	12.13	353	52	X	X	X							Master
F	12.15	328	60										Splay
F	12.16	033	81	X									
F	12.19	322	58										
F	12.25	320	60	X								T	
F	12.28	326	59	X								T	
V	12.29	156	80										
F	12.33	062	82	X								T	
V	12.36	156	82										
F	12.43	056	76	X								T	
V	12.64	155	85										
V	12.84	146	82										

Type	BH depth	Azimuth of dip	Dip	EP	CHL	CA	FE	PY	FL	MU	LAU	T/O	Remarks
V	12.93	158	80										
V	13.02	155	85										
F	13.23	304	41	X									
V	13.41	156	80										
F	13.46	328	46	X	X								
V	13.65	156	80										
F	13.74	250	66	X								T	
V	13.76	162	64										
F	13.80	172	52	X								T	
V	13.88	156	66										
F	13.99	338	82	X	X	X					X	O	
F	14.04	154	83	X		X						T	
F	14.09	321	68	X		X							
F	14.11	296	58	X	X								2 mm
F	14.18	310	50										Master, small splays
F	14.19	315	58										Master, small splays
F	14.23	333	78	X	X								
V	14.32	153	84										
F	14.44	327	71	X		X							
V	14.47	161	78										
F	14.51	026	60	X		X							
V	14.53	150	86										
V	14.65	146	86										
V	14.83	162	88										
V	15.08	153	66										
F	15.14	083	77	X	X								Qz
V	15.17	156	67										
F	15.23	150	84	X									
F	15.24	221	70	X									
F	15.26	216	70	X									
V	15.35	158	83										
V	15.56	332	78										
F	15.56	216	53		X								
V	15.59	342	80										
V	15.74	157	80										
F	15.78	064	48	X									
F	15.88	202	80										
V	16.00	156	82										
V	16.13	148	78										
F	16.27	031	90	X									
V	16.45	166	82										
V	16.50	166	82										
F	16.55	166	80	X	X								With splays
F	16.75	035	82	X	X								Qz
V	16.90	151	85										
F	17.00	346	78	X	X								With splay
V	17.06	152	82										
F	17.14	338	82	X	X								With splays
F	17.26	036	62									T	Not visible
V	17.29	164	78										

Type	BH depth	Azimuth of dip	Dip	EP	CHL	CA	FE	PY	FL	MU	LAU	T/O	Remarks
V	17.43	154	77										
F	17.51	238	48	X	X								
V	17.55	161	84										
F	17.67	261	30	X									
V	17.73	150	84										
F	17.78	320	74	X	X								
V	17.92	154	82										
V	18.13	154	84										
V	18.38	158	83										
V	18.58	154	80										
F	18.72	186	78	X	X	X							4 mm, with splays
V	18.83	156	78										
F	19.00	258	62	X	X								
F	19.05	311	88	X									2-3 mm
V	19.08	150	72										
F	19.09	305	80	X	X								
F	19.14	336	82	X	X								
F	19.15	146	78	X	X								
F	19.35	175	66	X									2 mm
V	19.35	156	64										
V	19.38	356	45										
V	19.60	335	74										
V	19.71	156	78										
F	19.77	066		X	X								Qz, subparallell
V	19.89	322	72										
F	19.92	156	82										
F	19.98	329	90	X									Qz
V	20.09	326	80										
V	20.23	328	74										
F	20.24	284	62	X	X								Qz
F	20.25	268	72	X	X								Qz
F	20.27	272	60	X	X			X					Qz
V	20.44	068	60										
F	20.63	330	66	X	X						X	O	
V	20.69	058	52										
F	20.77	232	60									T	No visible filling
F	20.92	212	52	X	X								Qz, possibly a splay
F	21.08	124	42	X	X								Qz
V	21.09	130	70										
F	21.10	041	24	X	X								Qz
F	21.14	074	30	X	X								Qz
V	21.25	328	70										
V	21.47	149	72										
V	21.63	087	48										
F	21.67	236	40									T	No visible filling
V	21.73	125	76										
V	21.77	232	76										
V	21.96	329	76										
V	21.98	234	74										
V	22.03	152	74										

Type	BH depth	Azimuth of dip	Dip	EP	CHL	CA	FE	PY	FL	MU	LAU	T/O	Remarks
F	22.05	359	78	X	X							T	Qz
V	22.08	064	62										
V	22.13	160	78										
F	22.17	000	88	X	X							T	
F	22.20	356	64	X	X							T	
V	22.25	142	80										
V	22.43	149	76										
V	22.66	162	80										
F	22.76	070	78	X		X							
V	22.81	148	76										
F	22.88	064	75	X						X			
F	23.02	346	62	X	X		X						Qz, with splays
V	23.03	146	80										
F	23.09	336	70	X	X	X							
F	23.11	316	78	X	X	X							
V	23.11	158	84										
F	23.20	049	58	X								T	
F	23.27	056	70	X	X								With splay
V	23.28	149	74										
V	23.43	156	85										
F	23.50	345	74	X								T	Qz
V	23.61	150	78									T	
F	23.70	063	74	X								T	
F	23.00	140	335	70									
V	23.81	164	78									T	
F	23.95	052	64	X	X								
V	24.12	159	76										
F	24.25	053	75	X	X							T	Qz
F	24.27	050	70	X	X							T	
V	24.34	146	70										
V	24.35	311	56										
F	24.56	051	78	X								T	Qz
V	24.64	153	72										
F	24.70	228	80	X								T	
F	24.75	044	76	X								T	Qz
V	24.76	345	74										
F	24.81	170	78		X		X						
F	25.22	216	72	X									Qz, in mylonite
F	25.27	225	72	X									Qz, in mylonite
F	25.34	232	72	X									Qz, in mylonite
V	25.46	343	82										
F	25.52	351	72	X	X		X						
V	25.57	156	80										
F	25.72	356	79	X	X		X						Qz
V	25.73	338	78										
F	25.75	324	76	X	X		X						
F	25.80	323	56										
V	25.83	330	70										
F	25.85	353	66										
F	25.93	348	62										

Type	BH depth	Azimuth of dip	Dip	EP	CHL	CA	FE	PY	FL	MU	LAU	T/O	Remarks
F	25.97	344	68										
F	26.04	317	50			X							
V	26.06	338	85										
F	26.16	325	70										
V	26.38	336	78										
F	26.44	059	78	X									
V	26.58	147	72										
V	26.66	336	82										
V	26.70	338	76										
F	26.70	102	28			X	X						4 mm
F	26.75	316	76			X							
F	26.85	042	76	X		X							
F	26.88	231	80	X		X							
F	27.14	042	62	X	X								Qz
F	24.15	319	62			X						T	
V	24.16	330	74										
V	27.26	329	73										
F	27.30	216	83	X								T	
V	27.39	328	69										
F	27.44	214	80	X									Qz, double
V	27.61	342	80										
F	27.76	048	79	X	X		X						Qz
V	27.85	332	74										
F	27.93	112	63										Qz
V	28.09	137	69										
V	28.20	143	46										
V	28.35	121	45										
F	28.40	276	28	X	X								
F	28.45	359	70	X	X								
V	28.59	341	80										
F	28.65	224	85	X	X								Qz
V	28.77	330	80										
F	28.91	248	42	X									3 mm
V	28.96	343	78										
V	29.15	150	82										
F	29.16	326	64	X									Qz, 4 mm
F	29.22	332	83		X							T	Qz
F	29.35	233	44	X	X								Qz, parallelles
F	29.55	155	80	X									Qz, mylonite
F	29.70	024	82	X									Qz, mylonite
F	29.82	030	78	X									Mylonite
F	30.00	026	72	X									Qz, 2-3 mm, contact
F	30.25	032	52	X									2-3 mm
F	30.44	049	50	X									Several parallells
F	30.65	080	80	X	X								15 mm
F	30.70	049	78	X									Qz, contactzone
F	30.75	046	76		X							T	
F	30.84	052	50										
V	30.85	059	46										
F	30.93	074	78										

Type	BH depth	Azimuth of dip	Dip	EP	CHL	CA	FE	PY	FL	MU	LAU	T/O	Remarks
F	31.01	063	52	X									
V	31.08	055	46										
F	31.10	064	60	X									
F	31.13	040	78	X									
F	31.20	087	86	X									
F	31.25	072	42	X	X								Qz
F	31.35	070	27										
F	31.37	127	42										
F	31.73	058	50	X	X								Several parallells
F	31.93	062	24	X	X								
F	32.15	050	60	X									
F	32.20	050	60	X									
F	32.25	050	60										
V	32.34	060	40										
F	32.55	044	68		X								
F	32.66	048	36	X									2 mm, contactarea
F	32.75	051	38	X									Qz
F	32.82	056	52	X	X								
F	33.14	171	74	X								T	
F	33.10	059	50	X	X								
F	33.15	062	48	X								T	
V	33.16	140	38										
F	33.25	340	42				X					T	
F	33.31	125	80		X								
V	33.33	070	38										
F	33.34	082	62		X								
F	33.37	048	54		X								
F	33.42	050	68		X								
F	33.50	050	64		X								
F	33.53	043	62		X								
V	33.55	056	42										
F	33.58	056	43		X								
F	33.65	071	66		X								Qz
V	33.68	061	54										
F	33.74	065	52	X									Qz
F	33.78	065	62		X								Qz
F	33.85	051	50	X								T	Qz
F	33.91	040	60	X									Qz
F	33.97	087	58		X								Qz
F	34.03	054	48	X	X							T	
V	34.05	316	58										
F	34.15	222	76	X	X								
F	34.16	138	50	X	X								
F	34.37	164	56	X	X								Qz
F	34.45	090	35										
F	34.50	140	50										
F	34.56	118	42		X								
F	34.57	068	46		X								
F	34.60	040	48		X								
F	34.67	054	64	X	X								Qz

Type	BH depth	Azimuth of dip	Dip	EP	CHL	CA	FE	PY	FL	MU	LAU	T/O	Remarks
V	34.69	049	73										
V	34.79	053	68										
F	34.84	094	78	X								O	Qz
F	34.94	066	48										
V	34.94	046	72										
F	35.01	054	58		X							T	Qz
V	35.06	063	68										
F	35.09	054	58	X	X							T	
F	35.10	054	67	X	X							T	
F	35.12	056	65	X	X							T	
F	35.20	064	65	X	X							T	
V	35.21	064	68										
F	35.25	156	73		X							T	
F	35.30	058	70	X	X							T	
F	35.35	062	54	X	X							T	Qz
V	35.38	054	60										
F	35.40	052	71	X								T	Qz
F	35.43	052	71	X								T	Qz
F	35.55	056	50		X			X				O	
F	35.58	061	60		X							T	Qz, trippel
V	35.60	048	52										
F	35.68	077	67		X							T	Qz, double
F	35.73	052	58	X								T	Qz
V	35.76	061	50										
F	35.80	338	43			X	X					T	
F	35.92	046	64	X								T	Qz, 3 mm
V	35.94	054	52										
F	35.94	054	68	X								T	Qz, 5 mm
F	36.01	074	60	X								T	Qz
F	36.04	068	60	X								T	Qz
V	36.04	071	39										
F	36.08	058	60		X							T	Qz, trippel
V	36.08	081	40										
F	36.14	060	40		X							T	Qz, quadruppel
F	36.25	059	60		X							T	
V	36.26	066	39										
F	36.30	065	58		X							T	Qz, quadruppel
V	36.39	073	50										
F	36.40	060	67	X								T	Qz, quadruppel
F	36.45	065	58	X		X						T	Trippel
V	36.48	061	44										
V	36.53	075	35										
V	36.62	062	44										
F	36.63	068	64	X	X							T	Several of parallells
F	36.66	088	57	X	X							T	Several of parallells
V	36.67	066	47										
V	36.68	326	58										
F	36.73	068	60	X								T	Qz
F	36.74	064	58	X								T	Qz
V	36.74	330	56										

Type	BH depth	Azimuth of dip	Dip	EP	CHL	CA	FE	PY	FL	MU	LAU	T/O	Remarks
F	36.79	075	67	X	X							T	
V	36.79	324	58										
V	36.81	070	52										
F	36.81	062	57	X	X							T	Several of parallells
F	36.85	061	71	X			X	X				O	3 mm
V	36.87	056	58										
F	36.90	216	74			X						O	
V	36.95	073	57										
F	36.96	070	64	X									
F	37.05	162	90		X	X						O	
F	37.13	088	54	X								T	4 mm
F	37.14	333	58	X	X							T	
F	37.145	170	70									T	Tiny fault fracture
F	37.15	188	70	X						X		T	
F	37.19	140	76									O	Break?
V	37.23	054	50										
F	37.25	219	82	X	X	X	X					O	
V	37.28	146	66										
F	37.30	026	90			X						O	
V	37.31	056	62										
F	37.35	316	82		X	X						O	
F	37.40	298	70	X								T	1-2 mm, double
V	37.43	072	47										
F	37.43	164	40	X			X					O	
F	37.435	071	50	X								T	Qz, syst. of parallells
F	37.45	098	54	X								T	
F	37.48	137	78			X	X					O	
F	37.50	034	80	X		X	X					O	
V	37.55	098	38										
F	37.56	305	81	X			X					O	
V	37.63	073	48										
F	37.64	284	26	X			X					T	
F	37.65	075	42	X			X					T	
V	37.66	322	56										
F	37.67	070	50	X			X					T	
F	37.74	310	85			X	X					O	
V	37.78	070	40										
F	37.80	061	66	X			X					T	Qz
F	37.87	084	72	X			X					O	
F	37.90	074	61				X	X				T	Qz
V	37.93	069	38										
F	38.01	088	36	X	X							T	
V	38.02	082	40										
F	38.05	344	48	X		X						T	
F	38.10	054	62	X			X					T	Qz
V	38.26	106	35										
V	38.30	113	30										
F	38.34	332	82	X			X					O	
V	38.39	114	39										
F	38.51	119	60	X								T	

Type	BH depth	Azimuth of dip	Dip	EP	CHL	CA	FE	PY	FL	MU	LAU	T/O	Remarks
F	38.57	090	58									T	Qz, 2mm
V	38.58	330	74										
F	38.65	054	50	X									Qz
F	38.69	076	64	X								T	
V	38.71	117	50										
V	38.78	075	46										
V	38.81	316	64										
F	38.85	082	54	X								T	Qz
F	38.89	066	70	X								T	Qz
F	38.90	312	80			X						O	
F	38.95	077	63	X									Qz, residue
V	38.97	327	60										
V	38.98	336	64										
V	38.99	108	45										
F	39.00	112	60	X			X					T	Qz, 2 mm
V	39.03	103	44										
V	39.04	338	65										
F	39.05	306	70									O	
V	39.13	072	38										
F	39.20	056	37	X			X					T	
F	39.22	311	78				X					O	
F	39.23	103	43	X	X		X					T	
F	39.30	066	74	X			X					T	
F	39.35	333	68									T	
V	39.38	336	66										
V	39.40	116	48										
F	39.40	035	60	X			X					T	Qz
F	39.405	084	63	X			X					T	Qz
F	39.44	352	75				X					O	
F	39.50	065	58	X			X					T	Qz
V	39.53	074	42										
V	39.53	306	50										
F	39.54	032	66	X		X						O	
F	39.56	322	62			X						O	
F	39.64	300	72				X					O	Black oxide
F	39.67	328	44				X					O	Black oxide
V	39.68	076	58										
F	39.80	286	58			X						O	
V	39.82	092	40										
V	39.85	110	52										
F	39.86	286	64			X						T	
V	39.89	110	46										
F	39.90	116	52	X								T	Qz, trippel
V	39.94	094	48										
F	39.98	128	68	X			X					T	Qz, 4 mm
F	40.01	127	62		X							T	Qz, trippel
F	40.05	108	50		X							T	Qz, trippel
V	40.07	084	44										
V	40.16	110	42										
F	40.20	112	76			X						O	Black oxide

Type	BH depth	Azimuth of dip	Dip	EP	CHL	CA	FE	PY	FL	MU	LAU	T/O	Remarks
V	40.30	104	42										
F	40.35	076	39										
F	40.44	309	72				X					O	
V	40.48	082	38										
F	40.50	088	60				X					T	Trippel
V	40.51	066	42										
F	40.55	286	60			X						O	
V	40.56	073	46										
F	40.58	110	52		X							T	Trippel
V	40.61	077	45										
F	40.71	105	64				X					T	Double
F	40.73	286	64				X					O	Black oxide
V	40.75	084	40										
F	40.83	298	62			X						O	Black oxide
V	40.86	098	46										
F	40.92	246	54	X			X						
V	40.92	098	46										
F	41.03	108	70	X								T	15 mm
V	41.04	090	44										
F	41.05	284	80				X					O	Black oxide
F	41.055	034	56				X					O	Black oxide
V	41.08	068	40										
F	41.24	096	56	X								T	Black oxide, trippel
F	41.245	070	58			X						O	
F	41.25	048	55			X						O	
F	41.38	270	58				X					O	Black oxide
F	41.40	268	84									O	Black oxide
V	41.46	088	58										
F	41.50	294	80	X								O	
F	41.51	110	66	X								T	
F	41.56	123	63	X	X							T	
V	41.58	103	46										
F	41.60	113	69	X	X							T	
F	41.61	110	58	X	X							T	
F	41.67	112	70	X	X							T	Trippel
V	41.69	131	54										
F	41.73	254	43				X						
F	41.79	102	79		X							O	
F	41.80	109	52	X	X							T	
F	41.84	118	53	X	X							T	
V	41.85	120	56										
F	41.88	248	49				X					T	
V	41.93	116	55										
F	41.99	105	49		X							T	
V	42.08	126	58										
F	42.10	132	68	X								T	System of parallells
F	42.15	128	60	X								T	System of parallells
V	42.20	127	48										
F	42.20	246	60	X		X	X					O	
V	42.30	328	66										

Type	BH depth	Azimuth of dip	Dip	EP	CHL	CA	FE	PY	FL	MU	LAU	T/O	Remarks
F	42.30	109	56	X			X					T	
F	42.35	109	64	X			X					T	
F	42.45	026	38										
F	42.49	283	77	X		X						O	
F	42.50	298	46	X								T	
F	42.55	117	50	X								O	
V	42.58	133	65										
F	42.60	104	64	X			X					T	
V	42.68	144	72										
F	42.69	128	58		X		X	X				T	System of parallells
V	42.76	148	55										
F	42.80	288	46		X							O	Black oxide?
F	42.88	268	40	X								T	
F	42.96	290	70	X								O	
F	43.61	251	64			X						O	
V	43.62	129	52										
V	43.64	312	68										
F	43.65	088	76	X								T	15 mm, at 43.4 on BIBS 210/84
V	43.73	310	71										
V	43.78	330	70										
F	43.79	103	70	X									
V	43.81	123	44										
F	43.86	126	66	X								T	
V	43.92	132	47										
V	43.93	320	67										
F	43.94	123	68	X								T	Trippel
F	43.99	108	68			X						O	
F	44.00	050	82	X				X					3 mm
V	44.05	057	86										
V	44.16	062	82										
F	44.20	206	70		X								Subparallell
V	44.26	052	82										
F	44.28	036	56		X							T	Subparallell, foliation
V	44.28	036	56										
F	44.33	221	80			X						T	
V	44.35	054	80										
F	44.35	096	80	X								T	
F	44.39	084	82	X								T	
V	44.46	058	88										
F	44.49	053	90		X							O	With ortogonal splay
F	44.55	110	88	X								T	5 mm
F	44.56	319	75									O	Break?
V	44.65	055	76										
F	44.67	028	84									T	Dark fault, subparralell
F	44.68	103	80	X								T	Offset by fault above
F	44.73	097	68	X								T	
V	44.76	052	82										
F	44.83	228	88		X								
V	44.85	046	83										

Type	BH depth	Azimuth of dip	Dip	EP	CHL	CA	FE	PY	FL	MU	LAU	T/O	Remarks
F	44.91	057	71		X							O	Slickens 46to356
F	44.93	075	78		X								
V	44.96	051	86										
F	44.98	062	88										A-feature, bad match
V	45.05	051	85										
F	45.07	078	78	X									
F	45.08	074	85	X								T	Mylonite
F	45.09	058	83										Fault
V	45.16	053	83										
F	45.21	280	78										Break?
V	45.25	055	81										
V	45.35	056	88										
F	45.41	273	85	X								T	
V	45.45	057	88										
V	45.55	056	88										
F	45.62	336	64										Qz-vein
V	45.65	054	87										
V	45.76	058	86										
F	45.78	306	78										Break?
V	45.85	058	84										
F	45.90	085	82		X								
V	45.96	060	82										
V	46.03	075	70										
F	46.07	268	84		X							O	
F	46.15	076	84		X							O	
V	46.20	080	52										
F	46.27	070	67	X								T	5 mm
V	46.30	062	67										
F	46.35	071	47	X								T	3 mm
V	46.39	060	66										
F	46.45	285	45		X							O	
F	46.49	268	52		X								
V	46.54	056	56										
F	46.61	292	48				X					T	
V	46.63	046	52										
F	46.65	111	60			X						O	
V	46.71	239	53										
V	46.77	226	70										
V	46.81	246	72										
F	46.88	144	82	X			X					O	
V	46.91	073	60										
F	46.96	168	38	X	X	X	X					O	
F	47.07	231	78	X		X	X	X				O	
F	47.19	124	56	X			X					T	
F	47.23	277	78	X		X	X			X		O	
F	47.24	044	60			X						O	
F	47.29	067	82	X		X	X					O	
F	47.31	239	83	X			X					O	
V	47.34	051	68										
F	47.37	264	85	X			X					O	

Type	BH depth	Azimuth of dip	Dip	EP	CHL	CA	FE	PY	FL	MU	LAU	T/O	Remarks
F	47.44	239	74	X		X	X					T	
V	47.45	065	46										
F	47.47	043	85	X		X	X					T	
F	47.49	271	78	X		X	X					T	
F	47.54	258	80				X					O	
V	47.57	063	58										
F	47.63	246	76	X								O	
F	47.64	056	54	X		X						T	
F	47.67	062	55	X								O	
F	47.71	081	40	X		X						T	
F	47.75	080	86	X	X		X					O	
V	47.80	050	67										
F	47.85	062	84			X	X					O	
V	47.93	054	68										
F	47.95	090	70	X								T	3 mm
F	47.96	102	55	X								T	
F	48.01	034	77	X		X						O	
F	48.06	076	74	X								T	Trippel
V	48.11	056	75										
F	48.20	052	76	X			X					O	
F	48.22	050	74	X			X					O	
F	48.24	044	86	X			X					O	
V	48.27	058	68										
F	48.34	291	74			X						O	
V	48.37	058	64										
F	48.43	042	86										
V	48.48	060	67										
F	48.48	115	80										
V	48.66	060	65										
F	48.75	227	84	X		X						O	
F	48.80	313	80	X		X						O	
F	48.81	050	68	X								T	10 mm
V	48.83	053	74										
V	48.94	049	74										
V	49.02	047	55										
F	49.08	160	69	X								T	Qz
V	49.26	048	65										
F	49.37	218	88			X						O	
V	49.44	052	62										
F	49.46	072	62	X								T	
V	49.59	057	48										
V	49.71	068	52										
F	49.75	164	79	X								T	
V	49.88	056	48										
F	49.97	304	74	X	X							O	
F	50.00	342	52		X							T	
V	50.04	054	50										
F	50.10	346	42	X		X	X					O	
V	50.15	056	40										
V	50.30	060	46										

Type	BH depth	Azimuth of dip	Dip	EP	CHL	CA	FE	PY	FL	MU	LAU	T/O	Remarks
V	50.41	054	50										
F	50.56	076	72	X								T	System of paralells
V	50.62	046	48										
F	50.65	358	50										Fault
F	50.66	071	58	X								T	Displaced by the above
F	50.68	093	56	X								T	Displaced by the above
F	50.72	085	50	X								T	Displaced by the above
F	50.76	084	56	X								O	Break, 1 mm
V	50.80	056	54										
F	50.88	003	58			X						O	
F	50.99	093	56	X		X						O	
F	51.04	094	78			X						O	Break?
V	51.06	050	68										
F	51.11	094	82			X						O	Break?
V	51.17	054	52										
V	51.20	148	68										
V	51.28	063	52										
V	51.30	138	64										
V	51.59	052	62										
V	51.70	062	62										
V	51.82	063	64										
V	51.90	072	64										
F	51.94	250	86	X								O	
V	52.10	057	56										
V	52.19	054	64										
F	52.24	116	85									O	
F	52.28	348	75	X	X							T	
F	52.38	252	77	X			X					O	
F	52.45	256	86			X						O	
F	52.69	268	60	X								T	
F	52.70	102	37	X								T	
F	52.77	296	64			X						O	Black oxide
V	52.85	054	60										
V	52.94	071	58										
F	53.00	138	74	X	X							T	
F	53.06	110	70	X		X						O	
V	53.61	51	54										
V	53.72	83	46										
V	53.73	166	68										
F	53.77	296	68	X		X						O	
F	53.84	110	82	X		X						O	
F	53.89	105	90			X						O	
V	53.93	66	54										
V	54.25	63	64										
V	54.31	62	54										
V	54.55	234	70										
F	54.58	270	70			X						O	
V	54.62	234	72										
F	54.65	354	50	X								O	
F	54.70	54	33	X	X	X						O	

Type	BH depth	Azimuth of dip	Dip	EP	CHL	CA	FE	PY	FL	MU	LAU	T/O	Remarks
V	54.70	150	64										
V	54.87	240	72										
F	54.87	176	52	X								T	
F	54.98	151	78	X		X						O	
F	55.02	118	40									O	
F	55.09	66	58	X	X							T	Quadruppel
V	55.10	66	58										
F	55.15	156	60									O	
V	55.20	62	60										
V	55.35	56	64										
V	55.45	234	78										
V	55.55	228	80										
F	55.58	328	70	X								T	2 mm
F	55.69	288	80	X								T	1 mm
V	55.69	46	72										
V	55.89	328	78										
V	55.91	259	72										
F	55.91	85	64	X								T	
F	56.04	311	88									O	Black oxide
V	56.06	328	80										
V	56.18	40	60										
F	56.19	240	62	X								T	
V	56.22	339	70										
V	56.25	230	78										
F	56.29	148	76	X								O	
V	56.35	342	74										
V	56.38	32	62										
F	56.62	108	82	X								O	
V	56.64	243	80										
V	56.65	326	73										
V	56.78	344	73										
V	56.80	46	66										
F	56.85	135	78									O	
V	56.90	56	68										
F	56.91	64	66	X								T	2 mm
F	56.98	84	62	X								T	Qz
F	57.01	166	86	X								O	
V	57.13	158	68										
F	57.20	91	81				X					O	
F	57.21	336	68	X								O	
V	57.30	160	68										
F	57.30	312	62			X						T	
F	57.35	283	51			X						O	
F	57.36	276	55			X						T	
V	57.39	148	70										
F	57.44	274	48			X						O	
F	57.46	136	60	X								T	

Appendix 1.2
Deformation-alteration-rock data

Legend:

Rock	Rock type
Cat	Cataclastic deformation
Duc	Ductile deformation
A	Altered rock
AD	Äspö diorite
AG	Äspö granite
Myl	Mylonite
FGG	Fine grained granite
Ep	Epidote
Py	Pyrite
Chl	Chlorite
Qz	Quartz
kFsp	Potassium feldspar

Drillcore KXTT1

Type	From	To	Degree	Rocktype	Fabric/Texture	Remarks
CAT	2.17	2.22	1	ÄG	Medium grained	Lots of Ep-veins
ROCK	2.25	2.40		ÄG/ÄD	Medium grained	Transitional
DUC	2.41	2.43	1	ÄG/ÄD		Ep in upper contact
DUC	2.43	2.6	3	MYL		
A	2.42	2.43	1.5	ÄG/ÄD		Hematite im-pregnation
A	2.43	2.60	1.5	MYL		Hematite im-pregnation
DUC	2.60	2.70	2	MYL/ÄD		Transitional
DUC	2.70	2.76	1	ÄD	Medium grained	
CAT	3.19	3.22	1	ÄD	Medium grained	
A	3.19	3.22	1	ÄD	Medium grained	
CAT	3.54	3.57	1	ÄD	Medium grained	
ROCK	4.09	4.27		ÄG		Bits (by faults)
CAT	4.75	4.80	1	ÄG		
CAT	4.26	4.27	1	ÄG		
A	4.26	4.27		ÄG		
ROCK	4.27	4.60		ÄD	Medium grained	
CAT	4.615	4.62	1	ÄD	Medium grained	
ROCK	4.62	5.08		ÄD	Medium grained	Streaks of granitic rock
DUC	5.08	5.56	1	ÄD		Transitional
A	5.07	5.08	1	ÄD	Fine grained	
CAT	5.07	5.075	2	ÄD	Fine grained	
DUC	5.56	5.57	2	ÄD	Fine grained	
DUC	5.57	5.76	3	MYL		Ep in center
DUC	5.76	5.91	1	ÄD	Fine grained	
ROCK	5.91	6.68			Medium grained	
A	5.277	5.283	1			
DUC	6.69	6.70	1		Fine grained	
DUC	6.70	6.72	2			Ep, Qz lower boundary
DUC	6.72	6.75	3	MYL		
DUC	6.75	6.80	2		Fine grained	Ep upper boundary
A	6.66	6.75	1			Hematite im-pregnation
ROCK	6.75	8.21		ÄD	Medium grained	
CAT	7.347	7.352	1			Fragments
A	7.345	7.352	1			
CAT	8.215	8.225	1			Microfractures
A	8.20	8.23	1			Hematite im-pregnation
ROCK	8.61	9.21		ÄD	Medium grained	
ROCK	9.21	9.38		FGG		
ROCK	9.38	9.65		ÄD	Medium grained	
A	9.515	9.52	1			
CAT	9.635	9.64	1.5			Fragments
DUC	9.65	9.72	2	ÄD	Very fine grained	

Type	From	To	Degree	Rocktype	Fabric/Texture	Remarks
ROCK	9.72	10.62		ÄD	Fine grained, augen and phenocryst bearing	
A	10.60	10.70	1.5			
DUC	10.62	10.63	1			
DUC	10.63	10.68	2		Mylonitic	
DUC	10.68	10.85	3	MYL		
DUC	10.85	10.91	1		Medium grained	
DUC	10.91	10.95	3			
ROCK	10.86	10.96		ÄG		Contact 345/62
ROCK	10.96	11.43		ÄD	Medium to fine grained	
ROCK	11.43	11.57		ÄD/ÄG		Transitional
ROCK	11.57	11.59		ÄD	Fine grained, some phenocrysts	
ROCK	11.59	11.64		FGG		
ROCK	11.64	11.80		ÄD	Fine grained, foliated, phenocrysts	
DUC	11.83	11.86	3	MYL		Black
A	11.83	11.86	1.5			Ep, Py
CAT	11.92	11.94	1			Microfractures
ROCK	11.86	11.95		ÄD	Large k-fsp x:tals, <20 mm	
ROCK	11.95	12,04			Fine grained	Clouds of Ep
DUC	12.04	12.05	3	MYL		
A	12.04	12.05	1			Py, Ep
DUC	12.06	12.08	3	MYL		
A	12.06	12.08	1			Py, Ep
DUC	12.16	12.165	3	MYL		
ROCK	12,08	12.35		ÄD	<30 mm, phenocrysts (fractured)	
DUC	12.35	12.4	3	MYL		
A	12.35	12.4	1			Py
CAT	12.47	12.475	1			Fragments
A	12.47	12.48	1			
ROCK	12.4	12.47		FGG		
ROCK	12.47	12.61		ÄD	Fine grained, pheno-crysts <10 mm	
ROCK	12.61	13.12		ÄG		Hematite im-pregnation
A	12.66	12.67	1			
ROCK	13.12	13.61		ÄD	Medium grained, some phenocrysts	
ROCK	13.61	14,76		ÄD	Phenocrysts < 20-30 mm, foliated	
A	14.32	14.35	1			
DUC	14.42	14.47	3	MYL		
A	14.42	14.47	1			Py, Ep
DUC	14.50	14.60	1.5			
DUC	14.6	14.70	2			
DUC	14.7	14.80	1.5			
DUC	14.8	14.85	1			
DUC	14.85	14.92	0.5			
ROCK	14.76	14.82		ÄD/ÄG		Transitional

Type	From	To	Degree	Rocktype	Fabric/Texture	Remarks
ROCK	14.82	14,90		FGG		
ROCK	14.90	15.30		ÄG		
CAT	15.25	15.251	2			
A	15.24	15.25	1			
A	15.25	15.26	2			
A	15.26	15.265	1			
ROCK	15.30	15.48		ÄD		Transitional
DUC	15.23	15.24	0.5			
DUC	15.25	15.252	2			
DUC	15.25	15.30	0.5			
DUC	15.30	15.33	1			
DUC	15.33	15.46	0.5			
DUC	15.46	15.48	1			
DUC	15.48	15.5	3			Lithological contact
CAT	15.49	15.49	1			
ROCK	15.48	15.62		FGG		
DUC	15.60	15.62	2			
ROCK	15.62	15.82		MYL		
DUC	15.62	15.82	3	MYL		
A	15.57	15.59	1			
A	15.59	15.62	2			
A	15.62	15.83	3			
CAT	15.76	15.77	3			
CAT	15.79	15.81	3			
A	15.83	15.91	1			
A	15.91	15.93	2			
DUC	15.92	15.93	3	MYL		
ROCK	15.82	16.16		ÄD	Fine grained, strongly foliated	
ROCK	16.16	16.70		ÄD	Foliated, with pheno-crysts	
DUC	16.62	16.70	2			Towards contact
ROCK	16.70	17.66		ÄD	COARSE, <50 mm k-fsp x:tals	
ROCK	17.66	18.20		ÄD		Ep-clouds
ROCK	18.20	18.60		ÄD	Med. to fine grained	
A	18.45	18.48	1			
ROCK	18.60	18.97				
A	18.84	18.89	0.5			
CAT	18.97	19.00	1			Fragments
DUC	18.97	19.00	2		Very fine grained	
A	18.97	19.00	1			Ep, Py
CAT	19.07	19.10	1			
A	19.07	19.105	0.5			Hematite im-pregnation, Epidote
CAT	19.24	19.25	2.5			
A	19.20	19.60	1			Hematite im-pregnation
ROCK	18.97	19.81		ÄD	Some k-fsp x:tals < 30 mm	

Type	From	To	Degree	Rocktype	Fabric/Texture	Remarks
CAT	19.55	19.61	1			Fragments
DUC	19.55	19.60	2		Very fine grained	
A	19.55	19.60	1			Ep, Py
ROCK	19.81	20.00				More <30 mm x:tals
DUC	20.00	20.08	2		Very fine grained	
CAT	20.00	20.08	1			
A	20.00	20.08	1			Ep, Py
ROCK	20.08	20.60			Med. to Fine grained, phenocrysts	
CAT	20.14	20.16	0.5			
ROCK	20.60	20.80		ÄG		Hematite im-pregnation
CAT	20.65	20.651	2			Brecciated
A	20,62	20,80	1			Hematite im-pregnation
CAT	20,85	20,91	1,5			Brecciated ap-pearance
CAT	20,97	20,98	1			
DUC	20.97	21	1			
A	20,97	20,985	1			
ROCK	20,80	21,30		ÄD	Fine grained, <10 mm phenocrysts	
CAT	21,05	21,15	1			Broken pheno-crysts
CAT	21,15	21,18	1,5			
CAT	21,18	21,24	1			
A	21,13	21,25	0,5			Hematite im-pregnation
ROCK	21,30	21,50			Fine grained, some 5-10 mm k-fsp	
A	21,69	21,71	1			Hematite im-pregnation
ROCK	21,50	21,70		ÄD		CRUSHED
ROCK	21,70	22,00				BITS
CAT	22,05	22,055	1			
A	22,05	22,055	1			
CAT	22,36	22,375	1,5			
CAT	22,375	22,38	3			
CAT	22,38	22,39	1,5			
A	22,37	22,38	1			
ROCK	22,00	22,56		ÄD	Fine grained, phenocryst bearing	
CAT	22,545	22,55	1			
CAT	22,59	22,595	3			Contact
CAT	22,645	22,65	1			
CAT	22,68	22,685	1			
ROCK	22,50	23,30				BITS
ROCK	22,58	22,76		P		
ROCK	22,76	24,13		ÄD	Finegraind, some 5-10 mm grains	
A	23,00	23,01	1			
A	23,29	23,295	1			

Type	From	To	Degree	Rocktype	Fabric/Texture	Remarks
A	23,305	23,31	1			
ROCK	23,30	23,40				CRUSHED
ROCK	24,00	24,12				CRUSHED
ROCK	24,13	25,10			Medium grained	
ROCK	24,32	24,48				Rich in Epidote
ROCK	24,31	24,49			Fine grained	Dark
A	24,45	24,46	1			
ROCK	24,26	24,90				BITS
A	24,77	24,78	1			
A	24,83	24,835	1			
ROCK	25,10	25,38			Bearing <30 mm phenocrysts	
ROCK	25,38	25,70		P	Fine grained	Lower contact black
ROCK	25,70	26,12		ÄD	Foliated in lower parts	
A	26,095	26,125	1			Ep
CAT	26,105	26,13	2			
CAT	26,13	26,47	1			Fractured and fragmented
A	26,19	26,51	1			Hematite and Ep
ROCK	26,12	26,20		ÄD		Veins and clouds of Ep
ROCK	26,20	26,48				Grains are fragmented
ROCK	26,48	26,52				Ep, Chl veins, tight
ROCK	26,54	26,62			Phenocrysts <30 mm	
ROCK	26,62	26,93		ÄD		Ep-rich
ROCK	26,93	27,00		FGG		Ep, chl in contact
CAT	26,92	26.93	1			
CAT	26.93	26.98	2			
DUC	26.92	26.93	1			
DUC	26.93	26.98	3	MYL		
DUC	26.98	26.99	1			
ROCK	27.00	27.15		ÄD		Mylonitic
CAT	27.15	27.155	1			
CAT	27.17	27.20	1			
ROCK	27.15	27.57			Fine grained, phenocrysts	
A	27.17	27.3	1			Hematite impregnation
ROCK	27.57	27.76		P		Vein
CAT	27.58	27.73	0.5			
CAT	27.81	27.82	1			
A	27.82	27.82	1			
ROCK	27.76	28.07		ÄD	Fine grained, occasional phenocrysts, slightly foliated	
ROCK	28.07	28.3		P		Mylonitic, cataclastic
CAT	28.2	28.205	3	MYL		

Drillcore KXTT2

Type	From	To	Degree	Rocktype	Fabric/Texture	Remarks
CAT	2.1	2.13	2	ÄD	Medium grained	Microfractures
A	2.1	2.14	1.5		Fine grained	
CAT	2.365	2.37	1			
A	2.34	2.39	1			Hematite impregnation
ROCK	2.39	3.55		ÄD	Medium to fine grained, slightly foliated.	
CAT	2.5	2.52	1			
DUC	2.5	2.52	2			
CAT	2.71	2.72	1			
A	2.92	2.99	1			Hematite impregnation
CAT	3.135	3.14	1			
DUC	3.135	3.14	2			
A	3.135	3.14	1.5			
CAT	3.18	3.185	0.5			
A	3.18	3.1825	1			
ROCK	3.55	4.23		ÄG	Medium grained, slightly foliated	
CAT	3.54	3.56	1			
DUC	3.54	3.56	1			
CAT	3.62	3.625	1			
CAT	3.695	3.705	1			
CAT	3.83	3.835	1			
CAT	3.94	3.96	1			Ep in microfractures
DUC	3.94	3.96	1.5			
A	3.94	3.97			Fine grained	
CAT	4.13	4.15	1			
ROCK	4.23	4.33		ÄG/ÄD	Increase in foliation	Transitional
CAT	4.35	4.355	1			
A	4.35	4.355	1			
CAT	4.405	4.41	1.5			
DUC	4.405	4.41	3			
A	4.40	4.43	1			Hematite impregnation
ROCK	4.33	4.47		ÄG	Fine grained, foliated	
ROCK	4.47	4.50		ÄG/ÄD		Transitional
ROCK	4.50	4.84		ÄD	Medium grained	
CAT	4.545	4.55	1			
A	4.545	4.55	1			
CAT	4.595	4.6	1			
A	4.595	4.605	1			
CAT	4.65	4.655	1			
DUC	4.85	4.87	1			
A	4.84	4.85	1		Fine grained	
CAT	4.96	4.97	1			
DUC	4.96	4.98	1			
A	4.96	4.97	1		Fine grained	

Type	From	To	Degree	Rocktype	Fabric/Texture	Remarks
ROCK	4.84	4.96		FGG		
ROCK	4.96	5.22		ÄD	Fine grained	
DUC	5.295	5.40	2.5		Fine grained	Mylonitic
DUC	5.40	5.50	1			Lots of Ep-veins
A	5.40	5.50	1			Hematite impregnation
ROCK	5.40	6.20		ÄD	Fine to medium grained	
DUC	5.68	5.695	1			
CAT	6.03	6.04	1			
CAT	6.06	6.065	1			
CAT	6.125	6.13	1			
A	6.125	6.13	1			
CAT	6.19	6.20	1			
CAT	6.29	6.302	1			
A	6.26	6.35	1			
ROCK	6.20	6.40		ÄG	Medium grained	Cataclastic overprint
ROCK	6.40	6.56		ÄD		
CAT	6.57	6.59	2			
CAT	6.64	6.67	1			
A	6.57	6.77	1			
ROCK	6.57	6.67		ÄG	Medium grained	Cataclastic character
ROCK	6.67	8.14		ÄD	Medium grained, foliated	
CAT	6.775	6.78	1			
CAT	6.78	6.79	1			
CAT	7.01	7.02	1			
A	7.01	7.02	2		Fine grained	
CAT	7.12	7.125	1			
CAT	7.345	7.355	0.5			
ROCK	8.14	8.29		ÄD		Weird foliation
ROCK	8.29	8.59		ÄD	Medium to fine grained	
CAT	8.58	8.88	2			
DUC	8.58	8.88	1			
A	8.56	9.00	1		Fine grained	
ROCK	8.59	8.83				Ep, chl, qz, k-fsp in contact to Qz-vein
ROCK	8.83	9.00				Qz-vein, fractured
ROCK	9.00	9.10		ÄD	Fine grained	
ROCK	9.10	12.52		ÄD	Medium grained	
CAT	9.75	9.81	1			
DUC	9.75	9.81	1			
A	9.74	9.81	0.5			
A	9.93	9.96	0.5			
CAT	10.07	10.085	1			Microfractures
A	10.07	10.085	1			
CAT	10.42	10.46	1			
A	10.41	10.50	1		Fine grained	Enrichm of felsic and mafic minerals
CAT	10.77	10.80	2	MYL		

Type	From	To	Degree	Rocktype	Fabric/Texture	Remarks
DUC	10.77	10.80	3			
CAT	11.12	11.125	1	ÄD	Medium grained	
CAT	11.54	11.55	1			Microfractures
DUC	11.54	11.55	1			
CAT	11.63	11.66	1			
DUC	11.63	11.66	1			
ROCK	12.52	12.80		ÄG		
CAT	12.55	12.56	1			Microfractures, fragment
A	12.54	12.61	1		Fine grained	
A	12.63	12.66	1			
ROCK	12.80	14.08		ÄD	Phenocrysts 10-15 mm, foliated	Ep rich
CAT	13.145	13.15	1			
A	13.14	13.15	2		Fine grained	
ROCK	14.08	16.05		ÄD	Fine grained, phenocrysts	
DUC	14	14.12	1.5			
DUC	14.12	14.13	3			
DUC	14.13	14.15	1.5			
DUC	14.15	14.42	1			BACKGROUND
DUC	14.42	14.425	2.5			
DUC	14.425	15.64	1			BACKGROUND
A	14.12	14.13	3			
A	14.29	14.31	2			
DUC	14.64	14.66	1.5			
DUC	14.66	14.81	1			
DUC	14.81	14.92	1.5			
DUC	14.92	14.925	3	MYL		
DUC	14.925	14.98	2			
DUC	14.98	15.05	2.5			
DUC	15.05	15.12	3	MYL		
DUC	15.12	15.18	2			
DUC	15.18	15.29	1			
DUC	15.29	15.32	3	MYL		
DUC	15.32	15.55	1			
CAT	15.115	15.12	3			
A	15.00	15.40	1			
A	15.40	15.12	3			
A	15.295	15.32				
DUC	15.55	15.605	2			
DUC	15.605	15.61	3	MYL		
DUC	15.61	15.70	2			
DUC	15.70	16.00	1			BACKGROUND
A	15.605	15.61	2			
ROCK	16.05	16:53		ÄD	Fine grained, phenocrysts 10-15 mm, foliated	Ep-rich
CAT	16.52	16.53	1			
A	16.51	16.55	1	ÄG		
ROCK	16.55	17.31		ÄD		Overall cataclastic

Type	From	To	Degree	Rocktype	Fabric/Texture	Remarks
ROCK	17.31	17.37		ÄD	Fine grained	
ROCK	17.37	17.49			With large(<20 mm) fragmentet phenocrysts	
ROCK	17.49	17.59			Fine grained, fragmented phenocrysts	
CAT	17.31	17.36	2			
DUC	17.31	17.36	3	MYL		
ROCK	17.59	17.66		ÄG		
ROCK	17.66	18.24		ÄD	Fine grained	
CAT	17.68	17.70	3	MYL		
DUC	17.68	17.70	2.5			
CAT	17.76	17.77	1			
ROCK	17.93	18.00			Fine grained	Clouds of Epidote
ROCK	18.05	18.24		ÄD	Fine grained, <10 mm-sized fragments	

Drillcore KXTT3

Type	From	To	Degree	Rocktype	Fabric/Texture	Remarks
ROCK	2	2.13		ÄD/ÄG		Transitional
ROCK	2.13	3.08		ÄG		
CAT	2.635	2.64	1			
A	2.62	2.63	1			Hematite impreg-nation.
CAT	2.83	2.84	1.5			
DUC	2.83	2.84	1			
A	2.83	2.85				
CAT	3.005	3.04	1			
CAT	3.05	3.06	1			
A	3.00	3.07	1			
ROCK	3.08	3.22		ÄD		
ROCK	3.22	3.56		ÄG		
A	3.41	3.42	2			Hematite impreg-nation
CAT	3.67	3.675	0.5			
ROCK	3.56	3.90		ÄD	Medium grained	
ROCK	3.90	4.00		FGG	Fine grained	
ROCK	4.00	4.27			Fine grained	Mylonitic
CAT	4.05	4.06	1			
DUC	4.05	4.28	3			
ROCK	4.27	4.95		ÄG/ÄD	Medium grained	Transitional
A	4.51	4.52				
CAT	4.82	4.825	1			
A	4.82	4.825	1			
CAT	4.87	4.875	1			
A	4.85	4.92	1			
ROCK	4.95	5.23		ÄD	Medium grained	
CAT	5.22	5.225				
CAT	5.46	5.465	0.5			
ROCK	5.23	5.62		ÄD	Fine grained	Mylonitic
DUC	5.61	5.63	2		Increasing foliation	
DUC	5.63	5.69	3	MYL		
DUC	5.69	5.73	2			
A	5.63	5.70	2			Only felsic
CAT	5.645	5.65	2			
CAT	5.655	5.66	2			
CAT	5.675	5.68	2			
CAT	5.695	5.70	2			
DUC	5.84	5.85	3			
A	5.84	5.85	2			
CAT	5.84	5.845	2			
CAT	5.90	5.905	1			
ROCK	5.62	5.70		ÄG		
ROCK	5.70	5.84		ÄD	Fine grained	Mylonitic
ROCK	5.84	6.21		ÄG	Fine grained	
DUC	6.1	6.12	3	MYL		
A	6.12	6.10	2			

Type	From	To	Degree	Rocktype	Fabric/Texture	Remarks
CAT	6.05	6.06	2			Fragments, micro-fractures
CAT	6.24	6.245	2			Fragments
A	6.24	6.245	2			
CAT	6.45	6.455	1			
A	6.45	6.455	1			
ROCK	6.21	7.66		ÄD	Medium grained	
CAT	6.88	6.885	1			Fragments, micro-fractures
DUC	6.88	6.885	1			
A	6.88	6.89	1			Finegrained
CAT	7.48	7.485	1			
A	7.48	7.485	1			
CAT	7.52	7.525	1			
A	7.52	7.525	1			
CAT	7.71	7.78	1			
CAT	7.90	7.92	1			
CAT	7.98	8.00	1			
ROCK	7.66	7.90		ÄD	Fine grained, pheno-crysts, foliated	Clouds of Ep
ROCK	7.90	8.63			Fine grained, fragmented phenocrysts 25 mm	Some clouds of Ep
CAT	8.03	8.035	1			
CAT	8.345	8.35	1			
A	8.57	8.58	1			
CAT	8.575	8.58	2			
CAT	8.63	8.635	2			
A	8.81	8.82	1			
CAT	8.815	8.82	1			
ROCK	8.63	9.13		ÄD	Fine grained, crystal fragments	
ROCK	9.13	9.25		ÄD		Fracture zone
ROCK	8.87	8.90				Py-mineralization
CAT	9.14	9.145	2		Microfractures	
A	9.13	9.25	2		Fine grained	
ROCK	9.25	9.34		ÄD		Clouds of Ep.
ROCK	9.34	11.76		ÄD	Fine grained, phenocryst bearing	
CAT	9.655	9.66	1			
CAT	10.08	10.095	0.5			
A	10.28	10.31	1			
A	10.62	10.66	1			
ROCK	11.76	11.88			Pronounced foliation	
ROCK	11.88	12.29			Increased phenocryst frequency	
ROCK	12.29	12.68			Fine grained, phenocryst bearing	
A	12.65	12.66	1			
ROCK	12.29	13.00			Overall pronounced foliation	
ROCK	12.70	12.89				Slabs of porphyric rock

Type	From	To	Degree	Rocktype	Fabric/Texture	Remarks
ROCK	12.88	13.00			Fine grained, medium-sized fragments	Ep in foliation planes
DUC	13	13.07	1			
A	13.07	13.08	3			
DUC	13.08	13.14	2			
DUC	13.14	13.185	2.5			
DUC	13.185	13.22	1.5			
DUC	13.22	13.61	1			
ROCK	13.00	13.88		ÄD	Foliated	
DUC	13.61	13.69	2			
DUC	13.69	13.85	1			
DUC	13.85	13.89	1.5			
DUC	13.89	13.97	3	MYL		
CAT	13.89	13.96	3			
ROCK	13.88	14.11		ÄD	Fine grained	
DUC	13.97	14.10	1			
DUC	14.10	14.16	3	MYL		
DUC	14.16	14.18	2			
DUC	14.18	14.21	3	MYL		
DUC	14.21	14.24	1			
DUC	14.24	14.26	2			
DUC	14.26	14.55	1			
CAT	14.1	14.12	1			
CAT	14.12	14.15	3			
ROCK	14.11	15.32		ÄD	Fine grained, phenocryst bearing, foliated	
DUC	14.55	14.74	1.5			
DUC	14.74	14.85	1			
DUC	14.85	14.92	1.5			
DUC	14.92	15.00				
A	15.15	15.22	1			Overall Ep and Hematite impreg-nated
ROCK	15.32	16.54		ÄD	Medium grained	Hematite impreg-nation.
DUC	15.75	15.80	3	MYL		
CAT	15.75	15.80	2			
A	15.75	15.82	3		Fine grained	Hematite impreg-nation
A	15.92	15.96	1			Hematite impreg-nation.
ROCK	16.54	16.66			Fine grained	Fining
ROCK	16.66	16.97		MYL		Red, Qz and Ep
ROCK	16.97	17.00		QZ		
ROCK	17	17.34		ÄD		Fractured and fragmented

Drillcore KXTT4

Type	From	To	Degree	Rocktype	Fabric/Texture	Remarks
ROCK	3.00	3.51		ÄG		
ROCK	3.51	3.86		ÄD		
ROCK	3.86	4.02		ÄG		
ROCK	4.02	4.40		FGG		Hematite impregnation
ROCK	4.40	4.60		ÄD		
ROCK	4.60	4.74		P	Fine grained	
CAT	4.60	4.70	1.5			
DUC	4.60	4.75	1.5			
A	4.59	4.75	1			Hematite
ROCK	4.74	4.88		ÄD		Transitional
ROCK	4.88	5.32		ÄD		
A	5.14	5.15	0.5			
CAT	5.34	5.47	1			
DUC	5.28	5.48	1			
A	5.28	5.34	1			
A	5.34	5.46	1.5			
A	5.46	5.48	1			
ROCK	5.32	5.48		ÄD		
ROCK	5.48	5.90		ÄD		
A	5.62	5.64	1			Hematite, Ep
DUC	5.61	5.63	1.5			
DUC	5.76	5.78	1			
A	5.76	5.78	1.5			Ep, mafic minerals
A	5.88	5.95	1.5			Mafic minerals
ROCK	5.90	6.45		ÄD	Fine grained	
DUC	6.05	6.10	2			
DUC	6.10	6.32	3	MYL		
DUC	6.32	6.36	2			
CAT	6.10	6.30	2			
A	6.05	6.20	1			Hematite
A	6.20	6.34	2			Ep, Hematite
ROCK	6.45	7.78		ÄD	Medium grained	Ep-rich
A	6.58	6.61	2			Hematite
CAT	7.75	7.76	1			
A	7.69	7.71	1			
DUC	7.65	7.84	1			
DUC	7.84	7.95	3	MYL		
DUC	7.95	7.99	1			
CAT	7.86	7.97	2			
A	7.84	7.98	2			
ROCK	7.95	8.34		ÄD		Ep-rich
ROCK	8.34	8.65		P		Red, with Ep
ROCK	8.65	9.46		ÄD		Ep-rich
A	8.97	8.99	1			Mafic minerals
ROCK	9.40	9.45			Fine grained	
ROCK	9.67	9.78		ÄD	Fine grained, foliated	Ep-rich
ROCK	9.78	9.83				Red vein of only

Type	From	To	Degree	Rocktype	Fabric/Texture	Remarks
						felsic
ROCK	9.83	10.10		ÄD	Fine grained, with phenocrysts. Foliated	
ROCK	10.12	10.20		FGG		
ROCK	10.20	10.50		ÄD	Fine grained, foliated	With chlorite
ROCK	10.50	10.62		FGG		Red
ROCK	10.62	11.02		ÄD	Fine grained, foliated	Ep- and Chl-rich.
ROCK	11.02	11.08			Fine grained	Felsic minerals mostly
ROCK	11.08	12.10		ÄD	Coarse, large phenocrysts and augens, foliated	
DUC	11.12	11.23	1.5			
DUC	11.23	11.27	1			
DUC	11.27	11.275	3	MYL		
DUC	11.275	11.30	2			
DUC	11.30	11.305	3	MYL		
DUC	11.305	11.345	2			
DUC	11.345	11.35	3	MYL		
DUC	11.35	11.45	1.5			
DUC	11.45	11.46	3	MYL		
DUC	11.72	11.73	3			
DUC	11.88	11.90	3			
CAT	12.09	12.10	3	MYL		Feature A
DUC	12.09	12.12	3			
DUC	12.33	12.37	2			Contact
ROCK	12.10	12.33		FGG		
ROCK	12.33	12.63		ÄD	Coarse, large phenocrysts and augens, foliated	
ROCK	12.63	13.90			Fine grained with fragmented phenocrysts, foliated	
DUC	13.00	13.01	3			
CAT	13.00	13.01	3			
CAT	13.02	13.05	2			
CAT	13.05	13.06	1			
DUC	13.05	13.06	1			
DUC	13.06	13.11	2.5			
DUC	13.11	13.12	2			
A	13.08	13.14	2			
DUC	13.24	13.25	1			
DUC	13.25	13.33	1.5			
A	13.25	13.32	1.5			
CAT	13.43	13.48	1.5			
A	13.43	13.46	1.5			
ROCK	13.90	14.35		ÄG		
A	14.35	14.36	1			Contact
ROCK	14.35	14.77		ÄD	Fine grained with fragmented phenocrysts, foliated	
DUC	14.65	14.78	1			
A	14.65	14.78	1			
CAT	14.77	14.83	1			
ROCK	14.77	15.50		ÄG		

Type	From	To	Degree	Rocktype	Fabric/Texture	Remarks
CAT	15.1	15.15	1			
A	15.12	15.14	1.5			
CAT	15.19	15.21	1			
CAT	15.24	15.26	1			
A	15.19	15.21	1			
DUC	15.19	15.27	3	MYL		CRUSHED
ROCK	15.50	15.70		ÄD	Fine grained	
ROCK	15.70	17.90		ÄD	Slightly foliated	
DUC	17.10	17.25	1			
DUC	17.54	17.55	2			
CAT	17.84	17.86	1.5			
ROCK	17.90	19.54		ÄD		Starry sky
CAT	18.22	18.48	1			Microfractures
A	18.47	18.50	1.5			
A	18.65	18.67	1			
DUC	19.16	19.18	1			
DUC	19.50	19.56	1			Contact zone
ROCK	19.55	21.50		ÄG		
CAT	20.41	20.415	2			
ROCK	20.45	20.50				MISSING
A	21.14	21.15	2			
DUC	21.34	21.345	1			
A	21.34	21.345	1			
CAT	21.48	21.52	1			
DUC	21.48	21.52	3			
A	21.48	21.54	1			
ROCK	21.50	21.60		ÄG/ÄD		Transitional
ROCK	21.60	23.62		ÄD	With increasing foliation	
DUC	21.83	21.835	2			
CAT	22.26	22.35	1			
DUC	22.26	22.28	2			
A	22.26	22.29	2			
A	22.43	22.50	1			
A	22.50	22.55	2			
A	22.55	22.57	1			
DUC	22.50	22.51	1			
DUC	22.51	22.53	2			
DUC	22.53	22.57	1			
DUC	22.86	22.865	2			
DUC	23.48	23.49	1			
DUC	23.49	23.54	2			
DUC	23.54	23.55	1			
A	23.48	23.59	1		Increasing foliation	
ROCK	23.62	23.94		FGG		
ROCK	23.94	24.10		ÄD	Fine grained	Dark
ROCK	24.10	24.58		ÄD	Fine grained	Hematite impreg-nation BITS
DUC	24.57	24.58	3	MYL		
ROCK	24.58	25.23		ÄD		Heavy Hematite impregnation BITS

Type	From	To	Degree	Rocktype	Fabric/Texture	Remarks
ROCK	25.23	25.71		ÄD		Heavy Hematite impregnation BITS
CAT	25.44	25.49	1			
ROCK	25.71	26.12				Heavy Hematite impregnation BITS
ROCK	26.12	27.69		ÄG		
CAT	26.595	26.60	1			
A	26.65	26.655	1			
CAT	26.935	26.94	1			
A	26.94	27.05	1			Fine grained
CAT	27.05	27.06	1			
ROCK	27.69	29.24		ÄD	Slightly foliated	
DUC	28.70	28.73	2			
DUC	28.73	28.76	3	MYL		
DUC	28.76	28.77	2			
CAT	28.75	28.76	1.5			
A	28.74	28.95	1			Hematite impreg-nation.
CAT	29.24	29.245	1			
A	29.24	29.46	1	ÄD		Hematite impreg-nation
DUC	29.40	29.44	2			
DUC	29.44	29.47	3	MYL		
DUC	29.47	29.52	1.5			
DUC	29.52	29.58	3	MYL		
DUC	29.58	29.62	1			
CAT	29.46	29.49	2			
ROCK	29.46	31.37		ÄD		
CAT	29.53	29.60	2			
CAT	31.36	31.43	1			
DUC	31.36	31.40	2			
ROCK	31.40	31.63		ÄG		
ROCK	31.63	32.38		ÄD		
DUC	31.84	31.86	1			
A	32.28	32.29	1			
A	32.36	32.37	1			
CAT	32.39	32.43	1			
DUC	32.36	32.43	1			
ROCK	32.38	32.46				CRUSHED
ROCK	32.46	34.75		ÄG(?)		Overall "brittle" appearance
DUC	32.925	32.935	1			
A	32.925	32.935	1			
CAT	33.565	33.575	1			
CAT	33.625	33.63	1			
CAT	34.11	34.12	1			
ROCK	34.75	34.77		FGG		
ROCK	34.77	35.00		ÄD		
ROCK	35.00	35.30		ÄG		
ROCK	35.30	35.65		ÄD		

Type	From	To	Degree	Rocktype	Fabric/Texture	Remarks
ROCK	35.65	35.67		P		
ROCK	35.67	36.10		ÄD		
A	35.89	35.92	1			
A	35.945	35.95	1			
A	36.097	36.102	1			Hematite
A	36.29	36.31	1			
ROCK	36.10	36.50		ÄD	With large x:tals, 10-20 mm	
DUC	36.47	36.54	1			
DUC	36.54	36.58	3	MYL		
DUC	36.58	36.63	1			
DUC	36.63	36.77	2			
DUC	36.77	36.90	1			
ROCK	36.60	37.03		ÄD	Fine grained	
CAT	36.57	36.64	1			
ROCK	37.03	37.05		FGG		
DUC	37.00	37.03	1			
DUC	37.03	37.24	2			
DUC	37.24	37.29	1			
A	37.10	37.17	1			
ROCK	37.05	37.30		ÄD	Fine grained	
ROCK	37.30	37.55		ÄD	Medium grained	
ROCK	37.55	42.90		ÄD	Augen bearing, foliated	
A	37.74	37.76	1			
CAT	37.87	37.91	1			
CAT	37.96	37.965	0.5			
DUC	37.96	37.965	0.5			
A	38.02	28.08	0.5			
A	38.94	38.98	0.5			
CAT	39.01	39.60	0.5			
DUC	39.01	39.09	1			
DUC	39.09	39.70	3	MYL		
DUC	39.70	39.74	2			
DUC	39.74	39.80	1			
A	39.50	39.52	1			
A	39.52	39.60	2			
A	39.60	39.63	1			
A	39.76	39.79	1			
DUC	40.16	40.23	3	MYL		
DUC	40.28	40.36	3	MYL		
A	40.28	40.36	1			
CAT	40.28	40.36	0.5			
CAT	40.38	40.46	1			
DUC	40.38	40.45	2			
A	40.38	40.43	2			
DUC	40.61	40.64	1			
A	40.61	40.64	1			
A	40.74	40.76	0.5			
DUC	40.74	40.75	0.5			
A	40.93	40.96	0.5			
A	40.96	41.00	1			

Type	From	To	Degree	Rocktype	Fabric/Texture	Remarks
DUC	42.245	42.25	1			
DUC	42.345	42.35	1			
DUC	42.54	42.55	1			
ROCK	42.90	43.24		ÄD	Medium grained	
CAT	43.05	43.07	2			
A	43.03	43.08	1			
CAT	43.14	43.16	1			
DUC	43.14	43.16	1			
A	43.13	43.17	1			
DUC	43.18	43.50	2			
A	43.35	43.36	0.5			
ROCK	43.24	43.47		ÄD	Fine grained	With Py
ROCK	43.47	43.53		ÄG		
ROCK	43.53	43.64		ÄD	Fine grained, black	
ROCK	43.64	43.65		FGG		5 mm vein
ROCK	43.65	45.00		ÄD	Medium grained	
A	43.76	43.77	1			Hematite
A	43.80	43.85	1			
CAT	43.90	43.97	1			
CAT	43.97	43.99	1.5			
DUC	43.97	43.98	1			
DUC	43.98	44.00	2		Fine grained	
A	43.92	43.97	1			
A	43.97	43.98	2			Hematite
A	43.98	44.00	1			
ROCK	44.10	44.20		ÄD		Slightly more felsic
A	44.32	44.325	1			
A	44.89	44.895	1			
ROCK	45.00	45.91		ÄD/ÄG		Transitional
CAT	45.90	45.91	1			
ROCK	45.91	48.50		ÄG		
A	45.05	45.055	1			
ROCK	46.36	46.40				CRUSH
DUC	46.92	47.00	2			Lots of Ep-veins
ROCK	47.17	47.40				Crush breccia
CAT	48.04	48.05	3			
DUC	48.04	48.05	1			
A	48.00	48.01	1			
A	48.02	48.06	1			Hematite
ROCK	48.50	48.82		ÄG/ÄD		Transitional
ROCK	48.82	49.25		ÄD	Fine grained	
CAT	48.74	48.81	2			Lots of Ep
DUC	48.74	48.81	1			

Drillcore KA3005a

Type	From	To	Degree	Rocktype	Fabric/Texture	Remarks
ROCK	0.00	0.20		ÄD		
ROCK	0.20	0.21		FGG		Vein
ROCK	0.21	0.53		ÄD		
ROCK	0.53	1.13		FGG		
DUC	0.90	0.94	0.5			
DUC	0.94	0.97	1			
DUC	0.97	1.00	0.5			
ROCK	1.13	6.08		ÄD	Medium grained, slightly foliated	
A	1.56	1.57	1.5			Hematite
A	2.56	2.58	3			Hematite, Qz-deficiency
A	2.58	2.74	1			
DUC	3.25	3.30	1			
A	3.25	3.30	2			Dark chl-alteration
CAT	5.25	5.26	2			Cataclasite
DUC	5.25	5.30	1			
A	5.22	5.23	1.5			
A	5.23	5.30	3			
DUC	5.64	5.66	1			
DUC	5.66	5.67	2			
DUC	5.67	5.68	1			
CAT	5.665	5.67	0.5			
A	5.64	5.65	1			
A	5.65	5.67	2			
A	5.67	5.68	1			
DUC	5.75	5.76	2			
A	5.75	5.76	1			
A	5.86	5.865	1			
A	5.90	5.96	1.5			
A	5.96	6.03	0.5			
A	6.03	6.08	3			Contact zone
ROCK	6.08	6.50		FGG		
ROCK	6.50	6.70		ÄD	Medium grained	
ROCK	6.70	6.71		FGG		Vein
ROCK	6.71	7.40		ÄD	Medium grained	
ROCK	7.40	7.60			Fine grained	
ROCK	7.60	8.53			Medium grained	
CAT	7.46	7.50	1			
DUC	7.46	7.49	1			
DUC	7.49	7.50	2			
A	7.85	7.86	1			
A	8.55	8.75	1			Hematite
A	9.19	9.28	0.5			
A	9.28	9.36	1			
A	9.36	9.38	3			
A	9.38	9.50	0.5			
CAT	9.24	9.25	1			Microfractures

Type	From	To	Degree	Rocktype	Fabric/Texture	Remarks
ROCK	8.53	8.73		ÄD	Fine grained	
ROCK	8.73	12.26		ÄD	Medium grained	
A	9.51	9.53	1			
A	9.53	9.54	3		Fine grained	
A	9.54	9.57	1			
A	9.65	9.655	1			
CAT	9.53	9.54	0.5			
A	10.01	10.14	1			Where pro-nounced foliation
A	10.19	10.22	2			
A	10.50	10.60	0.5			
A	10.60	10.64	1			
A	10.64	10.73	2			
A	10.73	10.83	1			
A	10.83	10.85	2			
A	10.85	10.86	3			
A	10.86	10.91	1			
A	10.91	10.93	3			
A	10.93	10.97	1.5			
A	10.25	10.35	2			
A	11.53	11.54	1			
CAT	11.87	11.96	1			Microfractures
A	11.86	11.96	1.5			Hematite , mafic minerals
A	12.02	12.13	2			
A	12.13	12.15	3			
A	12.15	12.25	1			
ROCK	12.26	13.15		ÄD	Occasional larger pheno-crysts	
ROCK	13.15	13.23		FGG		
ROCK	13.23	15.64		ÄD	Medium grained	
A	13.20	13.26	1			
A	13.93	14.03	2			Finer grains
A	14.03	14.20	1			
A	14.43	14.44	0.5			
A	14.70	14.74	1			Mafic minerals
A	15.10	15.29	2			
A	15.39	15.42	2			Mafic minerals
ROCK	15.64	15.94		FGG		Almost porhyric
A	15.62	15.65	2			Enrichment of felsics
A	15.65	15.80	1			
A	15.90	15.95	2			Enrichment of felsics
ROCK	15.94	16.66		ÄD		
A	16.28	16.36	2			Mafic alternat-ingly felsic
CAT	16.265	16.27	0.5			
A	16.545	16.55	1			
A	16.65	16.71	1			
A	16.71	16.80	1.5			Enrichm of Qz and K-fsp

Type	From	To	Degree	Rocktype	Fabric/Texture	Remarks
A	16.80	16.82	1			
ROCK	16.66	16.74				Qz, K-fsp
ROCK	16.74	20.00		ÄD	Medium grained, slightly foliated	
A	18.49	18.53	1			Enrichment of felsics
A	18.66	18.73	3		Fine grained	
A	19.04	19.05	1			
A	19.10	19.22	2			
A	19.97	19.98	1			
A	20.21	20.27	1.5			
ROCK	20.00	22.23		ÄD	Medium grained, occasional larger phenocrysts.	
A	21.10	21.15	1			
A	22.04	22.05	1			
ROCK	22.23	24.03		ÄD	Medium grained	
A	22.57	22.61	2			Mafic minerals
A	22.61	22.69	2			Felsic minerals
A	22.69	22.75	2			Mafic minerals
A	22.75	22.90	2		Fine grained	Felsic minerals
A	22.90	23.00	2			Mafic minerals
A	23.00	23.03	2			Hematite
ROCK	24.03	24.30		ÄD	With occasional large phenocrysts	
ROCK	24.30	24.76			Medium grained	
A	24.80	24.83	2			Hematite
A	24.83	24.98	1	ÄD	Fine grained	Mafic minerals
CAT	24.805	24.815	1			
ROCK	24.76	25.19		ÄD	Fine grained	Multidirectional fractures
DUC	25.19	25.35	3	MYL		
CAT	25.19	25.35	1.5			
A	25.15	25.37	3			Ep rich
ROCK	25.35	25.88		ÄD	Medium grained	
ROCK	25.88	26.00			Fine grained	
A	25.52	25.53	1			Hematite
A	25.74	25.75	1			Hematite
A	25.84	25.86	1.5			
A	25.91	25.98	2			
DUC	25.91	25.98	2			Mylonitic
CAT	25.91	25.98	1			
A	26.43	26.48	1			
A	26.85	26.88	1			Fe-mineralization
ROCK	26.00	30.00		ÄD	Medium grained, rather massive	
CAT	27.29	27.31	1			Microfractures
A	27.73	27.76	2			Hematite
A	27.91	27.93	2		Fine grained	
A	28.38	28,48	1.5			
A	28.62	28.66	0.5			
A	28.89	28.93	0.5			
CAT	28.91	28.94	1			Microfractures

Type	From	To	Degree	Rocktype	Fabric/Texture	Remarks
CAT	29.16	29.48	1			Microfractures
A	29.15	29.16	0.5			
A	29.34	29.53	1			
A	29.53	29.55	2			
DUC	29.53	29.55	3	MYL		
CAT	29.53	29.55	2			
CAT	29.68	30.27	1.5			
DUC	29.68	29.70	1			
DUC	29.70	29.73	3	MYL		Ep-rich
DUC	29.73	29.80	1			
DUC	29.80	30.27	3	MYL		Ep-rich
DUC	30.27	30.84	1			
A	29.70	29.73	2			
A	30.00	30.31	1			
A	30.31	30.70	2			
ROCK	30.00	30.70		FGG		
CAT	30.85	31.00	1			Microfractures
DUC	30.84	31.02	2			
A	30.70	30.80	1			
A	30.80	31.02	2			Ep
ROCK	30.70	31.12		ÄD		
CAT	31.12	32.20	1.5			Microfractures
DUC	31.12	32.13	3	MYL		
DUC	32.12	32.28	2			
A	31.10	31.13	2.5			
A	31.13	32.28	1.5			
ROCK	31.12	32.20		MYL		Hematite , Epi-dote
ROCK	32.20	32.65		ÄD		Dark
DUC	32.52	32.64	2			
DUC	32.64	32.85	3	MYL		
DUC	32.85	32.91	2			
CAT	32.53	32.84	1.5			Microfractures
A	32.58	32.64	1.5			Felsic minerals
A	32.64	32.85	2			Hematite , felsic
A	32.85	33.20	2			Mafic minerals
ROCK	32.65	32.83		MYL		Hematite, Epidote
ROCK	32.85	35.44		ÄD		
CAT	33.03	33.04	1			
CAT	33.43	33.50	1			
DUC	33.34	33.41	1			
A	33.35	33.42	2			Mafic minerals
A	33.42	33.55	2			Felsic minerals
A	33.64	33.66	1			
A	33.72	33.78	1			
A	33.97	34.19			Fine grained	Hematite
A	34.375	34.38	1			
A	34.43	34.60	2			Mafic minerals
A	34.84	34.85	1.5			
A	34,97	35.22	1			Mafic minerals
ROCK	35.44	35.50		ÄG		

Type	From	To	Degree	Rocktype	Fabric/Texture	Remarks
ROCK	35.50	36.50		ÄD	Medium grained, foliated	Dark
A	35.53	35.60	2			Mafic minerals
A	35.67	35.68	1			
A	35.72	35.73	2			
A	35.79	35.82	2			Hematite
CAT	35.72	35.73	1			
CAT	35.79	35.72	0.5			
ROCK	36.50	36.72		ÄD	Fine grained, foliated	
ROCK	36.72	36.80		ÄG	Foliated	
A	36.60	36.75	1.5			
A	36.75	36.79	1.5			Hematite
A	36.79	36.86	2			Mafic minerals
ROCK	36.80	38.20		ÄD	Fine grained, foliated	
CAT	37.12	37.15	1.5			
A	37.12	37.15	2			Hematite, only felsic
A	37.40	37.49	2			Hematite
A	37.55	37.56	1.5			
A	37.80	37.81	2.5			Hematite
A	37.81	37.90	2			Hematite , only felsic
A	37.90	37.91	2.5			Hematite
DUC	38.03	38.07	1			
A	38.00	38.20	1			Hematite
ROCK	38.20	40.20		ÄD	More Medium grained	
DUC	38.64	38.66	1			
A	38.64	38.66	1.5			Mafic minerals
DUC	38.75	38.90	1			
A	38.75	38.90	1			Mafic minerals
A	39.195	39.20	1			
A	39.215	39.22	1			
A	39.245	39.25	1			
A	39.30	39.302	1			
A	39.35	39.352	1			
A	39.63	39.68	1		Fine grained	Hematite
CAT	39.63	39.68	0.5			
ROCK	40.20	40.40		ÄD	Fine grained	
ROCK	40.40	40.60			Medium grained	
ROCK	40.60	42.24			Fine grained, some phenocrysts	Ep rich
DUC	40.54	40.60	1			
DUC	40.70	40.78	1.5			
DUC	40.78	40.80	3	MYL		
DUC	40.80	40.86	2			
DUC	40.86	41.33	3	MYL		With occasional Qz
CAT	40.70	41.33	1			
A	40.54	40.65	1.5			
A	40.70	40.78	1.5			
A	40.78	40.80	2			
A	40.80	40.86	1.5			

Type	From	To	Degree	Rocktype	Fabric/Texture	Remarks
A	40.86	41.13	2.5		Fine grained	Hematite
A	41.24	41.33	2			Hematite
ROCK	42.24	42.76		ÄD		Hematite impreg-nation
A	42.19	42.21	2			Hematite
A	42.35	42.46	1			Hematite
A	42.46	42.51	2			Hematite
A	42.59	42.73	2		Fine grained	Hematite
DUC	42.59	42.62	2			
DUC	42.62	42.67	3	MYL		
DUC	42.67	42.71	2			
CAT	42.59	42.72	1			
ROCK	42.76	44.86		ÄD	Fine grained, foliated	
A	43.64	43.66	1.5			Ep
A	43.78	43.785	1			
A	43.85	43.86	1			
A	43.93	44.01	1.5			Hematite, Epidote
DUC	44.00	44.005	3			
DUC	44.005	44.03	2			
DUC	44.03	44.09	1			
DUC	44.09	44.13	0.5			
DUC	44.13	44.17	1			
DUC	44.28	44.29	3			
DUC	44.29	44.35	0.5			
DUC	44.35	44.355	1.5			
DUC	44.36	44.36	2			
DUC	44.36	44.37	1			
DUC	44.37	44.375	1.5			
DUC	44.375	44.395	1			
DUC	44.395	44.405	2.5			
DUC	44.405	44.45	1.5			
DUC	44.45	44.51	2			
DUC	44.55	44.56	3			
A	44.53	44.55	2.5			
A	44.55	44.56	3			
A	44.56	44.57	2			
A	44.57	44.58	1			
DUC	44.59	44.62	1			
DUC	44.62	44.64	3			
DUC	44.64	44.67	1			
DUC	44.67	44.68	2			
DUC	44.68	44.83	1			
DUC	44.83	44.93	1.5			
DUC	44.93	44.95	2			
DUC	44.95	45.00	1.5			
DUC	45.00	45.05	1.5			
DUC	45.05	45.06	3			
DUC	45.06	45.07	2			
DUC	45.07	45.08	3			
DUC	45.08	45.35	2			
DUC	45.35	45.405	1			

Type	From	To	Degree	Rocktype	Fabric/Texture	Remarks
DUC	45.405	45.41	3			
A	45.37	45.39	1			
A	45.39	45.40	2			
A	45.40	45.41	1			
A	45.41	45.42	2			
DUC	45.41	45.43	1			
DUC	45.43	45.47	2			
DUC	45.47	45.62	1.5			
DUC	45.62	45.74	1			
DUC	45.74	45.80	1.5			
DUC	45.80	45.89	1			
DUC	45.89	45.95	1.5			
DUC	45.95	46.43	2			
DUC	46.43	46.55	1			
ROCK	44.86	45.48		ÄD	Bearing phenocrysts	
ROCK	45.48	45.60		ÄD		
ROCK	45.60	45.64		FGG		
ROCK	45.64	45.80		ÄD		
ROCK	45.80	45.90		ÄD	Bearing phenocrysts	
ROCK	45.90	46.41		ÄD	Occasional phenocrysts	
ROCK	46.41	46.54		FGG		Hematite impregnation
DUC	46.55	46.68	1.5			
ROCK	46.54	46.67		ÄD	Foliated	Hematite impregnated, Ep-rich
ROCK	46.67	46.71		FGG	Foliated	Hematite impregnated, Ep-rich
ROCK	46.71	48.18		ÄD	Foliated	Hematite impregnated, Ep-rich
CAT	47.06	47.30	0.5			
A	47.53	47.54	1			Hematite
DUC	47.60	47.64	2		Fine grained	
DUC	47.64	47.71	3	MYL		
DUC	47.71	47.85	2		Fine grained	
CAT	47.57	47.85	1			
A	47.63	47.72	2			Hematite impregnated, Ep-rich
A	47.72	47.83	1.5			Dark
ROCK	48.18	48.23		FGG	Foliated	Hematite impregnated, Ep-rich
ROCK	48.23	48.40		ÄD	Foliated	Hematite impregnated, Ep-rich
ROCK	48.40	48.48		FGG	Foliated	Hematite impregnated, Ep-rich
ROCK	48.48	48.86		ÄD	Foliated	Hematite impregn., Ep-rich
ROCK	48.86	49.31		ÄD	Occasional phenocrysts, foliated	
ROCK	49.31	49.75		ÄD		Dark, some Ep
ROCK	49.75	49.83		ÄD	Fine grained	
ROCK	49.83	50.02		ÄG		Hematite, more felsic

Type	From	To	Degree	Rocktype	Fabric/Texture	Remarks
ROCK	50.02	51.33		ÄD	Foliated	Hematite im-pregnated, Ep-rich
DUC	50.51	50.58	3	MYL		Ep-rich
DUC	50.58	50.71	2			
DUC	50.71	50.89	1.5			
CAT	50.51	50.80	1.5			Microfractures
CAT	50.80	50.90	1			
A	50.51	50.77	2			Hematite
A	50.77	50.90	1		Fine grained	Dark
ROCK	51.33	51.44		P		
ROCK	51.44	52.25		ÄD	Massive	Ep-rich
ROCK	52.25	52.60		P		Hematite , Ep, Ca and black oxide in fracture planes
ROCK	52.60	52.72		ÄD	Massive	Ep-rich
ROCK	52.72	52.80		P		
ROCK	52.80	54.10		ÄD	Massive	Ep-rich
ROCK	54.10	54.15		P		
ROCK	54.15	54.82		ÄD	Massive	Ep-rich
ROCK	54.82	54.85		P		
ROCK	54.85	55.40		ÄD	Slightly foliated	Ep-rich
CAT	55.03	55.10	0.5			
DUC	55.02	55.12	1.5			
A	55.05	55.12	1.5			
ROCK	55.40	55.70		ÄD	Massive	Ep-rich
ROCK	55.70	55.81		P		
ROCK	55.81	57.45		ÄD	Massive	Ep-rich
CAT	56.87	57.00	0.5			
DUC	56.88	57.00	1			
A	56.88	57.00	1			
ROCK	57.45	58.00		QZ		

SKB TR-01-21

Appendix 2

The BIP database

Appendix 2

The BIP database

	Depth	Azimuth of dip	Dip	Width	Sort	Form	Condition	Remarks
0	[m]	[°]	[°]	[mm]	Primary structure	Planar	Weathered	Quartz
1					Fracture	Undulating	Dull	Chlorite
2					Vein	Stepped	Cavities	Calcite
3					Fracture zone	Irregular	Open	Epidote
4					Contact	Network	Oxidised	Hematite
5					Structure (foliat.)	Breccia	Chloritised	Pyrite
6					Alteration	Shear	Epidotised	Hybride rock
7						Crushed	Tectonised	Clay
8						Flowstruct.		Granite
9						Foliation		Pegmatite
10								Fine grained Gr.
11								Mylonite

Borehole KXTT1

Meter along borehole	Azimuth of dip	Angle of dip	Width [mm]	Sort	Form	Condition	Remark
4.113	204	77	2	1	0	3	2
4.184	153	51	2	1	0	3	2
4.201	166	75	2	1	0	3	2
4.653	42	73	1	1	0	1	2
5.064	190	57	2	1	0	4	2
5.078	187	57	2	1	0	4	2
5.142	50	71	2	1	0	4	2
5.674	49	62	18	1	4	4	3
6.097	22	86	1	1	1	3	2
6.768	66	76	13	1	4	4	2
6.809	67	76	5	1	4	4	2
7.262	197	69	2	1	0	3	2
7.316	194	86	2	1	0	4	2
7.526	221	55	2	1	0	2	2
8.266	51	83	5	1	4	4	3
8.496	214	82	2	1	0	2	2
8.84	63	73	2	1	0	1	2
8.96	35	89	3	1	0	1	2
9.228	48	68	2	1	0	4	2
9.261	231	73	2	1	0	2	2
9.373	70	77	2	1	0	4	2
9.662	233	88	4	1	0	1	3
9.86	52	85	1	1	0	2	2
9.994	59	77	2	1	0	2	2
10.332	207	77	3	1	1	3	2
10.739	88	71	7	1	4	1	3
11.051	73	61	2	1	1	4	3
11.52	19	85	3	1	0	4	2
11.675	38	70	9	2	0	4	10
12.485	276	82	2	1	0	1	3
12.617	172	48	3	1	0	2	1
12.709	282	84	3	1	1	5	2
12.876	222	89	1	1	0	1	1
13.099	30	83	3	1	0	1	2
13.22	238	77	2	1	0	1	2
13.438	244	84	1	1	0	1	2
13.623	172	14	1	1	0	1	2
14.21	45	81	1	1	0	2	2
14.291	49	76	2	1	0	1	2
14.292	225	74	1	1	0	2	2
14.491	137	78	1	1	0	1	2
14.896	308	87	1	1	1	4	2
15.25	56	83	4	1	1	4	3
15.307	354	53	1	1	1	2	2
15.734	50	71	91	5	6	7	11
15.772	54	78	2	1	0	3	2

Meter along borehole	Azimuth of dip	Angle of dip	Width [mm]	Sort	Form	Condition	Remark
15.792	49	79	5	1	1	4	3
15.812	49	70	6	1	1	3	2
15.935	57	80	3	1	4	1	2
18.268	81	79	4	1	4	1	2
19.123	49	84	7	1	1	1	2
19.195	210	74	2	1	1	4	2
19.273	64	86	4	1	1	4	3
19.329	152	13	4	1	1	4	2
19.383	59	77	2	1	1	3	2
19.493	195	42	8	1	1	4	3
20.13	270	41	18	1	1	4	3
20.234	131	23	2	1	3	2	2
20.65	185	76	1	1	1	2	2
20.733	31	89	5	1	0	3	2
20.902	45	89	2	1	0	2	2
20.902	256	58	3	1	1	1	2
21.009	48	76	1	1	1	2	2
21.139	183	80	6	1	1	4	3
21.358	44	84	2	1	1	2	2
21.506	176	88	2	1	3	2	2
21.59	219	82	2	1	1	2	2
21.634	203	84	2	1	3	4	1
21.662	5	65	1	1	1	4	2
21.708	244	69	3	1	1	4	3
21.89	35	85	2	1	1	3	2
21.911	17	88	2	1	1	2	2
21.96	47	70	2	1	1	3	2
22.025	37	79	1	1	1	3	2
22.158	200	53	2	1	1	3	2
22.27	36	86	2	1	1	4	2
22.419	68	75	8	1	0	4	3
22.525	251	81	2	1	1	3	2
22.613	63	65	6	1	1	4	3
22.694	68	76	4	1	1	3	2
22.814	8	72	143	2	3	4	10
23.025	222	61	2	1	1	2	2
23.077	215	69	2	1	1	4	2
23.207	6	47	2	1	1	3	2
23.303	204	59	2	1	1	2	2
23.351	71	77	4	1	1	3	2
23.531	204	67	1	1	0	1	2
23.624	67	79	2	1	1	2	2
23.754	211	73	1	1	0	1	2
23.845	56	82	4	1	1	3	2
24.017	60	82	2	1	1	2	2
24.116	103	84	5	1	1	4	3
24.198	68	72	2	1	1	2	2
24.446	51	59	1	1	3	3	1

Meter along borehole	Azimuth of dip	Angle of dip	Width [mm]	Sort	Form	Condition	Remark
24.523	57	76	48	2	3	1	1
24.637	356	50	1	1	3	3	2
24.788	206	74	3	1	1	4	3
24.91	18	79	3	1	1	2	2
24.967	359	70	2	1	1	3	2
24.976	214	77	4	1	1	3	2
25.096	0	15	1	2	0	4	10
25.246	206	70	3	1	0	1	2
25.464	61	71	187	2	1	4	10
25.469	30	86	2	1	1	3	2
25.531	196	78	1	1	0	4	3
25.6	210	86	2	1	0	4	3
25.834	208	86	2	1	0	4	2
25.885	206	65	1	1	0	4	2
26.087	224	74	3	1	0	4	2
26.156	78	80	3	1	1	4	3
26.382	142	70	2	1	3	4	3
26.469	305	26	2	2	0	4	10
26.584	68	72	4	1	1	4	3
26.992	71	72	25	1	4	4	3
27.183	191	70	3	1	0	4	2
27.219	271	85	4	1	0	4	3
27.22	185	74	2	1	0	4	2
27.541	34	73	5	1	2	4	2
27.783	187	68	2	1	0	4	2
27.835	29	76	61	2	1	4	10
27.868	60	77	3	1	4	4	3
28.055	48	86	4	1	0	1	2

Borehole KXTT2

Meter along borehole	Azimuth of dip	Angle of dip	Width [mm]	Sort	Form	Condition	Remark
4.134	162	53	1	1	1	2	2
4.158	251	70	5	1	0	4	3
4.185	140	47	1	1	0	2	3
4.378	157	57	1	1	0	2	3
4.441	64	84	6	1	0	4	3
4.474	149	49	1	1	0	2	3
4.519	35	77	2	1	0	4	3
4.537	115	22	3	1	0	4	3
4.667	291	37	1	1	0	1	3
4.851	48	82	112	2	0	4	10
5.057	67	60	3	1	0	1	3
5.147	194	66	2	1	0	1	3
5.24	181	65	2	1	0	1	3
5.294	182	67	3	1	1	4	3
5.422	173	31	2	1	0	4	3
5.487	245	57	3	1	0	4	3
5.513	136	67	3	1	1	3	2
6.12	138	32	3	1	1	1	3
6.347	184	34	16	1	4	4	3
6.42	200	72	2	1	0	3	2
6.603	249	67	5	1	4	4	3
6.643	293	26	14	1	4	4	3
7.047	44	81	7	1	0	1	3
7.09	239	68	2	1	0	1	3
7.143	16	78	3	1	1	2	2
7.246	206	77	3	1	0	2	2
7.304	208	66	3	1	0	1	3
8.162	136	62	1	1	0	3	2
8.547	188	87	1	1	0	2	2
8.915	82	66	100	2	1	4	0
9.182	50	81	1	1	0	3	2
9.214	235	67	2	1	0	4	3
9.301	240	72	2	1	0	2	3
9.328	208	81	3	1	0	2	3
9.514	207	69	2	1	0	2	2
9.688	85	67	2	1	2	4	3
9.836	49	75	17	1	4	5	3
9.98	63	75	2	1	0	5	3
10.138	51	69	6	1	0	4	3
10.157	206	86	2	1	0	2	3
10.258	208	83	2	1	0	2	3
10.464	74	86	6	1	0	4	3
10.826	63	85	21	1	4	5	3
11.16	63	78	4	1	0	1	3
11.61	60	72	6	1	4	4	3
11.666	245	85	4	1	4	4	3

Meter along borehole	Azimuth of dip	Angle of dip	Width [mm]	Sort	Form	Condition	Remark
11.69	90	86	6	1	4	4	3
12.206	201	81	3	1	0	2	2
12.224	238	72	2	1	0	2	2
12.601	15	84	6	1	0	4	3
12.687	236	68	2	1	0	2	2
13.103	234	65	3	1	0	2	2
14.114	59	86	5	1	1	1	3
14.291	164	38	3	1	7	3	2
14.429	201	80	3	1	0	1	3
14.625	214	69	3	1	0	2	2
14.965	65	76	2	1	0	1	2
15.037	74	74	10	1	4	1	3
15.124	59	77	22	1	4	5	2
15.304	57	76	2	1	0	1	2
15.662	335	87	1	1	1	1	2
16.381	85	90	2	1	0	2	3
16.576	77	87	6	1	1	4	3
17.19	50	72	4	1	1	4	1
17.386	178	46	1	1	0	2	2
17.5	200	78	3	1	0	2	2
17.684	68	85	63	2	0	4	10
17.725	57	87	9	1	0	1	2
17.784	242	85	3	1	0	1	2

Borehole KXTT3

Meter along borehole	Azimuth of dip	Angle of dip	Width [mm]	Sort	Form	Condition	Remark
3.892	221	74	1	1	0	2	2
3.939	153	68	1	1	0	2	2
4.075	244	9	2	1	0	2	2
4.126	222	72	8	1	4	5	2
4.266	191	89	17	1	4	5	2
4.474	142	42	1	1	0	2	2
4.632	213	48	1	1	0	2	2
4.636	356	68	2	1	0	4	3
4.893	150	61	1	1	0	2	2
5.081	98	83	1	1	0	4	3
5.252	258	89	2	1	0	4	3
5.466	25	87	1	1	0	4	2
5.579	209	87	1	1	0	1	2
5.661	238	63	41	2	1	4	10
5.694	237	65	8	1	4	4	3
5.732	54	90	5	1	1	4	1
5.735	116	33	5	1	4	4	3
5.949	15	67	239	2	1	4	10
6.029	141	72	2	1	1	2	2
6.111	14	66	9	1	4	4	3
6.153	162	12	2	1	0	2	2
6.284	27	76	3	1	0	4	3
6.364	195	84	3	1	0	2	2
6.41	191	88	2	1	0	2	2
6.482	195	82	3	1	0	4	2
6.564	185	49	2	1	0	2	2
6.643	30	84	4	1	0	4	2
6.9	187	72	6	1	0	5	2
6.925	13	86	2	1	0	2	2
6.937	6	88	1	1	0	5	2
7.16	225	79	2	1	0	1	2
7.288	204	79	4	1	0	1	2
7.509	29	75	4	1	0	5	2
8.034	54	66	7	1	4	5	3
8.046	15	78	2	1	0	1	2
8.071	40	69	2	1	0	5	3
8.38	47	71	2	1	0	5	3
8.489	171	71	2	1	0	2	2
8.645	189	73	3	1	0	1	2
8.654	71	62	2	1	0	1	2
9.199	59	68	70	5	8	4	2
9.358	45	75	2	1	0	2	2
10.358	27	56	2	1	1	2	2
13.076	186	39	4	1	0	3	2
13.166	32	57	1	1	1	1	2
13.887	71	82	7	1	0	4	2

Meter along borehole	Azimuth of dip	Angle of dip	Width [mm]	Sort	Form	Condition	Remark
13.92	61	77	3	1	0	2	2
13.967	76	82	6	1	4	4	2
14.064	28	89	1	1	1	3	2
14.1	55	78	5	1	1	3	2
14.141	60	85	44	5	8	5	2
14.775	30	62	1	1	1	3	2
15.107	331	88	1	1	0	1	2
15.229	54	88	2	1	1	2	2
15.362	29	61	2	1	1	3	2
15.576	177	41	1	1	0	2	2
15.699	63	69	2	1	0	2	2
15.775	251	85	5	1	4	4	2
15.961	64	75	4	1	1	4	2
16.311	262	89	3	1	1	2	2
16.352	37	89	1	1	1	2	2
16.578	189	84	3	1	0	2	2
16.783	82	87	10	1	1	4	0
16.989	13	68	22	1	1	4	0

Borehole KXTT4

Meter along borehole	Azimuth of dip	Angle of dip	Width [mm]	Sort	Form	Condition	Remark
3.796	196	63	1	1	0	2	2
4.015	54	71	2	1	0	4	3
4.154	325	20	2	1	0	2	2
4.277	37	88	7	1	2	4	3
4.322	207	84	6	1	2	4	3
4.338	184	65	3	1	0	2	2
4.456	136	45	1	1	0	2	2
4.634	80	90	10	1	4	4	3
4.65	76	89	106	2	1	4	10
4.66	143	61	1	1	0	2	2
4.785	5	20	4	1	1	4	3
5.366	208	76	6	1	0	4	3
5.443	188	65	3	1	1	2	2
5.45	207	79	5	1	1	4	3
5.461	157	45	1	1	0	2	2
5.505	200	73	3	1	0	4	2
5.67	223	84	10	1	0	4	3
5.789	174	74	6	1	4	4	3
5.926	155	71	2	1	1	4	2
6.025	211	66	1	1	1	3	2
6.091	24	84	236	2	1	6	10
6.654	64	84	6	1	0	4	3
7.818	10	83	44	2	1	4	10
7.891	43	87	2	1	0	4	3
8.052	50	80	9	1	0	4	3
8.493	33	7	2	1	0	2	2
8.688	13	76	216	2	0	4	10
8.743	202	86	2	1	0	2	2
8.786	3	66	13	2	1	4	10
9.405	332	7	2	1	0	4	2
9.565	209	79	10	1	4	4	3
9.707	43	62	76	2	1	4	10
9.711	30	69	5	1	1	3	2
9.835	63	66	38	2	1	4	10
10.161	70	69	5	1	0	4	3
10.404	30	67	10	2	1	4	10
10.536	38	62	70	2	1	4	10
10.789	36	58	7	2	1	4	10
12.096	56	76	4	1	0	3	2
12.125	50	73	23	1	1	4	3
12.145	45	77	2	1	0	2	2
12.186	236	80	3	1	0	4	3
12.354	8	85	162	2	1	4	10
13.044	44	80	1	1	0	3	2
13.133	39	65	7	1	1	1	3
13.338	50	88	3	1	0	1	3

Meter along borehole	Azimuth of dip	Angle of dip	Width [mm]	Sort	Form	Condition	Remark
13.443	209	81	11	1	1	1	3
13.585	229	86	1	1	1	1	3
13.751	35	62	1	1	1	1	2
13.923	6	83	0	4	1	4	10
13.952	46	82	4	1	0	4	3
14.033	228	69	1	1	0	2	2
14.086	46	87	2	1	0	2	3
14.244	144	5	2	1	0	2	2
14.333	46	82	4	1	0	4	3
14.803	30	67	254	2	1	4	10
15.185	39	86	37	1	4	5	3
15.249	39	88	26	1	4	5	3
15.25	357	77	1	1	4	3	2
15.267	201	77	1	1	0	3	2
15.284	31	84	8	1	0	4	3
15.359	164	27	2	1	0	2	1
15.433	-63	24	2	1	0	4	3
15.473	177	56	2	1	0	4	2
15.493	187	46	1	1	0	4	2
15.523	340	86	1	1	1	2	2
15.851	180	77	8	1	0	4	3
16.082	286	27	2	1	0	4	3
16.44	45	86	4	1	0	4	3
16.783	154	53	4	1	0	4	3
17.185	299	84	2	1	0	1	2
17.283	93	67	7	1	1	1	0
17.572	69	5	10	2	1	1	1
17.896	220	69	13	1	0	1	0
18.258	223	89	8	1	0	1	3
18.335	255	64	4	1	1	1	3
18.493	69	87	8	1	0	4	3
18.514	53	76	21	2	1	4	10
18.707	170	37	2	1	0	3	2
19.092	183	72	2	1	0	1	2
19.256	37	60	5	1	0	1	2
19.338	219	83	17	1	0	3	2
19.567	66	82	0	4	0	1	8
19.574	70	80	4	1	0	1	3
19.771	204	75	3	1	1	3	2
19.787	23	75	3	1	1	2	2
20.017	306	36	2	1	0	2	2
20.124	59	89	2	1	0	2	2
20.228	69	75	5	1	0	3	2
20.413	221	84	3	1	0	3	2
20.485	203	78	4	1	0	4	2
20.514	215	82	3	1	0	3	2
20.646	8	71	1	1	1	2	2
20.733	49	70	2	1	1	3	2

Meter along borehole	Azimuth of dip	Angle of dip	Width [mm]	Sort	Form	Condition	Remark
20.957	201	77	1	1	0	2	2
20.981	235	82	4	1	1	3	2
20.996	38	81	1	1	1	3	2
21.099	204	77	2	1	0	3	2
21.352	61	76	4	1	0	3	2
21.367	52	1	2	1	0	2	2
21.531	63	61	4	1	0	3	3
21.552	57	59	8	1	4	4	3
21.822	279	52	11	1	4	4	3
21.85	238	23	3	1	1	4	3
21.905	163	49	2	1	1	2	2
22.251	292	82	213	2	1	4	10
22.308	71	81	3	1	1	2	2
22.35	73	80	4	1	1	3	2
22.503	278	84	8	1	4	4	3
22.56	70	81	3	1	0	4	2
22.739	226	72	4	1	0	4	2
22.786	85	82	4	1	0	4	2
22.837	58	72	3	1	1	2	2
23.065	20	62	1	1	0	2	2
23.692	202	57	3	1	0	5	3
23.779	188	51	3	1	0	4	3
23.878	211	54	4	1	0	4	3
23.971	33	87	281	2	0	4	10
24.173	37	72	3	1	0	2	2
24.281	26	69	2	1	1	3	2
24.316	29	64	12	1	1	3	2
24.34	35	81	1	1	0	2	2
24.434	70	63	2	1	1	2	2
24.532	90	59	1	1	1	2	2
24.626	88	71	10	1	0	4	3
24.767	298	10	2	1	0	2	2
24.865	229	87	3	1	0	3	2
25.037	29	85	2	1	0	2	2
25.122	49	80	4	1	1	3	2
25.144	62	63	2	1	1	3	2
25.302	33	59	2	1	1	2	2
25.56	13	60	6	1	1	2	2
25.733	13	85	5	1	1	3	2
25.878	21	77	4	1	1	3	2
26.088	355	75	5	1	0	2	1
26.312	55	74	1	1	0	2	2
26.587	218	85	2	1	0	2	1
26.637	34	63	2	1	0	2	1
26.762	8	72	3	1	1	2	2
26.951	56	69	3	1	1	3	1
27.053	248	82	3	1	0	2	2
27.095	43	82	1	1	0	2	2

Meter along borehole	Azimuth of dip	Angle of dip	Width [mm]	Sort	Form	Condition	Remark
27.42	46	85	3	1	0	2	2
27.524	37	89	3	1	0	2	2
27.771	33	79	2	1	0	1	2
28.173	245	71	2	1	1	1	3
28.285	61	70	2	1	1	1	2
28.433	52	12	1	1	1	1	2
28.777	56	65	127	2	0	4	10
28.791	54	65	9	1	0	4	3
28.849	52	76	1	1	0	4	2
28.9	73	66	4	1	0	3	1
29.007	52	64	1	1	0	1	2
29.095	203	90	3	1	0	2	2
29.137	45	70	5	1	0	4	3
29.164	208	87	1	1	0	2	2
29.174	200	70	1	1	0	4	2
29.249	74	82	5	1	4	4	3
29.296	64	83	4	1	1	3	2
29.454	34	73	29	1	0	4	3
29.567	189	85	14	1	0	4	3
30.009	26	81	4	1	0	3	2
30.121	218	26	9	1	1	4	3
30.513	222	69	4	1	0	4	3
30.532	37	89	3	1	0	3	2
30.879	72	73	2	1	0	1	2
30.911	73	73	2	1	0	1	2
31.18	59	74	2	1	0	1	2
31.314	156	59	3	1	0	2	2
31.416	73	68	9	1	0	3	3
31.466	43	75	3	1	0	4	2
31.564	51	65	2	1	0	2	2
31.706	74	79	6	1	0	4	3
31.937	73	69	2	1	0	4	3
32.173	74	66	2	1	0	4	2
32.428	32	58	2	1	1	3	2
32.567	40	63	1	1	0	2	2
32.913	37	90	2	1	0	4	2
33.101	73	75	2	1	0	3	2
33.178	62	80	6	1	0	2	2
33.588	38	72	3	1	1	4	1
33.784	98	69	1	1	0	4	2
34.121	224	78	2	1	0	4	2
34.14	330	41	1	1	0	4	1
34.394	32	65	2	1	0	2	2
34.479	30	73	1	1	0	2	2
35.233	24	80	2	1	1	2	2
35.938	43	67	2	1	1	2	2
36.049	46	80	2	1	0	2	2
36.343	43	62	1	1	0	4	1

Meter along borehole	Azimuth of dip	Angle of dip	Width [mm]	Sort	Form	Condition	Remark
36.496	260	72	3	1	0	4	3
36.594	70	81	57	2	0	4	10
36.635	63	80	2	1	0	3	2
36.796	60	59	6	1	0	1	3
37.078	21	67	14	2	0	1	9
37.155	26	66	33	2	0	4	10
37.173	21	67	7	1	0	4	3
37.887	326	14	2	2	0	4	10
37.909	52	76	5	1	0	1	3
38.774	222	85	1	1	0	1	2
39.531	94	78	85	5	6	4	11
39.585	95	79	6	1	0	3	2
39.819	99	74	2	1	0	4	2
40.282	77	90	42	5	6	7	11
40.444	65	64	50	5	6	7	11
40.792	29	66	2	1	1	1	2
40.983	78	68	2	1	1	4	2
41.762	225	77	3	1	0	3	2
42.777	59	76	1	1	0	1	2
42.809	196	80	2	1	0	1	2
43.078	244	86	21	1	0	1	3
43.253	80	69	3	1	0	1	3
43.421	145	53	2	1	0	1	2
44.025	68	72	13	1	0	3	3
44.084	65	72	4	1	0	1	2
44.465	185	54	1	1	0	4	2
44.557	61	89	2	1	0	4	2
44.615	63	82	2	1	0	4	2
44.756	56	74	3	1	0	4	3
45.435	167	56	2	1	0	2	2
45.492	235	80	3	1	0	4	2
45.996	95	79	9	1	0	4	0
46.291	134	52	2	1	0	2	2
46.293	59	88	2	1	0	2	2
46.4	176	56	1	1	0	2	2
46.617	156	57	3	1	0	5	2
46.743	136	48	4	1	1	3	2
46.885	233	86	3	1	0	2	2
46.936	53	86	2	1	0	4	2
47.003	239	90	27	1	4	4	3
47.018	230	81	1	1	1	4	2
47.055	53	77	3	1	1	4	2
47.229	250	83	6	1	3	4	2
47.595	151	60	3	1	1	2	2
48.05	267	76	5	1	1	4	3
48.407	220	4	2	1	0	2	2
48.837	63	80	39	1	4	4	3

Borehole KA3005a

Meter along borehole	Azimuth of dip	Angle of dip	Width [mm]	Sort	Form	Condition	Remark
5.302	172	26	11	1	0	4	3
11.685	109	87	3	0	3	2	6
15.398	295	52	10	2	0	5	9
26.745	95	18	4	1	0	4	2
35.133	67	81	5	1	0	4	3
35.188	53	76	2	1	0	1	3
35.284	40	76	1	1	0	1	3
35.591	52	76	4	1	0	1	3
35.646	334	44	3	1	0	4	2
35.795	49	61	6	1	0	1	3
35.813	65	64	6	1	0	1	2
35.872	74	52	5	1	0	1	3
36.206	69	60	3	1	0	1	3
36.259	78	66	6	1	0	1	3
36.589	66	41	4	1	0	2	2
36.714	80	69	9	1	0	4	3
36.813	216	74	3	1	1	3	1
36.815	78	67	2	1	0	4	3
36.997	82	71	2	1	0	4	3
37.038	42	76	33	2	0	4	9
37.171	214	67	4	1	1	3	1
37.356	222	66	1	1	0	3	1
37.405	98	68	3	1	0	4	3
37.717	94	69	2	1	0	4	1
37.741	81	66	61	2	0	4	9
37.887	278	75	5	1	0	4	3
37.937	64	57	3	1	0	4	3
38.085	154	88	2	1	0	4	1
38.346	103	61	6	1	0	1	3
38.733	69	89	3	1	0	0	3
38.826	97	65	3	1	0	0	3
39.367	224	72	2	1	0	2	2
39.479	212	75	2	1	0	2	2
39.537	351	70	1	1	0	2	2
39.54	203	81	1	1	1	1	2
39.644	305	79	1	1	0	1	2
39.746	108	52	10	1	4	4	3
40.33	321	79	1	1	0	1	2
40.466	234	63	4	1	0	4	3
40.698	339	45	3	1	0	6	1
40.785	87	80	12	1	4	4	3
40.917	245	88	3	1	0	4	3
40.926	216	71	4	1	0	2	2
41.03	241	88	2	1	0	2	2
41.067	222	78	2	1	0	2	2
41.519	348	72	2	1	0	4	1

Meter along borehole	Azimuth of dip	Angle of dip	Width [mm]	Sort	Form	Condition	Remark
41.627	156	57	2	1	0	4	1
41.885	101	76	4	1	0	4	3
41.93	108	59	3	1	0	4	3
42.076	303	82	2	1	0	4	3
42.177	212	68	2	1	0	4	2
42.192	47	59	4	1	0	4	3
42.202	119	83	5	1	0	4	3
42.313	87	82	3	1	0	4	3
42.444	109	54	6	1	0	4	3
42.718	243	89	34	1	4	4	3
42.897	260	60	6	1	0	4	3
42.971	81	66	4	1	0	1	3
43.169	110	82	4	1	0	1	3
43.273	275	71	4	1	0	1	3
43.404	300	84	14	1	0	1	3
43.54	106	87	2	1	0	1	3
43.623	95	74	2	1	0	1	3
43.719	95	79	50	6	0	4	3
43.974	61	82	12	1	0	1	3
44.288	210	80	1	1	0	2	2
44.296	51	56	14	1	4	1	3
44.366	23	49	2	1	0	1	3
44.388	76	79	5	1	0	1	3
44.477	45	89	2	1	0	2	2
44.553	107	87	4	1	0	1	3
44.673	94	77	5	1	0	1	3
44.74	88	66	3	1	0	1	3
44.766	42	72	2	1	0	1	3
44.797	53	76	3	1	0	1	2
44.974	70	88	1	1	0	2	1
45.045	69	79	2	1	0	1	3
45.087	240	90	5	1	0	1	3
45.647	342	64	11	1	0	4	0
46.162	83	87	4	1	0	1	3
46.271	257	81	3	1	0	1	3
46.342	64	79	4	1	0	1	2
46.491	331	71	1	1	0	2	2
46.619	335	45	3	1	0	2	2
46.979	170	34	4	1	0	4	1
47.214	308	68	2	1	0	4	1
47.329	295	70	3	1	0	4	0
47.484	249	61	2	1	0	4	2
47.563	86	83	4	1	0	4	3
47.723	67	47	45	1	4	4	3
47.944	104	77	3	1	0	1	3
48.052	50	77	2	1	0	1	3
48.237	239	68	2	1	0	3	1
48.252	236	71	3	1	0	3	1

Meter along borehole	Azimuth of dip	Angle of dip	Width [mm]	Sort	Form	Condition	Remark
48.253	77	72	3	1	0	4	3
48.453	233	73	5	1	0	3	1
48.759	223	64	2	1	0	1	3
48.829	56	80	10	1	0	4	3
49.253	90	73	2	1	0	1	3
49.422	224	62	4	1	0	3	1
49.481	243	86	3	1	0	4	3

Appendix 3

The line counting database

3-1 Line counting data parallel the tunnel axis

3-2 Line counting data normal to the tunnel axis

Appendix 3.1

Line counting data (**parallel to tunnel axis**). Line counting was carried out at the ceiling of the TRUE-1 section between 2950 and 2980 m. FGG is the fine grained granite, FA is azimuth of dip and FW is angle of dip

Interval from Line counting parallel to tunnel at 0 <=> 2950 m	To	Litho	No. of fractures	FA	FW	Trace length (m)
0	1	Diorite	0	0	0	0.00
1	2	Diorite	1	50	50	0.30
		Diorite	2	90	40	0.30
2	3	FGG	1	90	20	0.20
		FGG	2	210	30	0.20
		FGG	3	210	30	0.20
		Diorite	4	220	85	0.30
3	4	Diorite	0	0	0	0.00
4	5	Diorite	0	0	0	0.00
5	6	Diorite	1	90	40	1.00
		Diorite	2	70	50	1.50
6	7	Diorite	0	0	0	0.00
7	8	Diorite	0	0	0	0.00
8	9	Diorite	1	70	85	0.50
		Diorite	2	50	5	1.00
		Diorite	3	70	75	0.30
9	10	Diorite	0	0	0	0.00
10	11	Diorite	1	100	60	0.20
		Diorite	2	100	60	0.20
		Diorite	3	0	0	0.10
		Diorite	4	200	70	1.00
		Diorite	5	200	70	0.40
		Diorite	6	200	70	0.50
11	12	Diorite	1	240	45	1.70
12	13	Diorite	1	20	5	0.40
		Diorite	2	90	90	0.60
13	14	Diorite	1	0	60	0.40
		Diorite	2	270	15	1.60
		Diorite	3	270	25	3.00
14	15	Diorite	1	130	30	0.60
		Diorite	2	60	20	0.80
15	16	Diorite	1	210	45	0.20
		Diorite	2	270	20	0.80
16	17	Diorite	1	80	85	0.50

Interval from Line counting parallel to tunnel at 0 <=> 2950 m	To	Litho	No. of fractures	FA	FW	Trace length (m)
		Diorite	2	210	80	0.30
		Diorite	3	350	88	0.10
17	18	Diorite	1	50	70	0.15
18	19	Diorite	1	180	30	0.70
		Diorite	2	10	80	1.00
19	20	Diorite	1	180	35	0.40
20	21	Diorite	1	180	90	0.30
		FGG	2	0	80	0.10
		FGG	3	0	80	1.00
		FGG	4	140	30	0.10
21	22	FGG	1	130	5	0.10
		FGG	2	10	70	0.15
		Diorite	3	180	30	3.00
22	23	Diorite	1	180	30	0.40
		Diorite	2	210	20	0.20
23	24	Diorite	1	300	85	0.60
		Diorite	2	120	80	0.10
24	25	Diorite	1	150	70	0.40
25	26	Diorite	0	-	-	0.00
26	27	Diorite	0	-	-	0.00
27	28	Diorite	0	-	-	0.00
28	29	Diorite	1	180	30	1.00
		Diorite	2	300	70	2.00
		Diorite	3	230	30	0.30
29	30	Diorite	0	-	-	0.00
0	**30**	**TOTAL**				**31.20**

Appendix 3.2

Line counting data (**normal to tunnel axis**). Line counting was carried out at the ceiling of the TRUE-1 section between 2950 and 2980 m. FGG is the fine grained granite, FA is azimuth of dip and FW is angle of dip.

Interval from Line counting normal to tunnel at 0 <=> 2950 m	To	Litho	No. Of fractures	FA	FW	Trace length (m)
1	4	Diorite	1	200	70	0.40
		Diorite	2	70	70	0.30
		Diorite	3	220	10	4.00
		Diorite	4	90	70	0.40
		Diorite	5	0	0	5.00
at 5 <=> 2955 m		Diorite	1	130	45	0.40
		Diorite	2	0	85	1.00
		Diorite	3	130	50	0.50
		Diorite	4	120	40	0.10
		Diorite	5	0	0	0.20
		Diorite	6	100	15	2.50
		Diorite	7	40	30	1.00
at 10 <=> 2960 m from 1	4	Diorite	1	200	80	1.30
		Diorite	2	230	20	0.70
		Diorite	3	220	80	0.20
		Diorite	4	230	40	0.30
		Diorite	5	120	70	0.15
		Diorite	6	150	10	1.00
		Diorite	7	150	10	0.20
		Diorite	8	150	10	0.40
		Diorite	9	150	10	1.00
at 15 <=> 2965 m from 0	4	Diorite	1	130	20	1.50
		Diorite	2	190	90	4.00
		Diorite	3	160	40	0.20
		Diorite	4	300	5	0.10
		Diorite	5	300	10	0.30
		Diorite	6	300	10	0.10
		Diorite	7	0	0	0.50
		Diorite	8	270	20	1.20
		Diorite	9	130	10	0.60
		Diorite	10	110	45	0.20
		Diorite	11	270	20	2.50
at 20 <=> 2970 m from 0	0.5	FGG	1	160	85	0.50
		FGG	2	90	30	0.20
		FGG	3	30	50	0.50
		FGG	4	130	85	1.00

Interval from Line counting normal to tunnel at 0 <=> 2950 m	To	Litho	No. Of fractures	FA	FW	Trace length (m)
		FGG	5	160	80	0.20
0.5	2.5	Diorite	6	0	50	0.60
		Diorite	7	0	50	0.60
		Diorite	8	0	50	0.40
		Diorite	9	70	90	0.40
		Diorite	10	170	70	0.40
2.5	3	FGG	11	190	80	0.70
		FGG	12	320	10	0.40
		FGG	13	190	80	1.50
		FGG	14	190	80	0.20
		FGG	15	190	80	0.30
		FGG	16	150	70	0.10
2.5	3	FGG	17	190	80	0.40
		FGG	18	270	45	1.00
3	4	Diorite	19	200	15	1.20
		Diorite	20	270	40	0.50
		Diorite	21	90	40	0.30
		Diorite	22	0	0	2.00
		Diorite	23	300	60	0.40
at 25 <=> 2975 m from 0	4	Diorite	1	190	10	0.20
		Diorite	2	200	70	0.20
		Diorite	3	20	70	0.10
		Diorite	4	130	90	0.20
		Diorite	5	120	20	1.50
		Diorite	6	180	50	0.50
		Diorite	7	0	50	1.00
		Diorite	8	0	50	0.20
		Diorite	9	310	25	0.30
		Diorite	10	130	70	0.70
		Diorite	11	310	15	0.70
at 30 <=> 2980 m from 0	4	Diorite	1	150	60	0.50
		Diorite	2	210	20	1.00
		Diorite	3	210	20	0.60
		Diorite	4	220	50	0.80
		Diorite	5	140	75	2.50
0		**TOTAL**				**30.50**

Appendix 4

The tunnel wall fracture trace map of the TRUE-1 block

4-1 TRUE-1 block fracture-trace map along tunnel from 2944 – 2955 m

4-2 TRUE-1 block fracture-trace map along tunnel from 2949 – 2960 m

4-3 TRUE-1 block fracture-trace map along tunnel from 2960 – 2972 m

4-4 TRUE-1 block fracture-trace map along tunnel from 2972 – 2983 m

4-5 TRUE-1 block fracture-trace map along tunnel from 2983 – 2994 m

4-6 TRUE-1 block fracture-trace map along tunnel from 2994 – 3004 m

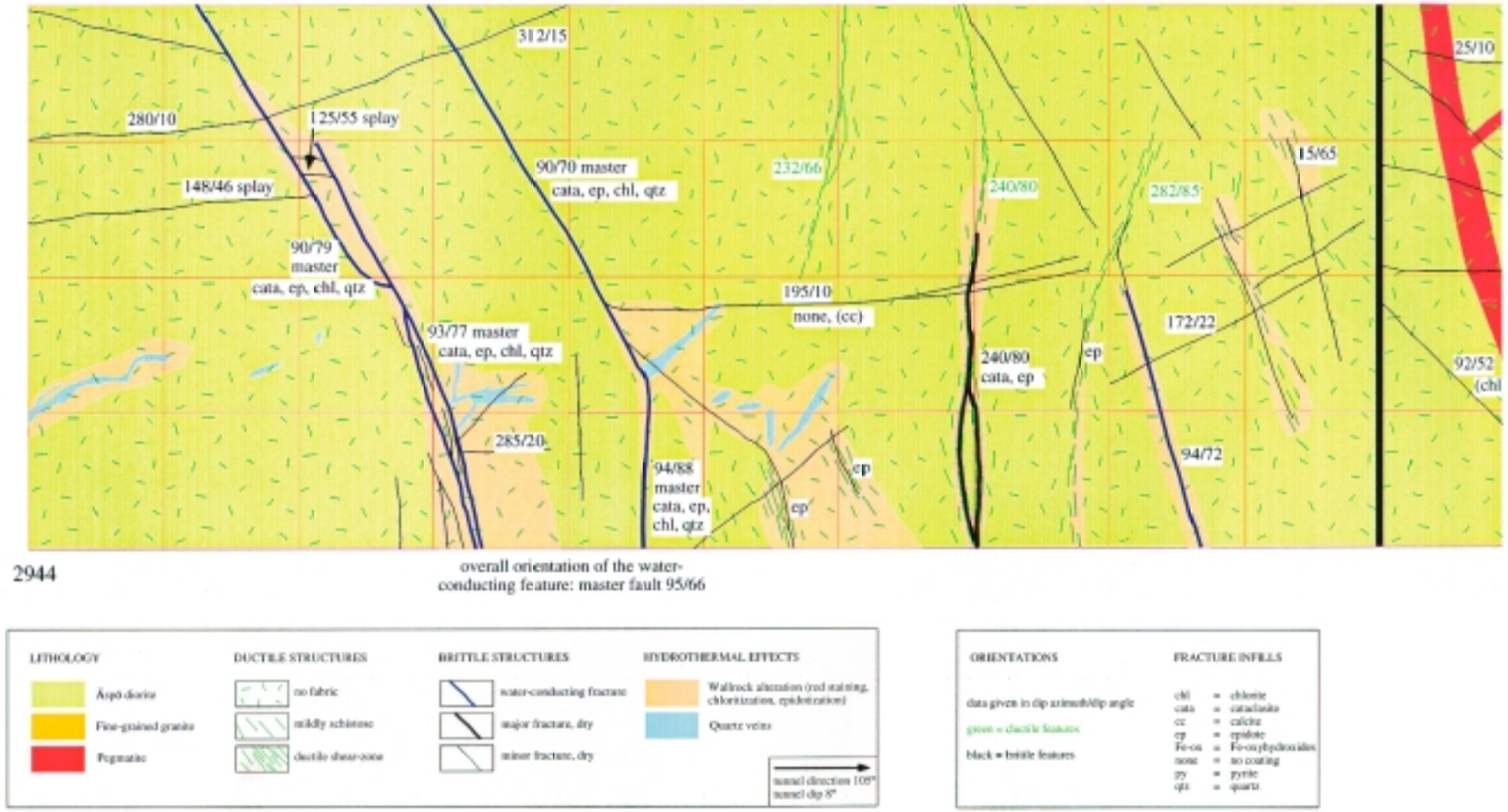

Appendix 4-1. *TRUE-1 block fracture-trace map along tunnel from 2944 – 2955 m.*

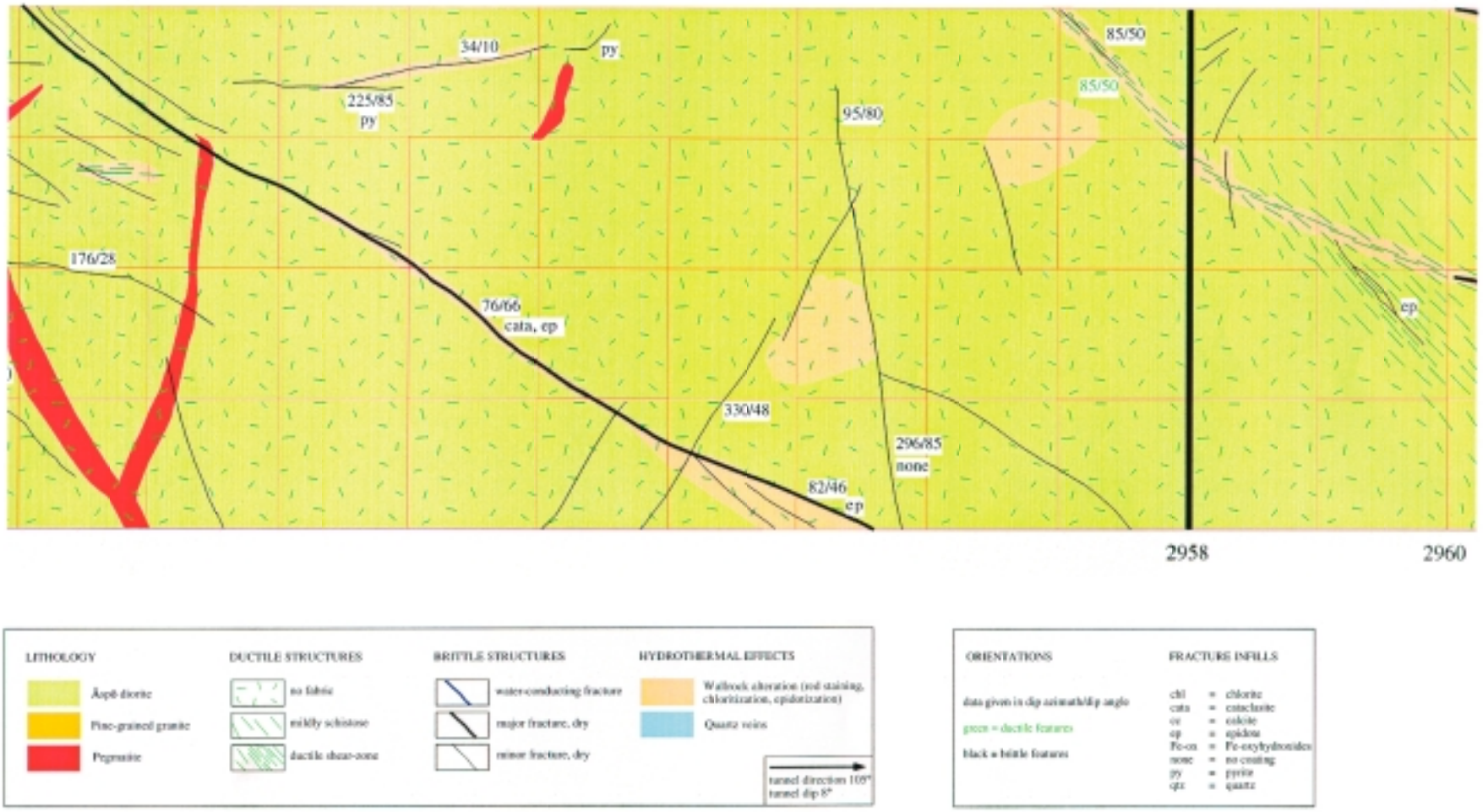

Appendix 4-2. *TRUE-1 block fracture-trace map along tunnel from 2949– 2960 m.*

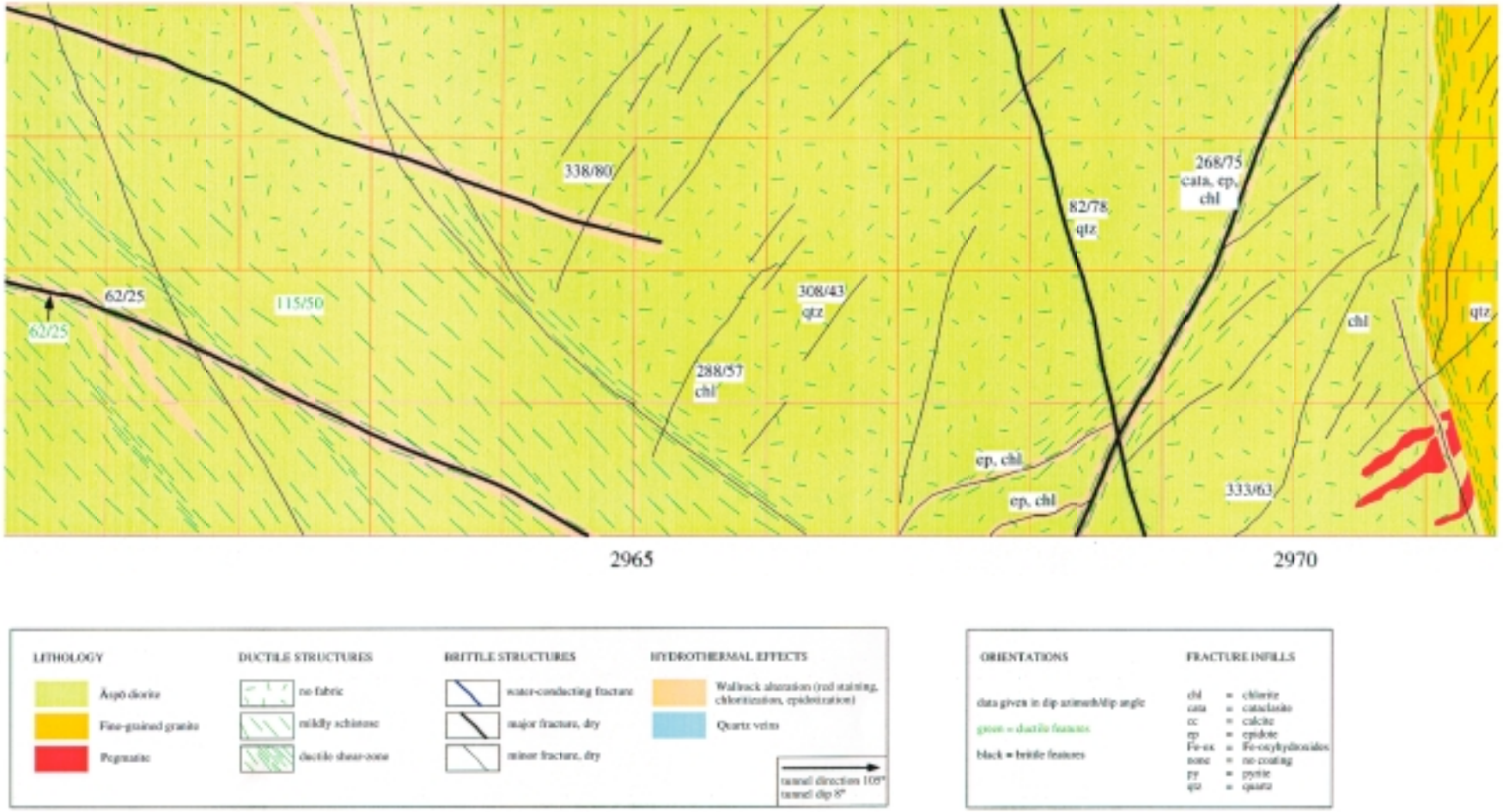

Appendix 4-3. *TRUE-1 block fracture-trace map along tunnel from 2960 – 2972 m.*

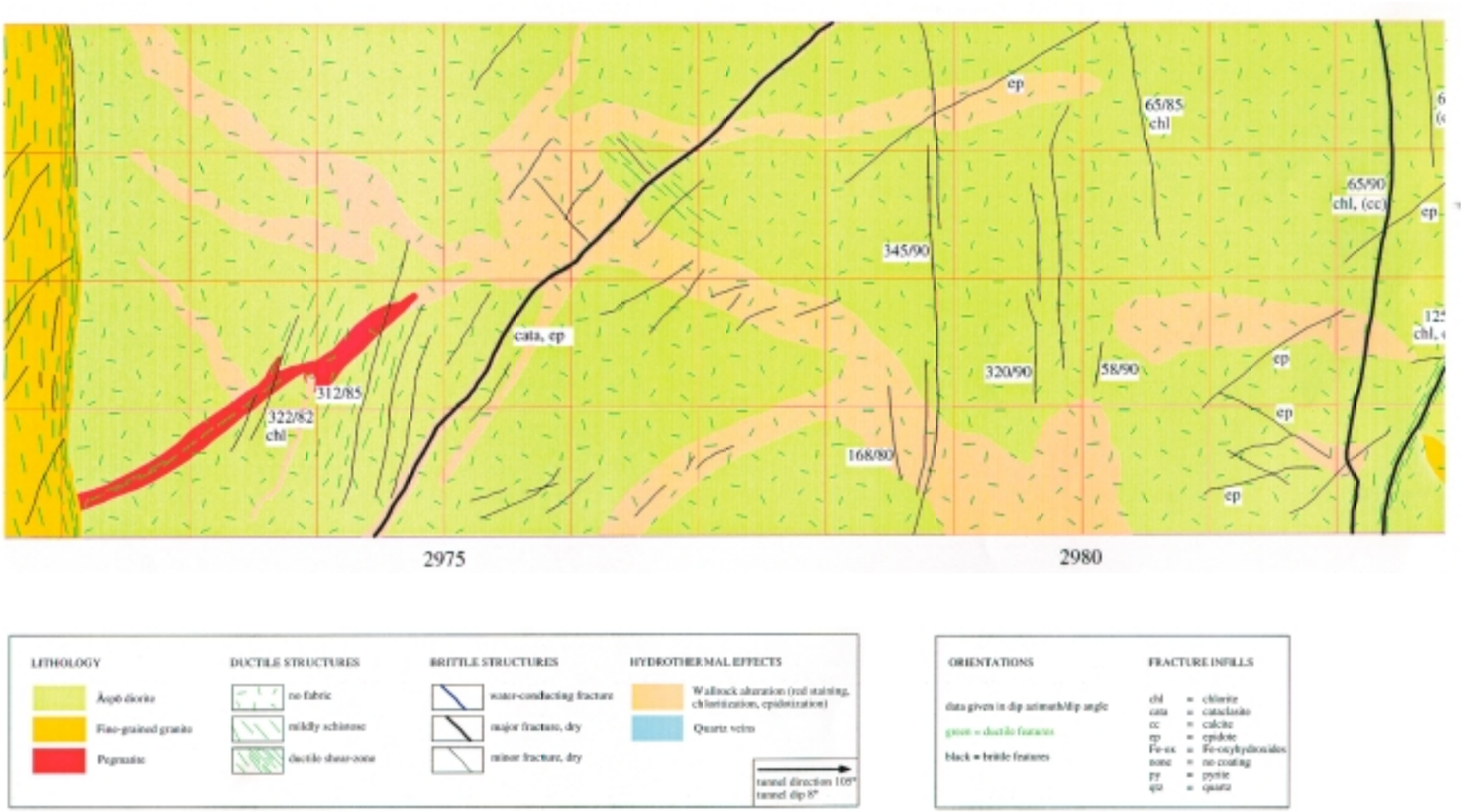

Appendix 4-4. *TRUE-1 block fracture-trace map along tunnel from 2972– 2983 m.*

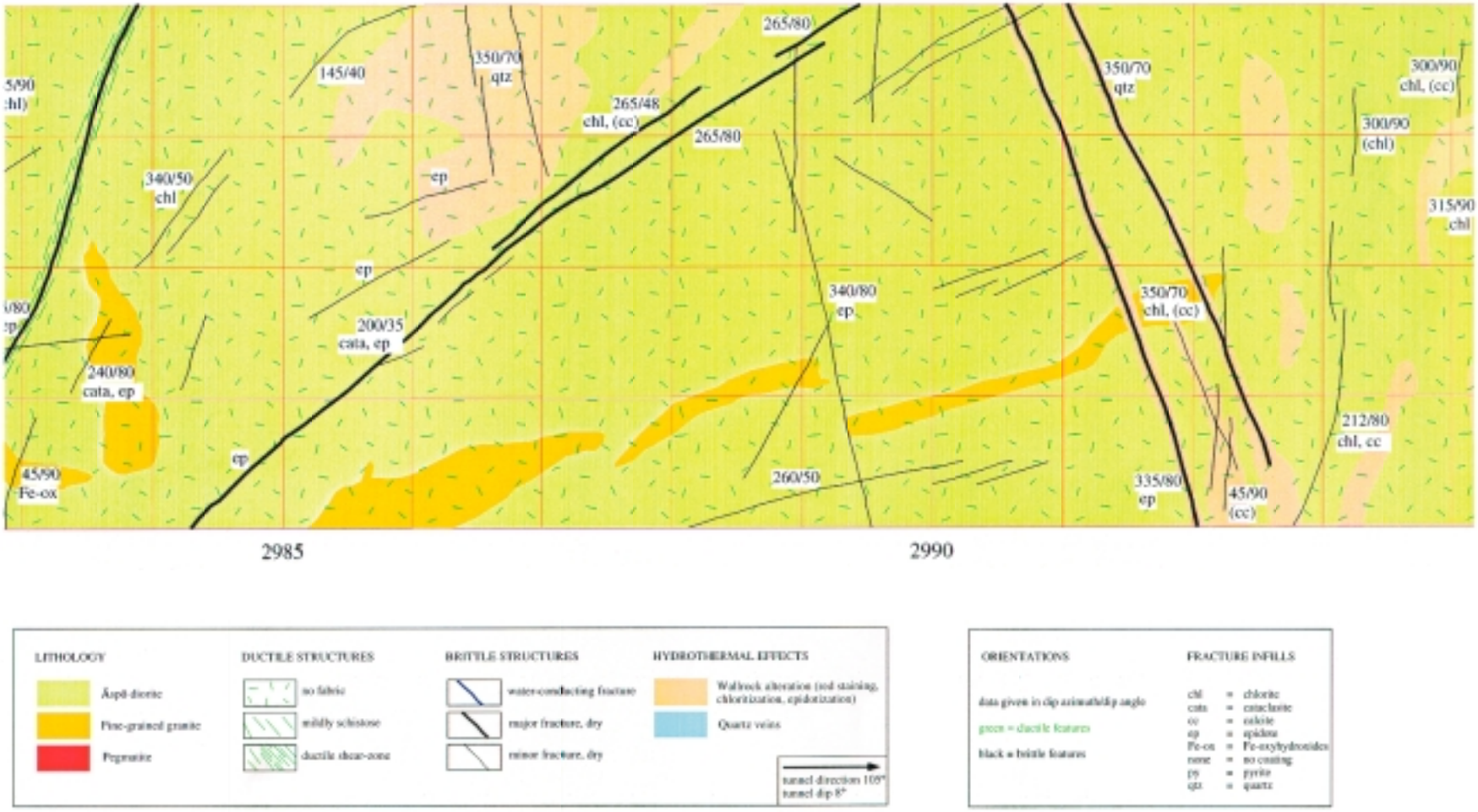

Appendix 4-5. *TRUE-1 block fracture-trace map along tunnel from 2983 – 2994 m.*

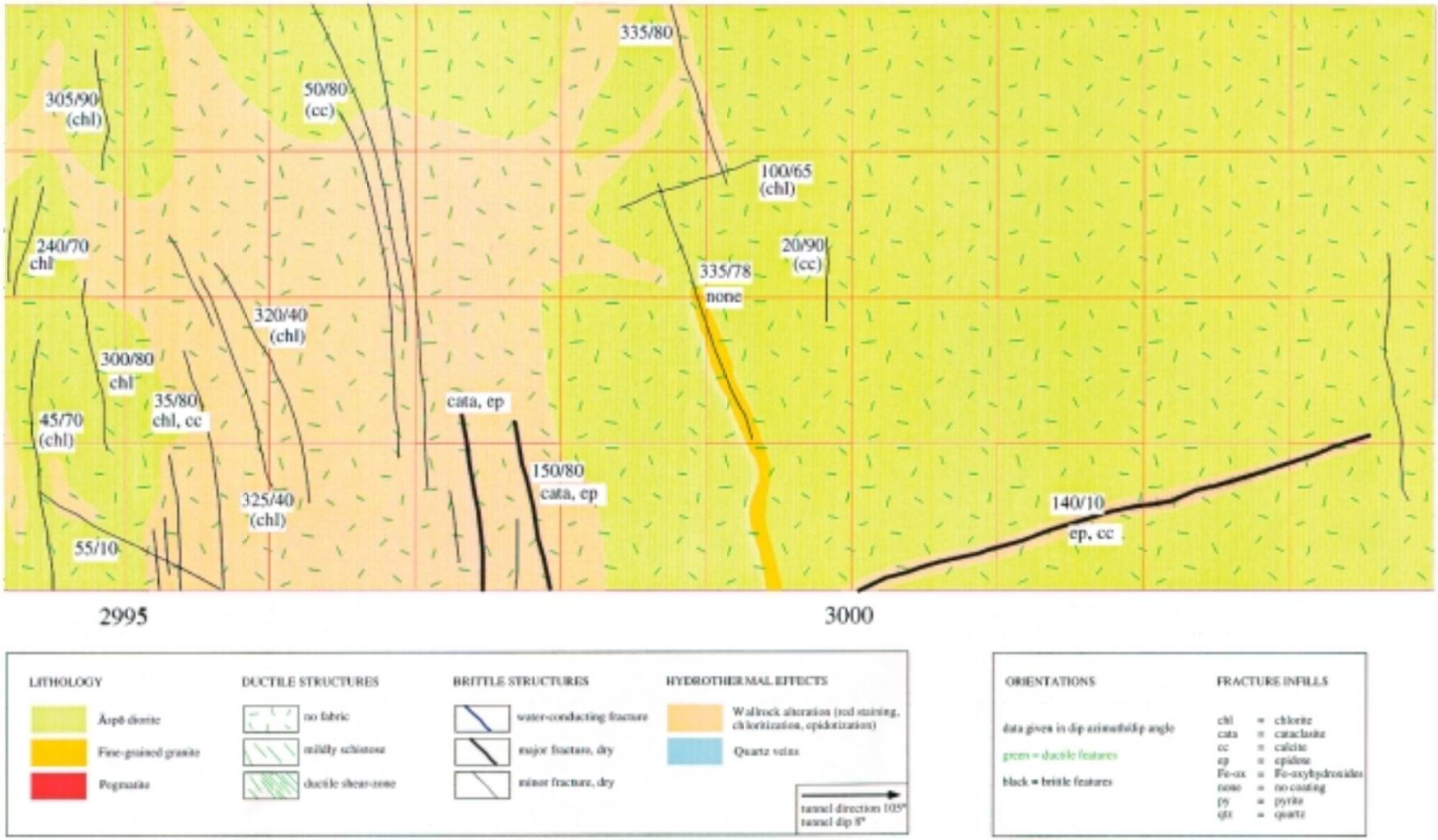

Appendix 4-6. *TRUE-1 block fracture-trace map along tunnel from 2994– 3004 m.*

Appendix 5

The deterministic structural model: visualisation of fractures in the TRUE-1 block

5-1 Visualisation of fractures from the drillcore database. Horizontal plane (–400m): all open structures, mylonites and lithologies.

5-2 Visualisation of fractures from the drillcore database. Horizontal plane (–400m): all open structures.

5-3 Visualisation of fractures from the drillcore database. 060/40 plane: all openstructures.

5-4 Visualisation of fractures from the drillcore database. Horizontal plane (–400m): all mylonites and fractures containing fault gouge.

5-5 Visualisation of fractures from the drillcore database. 060/40 plane: all mylonites and fractures containing fault gouge.

5-6 Visualisation of fractures from the drillcore database. Structural log of borehole KXTT1.

5-7 Visualisation of fractures from the drillcore database. Structural log of borehole KXTT2.

5-8 Visualisation of fractures from the drillcore database. Structural log of borehole KXTT3.

5-9 Visualisation of fractures from the drillcore database. Structural log of borehole KXTT4.

5-10 Visualisation of fractures from the drillcore database. Structural log of borehole KA3005A.

5-11 Visualisation of fractures from the BIP database. Horizontal plane (–400m): all open structures, mylonites and lithologies.

5-12 Visualisation of fractures from the BIP. Structural log of borehole KXTT1.

5-13 Visualisation of fractures from the BIP. Structural log of borehole KXTT2.

5-14 Visualisation of fractures from the BIP. Structural log of borehole KXTT3.

5-15 Visualisation of fractures from the BIP. Structural log of borehole KXTT4.

5-16 Visualisation of fractures from the BIP. Structural log of borehole KA3005A.

5-17 Selection of data: every fifth open structure from the BIP database (060/40 plane).

5-18 Selection of data: mylonites from the drillcore database (060/40 plane).

5-19 Selection of data: Mylonites from the drillcore database along the "Feature A" structures mapped from drillcores (060/40 plane).

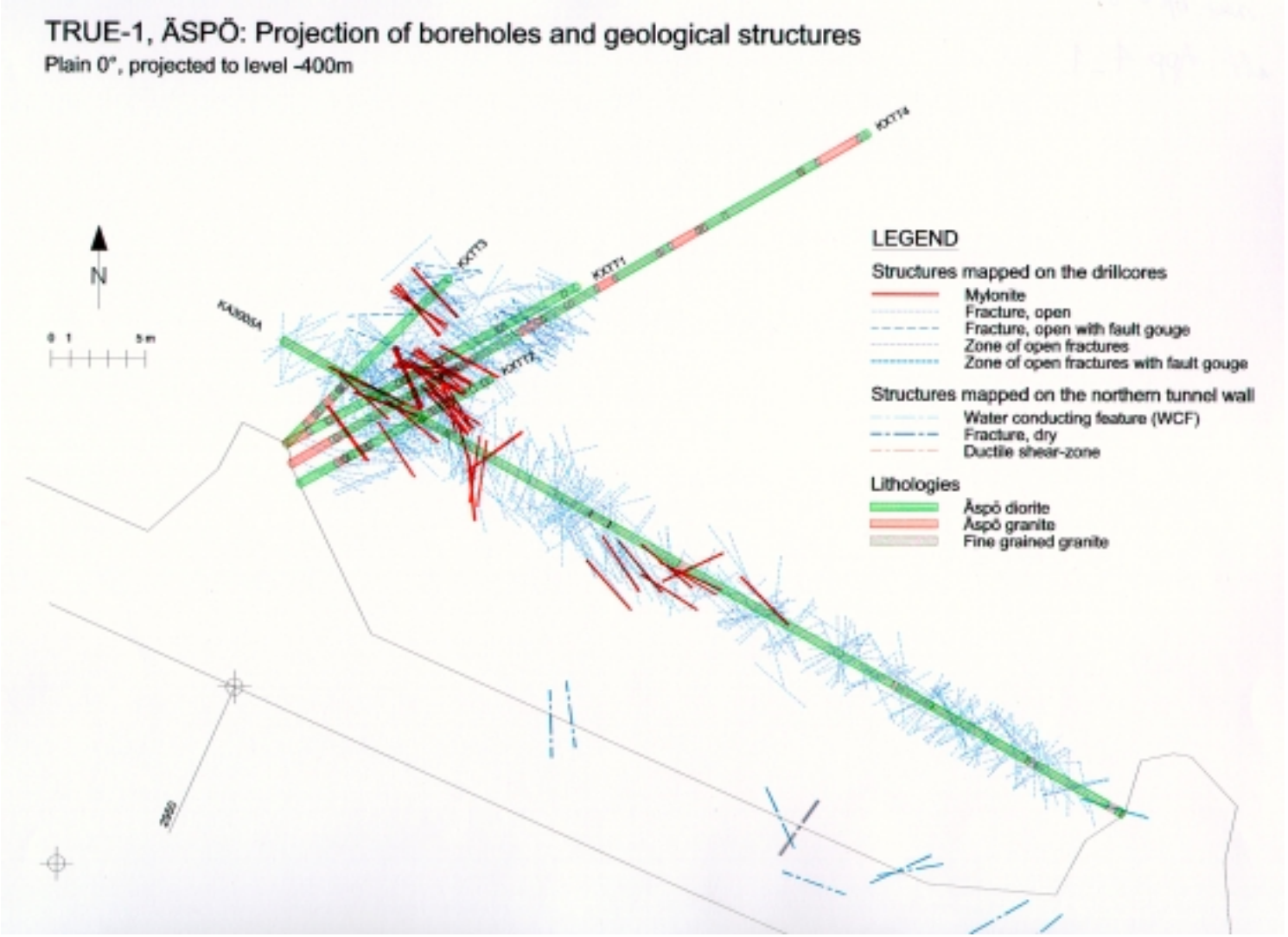

Appendix 5-1. *Visualisation of fractures from the drillcore database. Horizontal plane (-400m): all open structures, mylonites and lithologies.*

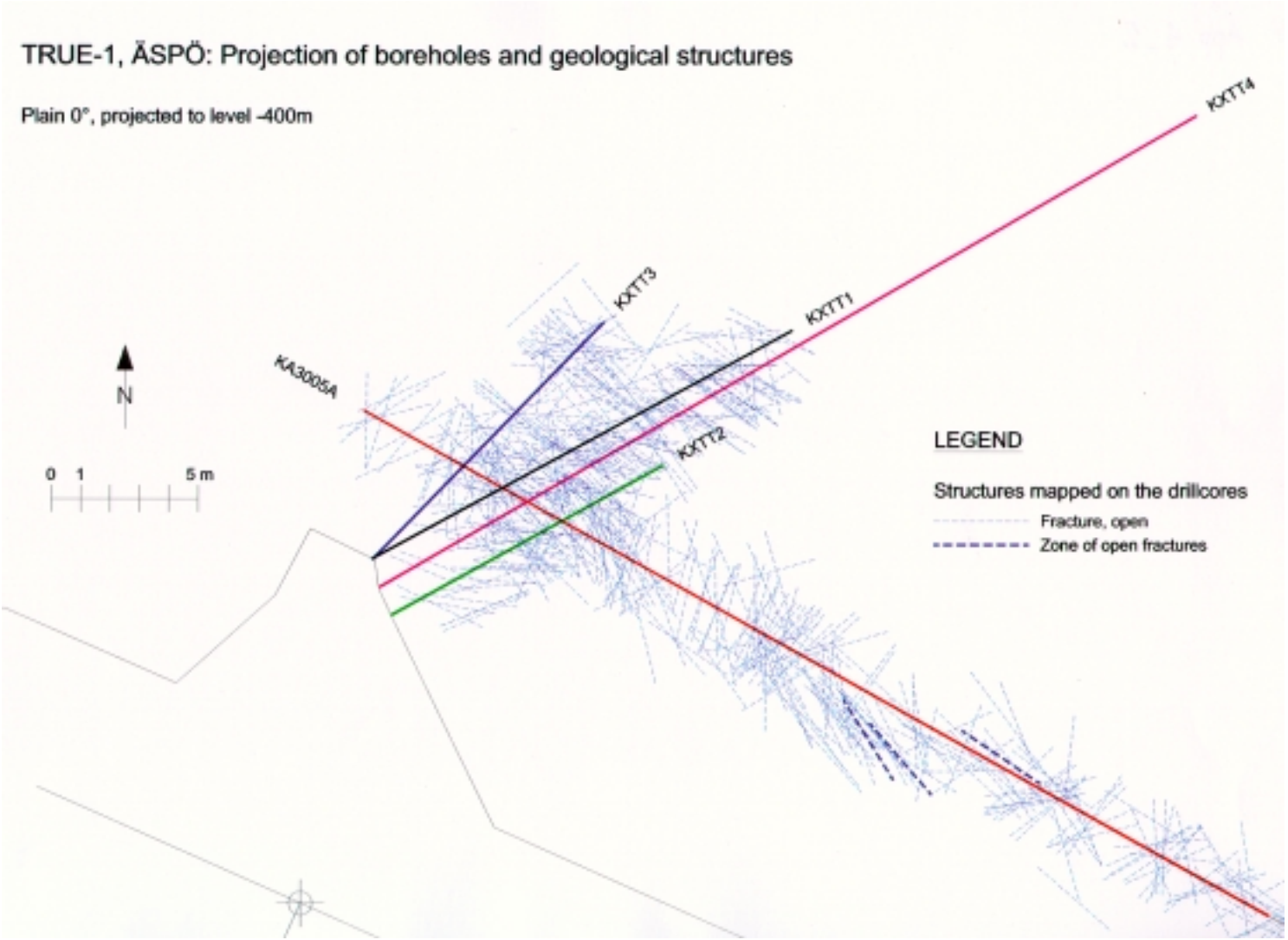

Appendix 5-2. *Visualisation of fractures from the drillcore database. Horizontal plane (-400m): all open structures.*

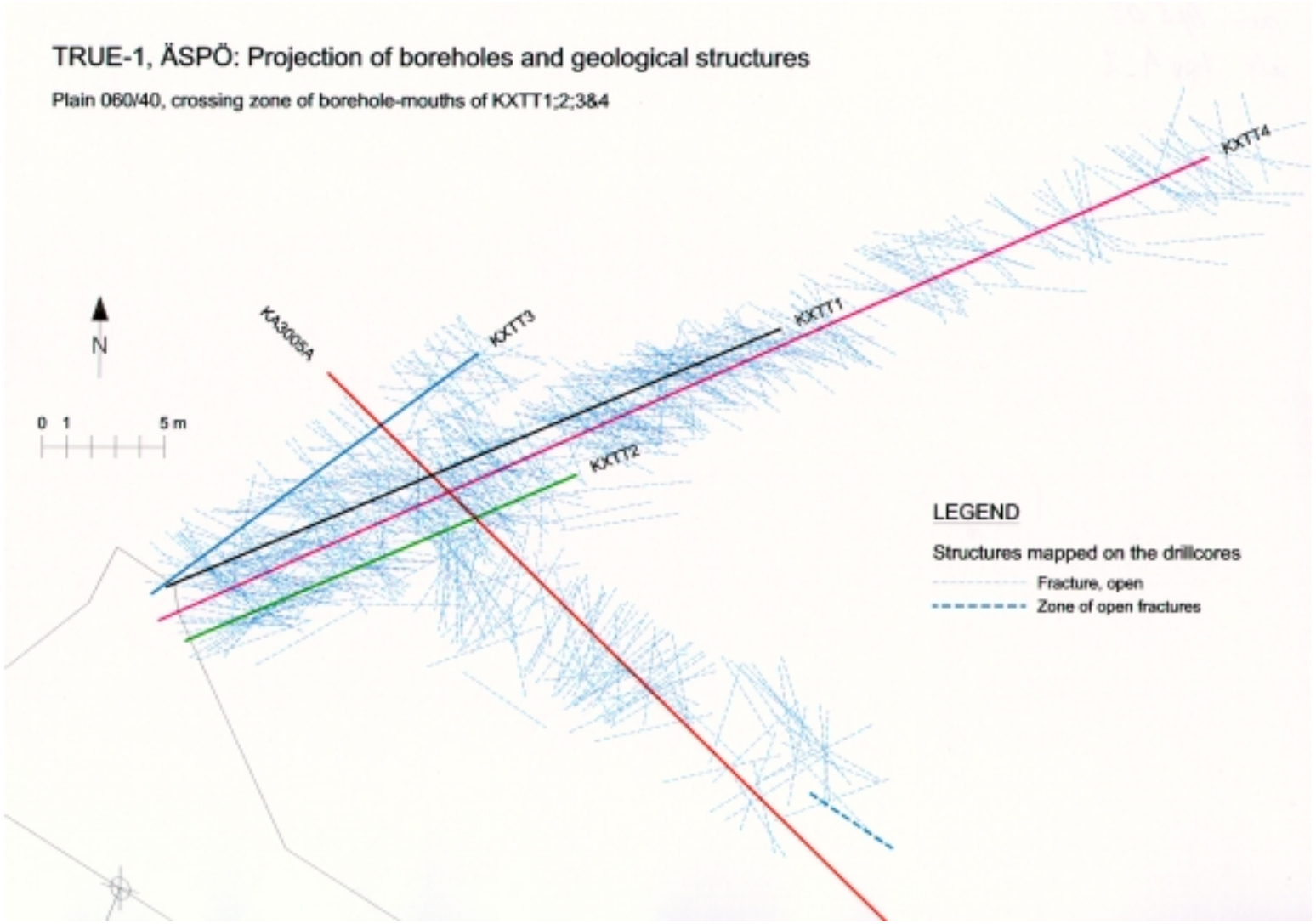

Appendix 5-3. *Visualisation of fractures from the drillcore database. 060/40 plane: all open structures.*

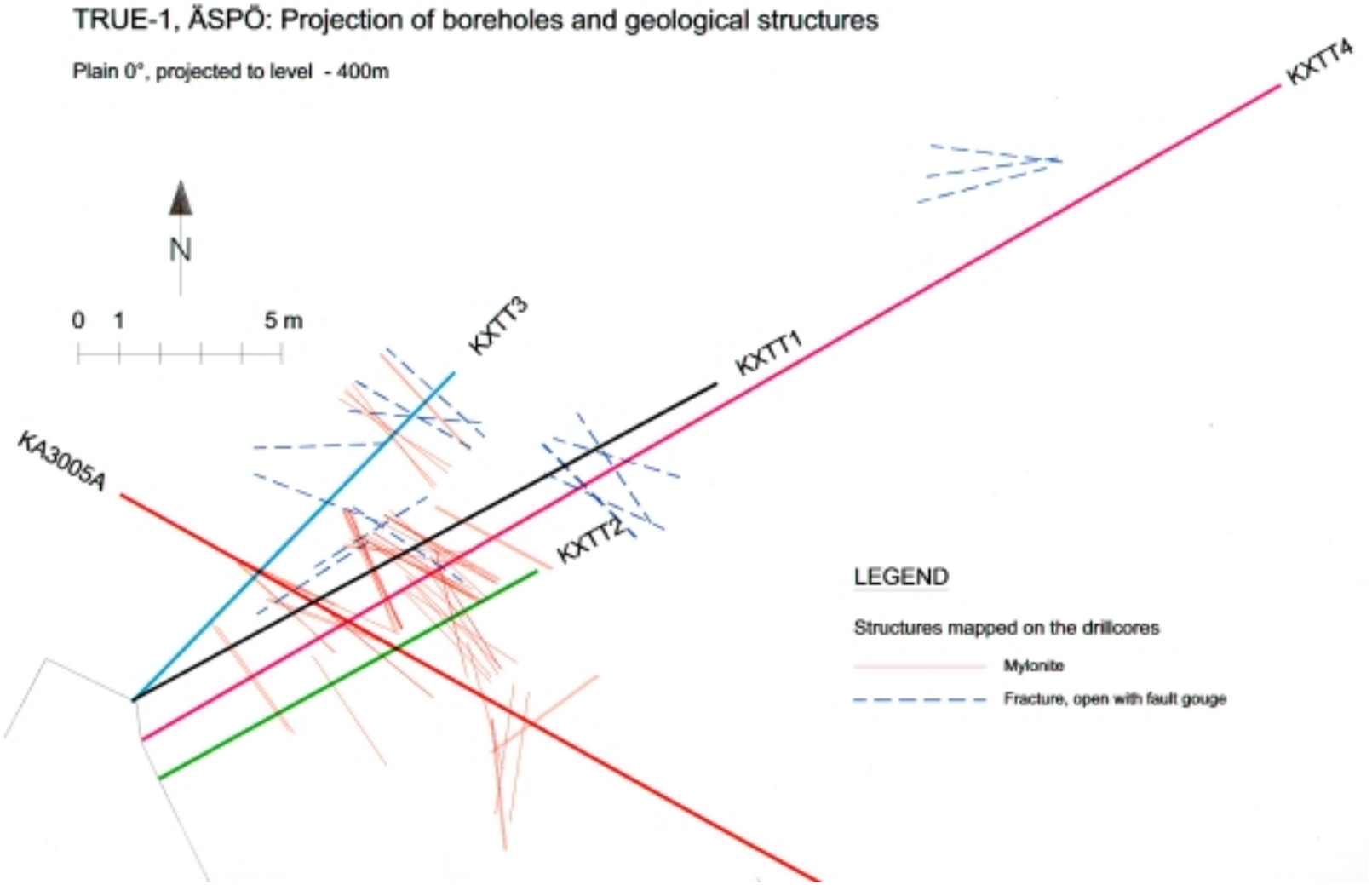

Appendix 5-4. *Visualisation of fractures from the drillcore database. Horizontal plane(-400m): all mylonites and fractures containing fault gouge.*

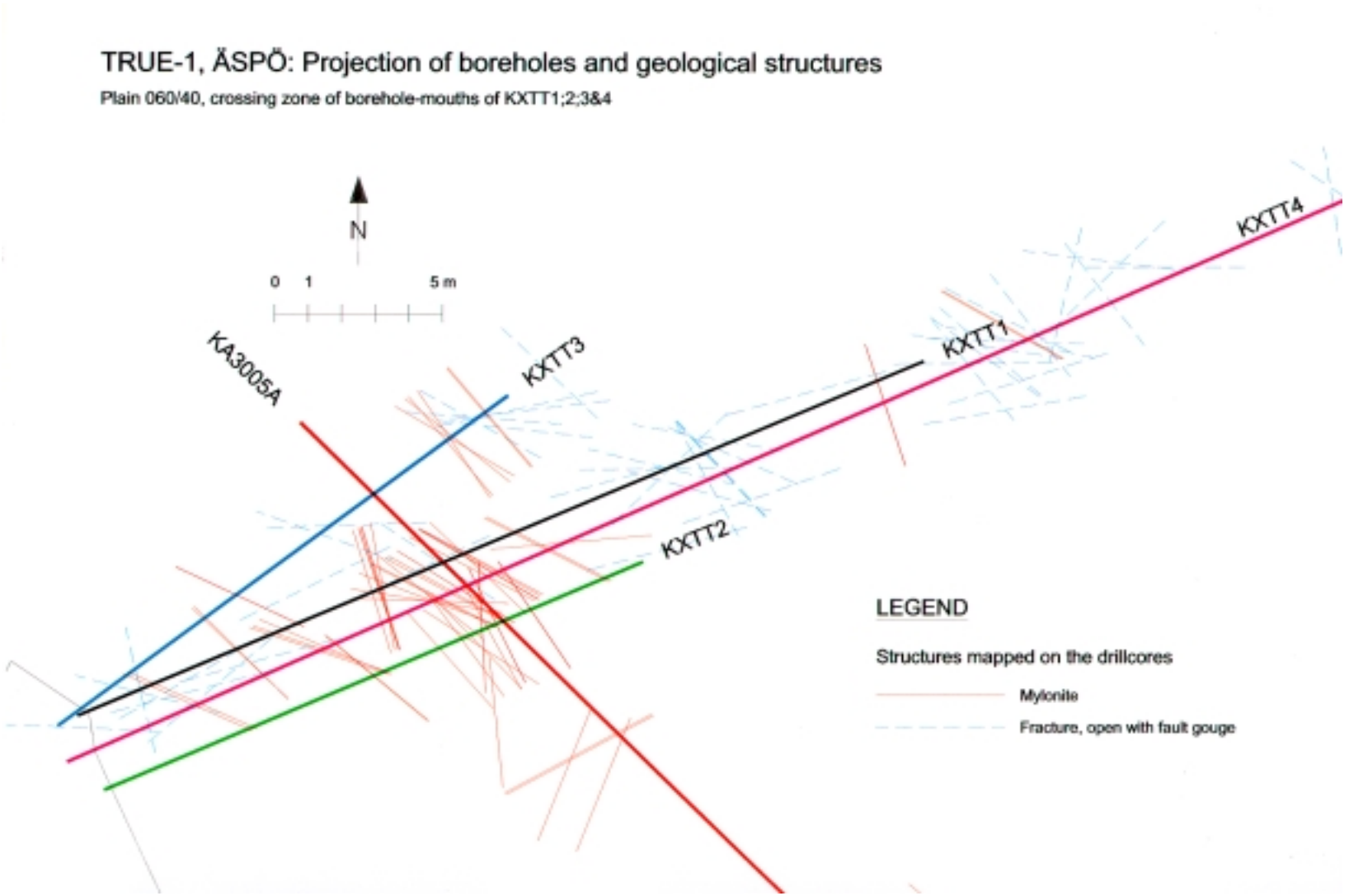

Appendix 5-5. *Visualisation of fractures from the drillcore database. 060/40 plane: all mylonites and fractures containing fault gouge.*

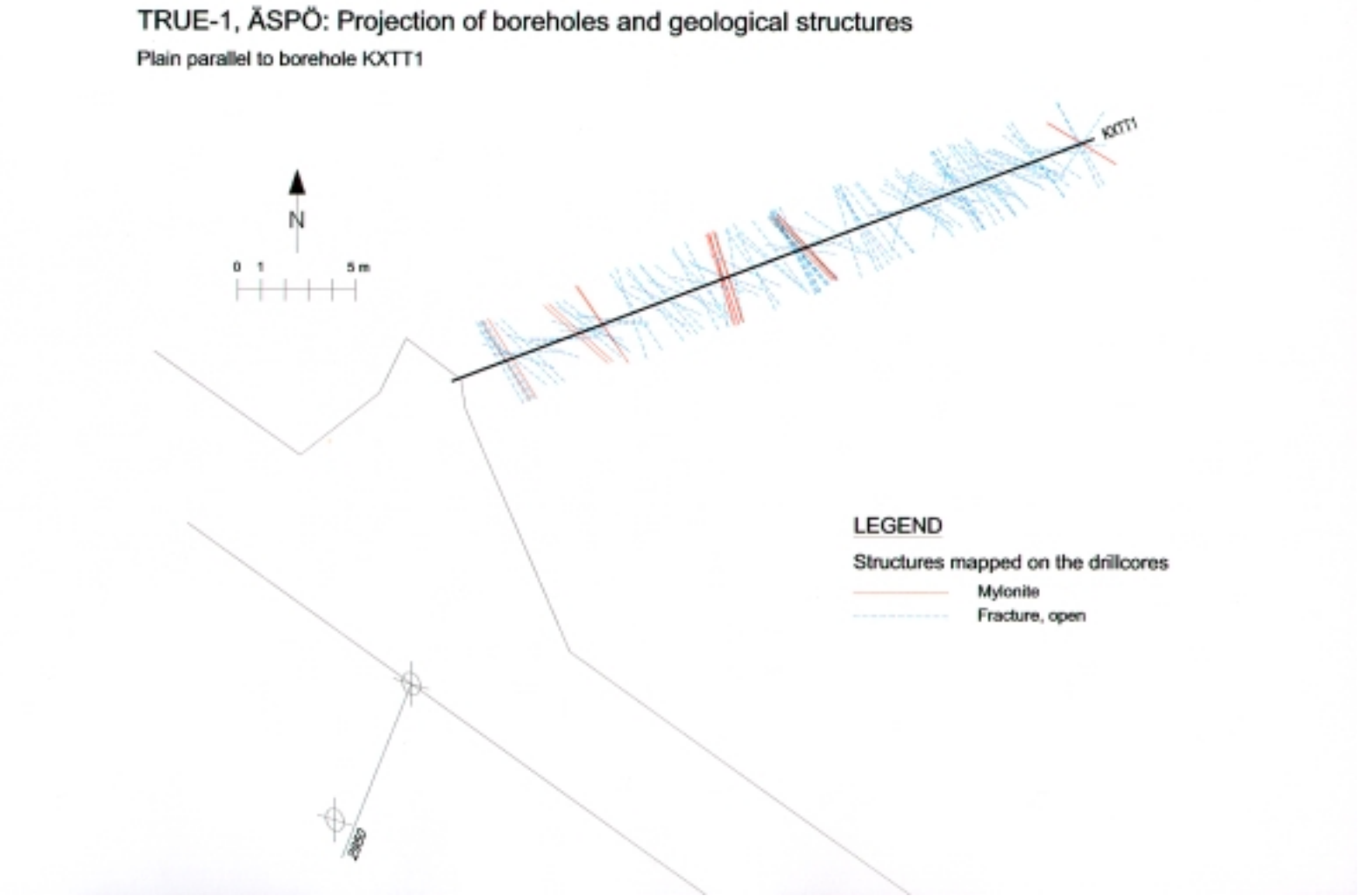

Apendix 5-6. *Visualisation of fractures from the drillcore database. Structural log of borehole KXTT1.*

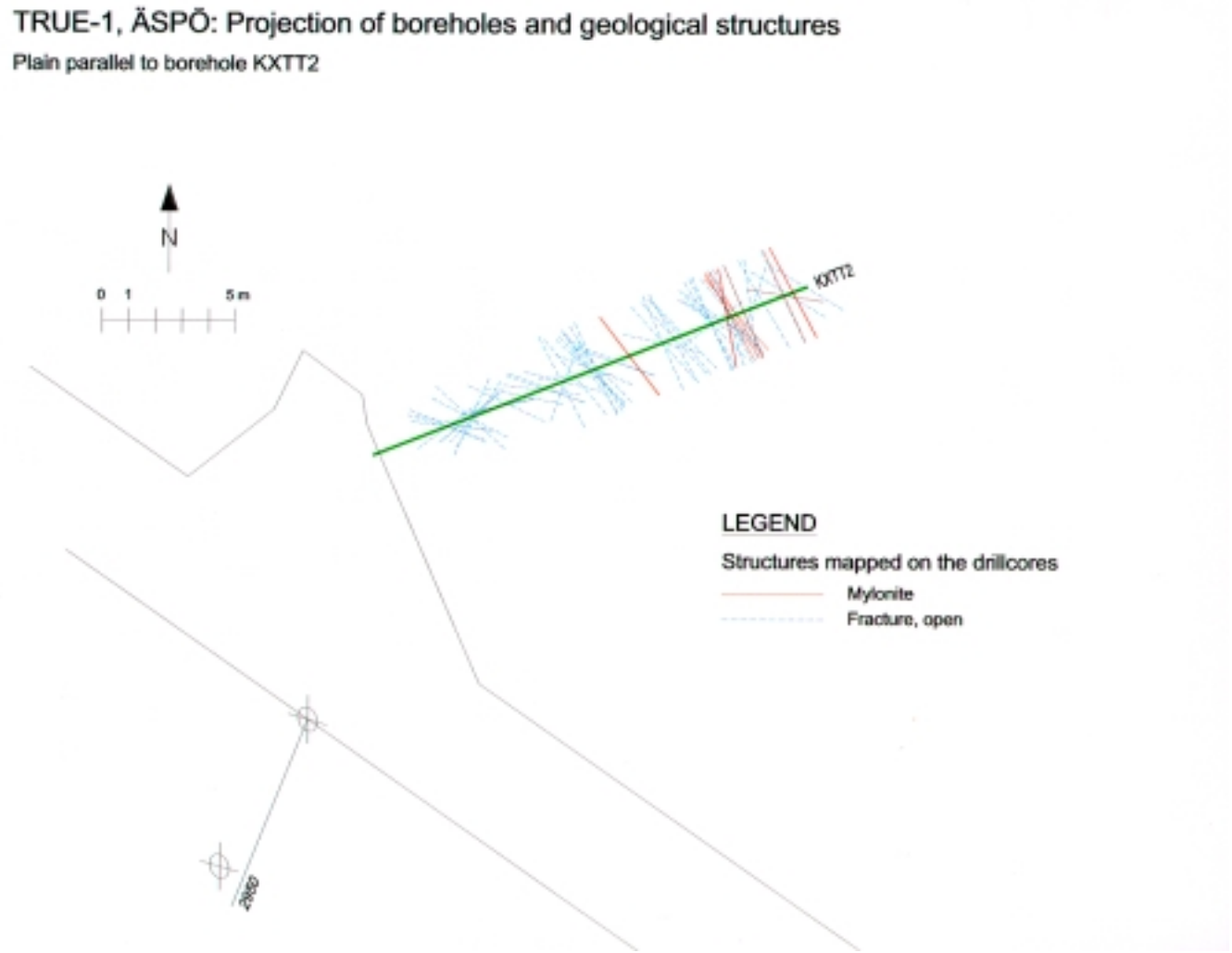

Appendix 5-7. *Visualisation of fractures from the drillcore database. Structural log of borehole KXTT2.*

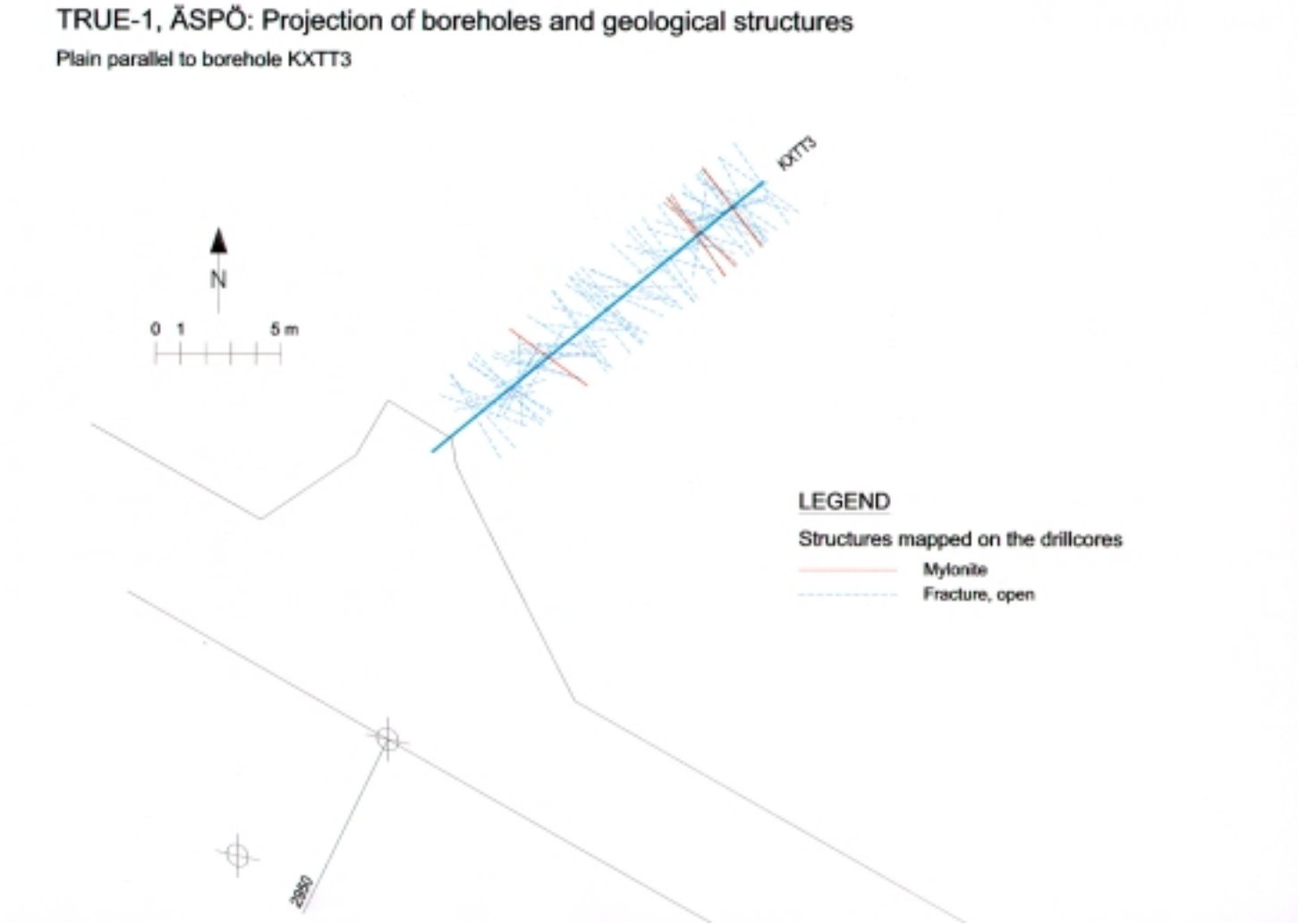

Appendix 5-8. *Visualisation of fractures from the drillcore database. Structural log of borehole KXTT3.*

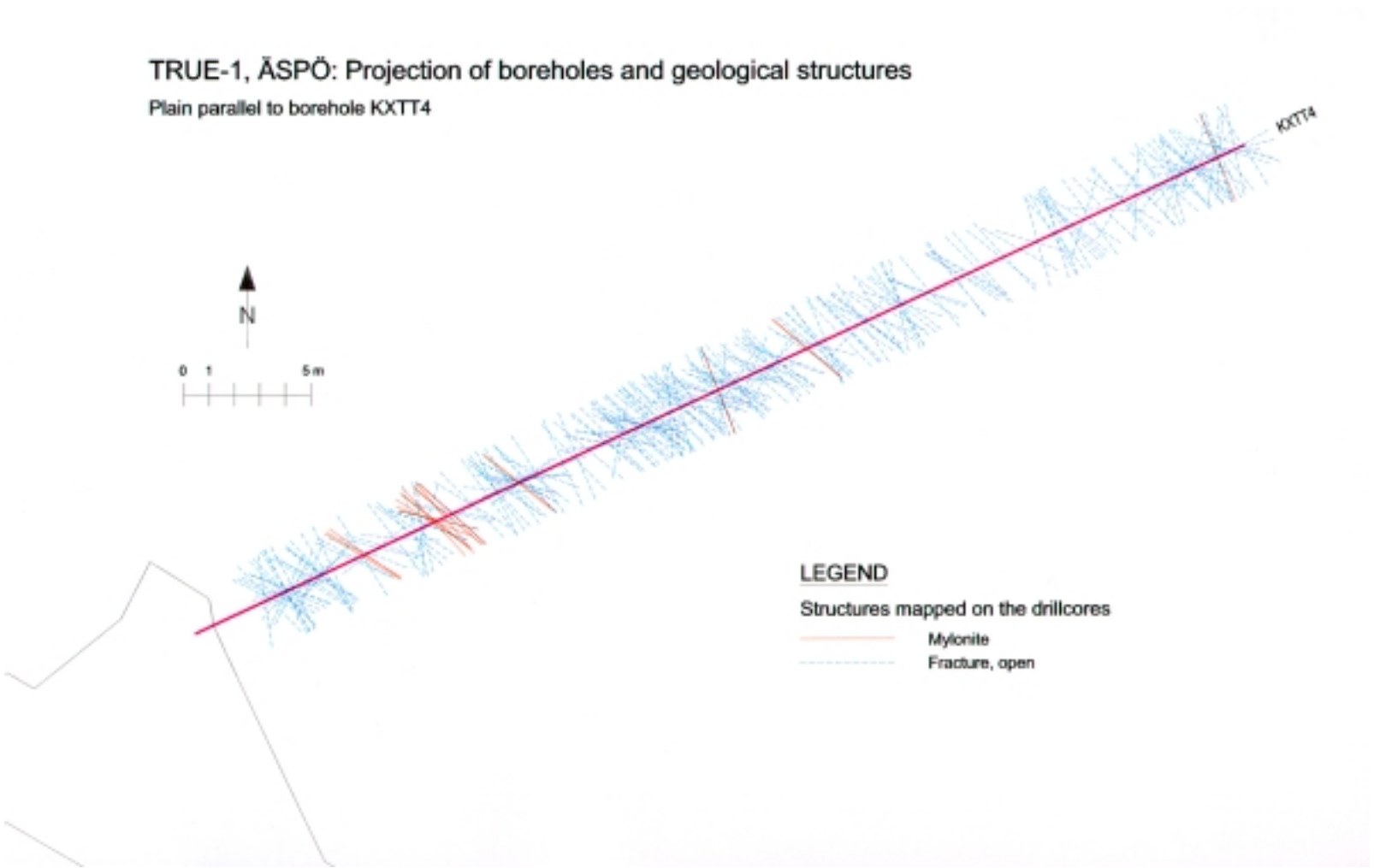

Appendix 5-9. *Visualisation of fractures from the drillcore database. Structural log of borehole KXTT4.*

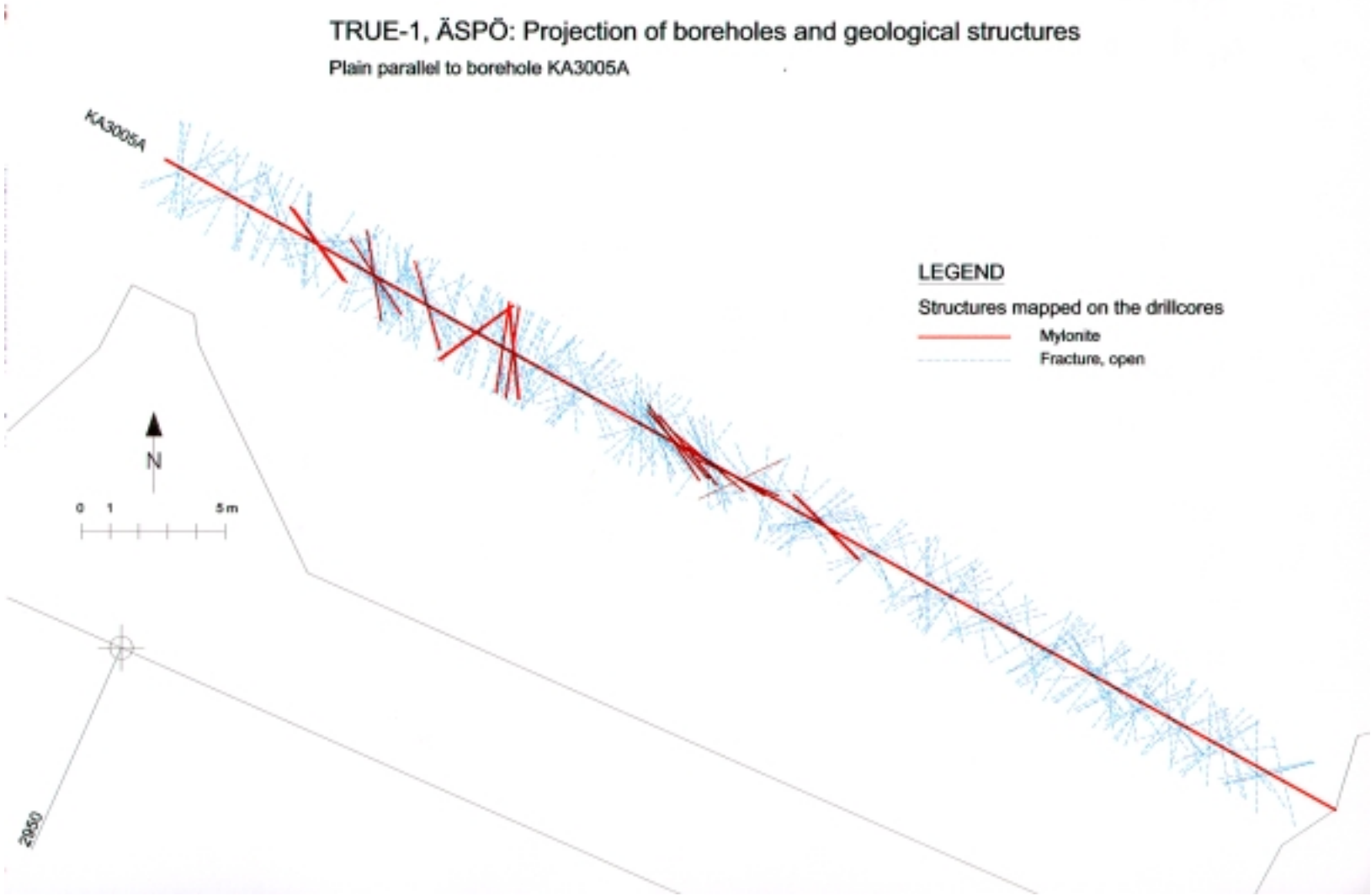

Appendix 5-10. *Visualisation of fractures from the drillcore database. Structural log of borehole KA3005A.*

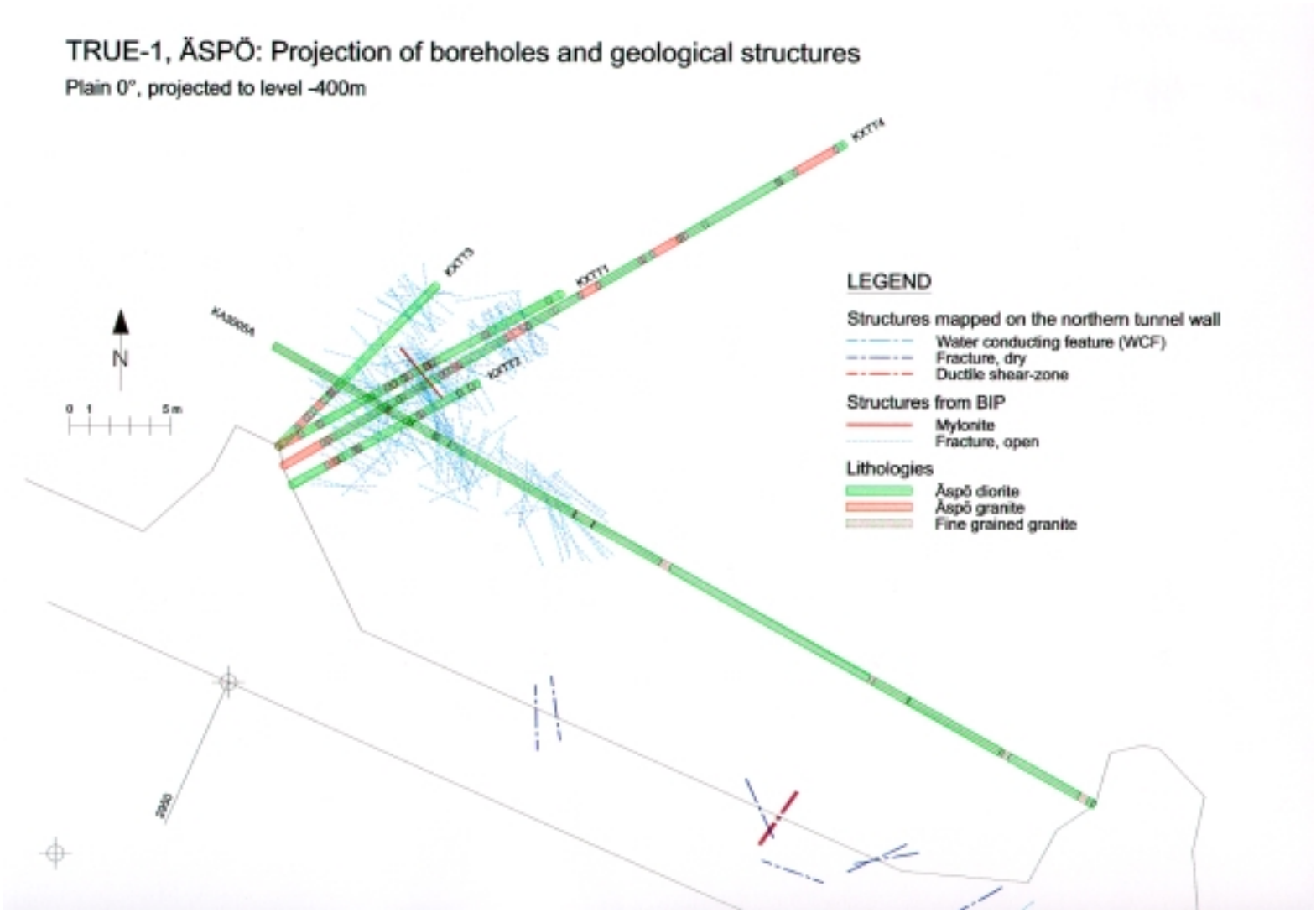

Appendix 5-11. *Visualisation of fractures from the BIP database. Horizontal plane (-400m): all open structures, mylonites and lithologies.*

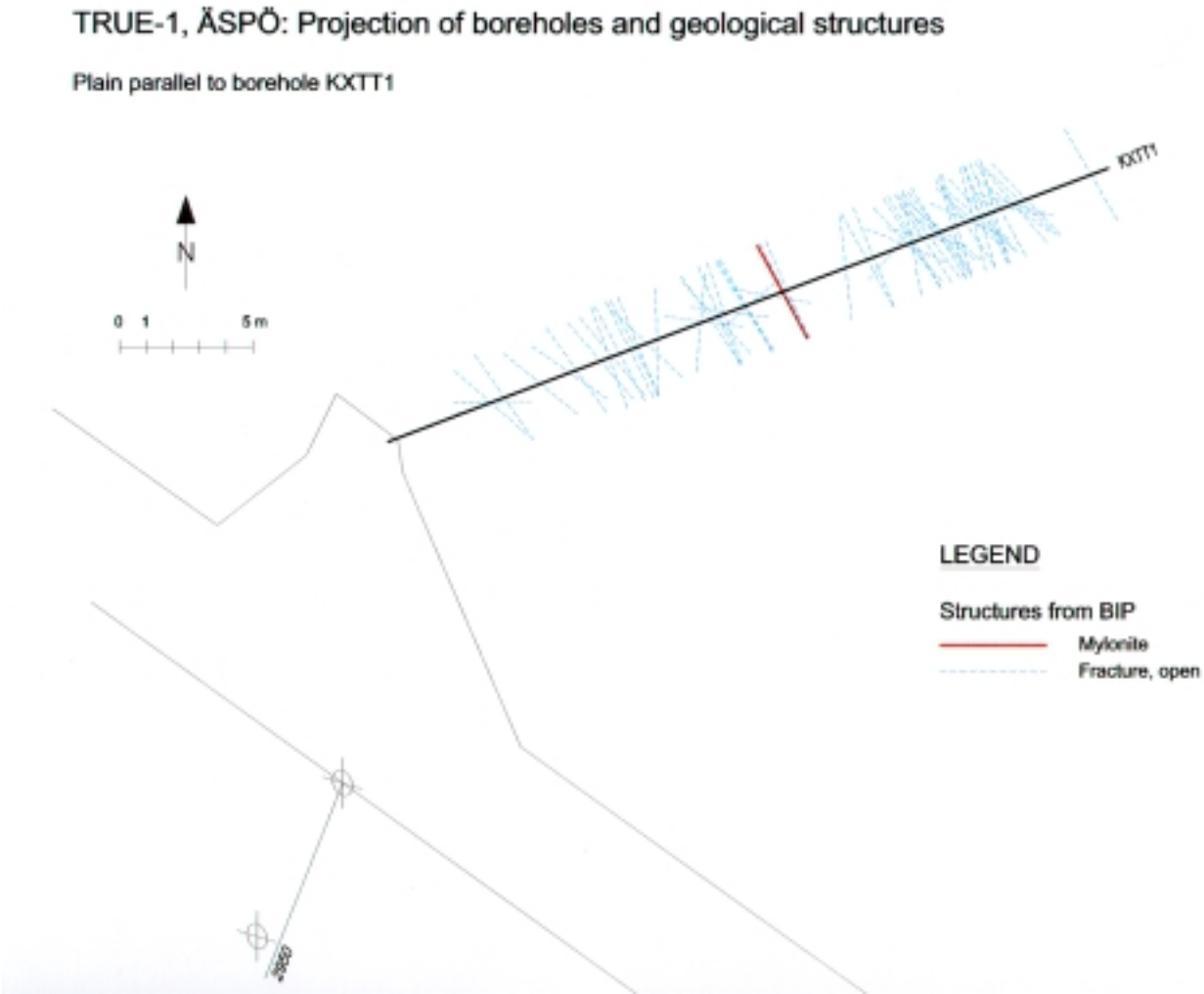

Appendix 5-12. *Visualisation of fractures from the BIP. Structural log of borehole KXTT1.*

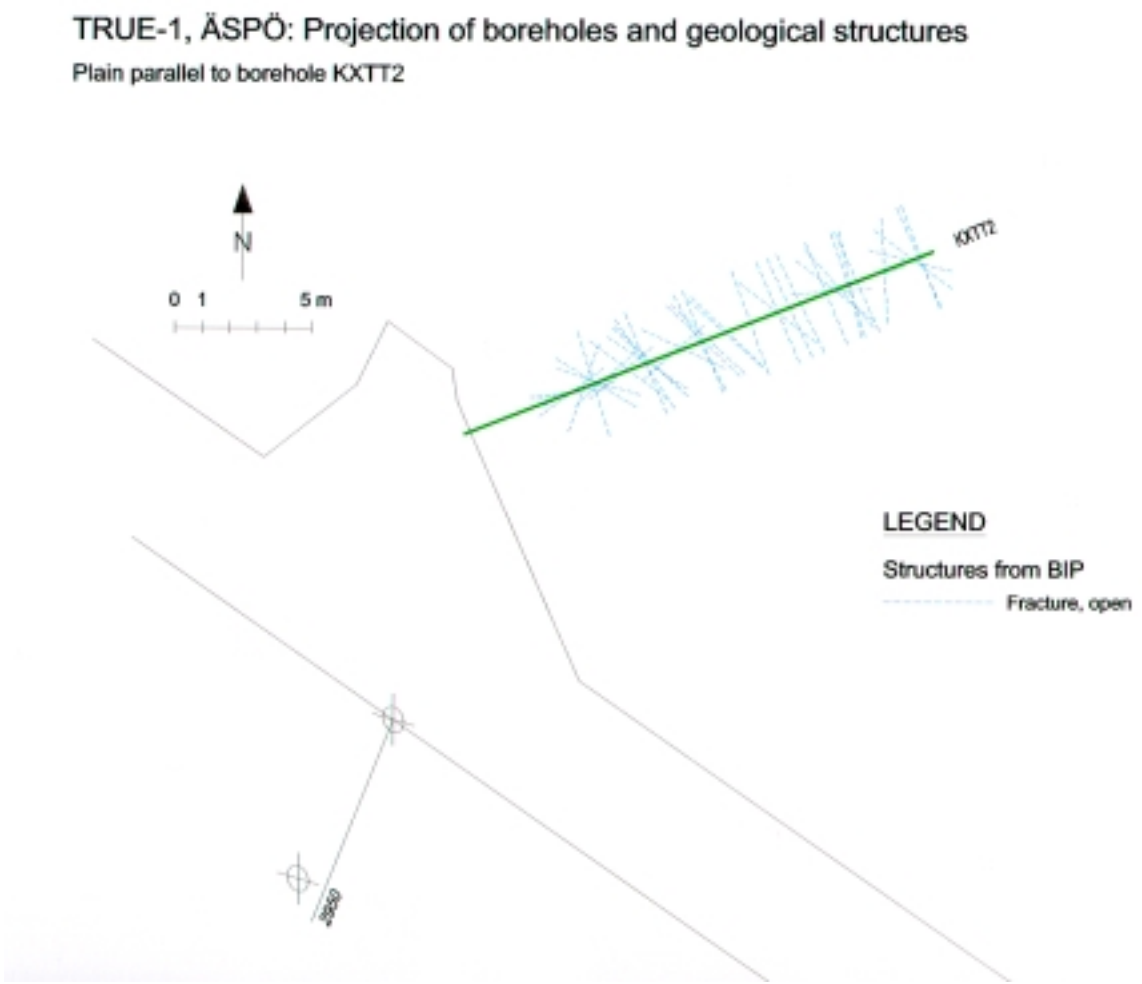

Appendix 5-13. *Visualisation of fractures from the BIP. Structural log of borehole KXTT2.*

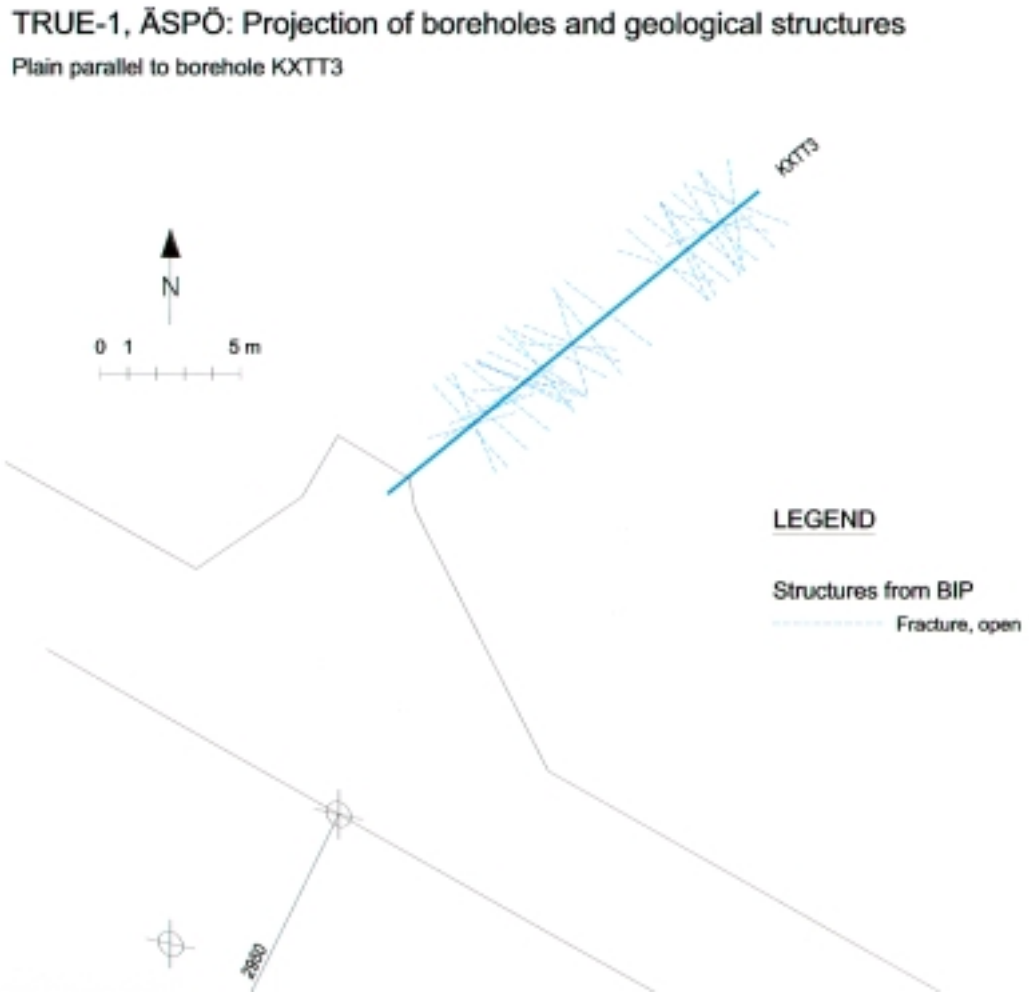

Appendix 5-14. *Visualisation of fractures from the BIP. Structural log of borehole KXTT3.*

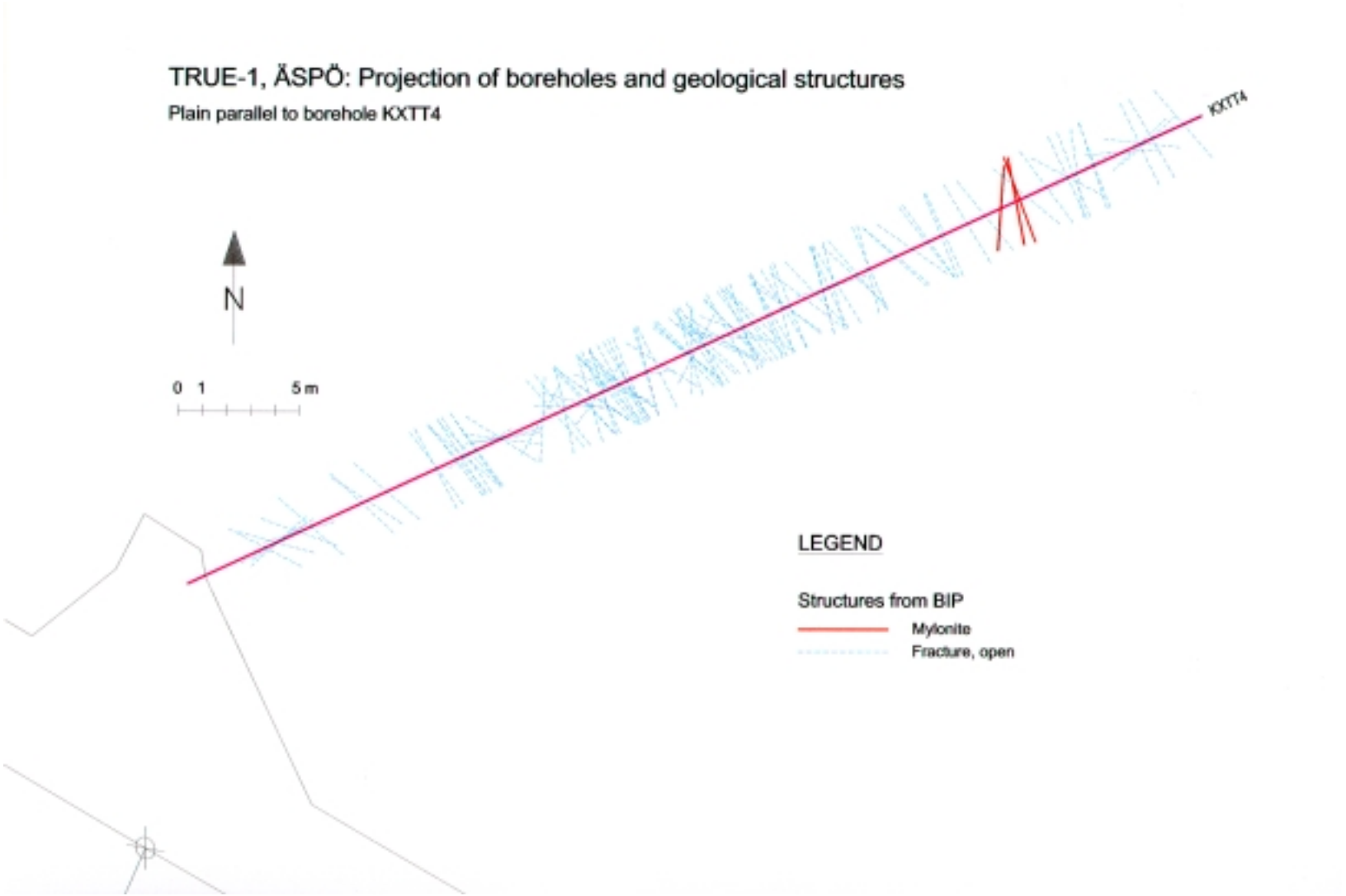

Appendix 5-15. *Visualisation of fractures from the BIP. Structural log of borehole KXTT4.*

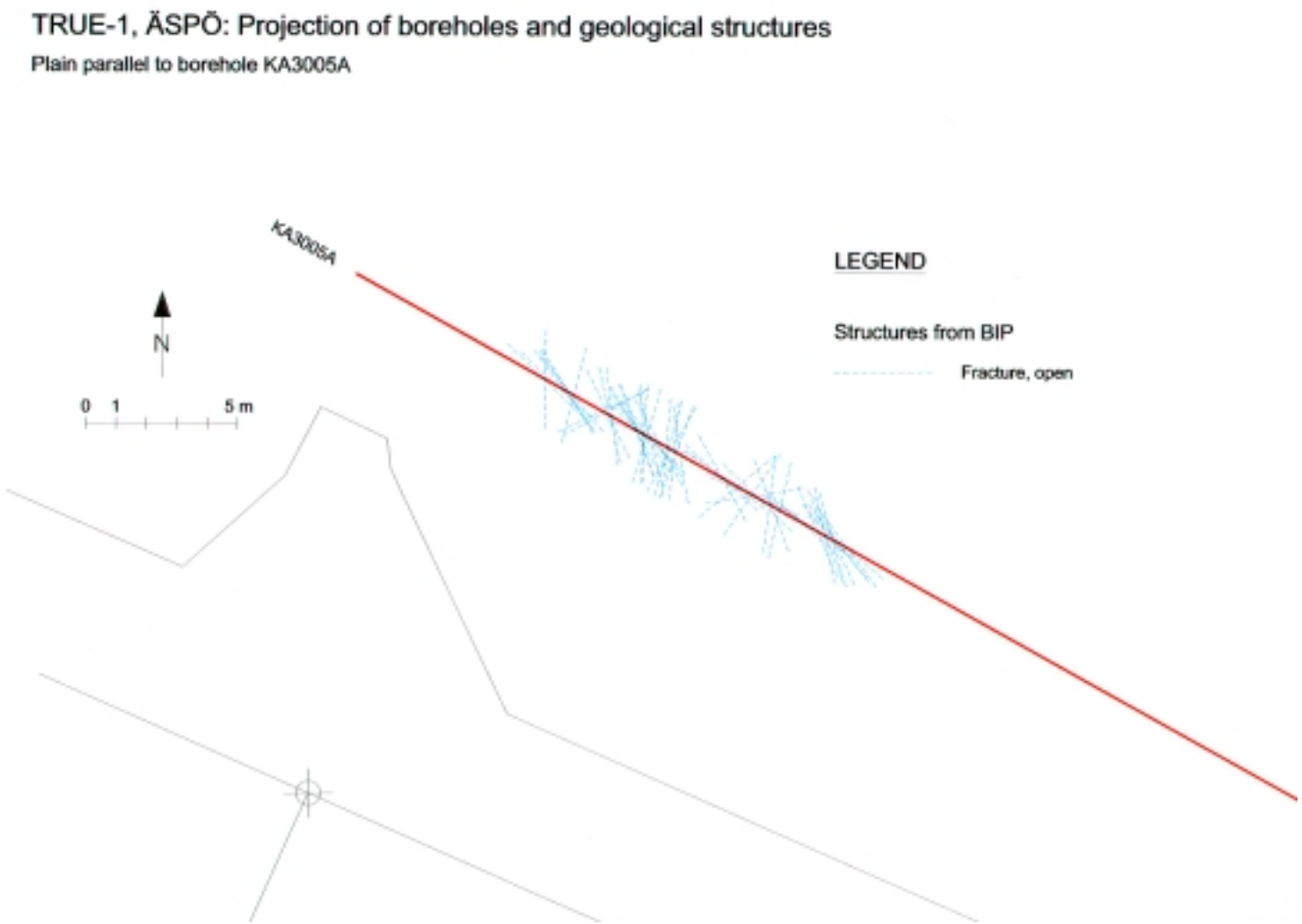

Appendix 5-16. *Visualisation of fractures from the BIP. Structural log of borehole KA3005A.*

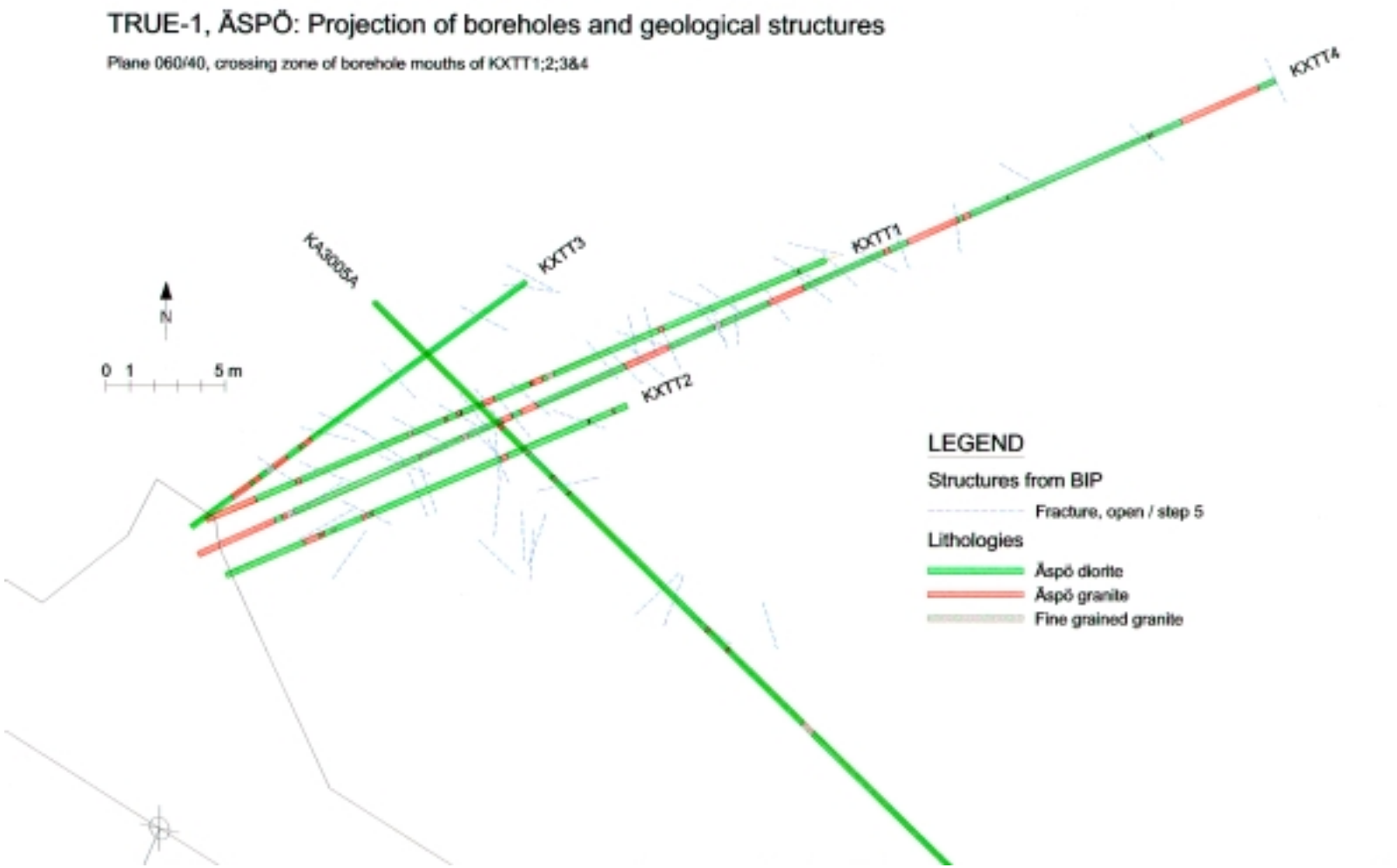

Appendix 5-17. *Selection of data: every fifth open structure from the BIP database (060/40 plane).*

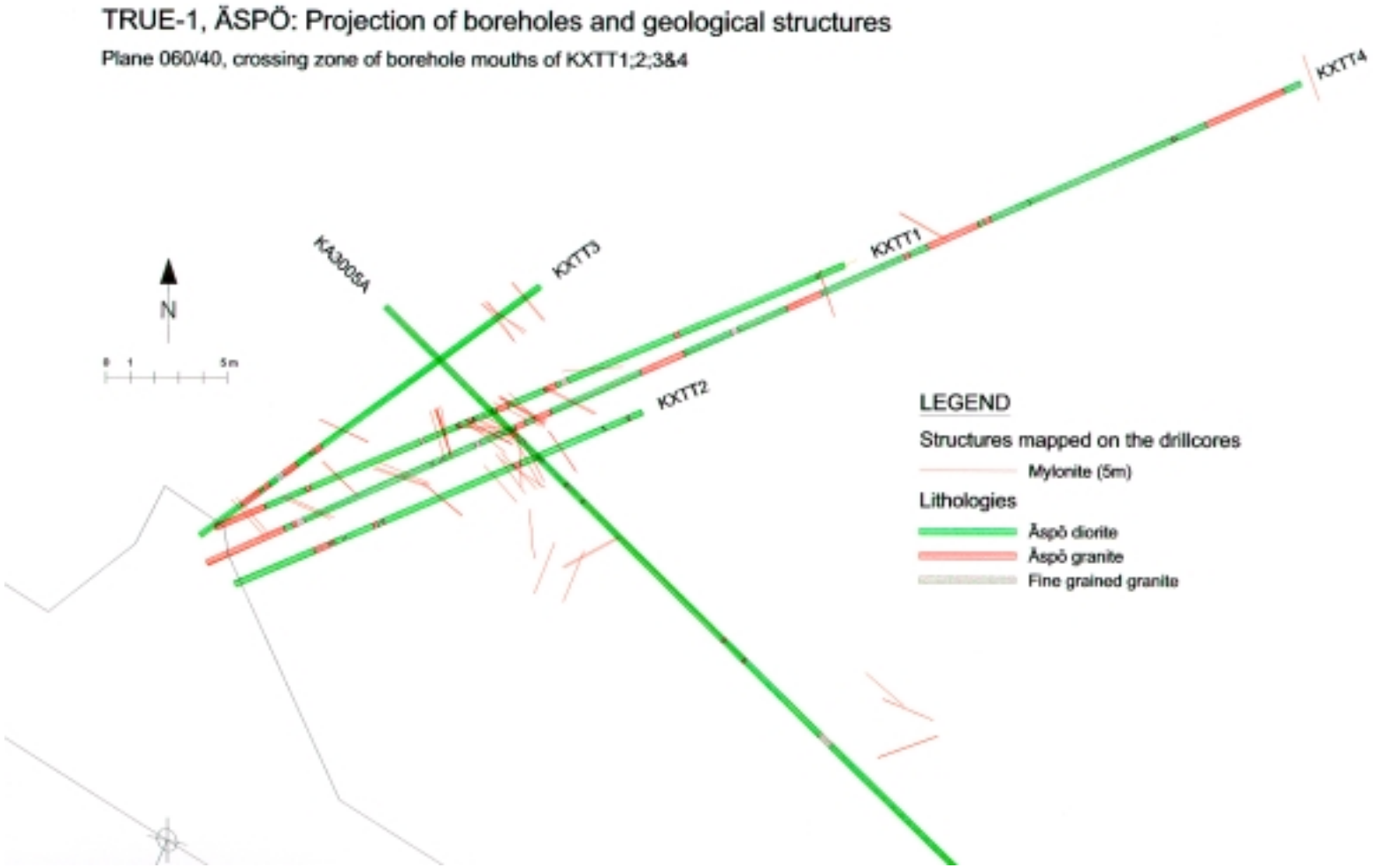

Appendix 5-18. *Selection of data: mylonites from the drillcore database (060/40 plane).*

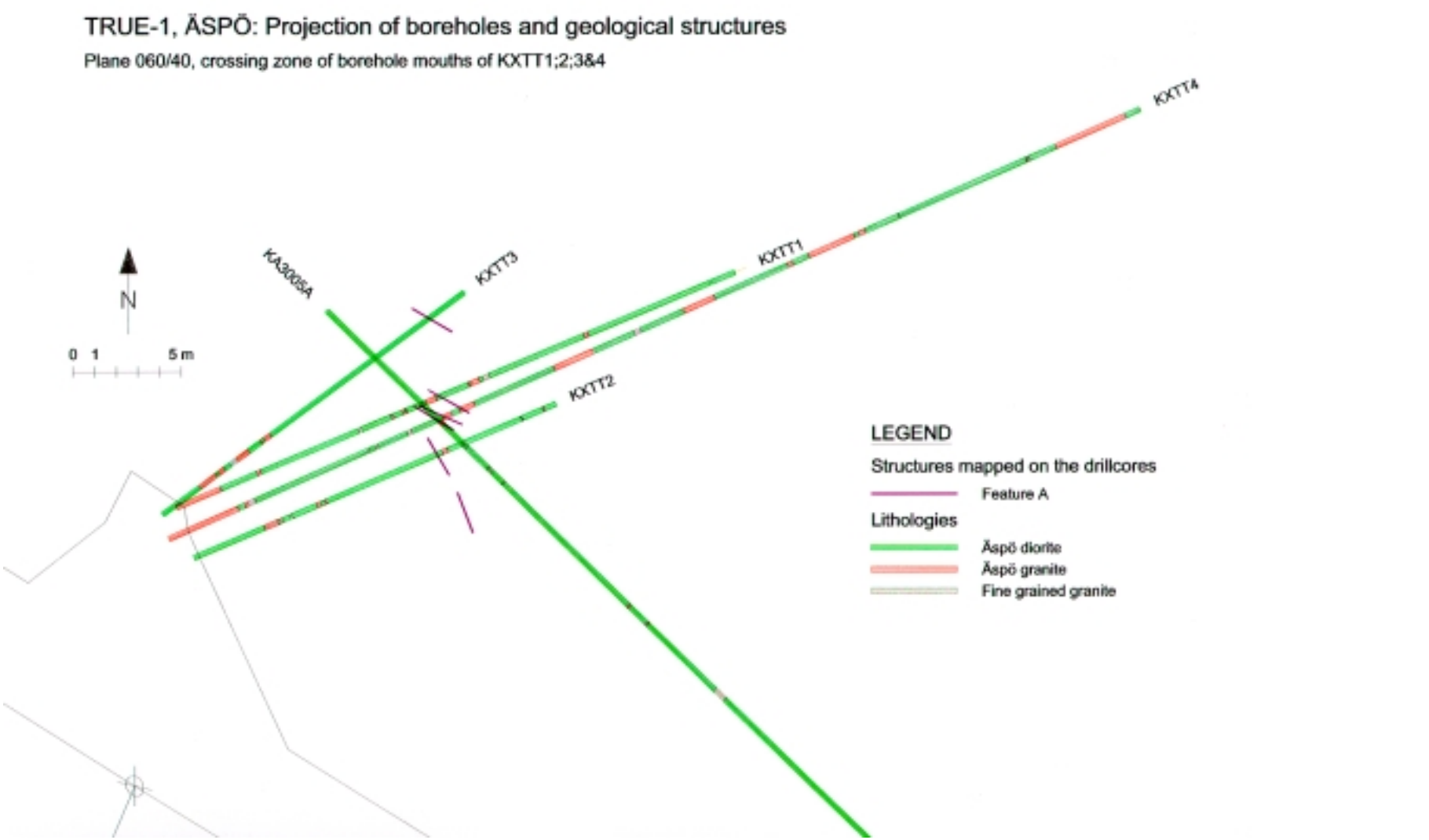

Appendix 5-19. *Selection of data: Mylonites from the drillcore database along the "Feature A" structures mapped from drillcores (060/40 plane).*

Appendix 6

Constraints on the structural model based on hydrogeological observations

6-1 Crosshole reactions in borehole KXTT4 and estimation of parameters.

6-2 Crosshole reactions in borehole KA3005A and estimation of parameters.

6-3 Inverse modelling of withdrawal test in borehole KXTT2, option 1: homogenous domain, no skin.

6-4 Inverse modelling of withdrawal test in borehole KXTT2, option 2: homogenous domain, positive skin factor.

6-5 Inverse modelling of withdrawal test in borehole KXTT2, option 3: homogenous domain, positive skin factor and fixed flow dimension.

6-6 Figure 2.44 Fracture logs and water inflows of boreholes a) KXTT1 b) KXTT2 c) KXTT3, d) KXTT4 and e) KA3005A. Inflows > 5 litres/min are shown with arrows and numbers. Inflows > 0.5 litres/min but < 5 litres/min are only indicated with arrows.

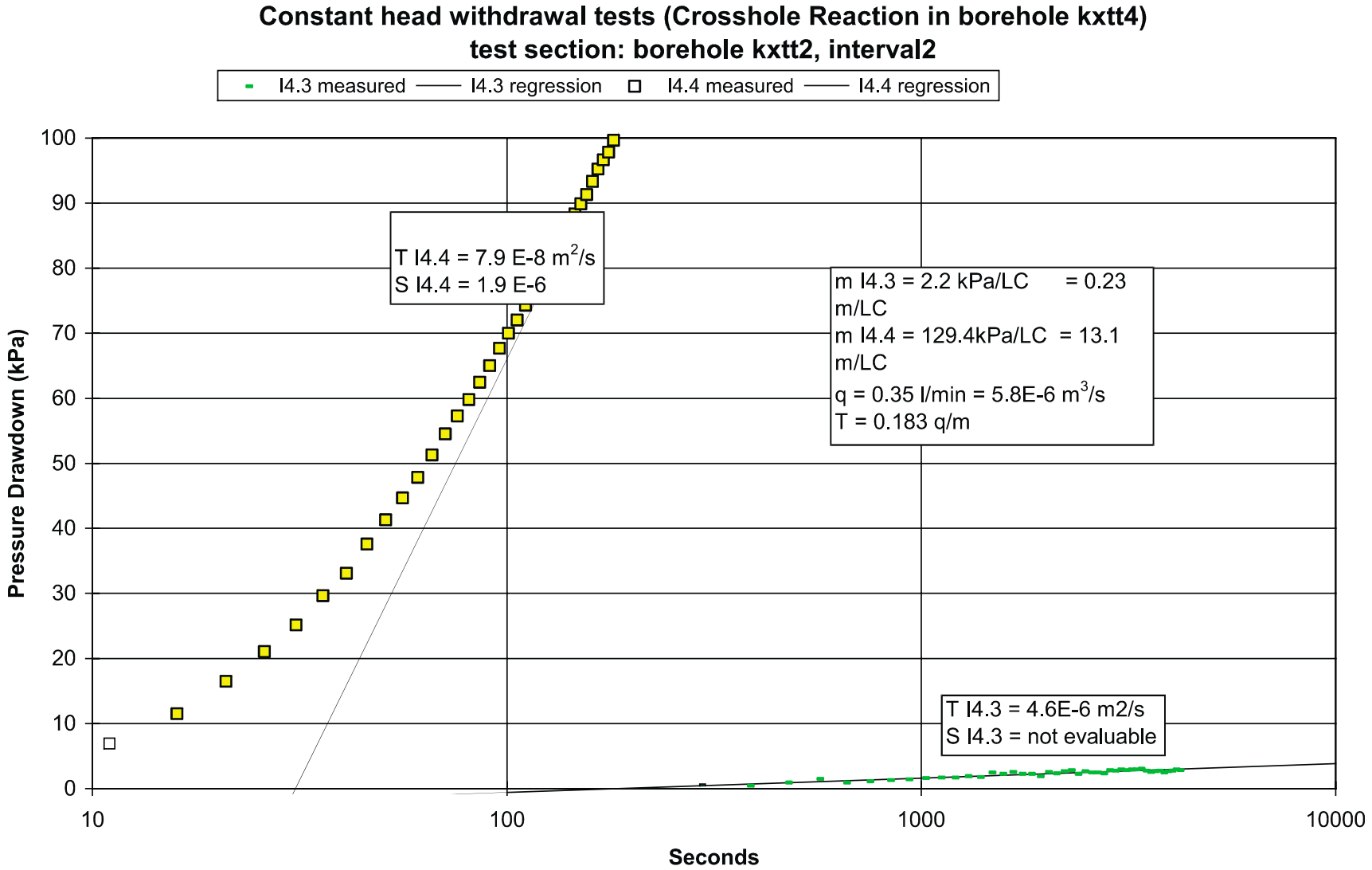

Appendix 6-1. *Crosshole reactions in borehole KXTT4 and estimation of parameters.*

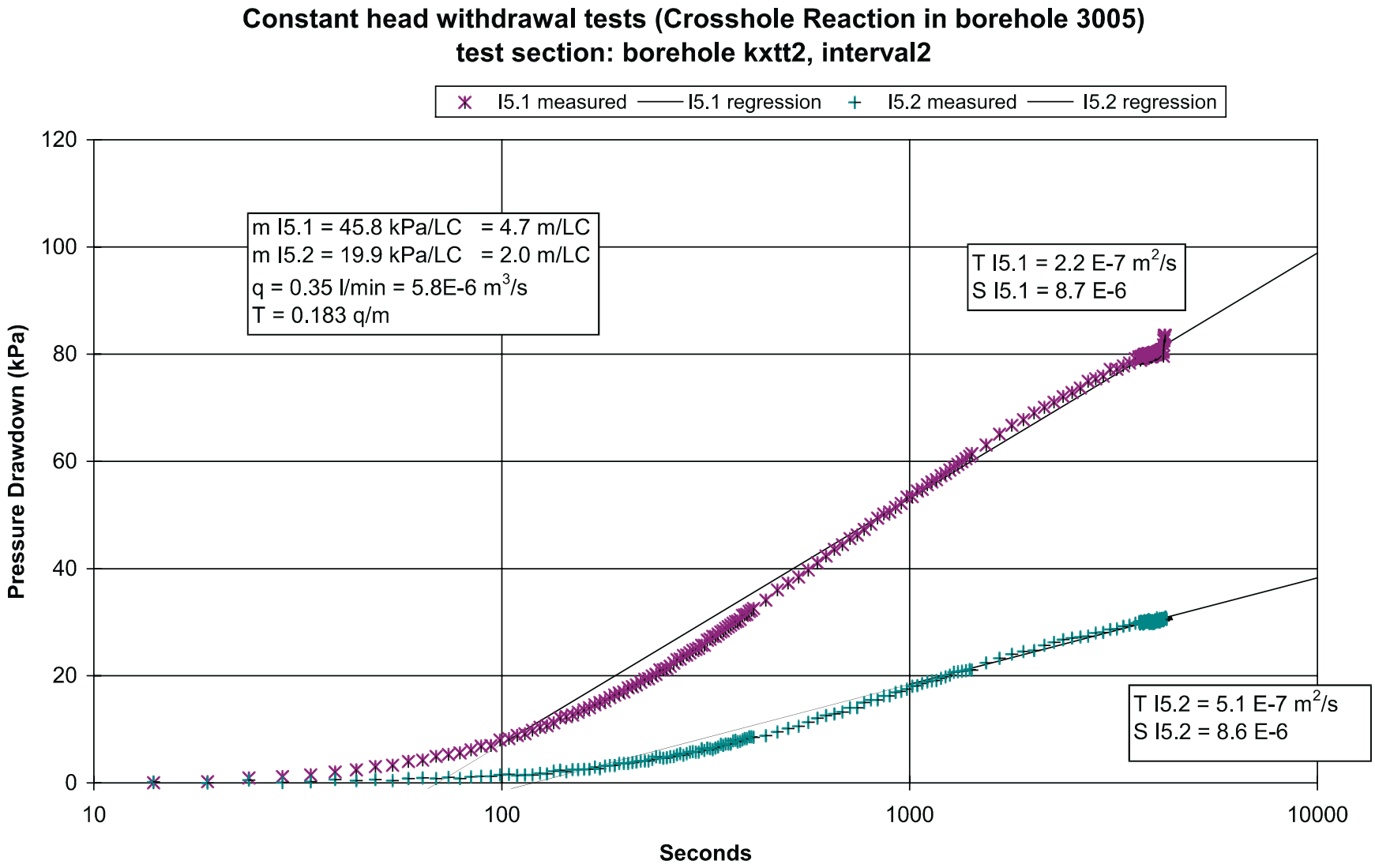

Appendix 6-2. *Crosshole reactions in borehole KA3005A and estimation of parameters.*

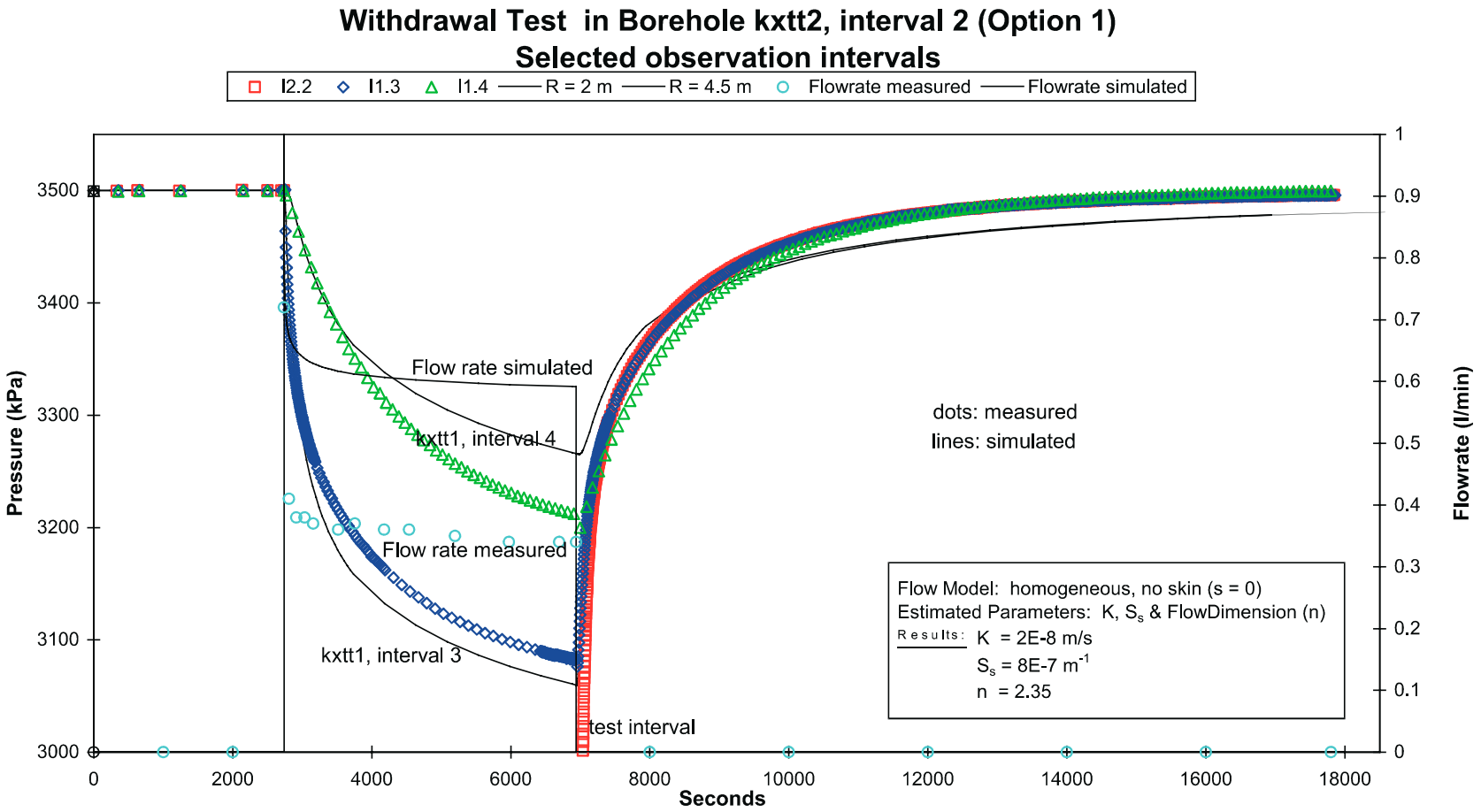

Appendix 6-3. *Inverse modelling of withdrawal test in borehole KXTT2, option 1: homogenous domain, no skin.*

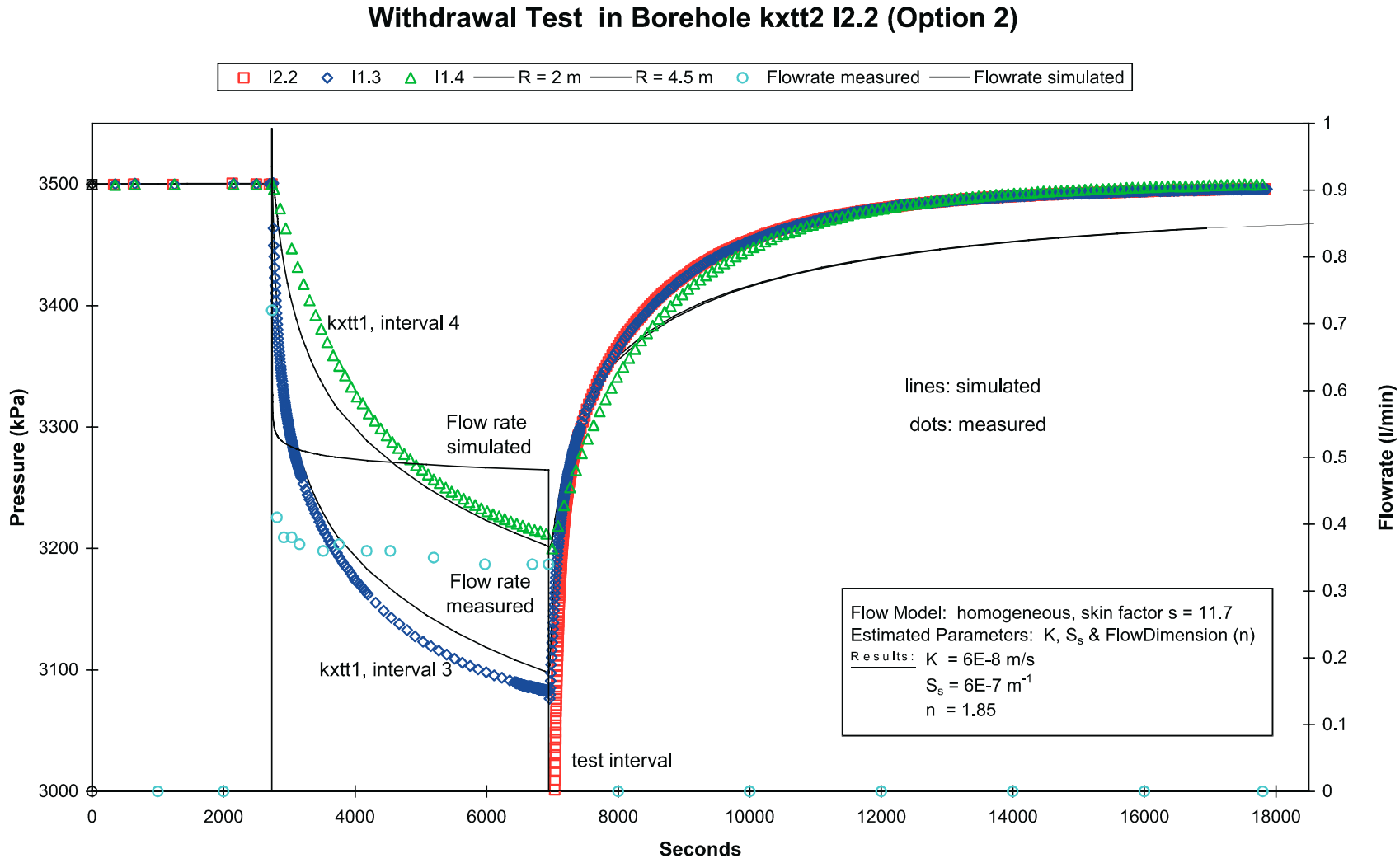

Appendix 6-4. *Inverse modelling of withdrawal test in borehole KXTT2, option 2: homogenous domain, positive skin factor.*

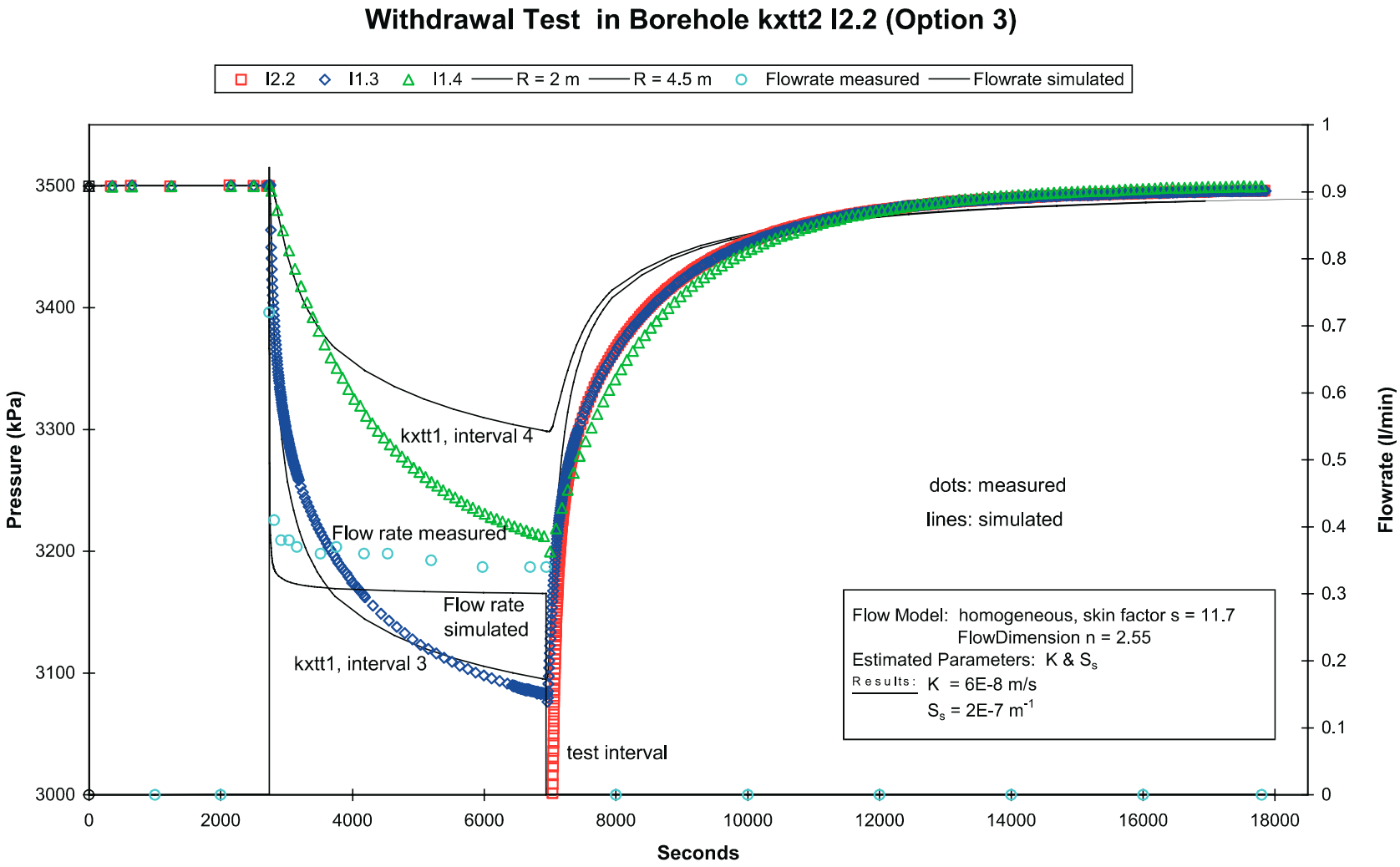

Appendix 6-5. *Inverse modelling of withdrawal test in borehole KXTT2, option 3: homogenous domain, positive skin factor and fixed flow dimension.*

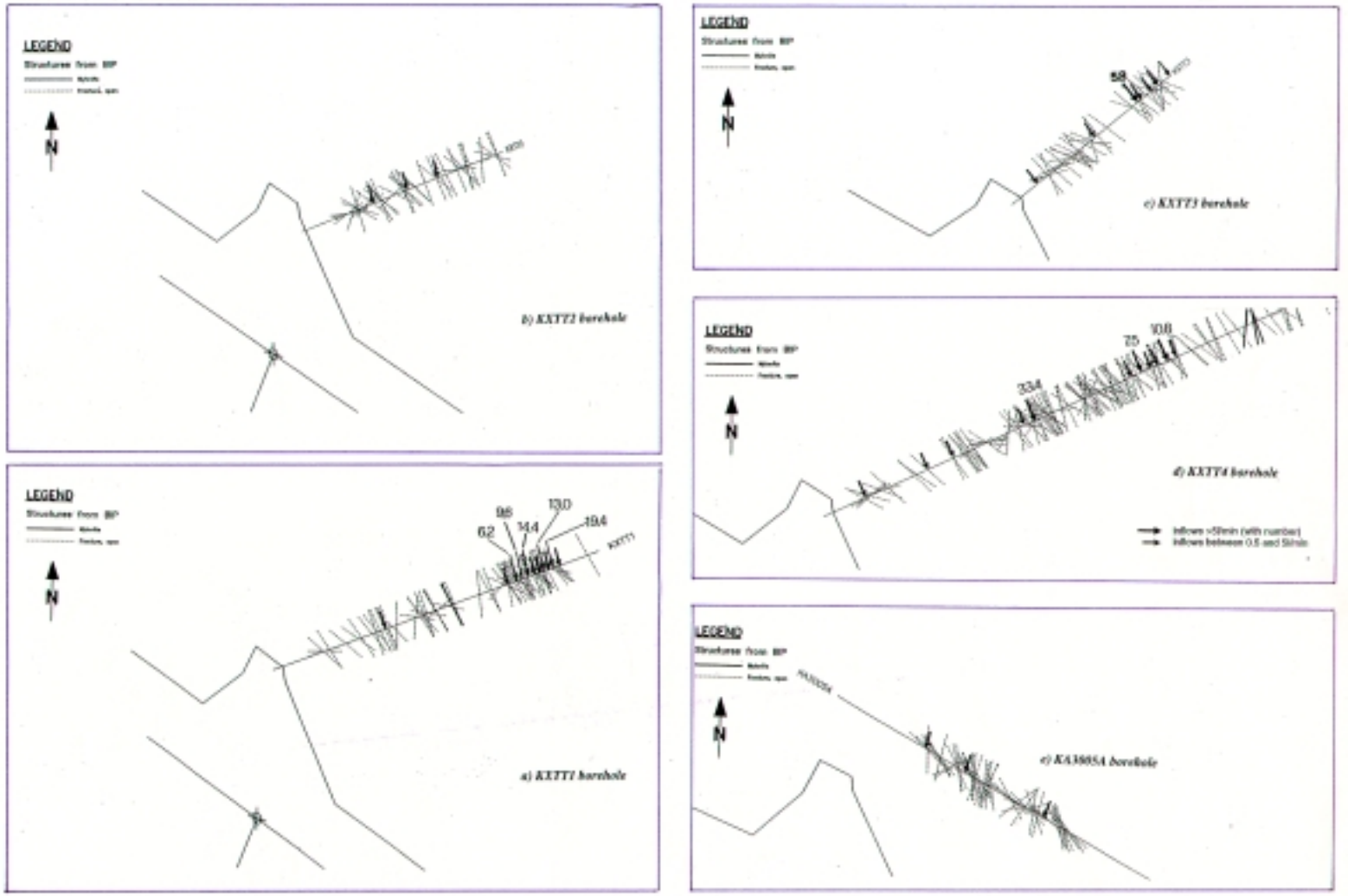

Appendix 6-6. *Figure 2.44 Fracture logs and water inflows of boreholes a) KXTT1 b) KXTT2 c) KXTT3, d) KXTT4 and e) KA3005A. Inflows > 5 litres/min are shown with arrows and numbers. Inflows > 0.5 litres/min but < 5 litres/min are only indicated with arrows.*

Scaling relationships: cumulative fracture frequencies of structural maps

7-1 **Cumulative frequency plots of fractures of structural map of Figure 3-1b, Äspö local scale, a) whole range of data and b) reduced range, linear segment.**

7-2 **Cumulative frequency plots of fractures of structural map of Figure 3-2a, Äspö West a) whole range of data and b) reduced range, linear segment.**

7-3 **Cumulative frequency plots of fractures of structural map of Figure 3-2b, Äspö village a) whole range of data and b) reduced range, linear segment.**

7-4 **Cumulative frequency plots of fractures of structural map of Figure 3-4, Äspö rock laboratory, tunnel metre 1978-2003, a) whole range of data and b) reduced range, linear segment.**

7-5 **Cumulative frequency plots of fractures of structural map of Figure 3-5b, Äspö rock laboratory, tunnel metre 2050, a) whole range of data and b) reduced range, linear segment.**

7-6 **Cumulative frequency plots of fractures of structural map of Figure 3-6, Äspö rock laboratory, tunnel metre 2232 – 2260, a) whole range of data and b) reduced range, linear segment.**

7-7 **Cumulative frequency plots of fractures of structural map of Figure 3-5 c, Äspö rock laboratory, tunnel metre 2963, a) whole range of data and b) reduced range, linear segment.**

7-8 **Cumulative frequency plots of fractures of structural map of Figure 3-7, tunnel wall of the TRUE-1 block, between tunnel metres 2944 and 3004, a) whole range of data and b) reduced range, linear segment.**

7-9 **Cumulative frequency plots of fractures derived from the line countings at the tunnel ceiling of the TRUE-1 block, between tunnel metres 2950 and 2980 (see also Appendix 3), a) whole range of data and b) reduced range, linear segment.**

7-10 **Cumulative frequency plots of fractures of structural map of Figure 3-8, Äspö rock laboratory, tunnel metre 3124, a) whole range of data and b) reduced range, linear segment.**

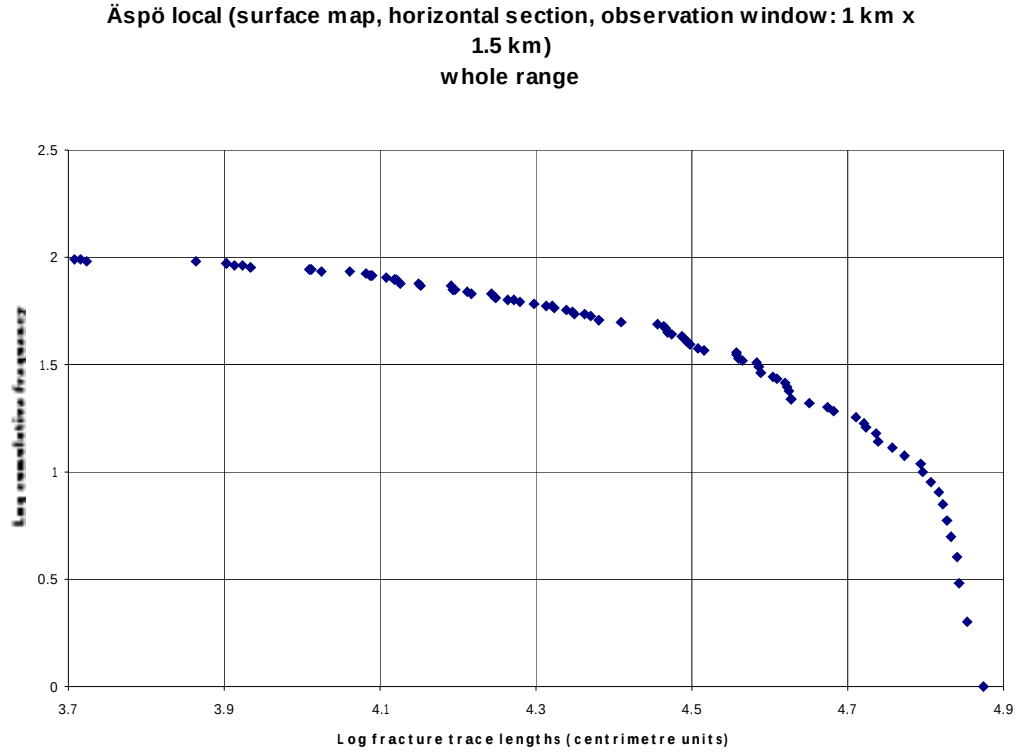

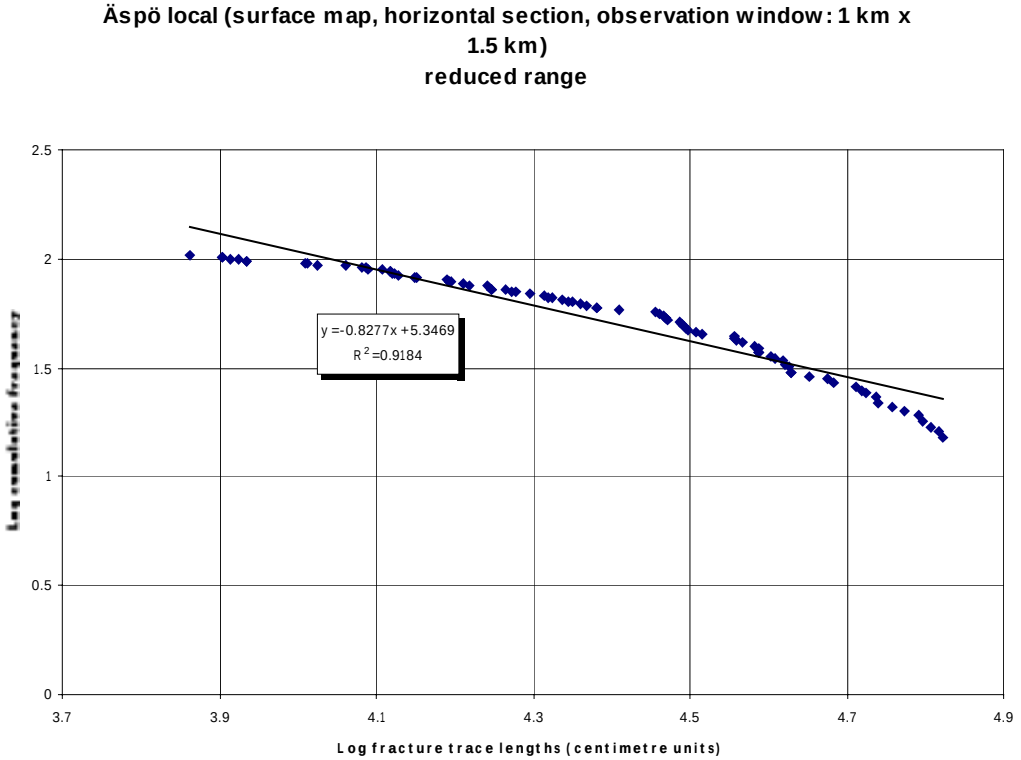

Appendix 7-1. *Cumulative frequency plots of fractures of structural map of Figure 3-1b, Äspö local scale, a) whole range of data and b) reduced range, linear segment.*

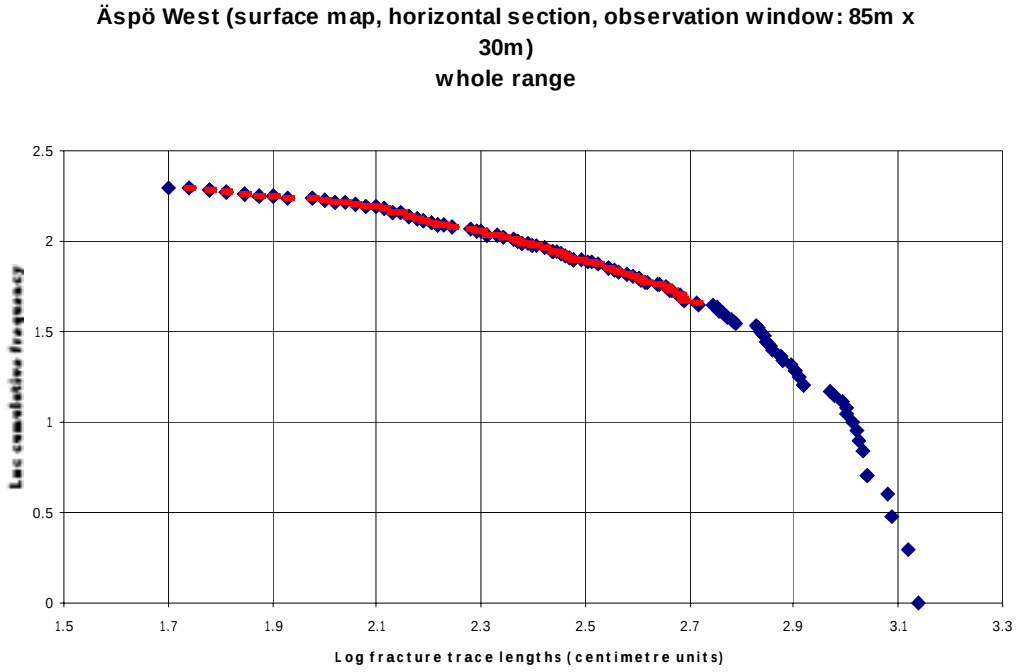

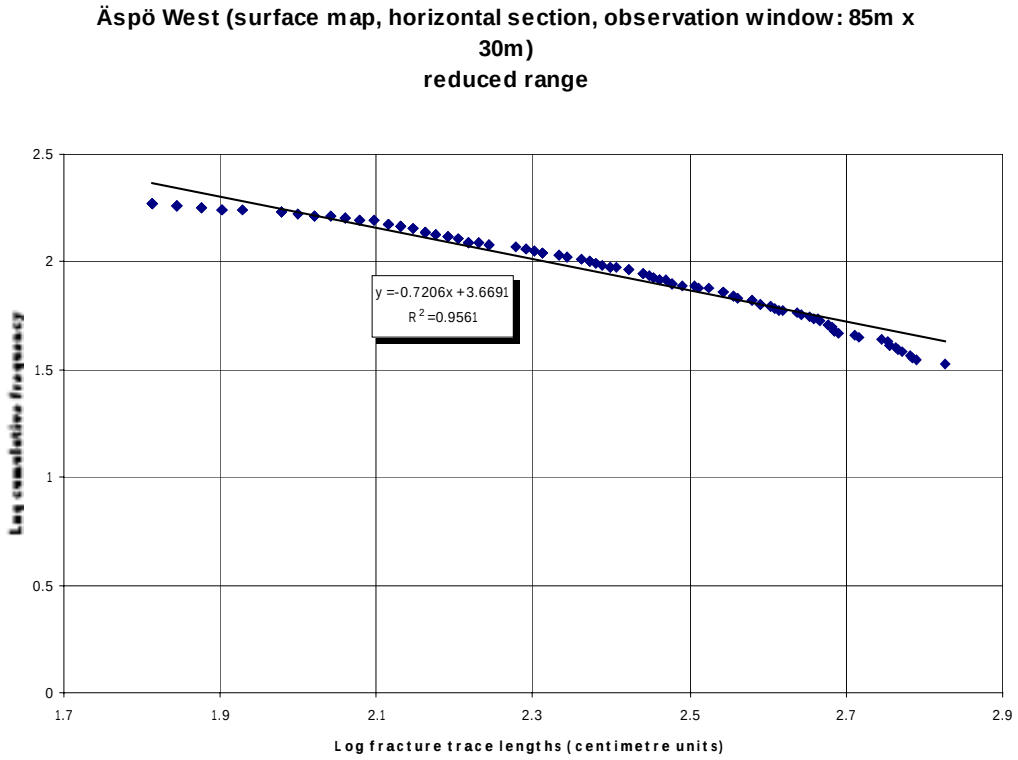

Appendix 7-2. *Cumulative frequency plots of fractures of structural map of Figure 3-2a, Äspö West a) whole range of data and b) reduced range, linear segment.*

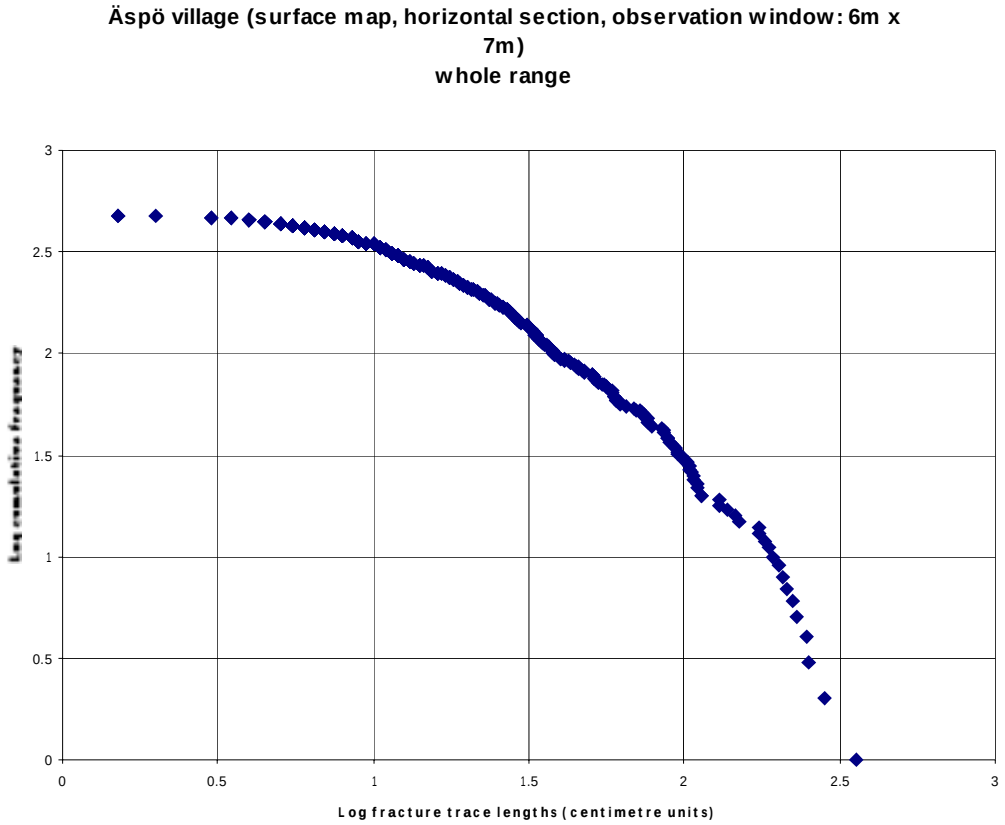

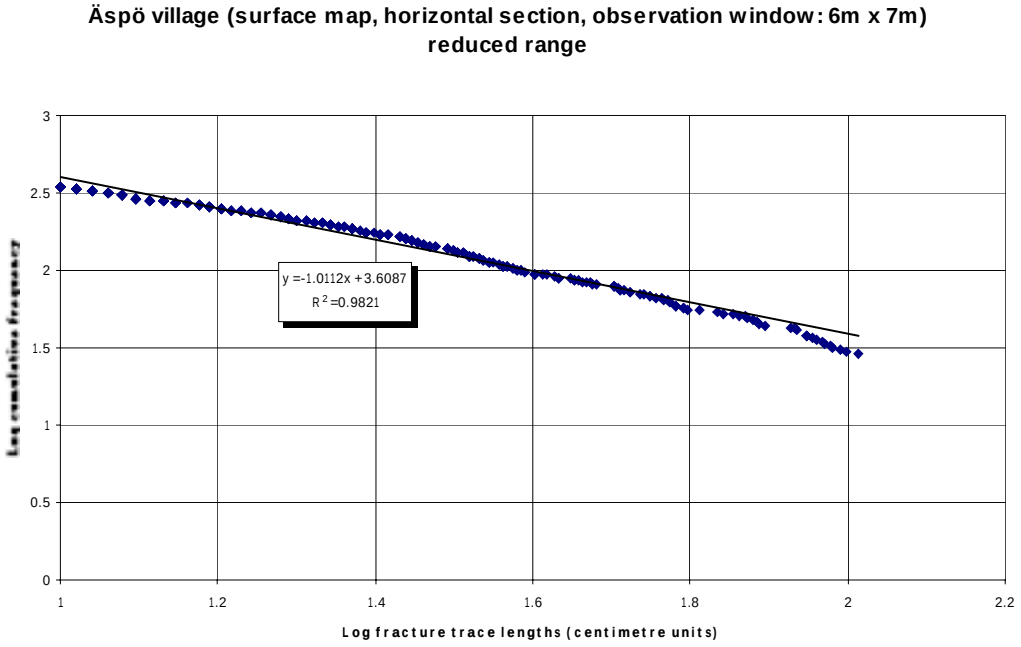

Appendix 7-3. *Cumulative frequency plots of fractures of structural map of Figure 3-2b, Äspö village a) whole range of data and b) reduced range, linear segment.*

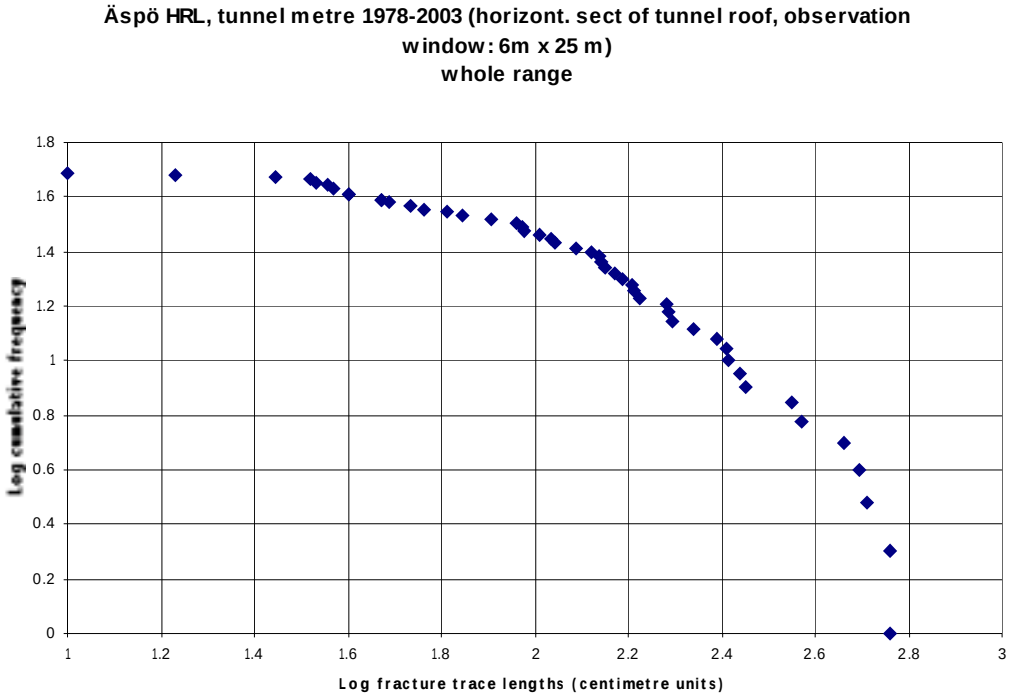

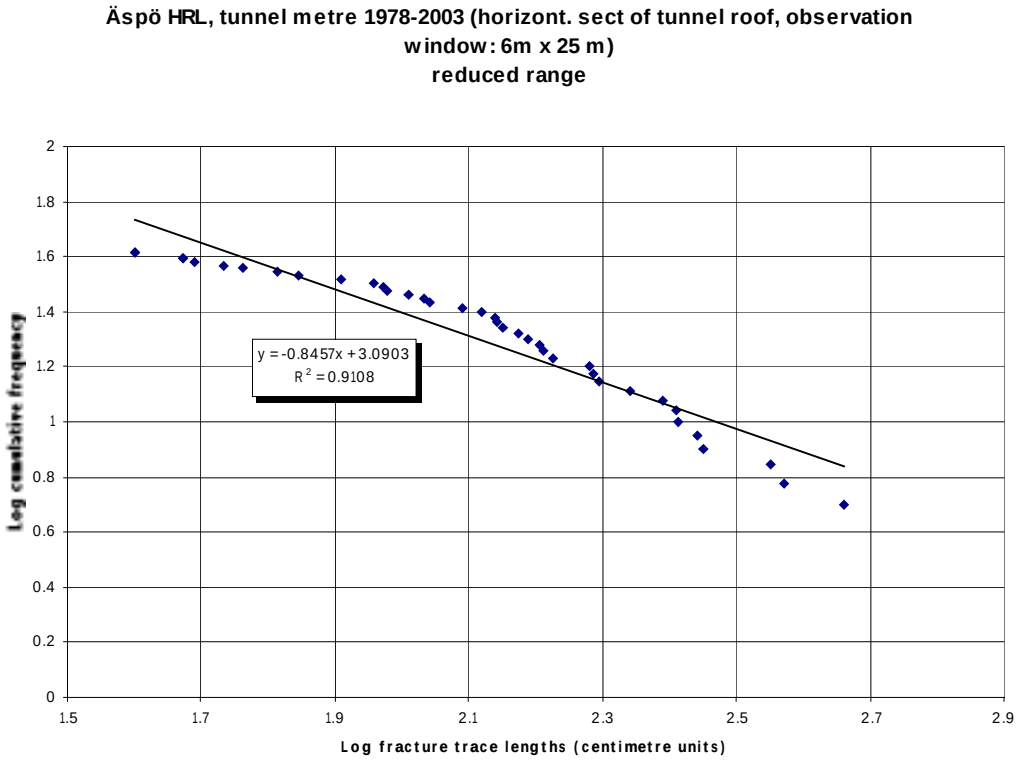

Appendix 7-4. *Cumulative frequency plots of fractures of structural map of Figure 3-4, Äspö rock laboratory, tunnel metre 1978-2003, a) whole range of data and b) reduced range, linear segment.*

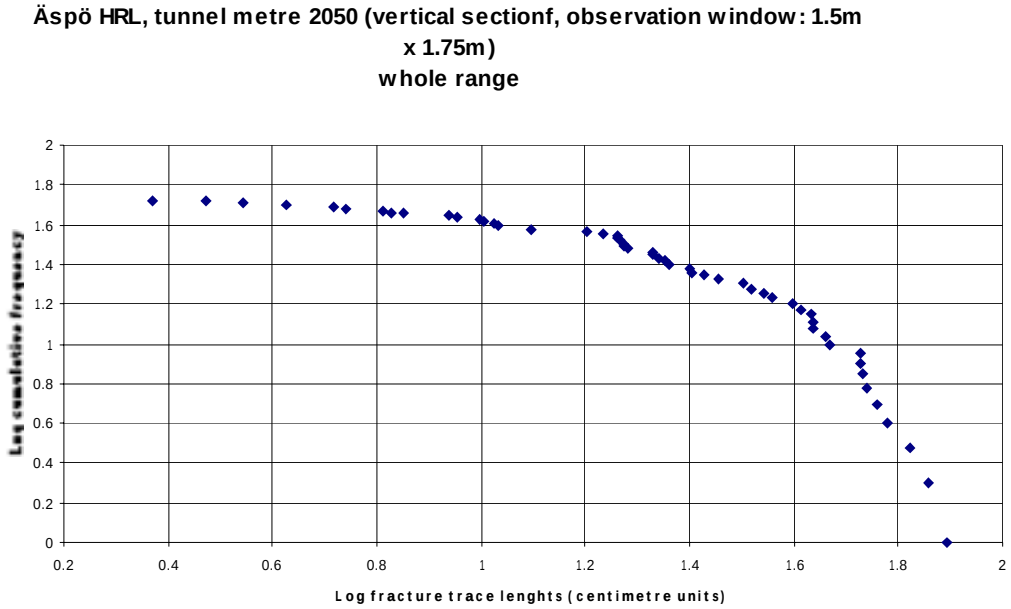

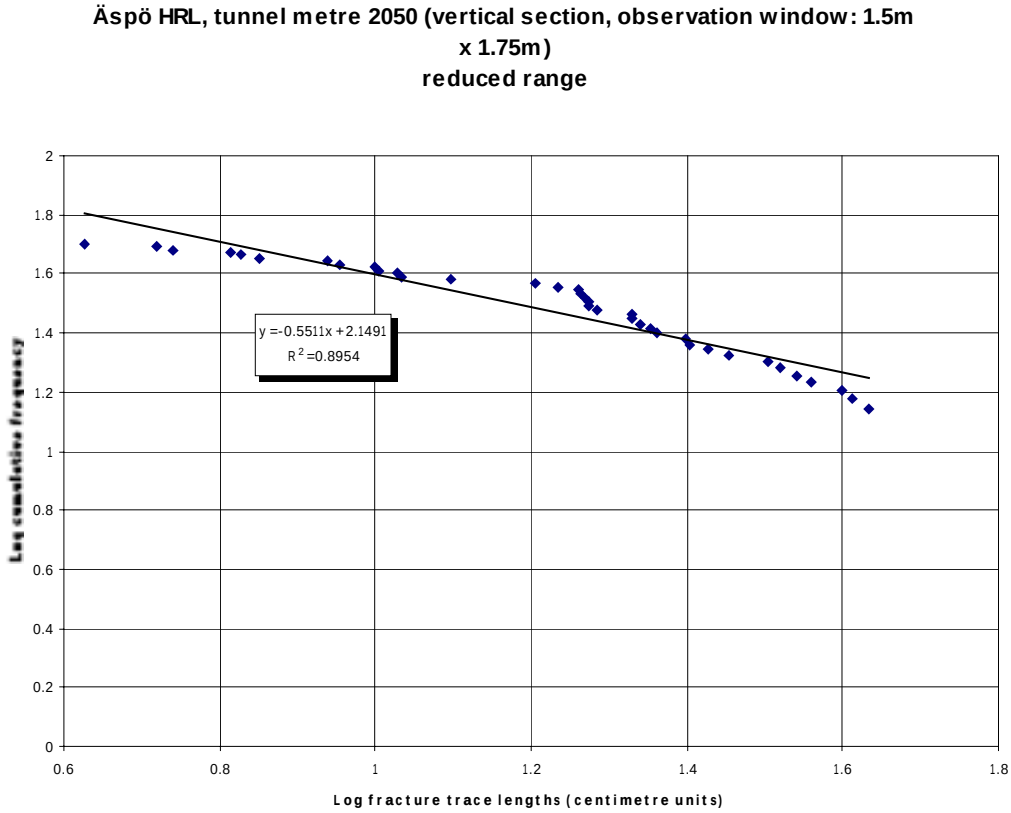

Appendix 7-5. *Cumulative frequency plots of fractures of structural map of Figure 3-5b, Äspö rock laboratory, tunnel metre 2050, a) whole range of data and b) reduced range, linear segment.*

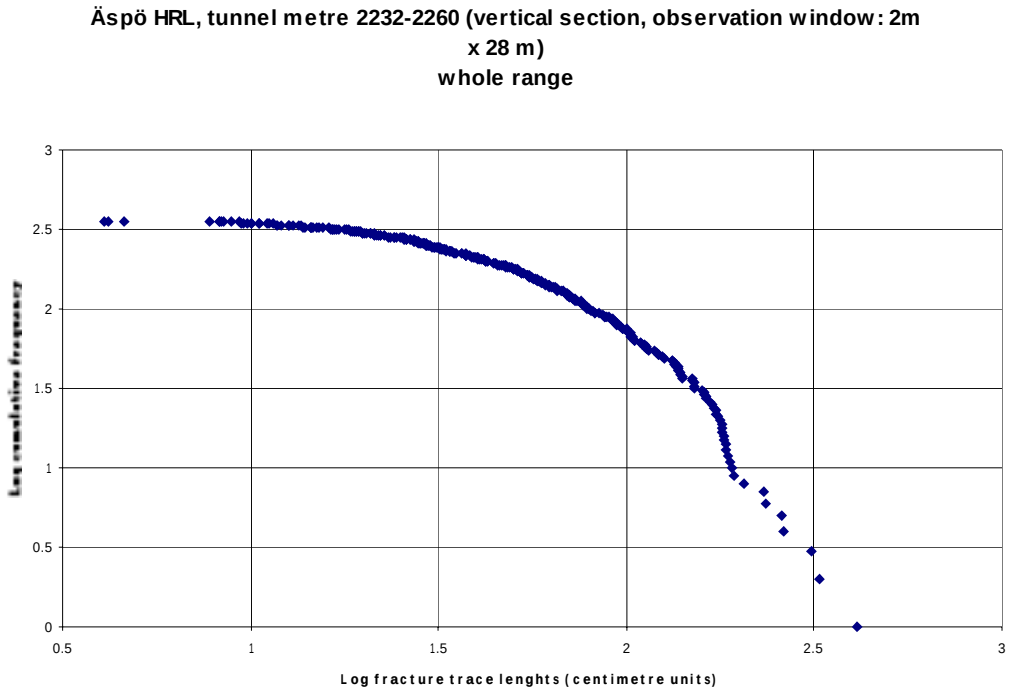

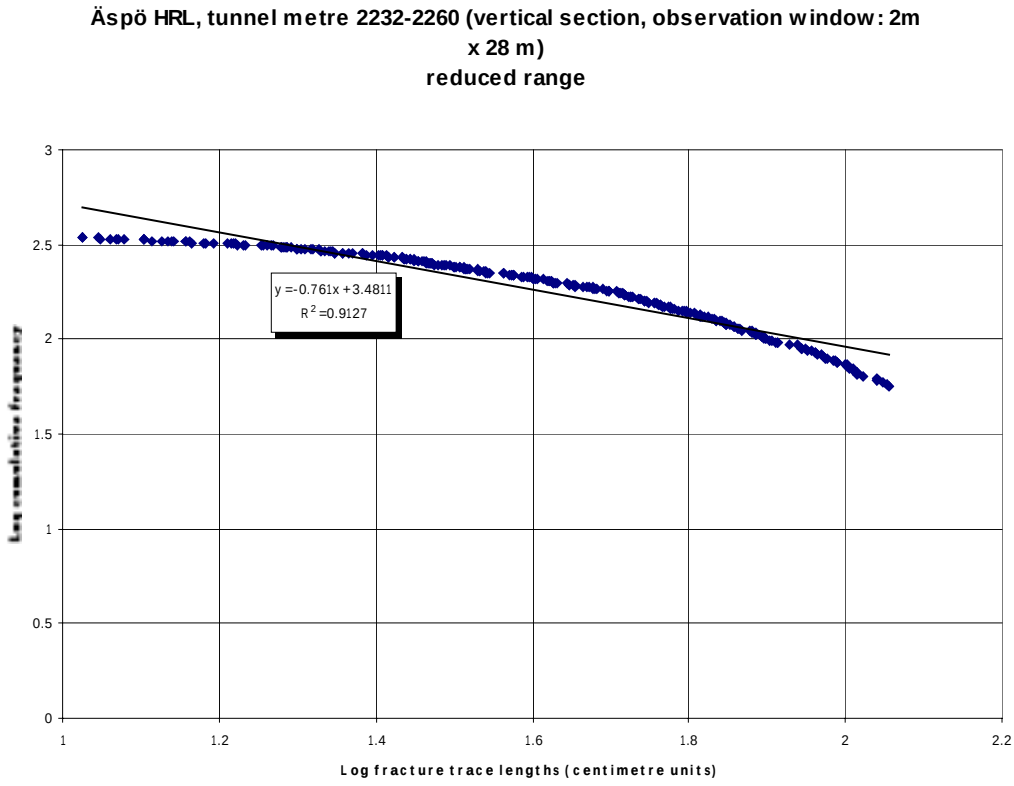

Appendix 7-6. *Cumulative frequency plots of fractures of structural map of Figure 3-6, Äspö rock laboratory, tunnel metre 2232 – 2260, a) whole range of data and b) reduced range, linear segment.*

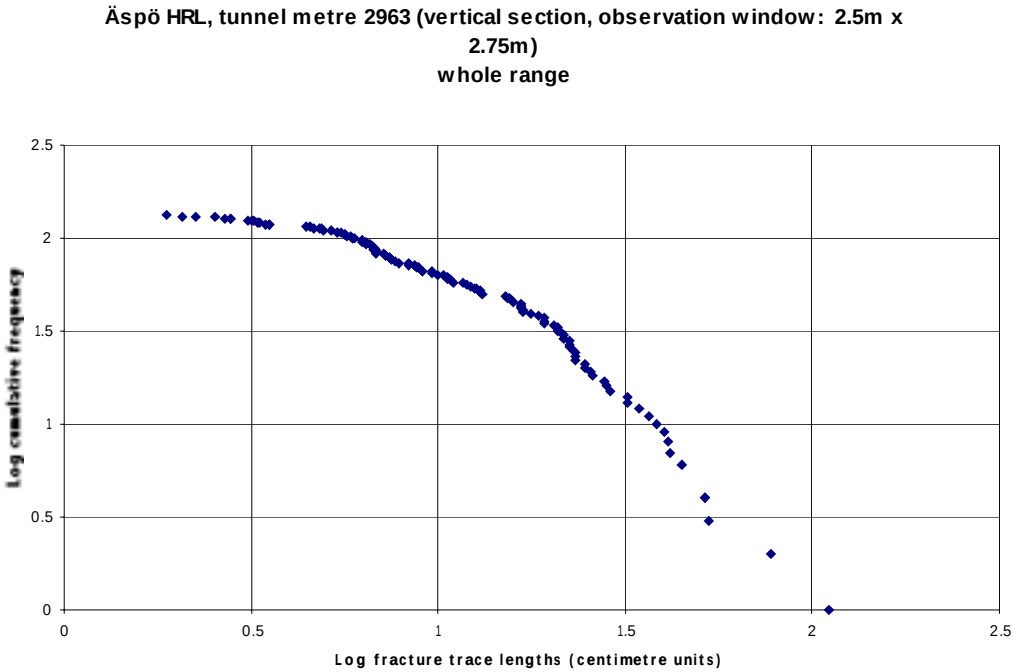

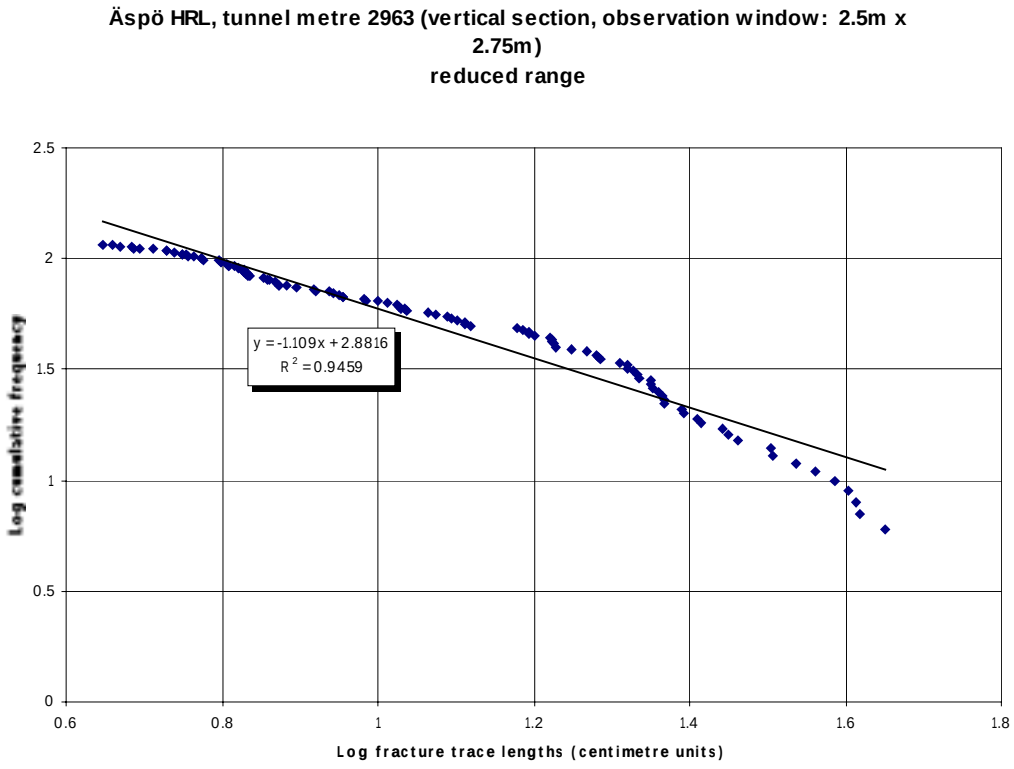

Appendix 7-7. *Cumulative frequency plots of fractures of structural map of Figure 3-5 c, Äspö rock laboratory, tunnel metre 2963, a) whole range of data and b) reduced range, linear segment.*

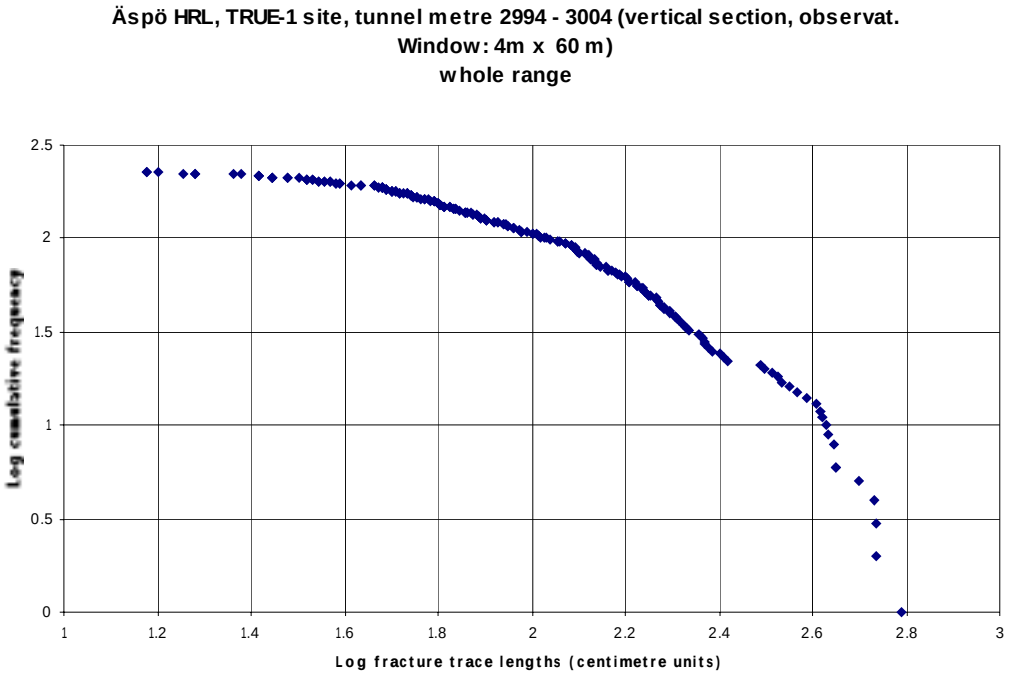

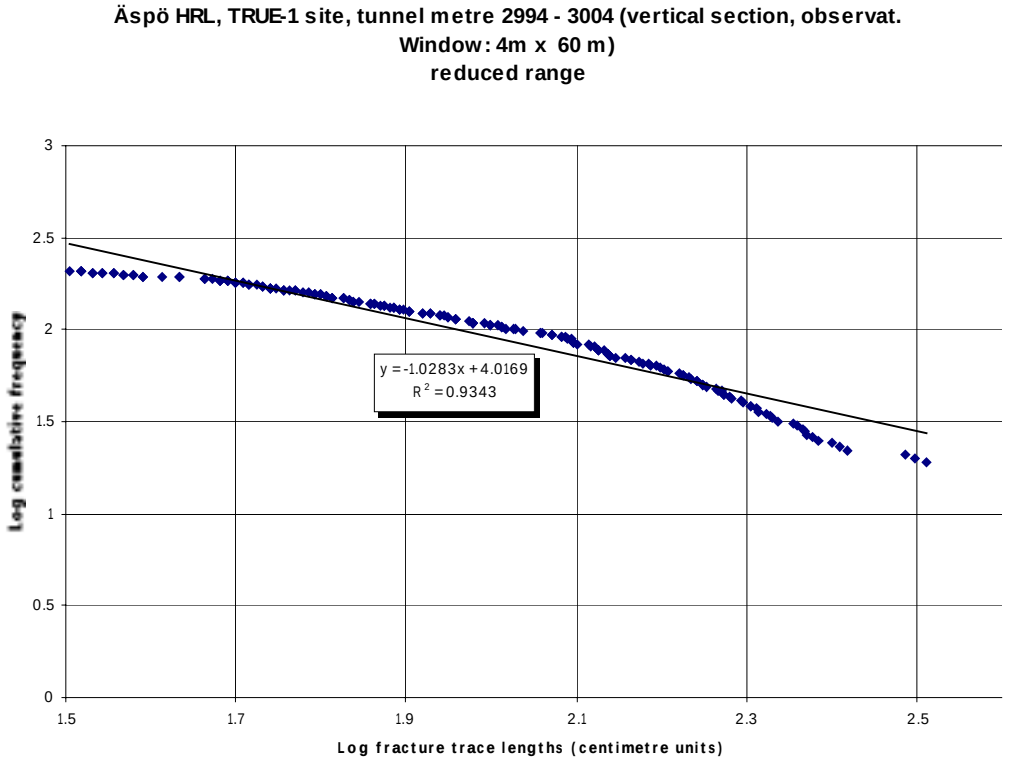

Appendix 7-8. *Cumulative frequency plots of fractures of structural map of Figure 3-7, tunnel wall of the TRUE-1 block, between tunnel metres 2944 and 3004, a) whole range of data and b) reduced range, linear segment.*

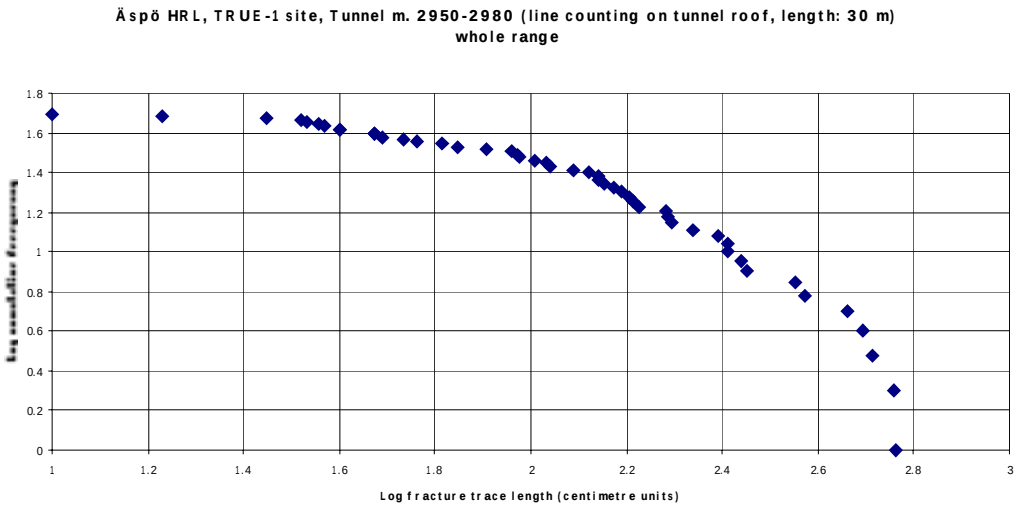

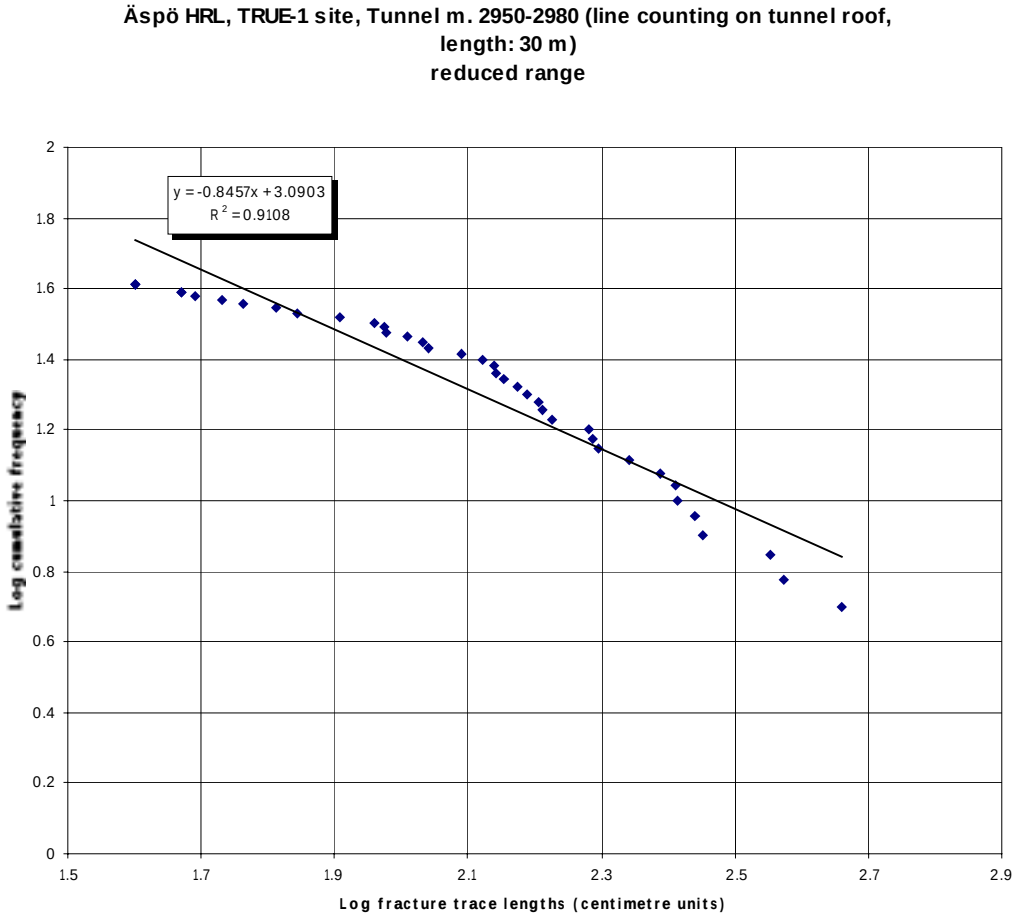

Appendix 7-9. *Cumulative frequency plots of fractures derived from the line countings at the tunnel ceiling of the TRUE-1 block, between tunnel metres 2950 and 2980 (see also Appendix 3), a) whole range of data and b) reduced range, linear segment.*

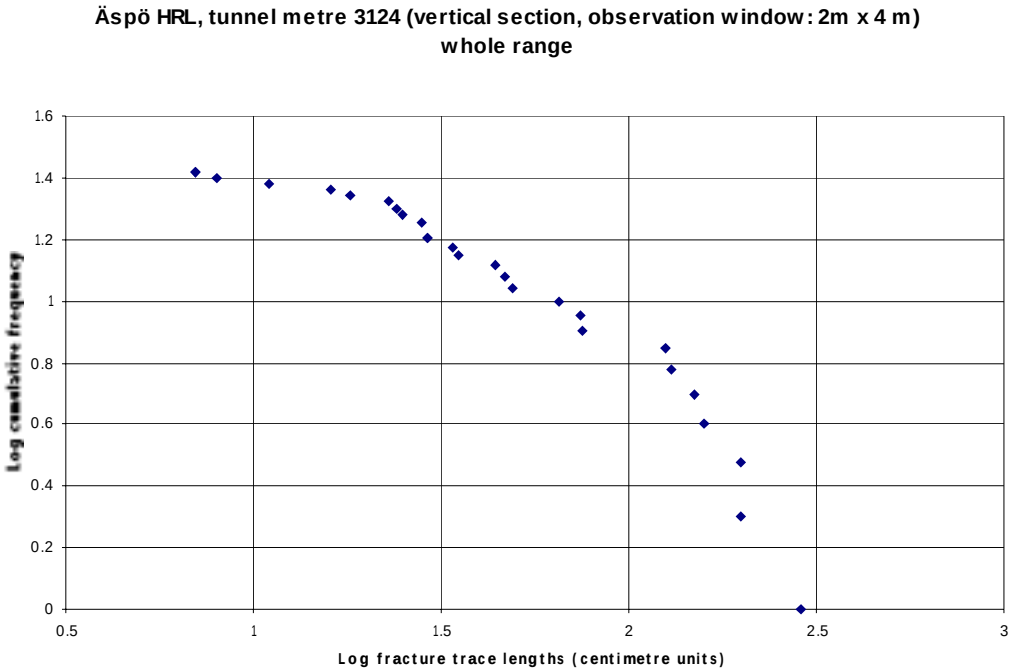

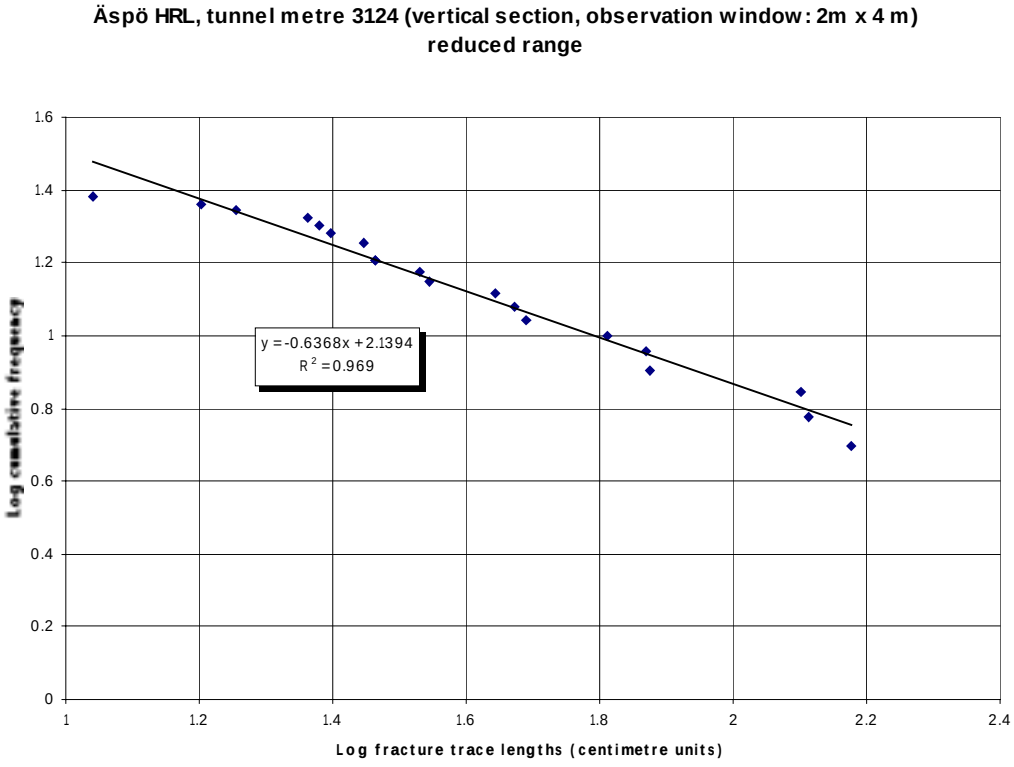

Appendix 7-10. *Cumulative frequency plots of fractures of structural map of Figure 3-8, Äspö rock laboratory, tunnel metre 3124, a) whole range of data and b) reduced range, linear segment.*